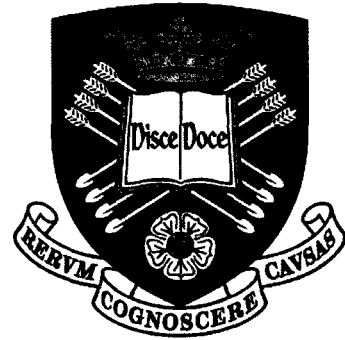


UNIVERSITY OF SHEFFIELD

Department of Civil and Structural Engineering



**COLUMN DESIGN
FOR
AXIAL COMPRESSION
AND
END ROTATION**

by Charles MacIan King

A thesis submitted in fulfilment of the requirements for the degree of Doctor of Philosophy

June 2010

SUMMARY

A column design method has been developed for use in braced frames with discontinuous columns using flexible cap and base plates and floor beams that are either simply supported or continuous. The method is intended to be used with shallow floor construction with concrete or steel/concrete composite slabs in which the floor slab occupies the depth of the floor beams and is fully grouted to the beams so that the slab restrains the full depth of the beams and was developed to simplify the design of discontinuous columns in frames using Corus ASB type floor construction without resorting to methods using nominal moments. Floor beams are therefore designed to carry the floor loads without interaction with the columns. Columns are designed to resist the floor beam reactions with column end-rotations equal to the slope of the floor beams at the top or bottom of the column, whichever is the greater.

The method incorporates the elasto-plastic behaviour of columns subject to axial compression and large end-rotations. The design procedure uses rectangular stress blocks of classic plastic cross-sectional resistance and includes the end-rotations of the columns and the effects of imperfections. Therefore the approach is similar to classic second-order rigid-plastic analysis but with the important additions of actual end-rotations and an initial imperfection. The method has been verified by physical tests on full-scale columns and finite element analysis using non-linear geometry and material properties.

The design method

1. is derived from simple geometry and simple statics
2. accounts for initial imperfections by deriving a design value from the strut resistance of whatever design code is specified
3. is limited to sections that cannot be affected by torsional, lateral torsional or torsional flexural buckling
4. is not applicable to sections with thin walls
5. has been verified for use with hot-finished square hollow sections by testing full-scale columns

The design method is defined in detail and illustrated by a worked example so that it can be used in normal design practice. Connection design and bracing requirements are discussed to enable the column design to be used to design complete frames.

ACKNOWLEDGEMENTS

I would like to thank Dr J B Davison for his energy and time given in supervision and encouragement.

The laboratory tests were funded by both the Construction & Industrial and the Tubes divisions of Corus and I would like to thank Corus for this funding without which the tests would not have been possible.

The PhD was partially funded by the SCI and I would like to thank the SCI for this funding.

These tests were conducted in the laboratories of the Department of Civil Engineering of the University of Sheffield. These were organised by Dr J B Davison and the rig was designed, constructed and operated by Mr S Waters. It is to the great credit of Mr Waters that very smooth curves were recorded on the falling branch of the test, including an unloading and re-loading cycle. I would like to thank both Dr Davison and Mr Waters for doing these tests with only limited input from me.

I especially thank my wife Stephanie for her generous support and encouragement throughout all the years of the project.

I would also like to thank following for their contributions:

Dr A R Gent for his original papers on elastic-plastic column stability

Dr Arun Kamtekar for pointing me to the Gent papers

Tom Cosgrove, for suggesting that I should conduct the research as a PhD

David Brown, for his support of the project and help in securing funding and travel time to Sheffield

Charles King

DECLARATION

Except where specific reference has been made to the work of others, this thesis is the result of my own work. No part of it has been submitted to any University for a degree, diploma or other qualification.

Charles Maclan King

CONTENTS

	Page No.
SUMMARY	ii
ACKNOWLEDGEMENTS	iii
DECLARATION	iv
FIGURES	ix
LIST OF SYMBOLS	xv
1 BACKGROUND	1
1.1 Introduction	1
1.2 Braced frames	1
1.3 Beam and column arrangements in traditional braced frames	2
1.4 Braced frames with discontinuous columns	3
2 REVIEW OF DESIGN METHODS	6
2.1 Introduction	6
2.2 Design of traditional braced frames	7
2.3 Orthodox design of braced frames with discontinuous columns	10
2.4 Unorthodox design methods for braced frames	24
2.5 Summary of design methods, orthodox and unorthodox	32
3 THE NEW DESIGN APPROACH	33
3.1 Introduction	33
3.2 Behaviour of columns in reality	33
3.3 New column design approach	36
3.4 Development of a method to apply the new design approach	37
3.5 Effects of breadth to thickness ratios of the walls of the members	54
3.6 Range of column end-rotations	54
3.7 Summary	57
4 ANALYSIS TOOLS	59
4.1 Introduction	59
4.2 Finite slice model	63
4.3 ABAQUS finite element model	65
4.4 Summary	69

5	FULL SCALE LABORATORY TESTS	70
5.1	Introduction	70
5.2	The test programme	71
5.3	Test rig	72
5.4	Instrumentation	74
5.5	Test duration	76
5.6	Material properties	76
5.7	Test results	77
5.8	Effect of wall thickness	97
5.9	Summary	98
6	COMPARISON OF TESTS WITH ANALYSIS	100
6.1	Introduction	100
6.2	Correlation factor for test v Abaqus	106
6.3	Straight members with asymmetrical eccentricities	110
6.4	Straight members with symmetrical eccentricities	114
6.5	Effects of breadth to thickness ratios of wall	132
6.6	Correlation factor, c_r , used for the design model	136
6.7	Summary	137
7	BREADTH TO THICKNESS LIMITS	139
7.1	Introduction	139
7.2	Parametric study	143
7.3	Calibration of Abaqus with laboratory test results	146
7.4	Design limits	146
8	VALIDATION OF THE DESIGN MODEL BY A PARAMETRIC STUDY AND CALIBRATION	150
8.1	Introduction	150
8.2	Load-rotation path sensitivity	151
8.3	Planes of rotations	155
8.4	Similarity with different slendernesses	155
8.5	Confirmation of the proposed design model	157
8.6	Conclusions	163
9	DESIGN METHOD	165
9.1	Scope of application	165
9.2	Column design model	166
9.3	Beam design	170

9.4	Frame effects	175
9.5	Connection design fundamentals	181
9.6	Avoiding disproportionate collapse	187
9.7	Connection design to avoid disproportionate collapse	190
9.8	Alternative methods to satisfy the regulation	195
10	WORKED EXAMPLE	196
10.1	Introduction	196
10.2	Structural arrangement	196
10.3	Loading	198
10.4	Slab	198
10.5	Main beams	200
10.6	Column	205
11	CONCLUSIONS	212
11.1	Summary of what has been achieved	212
11.2	Suggestions for further developments	213
APPENDIX A	SHS SECTION PROPERTIES	223
A.2	Axial not exceeding 50% squash load	224
A.3	Axial compression exceeding $0.5 N_{pl}$	227
APPENDIX B	BS 5950 CALCULATIONS	231
B.1	Buckling resistance of Square Hollow Sections	231
B.2	Single curvature	232
APPENDIX C	FINITE ELEMENT MODEL DETAILS	234
C.1	Introduction	234
C.2	Full model	234
C.3	Half model	244
APPENDIX D	STRUT RESISTANCE FROM INITIAL IMPERFECTIONS	247
D.1	Introduction	247
D.2	Equilibrium	247
D.3	Derivation of strut formula	248
APPENDIX E	TRANSVERSE BENDING OF WALLS	251
E.1	Introduction	251
E.2	Second order elastic behaviour	253
E.3	Elastic behaviour bending about X or Y axes	254

E.4	Effects of plastic flow	256
E.5	Elastic-plastic behaviour bending about X or Y axes	264
E.6	Summary	269
APPENDIX F	FINITE SLICE SPREADSHEET	271
F.1	Outline of spreadsheet calculations	271
F.2	Calculation of the 'line of thrust'	272
F.3	Generation of the curvature and the deflected shape	273
F.4	Calculation of the moment induced by curvature	281
APPENDIX G	TABLES OF RESULTS OF PARAMETRIC STUDY	294
G.3	1.5m columns	295
G.4	3.0m columns	299
G.5	6.0m columns	305
APPENDIX H	IMPROVED ECONOMY WITH VARIABLE IMPERFECTION	308
APPENDIX I	DEFORMED SHAPE OF TEST SPECIMEN	311
APPENDIX J	CMK 2007 SSRC MODEL	312

FIGURES

Figure 1.1 Typical braced frame	2
Figure 1.2 Columns and beams in a traditional frame	3
Figure 1.3 Columns and beams in a typical frame with discontinuous columns	4
Figure 1.4 Typical column-beam connection	5
Figure 2.1 Beam-column connection with thin end-plates and low axial compression	7
Figure 2.2 Typical column with a beam connected on one side	8
Figure 2.3 Typical column with beams connected on both sides	8
Figure 2.4 Beam on a thin cap plate on a $140 \times 140 \times 10$ SHS	11
Figure 2.5 Column loading and bending moment diagram for double curvature	14
Figure 2.6 Column loading and bending moment diagram for single curvature	15
Figure 2.7 Typical end plate deformations	16
Figure 2.8 Force distribution at a flexible column end plate	18
Figure 2.9 Plastic cross-section showing strips resisting bending moment	20
Figure 2.10 Moment shedding from increasing axial load	25
Figure 3.1 Single curvature with small end-rotation	35
Figure 3.2 Single curvature with large end-rotation	35
Figure 3.3 Single curvature bending in the column	37
Figure 3.4 Double curvature bending in the column	37
Figure 3.5 Triangular approximation to the bending in the column	39
Figure 3.6 Deformation with increasing end rotation	40
Figure 3.7 Comparison of typical actual v plastic stress distributions	41
Figure 3.8 Design bending moment in the column including imperfection	44
Figure 3.9 Comparison of actual v plastic stress distributions at low end rotations	45
Figure 3.10 Plastic cross-section to calculate N_b from M_x only	47
Figure 3.11 Plastic cross-section to calculate N_b from M_x and M_y	48
Figure 3.12 Mid-height displacements – rotations applied about rectangular axes	49
Figure 3.13 Mid-height displacements – rotation applied at 45° to rectangular axis	50
Figure 3.14 Spread of plasticity – column displacements in $X=Y$ plane	51
Figure 3.15 Mid-height displacements – rotation at 22.5° intervals	52
Figure 4.1 Imperfection and deflections in one plane only	60
Figure 4.2 Deflections in two planes	61
Figure 4.3 Imperfection and deflections in the $X = Y$ plane	62

Figure 4.4 Parabolic residual stress pattern (on all sides)	64
Figure 4.5 Finite element model mesh of full model	66
Figure 4.6 Finite element model mesh of half model	67
Figure 4.7 Bi-triangular residual stress pattern (on all sides)	68
Figure 5.1 Test rig with column in position	72
Figure 5.2 Shoe at bottom of test column	73
Figure 5.3 Spring grip frame, the “thing”, for LVDT connections	74
Figure 5.4 Unloading cycle with no friction in the bearings	77
Figure 5.5 Unloading/re-loading cycle with no friction and no Bauschinger effect	78
Figure 5.6 Unloading/re-loading cycle with no friction in the end fittings	78
Figure 5.7 Unloading/re-loading cycle test kc3	79
Figure 5.8 Rising and falling branches	79
Figure 5.9 Bending moment for ram extension	80
Figure 5.10 Rising and falling branches with unloading/re-loading cycle	81
Figure 5.11 Bending moment for ram retraction	81
Figure 5.12 Load v mid-height displacement (in-plane)	82
Figure 5.13 Load v mid-height displacement (in-plane), zero to 8mm	82
Figure 5.14 10mm wall SHS, mid-height displacements v 3mm half-sine	84
Figure 5.15 6.3mm wall SHS, mid-height displacements v 3mm half-sine	84
Figure 5.16 5mm wall SHS, mid-height displacements v 3mm half-sine	85
Figure 5.17 Load v mid-height displacement (out-of-plane)	86
Figure 5.18 Load v mean end-rotation	87
Figure 5.19 Normalised load v mean end-rotation	88
Figure 5.20 kc3 end rotations	89
Figure 5.21 kc3difference from mean end rotation	89
Figure 5.22 kc4 end rotations	90
Figure 5.23 kc4difference from mean end rotation	90
Figure 5.24 kc5 end rotations	91
Figure 5.25 kc5difference from mean end rotation	91
Figure 5.26 kc6 end rotations	92
Figure 5.27 kc6difference from mean end rotation	92
Figure 5.28 kc7 end rotations	93
Figure 5.29 kc7difference from mean end rotation	93
Figure 5.30 kc8 end rotations	94
Figure 5.31 kc8difference from mean kc8 end rotation	94
Figure 5.32 kc9 end rotations	95
Figure 5.33 kc9difference from mean end rotation	95

Figure 5.34 kc10 end rotations	96
Figure 5.35 kc10 difference from mean end rotation	96
Figure 5.36 kc6 and kc10 end rotations	97
Figure 6.1 End rotations from eccentric load at top of column	103
Figure 6.2 End rotations from eccentric load at bottom of column	104
Figure 6.3 Typical end-rotation v load from tests	106
Figure 6.4 Mean end-rotation v load: test v Abaqus	107
Figure 6.5 Top of the unloading/reloading cycle – kc3, test & Abaqus	108
Figure 6.6 End-rotations at top of unloading path – kc8, test & Abaqus	109
Figure 6.7 End-rotations – kc7, test & Abaqus	110
Figure 6.8 End-rotations – kc8, test & Abaqus	111
Figure 6.9 Asymmetric eccentricity of loading for test kc7	113
Figure 6.10 End-rotations – kc3, test mean & Abaqus	115
Figure 6.11 End-rotations – kc4, test mean & Abaqus	116
Figure 6.12 End-rotations – kc5, test mean & Abaqus	116
Figure 6.13 End-rotations – kc6, test mean & Abaqus	117
Figure 6.14 End-rotations – kc7, test mean & Abaqus	117
Figure 6.15 End-rotations – kc8, test mean & Abaqus	118
Figure 6.16 End-rotations – kc9, test mean & Abaqus	118
Figure 6.17 End-rotations – kc10, test mean & Abaqus	119
Figure 6.18 Initial end-rotations – kc3, test mean & Abaqus	119
Figure 6.19 Initial end-rotations – kc4, test mean & Abaqus	120
Figure 6.20 Initial end-rotations – kc5, test mean & Abaqus	120
Figure 6.21 Initial end-rotations – kc6, test mean & Abaqus	121
Figure 6.22 Initial end-rotations – kc7, test mean & Abaqus	121
Figure 6.23 Initial end-rotations – kc8, test mean & Abaqus	122
Figure 6.24 Initial end-rotations – kc9, test mean & Abaqus	122
Figure 6.25 Initial end-rotations – kc10, test mean & Abaqus	123
Figure 6.26 Correlation factors for rotation	125
Figure 6.27 Effect of out-of-plane displacements – kc9, test & Abaqus	127
Figure 6.28 End-rotations – kc9, test mean & Abaqus	127
Figure 6.29 possible initial imperfections – kc7	129
Figure 6.30 Unloading/reloading cycle – kc7, test	130
Figure 6.31 Initial end-rotations – kc7, test mean & Abaqus	130
Figure 6.32 End-rotations – kc7, test mean & Abaqus	131
Figure 6.33 Initial imperfections – effect of residual stresses kc7	132
Figure 6.34 Effect of local buckling – rotation capacity from tests	133

Figure 6.35 Effect of local buckling – kc5, test & Abaqus	134
Figure 6.36 Effect of local buckling – kc9, test & Abaqus	134
Figure 6.37 Effect of local buckling – kc6, test mean & Abaqus	135
Figure 6.38 Effect of local buckling – kc10, test mean & Abaqus	135
Figure 7.1 Out-of-plane loads on curved walls	139
Figure 7.2 Transverse bending of walls, both sides in compression	140
Figure 7.3 Transverse bending of walls, one side compression, one in tension	140
Figure 7.4 Increased curvature of wall towards the middle of the wall	141
Figure 7.5 Column in double curvature	143
Figure 7.6 140×140 SHS in single curvature in rectangular plane	144
Figure 7.7 140×140 SHS in single curvature at 45° to rectangular plane	145
Figure 7.8 Limiting wall breadth to thickness ratio from Abaqus	145
Figure 7.9 Wall slenderness limitations, test v Abaqus	146
Figure 7.10 Wall slenderness limitations, overall breadth/thickness, B/t	148
Figure 8.1 Load paths for a column resisting axial and bending	152
Figure 8.2 Load paths for a column subject to axial and end-rotation	152
Figure 8.3 Load paths for imposed rotation in the plane of the initial imperfection	153
Figure 8.4 All column lengths, end-rotations about a rectangular axis	156
Figure 8.5 Comparison of imperfections “in plane” with “out of plane”	157
Figure 8.6 Design bending moment in the column including imperfection	158
Figure 8.7 1.5 m columns, e0 required	160
Figure 8.8 3.0 m columns, e0 required	160
Figure 8.9 6.0m columns, e0 required	161
Figure 8.10 Abaqus v CMK 2009 design model, 3.0m height	162
Figure 8.11 Abaqus v CMK 2009 design model, 1.5m height	162
Figure 8.12 Abaqus v CMK 2009 design model, 6.0m height	163
Figure 9.1 Instabilities to be avoided in beams at top and bottom of columns	165
Figure 9.2 Wall slenderness limitations, overall breadth/thickness, B/t	167
Figure 9.3 Design eccentricity including imperfection	168
Figure 9.4 Plastic cross-section to calculate N_0 from M_y only	169
Figure 9.5 Simply supported beams (connections at column face)	172
Figure 9.6 Cantilever and suspended span	173
Figure 9.7 Continuous beams	174
Figure 9.8 Bending moment diagrams used to calculate slopes at columns	175
Figure 9.9 End-rotations assumed where there is no sway	176
Figure 9.10 End-rotations modified by sway	177
Figure 9.11 Columns not deflected to slope of beams	179

Figure 9.12: Column end-rotation equal to beam slope, simply supported beams	180
Figure 9.13 Column end-rotation equal to beam slope, continuous beams	180
Figure 9.14 Typical thin end-plate connection	183
Figure 9.15 Bending moments in end-plate	184
Figure 9.16 Typical beam-column connection for plastic rotations in the beam	186
Figure 9.17 Model assumed in BS 5950-1 tying	191
Figure 9.18 Example beam-column connection	193
Figure 9.19 End-plate yield line patterns	194
Figure 10.1 Structural arrangement	197
Figure 10.2 Slab variable load and bending moment diagram	199
Figure 10.3 Slab variable load for max reaction on main beams	200
Figure 10.4 Two-span slab	200
Figure 10.5 Main beam load and bending moment	201
Figure 10.6 Plastic stress blocks in column	208
Figure A.1 Plastic stress distribution, low axial load	224
Figure A.2 Plastic stress distribution, high axial load	228
Figure C.1 Node numbering of corner nodes of SHS	234
Figure C.2 Imperfections and nodes to apply eccentric load	235
Figure C.3 Node numbering of rigid bodies at ends	236
Figure C.4 Wall 1, node and element numbering	237
Figure C.5 Wall 2, node and element numbering	238
Figure C.6 Wall 3, node and element numbering	239
Figure C.7 Wall 4, node and element numbering	240
Figure C.8 Node numbering at mid-height and inclinometers	241
Figure C.9 Node numbering of SHS – half model	244
Figure C.10 Imperfections and eccentric load application – half model	245
Figure C.11 Node numbering at mid-height and inclinometers – half model	246
Figure D.1 Imperfections; e_0 at zero load and e_N at load N	248
Figure E.1 BMD with equal stresses in the compression and tension flanges	255
Figure E.2 Schematic comparison of (elastic strain) v (elastic strain + plastic flow)	260
Figure F.1 Bending moment in column	271
Figure F.2 Displacements of nodes from curvature at node “i”	276
Figure F.3 Correction of displacements	277
Figure F.4 Member shape at ends	278
Figure F.5 End-shape from curvature in end sections	280
Figure F.6 Residual stress distribution	281

Figure F.7	Average compression stress	282
Figure F.8	“Elastic” bending stresses	283
Figure F.9	Stress diagram for one wall of width $2X$	286
Figure F.10	Possible stress distributions	288
Figure F.11	Correction of axial force resisted	289
Figure F.12	Calculation of bending moment resisted	292
Figure G.1	Mid-height displacements – rotations at 22.5° intervals	294
Figure H.1	e_0 for failure load for rotations in a rectangular plane.	309
Figure H.2	e_0 for failure load for rotations not in a rectangular plane	310
Figure I.1	Deflected shape of test columns	311

LIST OF SYMBOLS

The symbols listed below exclude the symbols from Appendices F, H and J.

A	gross cross-sectional area amplification factor
A_{100}	amplification factor at a distance of 100 mm from the point of maximum curvature
A_{max}	amplification factor at the point of maximum curvature
A_b	area required, if stressed to yield stress, to resist the buckling resistance of a pin-ended strut
A_s	tensile stress area of bolt (EN 1993-1-8)
B	external breadth of SHS
B	breadth of a solid section (eg slice of wall)
b	distance mid-plane to mid-plane of walls of SHS breadth of the external flat face of SHS, between the rounded corners (BS 5950) breadth of section (AISC) breadth of cap-plate or base-plate
C	curvature of member
C_{Em}	maximum member curvature at the cross-section under consideration
C_{100}	maximum curvature of member at a distance of 100 mm from the point of maximum curvature
C_{max}	maximum curvature of the curvature
C_y	curvature when longitudinal strain is at 1.0 yield strain
c	flat portion of compression element for classification of compression elements (EN 1993-1-1)
c_a	half-depth of plastic stress block in “webs” resisting axial force
c_b	half-breadth of plastic stress block in “flanges” resisting bending moment
c_f	correlation factor
D	Depth of section (BS 5950) depth of a solid section (eg a slice of wall) factor relating transverse stress in wall, σ_2 , to the curvature C in the

	equation $\sigma_2 = DC$
d	factor in formula for deflection $\delta = d \frac{pb^4}{EI_{wall}}$
d_s	Depth of wall available to resist bending in plastic cross sectional analysis
E	Young's modulus
e_d	design eccentricity of load application on column from neutral axis
e	actual eccentricity of load application on column from neutral axis
	Eccentricity of column at mid-height from end-to-end line
e_p	edge distance of bolts in cap-plate or base-plate
e_0	initial imperfection along one rectangular axis
e_0	initial imperfection in the plane of buckling, geometrical imperfection increased to give strut resistance reduced by both the geometrical imperfection and the residual stresses
e_b	eccentricity of load at bottom of column
e_i	Additional eccentricity of column at mid-height from end-to-end line to represent the effect of imperfections
e_N	amplified geometrical imperfection in the plane of buckling
e_R	design deflection along one rectangular axis
e_s	imperfection at mid-height of a column that makes the column resistance at zero end-rotation equal to the buckling resistance of a pin-ended strut
e_t	eccentricity of load at top of column
e_θ	$c_f \times$ end-rotation calculated by Abaqus
e_{theta}	
F	factor relating longitudinal strain in wall, ϵ_1 , to the curvature C in the equation $\epsilon_1 = FC$
F_c	Applied axial compression
F_{tRd}	bolt tensile resistance (EN 1993-1-8)
F_y	yield stress (AISC)
f_{max}	maximum compressive residual stress
f_r	maximum compressive residual stress
f_u	minimum specified ultimate tensile strength (EN 1993-1-1)
f_{ub}	minimum specified ultimate tensile strength of bolt (EN 1993-1-8)
f_{wvd}	design strength of fillet weld (EN 1993-1-8)
f_y	minimum specified yield stress (EN 1993-1-1)

f_{yd}	factored yield stress which is the minimum specified yield stress reduced by the appropriate material factor for cross-sectional resistance in the specified design code. For example, using EN 1993-1-1, $f_{yd} = f_y/\gamma_{M0}$, BS 5950-1, $f_{yd} = p_y$, AISC, $f_{yd} = \phi F_y$,
h	Height of column
I	Second moment of area of member second moment of area/unit width of wall of SHS
i	radius of gyration (EN 1993-1-1)
k	axial stress ratio
k_2	bolt resistance factor (EN 1993-1-8)
L	Member length
L_a	distance from face of column to bolts in cap-plate or base-plate
L_{cr}	buckling length (EN 1993-1-1)
L_E	Nominal effective length of member (BS 5950)
l_{eff}	Half-wave effective length
M	Applied moment
M_b	moment at bottom of column
M_{bs}	Moment of resistance, major axis, for simple construction (BS 5950)
M	Applied moment
M_{cx}	Cross-sectional moment resistance about the major axis (BS 5950)
M_{Ed}	Moment in member (EN 1993-1-1)
M_{ext}	Externally applied moment on column, for example from wind load
M_{LT}	Moment about major axis causing lateral torsional buckling (BS 5950)
$M_{pl,Rd}$	plastic moment of resistance of cross-section subject to bending alone (EN 1993-1-1)
M_{pr}	plastic moment of resistance of section reduced by axial force
M_s	Reduced plastic moment of resistance of cross-section when resisting axial compression equal to the flexural buckling resistance of a pin-ended strut
M_t	moment at top of column
M_x	Applied moment, major axis (BS 5950)

M_y	Applied moment, minor axis (BS 5950)
m	Moment gradient factor (BS 5950)
m_{LT}	Moment gradient factor applied to major axis moments for lateral torsional buckling (BS 5950)
m_x	Moment gradient factor applied to major axis moments for flexural buckling (BS 5950)
N	Axial force
N_b	buckling resistance of a pin-ended strut using the specified design code
$N_{b,Rd}$	buckling resistance of a pin-ended strut (EN 1993-1-1)
N_{cr}	Elastic critical buckling load, Euler load
N_{Ed}	Axial force in member (EN 1993-1-1)
N_{pl}	squash load of section
N_u	Load at point of unloading measured in the laboratory tests
N_{θ}	resistance from new design model with imposed end-rotation θ
$N_{\theta,Rd}$	resistance from new design model with imposed end-rotation θ (EN 1993-1-1)
n	number of yield strains
P	axial compression resisted tension in bolts in cap-plate or base-plate
P_c	Axial compression resistance (BS 5950)
P_{cx}	Axial compression resistance, buckling about major axis (BS 5950)
P_{RC}	radial pressure on wall of SHS due to curvature and longitudinal compressive stress
P_{RCi}	inward radial pressure on wall of SHS due to curvature and longitudinal compressive stress
P_{RCo}	outward radial pressure on wall of SHS due to curvature and longitudinal compressive stress
P_{rT}	radial pressure on wall of SHS due to curvature and longitudinal tensile stress
p	radial pressure on wall of SHS due to curvature
P_{RC}	radial pressure on wall of SHS due to curvature
$P_{RC,100}$	radial pressure on wall of SHS due to curvature at distance of 100 mm from the point of maximum curvature
$P_{RC,max}$	radial pressure on wall of SHS due to curvature at distance the point of maximum curvature

p_y	yield stress (BS 5950)
Q	prying force on the column base-plate or cap-plate from tension in the bolts connecting the column to the beams
R	radius of curvature of loaded SHS
r	radius of gyration (BS 5400-3)
S_x	plastic modulus, major axis (BS 5950)
S_y	plastic modulus, minor axis (BS 5950)
t	wall thickness thickness of cap-plate or base-plate
V	Vertical shear in beam (BS 5950)
V	Vertical shear on the column base-plate or cap-plate from tension in the bolts connecting the column to the beams
V_H	Horizontal shear (sway shear) across column
W	total uniformly distributed load on member
W_e	elastic modulus in the plane of buckling
W_{pl}	plastic modulus of section (EN 1993-1-1)
w	uniformly distributed load (force/unit length)
y	distance from elastic neutral axis to the extreme fibre of the cross-section in the plane of buckling
y_m	displacement of member from end-to-end straight line
Z	elastic modulus (BS 5950)
Z_y	Elastic modulus, minor axis (BS 5950)
α	non-dimensional imperfection factor (EN 1993-1-1)
β	Ratio of end moments on member (BS 5950)
β_w	strength factor for fillet welds (EN 1993-1-8)
γ_{M0}	Partial safety factor for cross-sectional resistance (EN 1993-1-1)
γ_{M1}	Partial safety factor for buckling resistance (EN 1993-1-1)
γ_{M2}	Partial safety factor for net area tension resistance (EN 1993-1-1) Partial safety factor for bolt and weld resistance (EN 1993-1-8)
δ	deflection, displacement of wall at mid-width of wall
δ_{100}	displacement at mid-width of wall at 100 mm along the axis of the column from point of maximum curvature
δ_{max}	displacement at mid-width of wall at point along the axis of the column where the curvature of the column is a maximum

δ_t	total displacement at mid-width of wall, including effects of plasticity
$\delta_{t,100}$	total displacement at mid-width of wall, including effects of plasticity, at 100 mm along the axis of the column from point of maximum curvature
$\delta_{t,max}$	total displacement at mid-width of wall, including effects of plasticity, at point along the axis of the column where the curvature of the column is a maximum
$\delta\epsilon_1, \delta\epsilon_2, \delta\epsilon_3$	plastic flow vector (Calladine)
$\delta\epsilon_{2b}$	plastic flow vector for plastic strain increasing the curvature of the wall
ϵ	yield stress factor $= \sqrt{\frac{275}{p_y}}$ in BS 5950 $= \sqrt{\frac{235}{f_y}}$ in EN 1993-1-1
ϵ_{2b}	plastic strain that increases the curvature of the walls
ϵ_{2be}	elastic bending strain that increases the curvature of the walls
ϵ_y	yield strain
η	non-dimensional imperfection factor (BS 5400)
θ	End-rotation of column and/or slope of beam
θ_b	End-rotation at bottom of column
θ_{CA}	Mean value of end-rotation calculated by Abaqus at the load N_u equal to the load in the laboratory tests at the point of unloading
θ_{Ct}	Mean value of end-rotation measured in the laboratory tests at the point of unloading
θ_t	End-rotation at top of column
λ	slenderness of member $= \frac{L_{cr}}{i}$ in EN 1993-1-1 and $= \frac{L}{r}$ in BS 5400
λ_1	normalizing factor for slenderness $= \pi \sqrt{\frac{E}{f_y}}$ (EN 1993-1-1)

$\bar{\lambda}$	normalized slenderness = $\frac{\lambda}{\lambda_1} = \sqrt{\frac{\sigma_y}{\sigma_{cr}}}$
σ_0	yield stress (Calladine)
$\sigma_1, \sigma_2, \sigma_3$	stresses along orthogonal axes 1, 2 and 3 (Calladine)
$\sigma'_1, \sigma'_2, \sigma'_3$	deviatoric stress vector (Calladine)
σ_C	Longitudinal compressive stress in wall
σ_{max}	Maximum elastic stress in column
σ_a	Mean axial stress
σ_b	Elastic bending stress at extreme fibre
σ_{cr}	elastic critical buckling (Euler) stress
σ_y	yield stress
τ	shear stress
ϕ	sway angle of frame (EN 1993-1-1) factor in buckling resistance calculation $= 0.5 \left[1 + \alpha(\bar{\lambda} - 0.2) + \bar{\lambda}^2 \right]$ (EN 1993-1-1)
ϕ_R	Joint rotation (Gent & Milner)
χ	reduction factor for buckling resistance

1 BACKGROUND

1.1 Introduction

A new form of braced frame has appeared in Britain for residential construction and has already been used for frames up to 14 storeys high. In these frames, the columns are discontinuous. Each column segment is only one storey high and is fitted with end plates to bolt to the beams below and above. Columns are square hollow sections with the smallest possible size so they can be hidden in the thickness of the walls. The beams are continuous, passing uninterrupted through the column lines, giving the efficiency of continuous beams with minimum fabrication cost. Due to continuity of the beams across the line of the columns, some rotation at the top and bottom of the column is likely to be induced under certain loading arrangements resulting in curvature of the column. This may reduce the resistance of the column below that of an equivalent pin-ended strut. Traditional steel frame construction does not use discontinuous columns.

This thesis describes the development of a method for calculating the strength of columns in “braced” frames with discontinuous columns. This new method can give more economical column sizes than other methods and is easy to apply by designers by use of a simple column resistance model.

1.2 Braced frames

Braced frames are the most common type of frames used in UK beam and column steel frames. A typical braced frame is shown in Figure 1.1. The distinguishing feature of a braced frame is that the structure has a discrete system of parts that stabilise the structure against failure in a sway mode. The bracing in a “braced frame” need not be diagonal bracing as shown in Figure 1.1, but can be provided by any other stiff structure. Common alternatives are concrete shear walls, concrete cores and stiff portal frames.

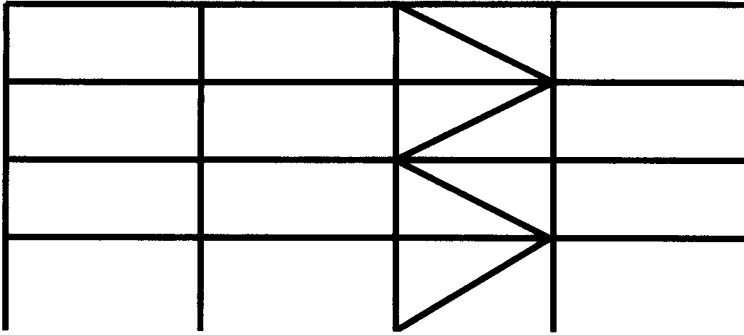


Figure 1.1 Typical braced frame

1.3 Beam and column arrangements in traditional braced frames

In traditional braced frames, the columns are continuous and the beams are connected between the columns. This is shown in Figure 1.2. In the UK, the connections between the beams and the columns are almost always intended to transfer vertical shear only from the beam to the column. This is because these connections are cheaper to fabricate than connections that also transmit bending moment and the cost of the connections is a significant proportion of the cost of a steel frame. In 1993 the cost of forming the connections was quoted as 30% of the cost of a typical steel frame even when the cost of handling is excluded [Fewster et al 1993], and although the cost of steel might have increased even more than labour costs for skilled labour, it is clear that the connections contribute a major part of the cost of steel frames.

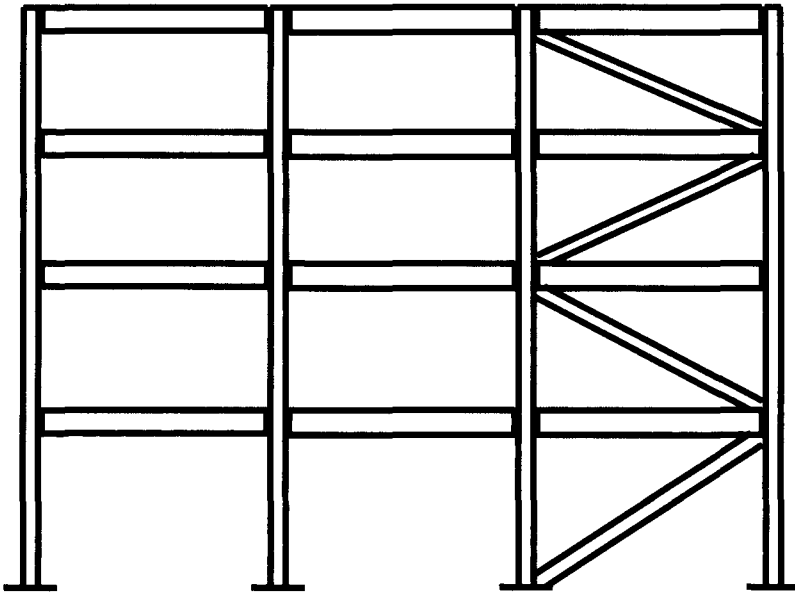


Figure 1.2 Columns and beams in a traditional frame

1.4 Braced frames with discontinuous columns

A typical frame using discontinuous columns is shown in Figure 1.3. Much larger frames have been constructed, up to 14 storeys high. Each column piece is only one storey high. To provide a shallow construction depth, the floor is supported on the bottom flange of asymmetric beams with a wider bottom flange. The floor may be composite construction using deep profile decking or may be pre-cast concrete. . Being built-in between the beams, the floor stabilises the beams, avoiding the potential local instability of the beams caused by the discontinuity of the columns, as shown in Figure 9.1.

Potential advantages of this type of construction are:

1. Shallow floor construction.
2. Beam continuity achieved with inexpensive connections.
3. Slender columns that can either be hidden in walls or are of low visual impact if not hidden.
4. Safe and easy crane hook access when lifting in pre-cast concrete floor units or metal decking because the columns do not extend above the floor beams until the next storey is erected.

Potential disadvantages are:

1. Storey height column lengths give more individual column pieces to lift, so more crane time for column erection.
2. Continuous beams give greater piece weights for the beams, so the crane requirements might be increased.
3. Column piece labelling must be carefully controlled if sections with different wall thicknesses but of the same column size are used.

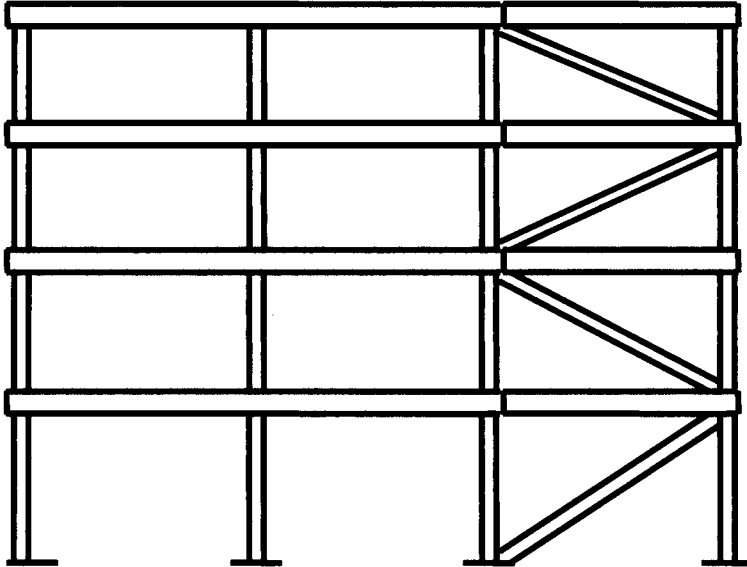


Figure 1.3 Columns and beams in a typical frame with discontinuous columns

Typical column to beam connections are shown in Figure 1.4. The column end plates are welded to the columns and bolted to the beams. Figure 1.4 does not show the web stiffeners that are used to prevent web buckling and web sway buckling. Where there are no secondary beams orthogonal to the main floor beams at the columns, steel strut/ties are provided for lateral restraint to the columns. These strut/ties are placed within the depth of the floor beam and connect the columns on one line of beams to the corresponding column on the adjacent line of beams as shown in AD 281 [SCI 2005a] and AD 283 [SCI 2005b].

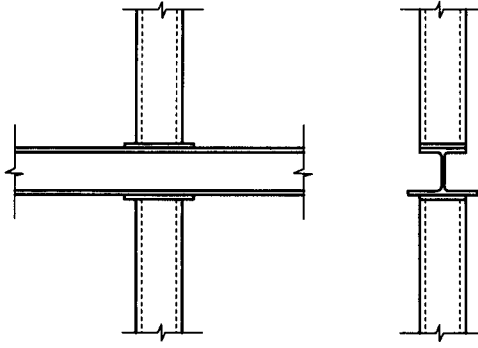


Figure 1.4 Typical column-beam connection

(floor and stiffeners to the beam web omitted for clarity)

2 REVIEW OF DESIGN METHODS

2.1 Introduction

The design methods available in the literature are reviewed in this Chapter. These methods include the current UK method for designing traditional braced frames and methods available for the design of braced frames with discontinuous columns.

Design methods comprise the complete process of selecting a form of construction, calculating the relevant forces and moments, choosing appropriate members and performing the necessary calculations to verify the design. A design method is not simply the verification of the resistance of a member. Therefore, the design methods reviewed below are from BS 5950-1 because it and its predecessor BS 449 provide advice on how to apply resistance checks to different forms of construction such as cap-plates and columns in “simple construction”. The Eurocodes do not provide this type of advice and the advice currently available for use of the Eurocodes in these forms of construction is based on the experience gained from earlier codes such as BS 5950-1 and BS 449.

There are two issues of special importance in frames with discontinuous columns.

The first issue is the stiffness of the column-beam joint. At the top of the building, the axial compression in the columns is small. If relatively thin column end-plates are used, the connections are flexible. In these cases, illustrated in Figure 2.1, the beam can rotate relative to the columns. This results in higher sagging moments in the beams than calculated in a rigid frame analysis. Either the analysis needs to include the joint flexibility or thicker end-plates must be used to reduce the flexibility of the connections. At the bottom of the building, the axial compression is high and this compression clamps the columns and beams so that very little rotation of the beam relative to the column is possible. Therefore, to use elastic analysis of the continuous frame, the designer must either determine the stiffness of the joints (which means including the effect of axial compression) or specify end-plates so thick that the joint is sensibly rigid even for low axial compression.

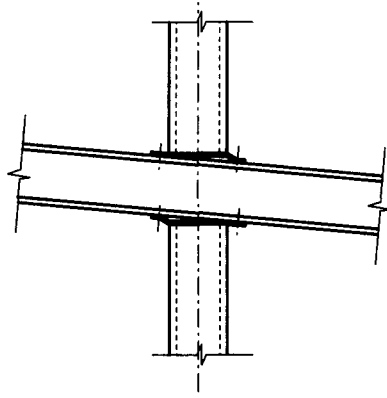


Figure 2.1 Beam-column connection with thin end-plates and low axial compression

The second issue is the effect of bending moments in the columns on the compression resistance. In a rigidly jointed frame, the bending moments in the columns calculated by elastic analysis can be so high that they cause a significant reduction in the resistance to axial compression. To compensate for this, larger column areas are required. Where the larger area is achieved by larger cross-sectional dimensions, the bending stiffness of the column is greater, attracting even more bending moment from the frame. This may lead to heavy columns, in contrast with the common preference of occupiers to have small column cross-sections, either to allow the columns to be hidden in the walls or to limit the visual impact of the columns when exposed.

2.2 Design of traditional braced frames

The design process for traditional braced frames, commonly known as “simple construction”, is given in BS 449 [BSI 1969] and BS 5950-1 [BSI 2000a]. The process is described for application to the Eurocodes in the Access-steel document SN005a-EN-EU [Access-steel SN005a 2005]. The process is as follows:

1. The beams are designed as simply supported beams spanning between the columns.
2. The effects of pattern loading are ignored and the columns are designed assuming that all the beams are fully loaded.
3. The columns are designed for the axial compression, from the sum of the shears from the beams plus the column weight, and a bending moment. In UK practice, this bending moment is calculated on the assumption that the beam shear, V , is applied to the column at an eccentricity of 100mm from the face of the column to which the beam is connected. A typical case for a column with beams connected to one side is shown in

Figure 2.2. A typical case for a column with beams connected to both sides is shown in Figure 2.3.

- Any relationship between the beam end rotations and the column rotations is ignored because the beams are assumed to be pin ended.

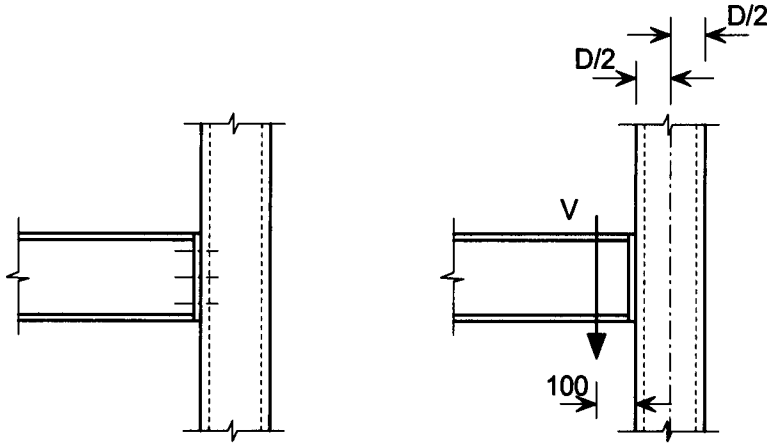


Figure 2.2 Typical column with a beam connected on one side

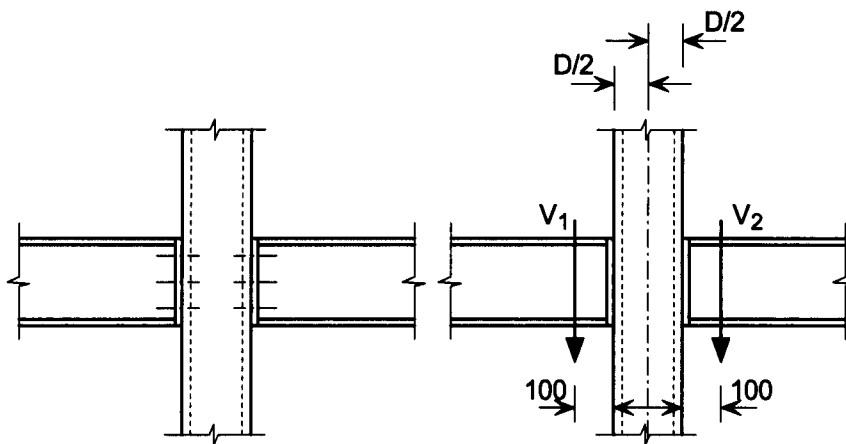


Figure 2.3 Typical column with beams connected on both sides

It can be seen from Figure 2.2 that a column with a beam connected on one side is designed to resist, in addition to the axial compression, a bending moment applied to the column of $V(100 + D/2)$ caused by the beam shear V . It can be seen in Figure 2.3 that a column with beams connected on both sides is designed to resist, in addition to the axial compression, the nett moment $(V_1 - V_2)(100 + D/2)$ caused by the beam shears V_1 and V_2 . Where the beam shears V_1 and V_2 are equal, the design moment is zero. The design method in BS 5950-1 [BSI 2000a] is made as simple as possible by designing only for the case of maximum load on all of the beams, so avoiding extra load cases from pattern loading.

To investigate the efficiency or inefficiency of this method of design and to allow a comparison with the design of discontinuous columns, a calculation for a typical external column is made below.

Assuming typical residential construction with columns on a 6.0 m × 7.5 m grid and a total factored floor load of 10 kN/m², the beam reaction is

$$V = 0.5(10 \times 6.0 \times 7.5) = 225 \text{ kN} \quad \text{Eq 2.1}$$

Assuming a 140 × 140 Square Hollow Section (SHS), the total nominal applied moment on an external column is given by:

$$M_x = 225(0.100 + 0.140/2) = 225 \times 0.170 = 38.25 \text{ kN-m} \quad \text{Eq 2.2}$$

This total moment is resisted in part by the column segment above the beam and the column segment below the beam. Assuming equal storey heights above and below, the moment on each segment of column is 38.25/2 = 19.1 kN-m.

The interaction equation in Clause 4.7.7 of BS 5950-1 [BSI 2000a] for use with traditional simple construction is:

$$\frac{F_c}{P_c} + \frac{M_x}{M_{bs}} + \frac{M_y}{p_y Z_y} \leq 1 \quad \text{Eq 2.3}$$

M_{bs} is the buckling resistance moment for simple columns which in the case of a square hollow section is equal to the plastic moment of resistance because square hollow sections are not prone to lateral torsional buckling. Therefore

$$M_{bs} = p_y \times S_x = 355 \times 246 \times 10^{-3} = 87.3 \text{ kN-m} \quad \text{Eq 2.4}$$

In the absence of minor axis bending, M_y , the equation can be re-written as follows:

$$\frac{F_c}{P_c} + \frac{M_x}{M_{bs}} \leq 1 \quad \text{Eq 2.5}$$

and re-written again as

$$F_c \leq P_c \left(1 - \frac{M_x}{M_{bs}} \right) \quad \text{Eq 2.6}$$

Assuming the column height is 3.0 metres, the column resistance P_c according to the SCI Blue Book [SCI 2001] for a 140 × 140 × 10 SHS in S355 steel is 1550 kN:

$$F_c \leq P_c \left(1 - \frac{M_x}{M_{bs}} \right) = 1550 \left(1 - \frac{19.1}{87.3} \right)$$

$$= 1550(1 - 0.219) = 1550 \times 0.781 = 1211 \text{ kN} \quad \text{Eq 2.7}$$

This is a reduction to 78% of the strut buckling capacity. It should be noted that this is the value for an external column. An internal column with equal span beams on opposite sides of the column and equal loads on the beams may be designed on the assumption that there is no moment applied to the column according to BS 5950-1.

The above summarizes column design for buildings using continuous columns and traditional UK “simple construction”.

2.3 Orthodox design of braced frames with discontinuous columns

2.3.1 Currently available design methods

The “simple construction” design method described in Section 2.2 is not appropriate for frames with discontinuous columns because of the structural form. In these frames, the beams are not even approximately pin-jointed at the face of each column. Therefore the method described in Section 2.2 is not applicable.

The design methods that are currently in use in design offices for multi-storey braced frames and that could be used for braced frames with discontinuous columns are:

1. Simple buildings using the method for a beam supported on a cap plate
2. Rigid jointed frame using elastic analysis
3. Flexibly jointed frame using elastic analysis
4. Rigid jointed frame with plastic analysis using member checks from current design codes

These methods are discussed below. The discussion is illustrated by calculations using $140 \times 140 \times 10$ SHS sections in all cases. One section size is used throughout to simplify comparison of results for different methods of calculation. The method of calculation is not affected by the size of section used.

2.3.2 Beam on a cap-plate – simple approach

The simplest design approach is to design the structure using the traditional methods for a beam on a cap plate, as shown in Figure 2.4. This design method is given in both BS 449 [BSI 1969] and BS 5950-1 [BSI 2000a]. BS 5950-1 Clause 4.7.7 says:

“The nominal moments applied to the columns by simple beams or other simply supported members should be calculated from the eccentricity of their reactions, taken as follows:

For a beam supported on the cap plate, the reaction should be taken as acting at the face of the column, or edge of packing if used, towards the span of the beam.”

This is shown in Figure 2.4 in which the column cap plate projecting beyond the face of the 140 × 140 × 10 SHS column is assumed to be too thin to support the reaction of the beam.

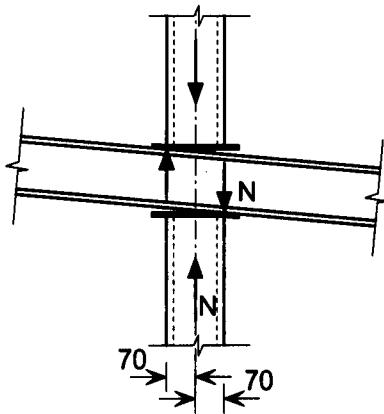


Figure 2.4 Beam on a thin cap plate on a 140 × 140 × 10 SHS

The effect of the cap plate design method on the calculated column resistance is evaluated below for the typical case of a 140 × 140 × 10 SHS with a storey height of 3.0 metres.

The column is checked by using the equation in BS 5950-1:2000 Clause 4.7.7 because that is the clause where the cap plate design guidance is found. This equation is:

$$\frac{F_c}{P_c} + \frac{M_x}{M_{bs}} + \frac{M_y}{p_y Z_y} \leq 1 \quad \text{Eq 2.8}$$

From Figure 2.4, M_x is equal to the axial load in the column multiplied by the eccentricity which is half the column width.

M_{bs} is the buckling resistance moment for a simple column and is equal to the plastic moment of resistance for a square hollow section.

In the absence of minor axis bending, M_y , the equation can be re-written as follows:

$$\frac{F_c}{P_c} + \frac{M_x}{M_{bs}} = \frac{F_c}{P_c} + \frac{F_c e}{M_{bs}} = F_c \left(\frac{1}{P_c} + \frac{e}{M_{bs}} \right) \leq 1 \quad \text{Eq 2.9}$$

$$\therefore F_c \leq \frac{1}{\left(\frac{1}{P_c} + \frac{e}{M_{bs}}\right)} \quad \text{Eq 2.10}$$

Substituting the values for this example:

$$F_c \leq \frac{1}{\left(\frac{1}{1550} + \frac{0.070}{87.3}\right)} = \frac{1}{0.645 \times 10^{-3} + 0.802 \times 10^{-3}}$$

$$= \frac{1}{1.447 \times 10^{-3}} = 691 \text{ kN} \quad \text{Eq 2.11}$$

This is a reduction to $691/1550 = 45\%$ of the strut buckling capacity.

The above applied the cap-plate design method to an internal column without unbalanced loading on the beams. If this method were applied, all columns would be very expensive.

2.3.3 Beam on a cap-plate – more exact approach

To try to find a more economical value of calculated resistance, a designer could use the more detailed checks in BS 5950-1:2000 Clause 4.8.3, as shown below. This requires checks on two different types of resistance:

1. Cross-sectional resistance.
2. Buckling resistance.

The buckling resistance checks are made below for cases of both single curvature and double curvature to show the effect of moment gradient.

The calculations are made using the equations for a square cornered section equivalent to a $140 \times 140 \times 10$ SHS developed in Appendix A, which gives the reduced section properties and resistances for square hollow sections with classic rectangular plastic stress blocks. The equivalent section has a perfectly square centreline, avoiding the complexities of rounded corners with varying thickness, with the dimensions and thickness calculated to give the same area and second moment of area as the real section. For this reason, the overall dimension taken in this worked example is 129.4 mm, which is the distance between the centre-lines of the walls of the equivalent section instead of the $140 - 10 = 130$ mm that might be expected for a $140 \times 140 \times 10$ SHS.

Firstly, find the compression resistance from the **cross-sectional resistance** checks:

$$\text{Squash load for a } 140 \times 140 \times 10 \text{ SHS} = 355 \times 5090 \times 10^{-3} = 1807 \text{ kN} \quad \text{Eq 2.12}$$

Assuming that the beam bears in line with the external face of the column, the eccentricity of load $e = 70 \text{ mm}$

Try case for axial compression $< 0.5 \times$ squash load and using the formula in Appendix A.2.2,

$$\begin{aligned} \therefore c_a &= e \left(\pm \sqrt{1 + \frac{3}{4} \left(\frac{b}{e} \right)^2} - 1 \right) \\ &= 70 \left(\pm \sqrt{1 + \frac{3}{4} \left(\frac{129.4}{70} \right)^2} - 1 \right) = 70 \times 0.888 = 62.1 \text{ mm} \end{aligned} \quad \text{Eq 2.13}$$

(The calculated half-depth c_a of the compression stress-block is less than $129.4/2 = 64.7 \text{ mm}$, confirming that the axial compression is less than half the squash load.)

The axial compression resisted $= P = 4t c_p y = 4 \times 9.83 \times 62.1 \times 355 = 867 \text{ kN}$. Taking the strut buckling capacity $= 1550 \text{ kN}$ from the “Blue Book” [SCI 2001], this is a reduction to $867/1550 = 56\%$ of the strut buckling capacity.

The moment resisted with the assumptions made above is:

$$P e = 867 \times 0.070 = 60.7 \text{ kN-m} \quad \text{Eq 2.14}$$

To investigate if this end moment might occur, the end-rotation necessary to induce this moment is calculated by traditional elastic analysis:

Assuming the pattern of loading shown in Figure 2.5, the end rotation of the column from the end moments of 60.7 kN-m would be:

$$\theta = \frac{ML}{6EI} = \frac{60.7 \times 10^6 \times 3000}{6 \times 205000 \times 14.2 \times 10^6} = 0.0104 \quad \text{Eq 2.15}$$

This end slope is smaller than the end rotation of many beams, so it is probable that the moment and axial load combination calculated above would occur in external columns in many frames. The rotation at the internal support of continuous beams might be less than this, in which case the moment would not be so large and the coincident axial resistance would be higher than the 867 kN calculated above. However, sway deformations of the structure from notional horizontal forces or wind loads will induce some end rotation.

Secondly, find the compression resistance from the **buckling resistance checks** assuming **double curvature** as shown in Figure 2.5.

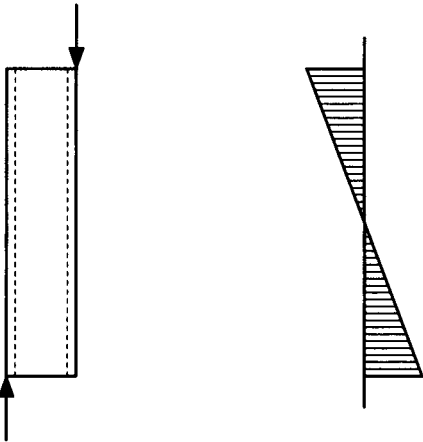


Figure 2.5 Column loading and bending moment diagram for double curvature

The check is made to BS 5950-1:2000 [BSI 2000a] Clause 4.8.3.3.3(a). Only the first of the three checks in 4.8.3.3.3(a) is needed, the check for major axis in-plane buckling, because the section is an SHS. The equation in 4.8.3.3.3(a) is:

$$\frac{F_c}{P_{cx}} + \frac{m_x M_x}{M_{cx}} \left(1 + 0.5 \frac{F_c}{P_{cx}} \right) \leq 1 \quad \text{Eq 2.16}$$

$P_{cx} = 1550 \text{ kN}$ from the Blue Book [SCI 2001]

$M_x = 60.7 \text{ kN-m}$ calculated above

$m = 0.4$ for double curvature from BS 5950-1:2000 Table 26

$$\therefore \frac{m_x M_x}{M_{cx}} = \frac{0.4 \times 60.7}{87.3} = 0.278 \quad \text{Eq 2.17}$$

$$\therefore F_c \leq \frac{\left(1 - \frac{m_x M_x}{M_{cx}} \right)}{\left(1 + 0.5 \frac{m_x M_x}{M_{cx}} \right)} P_{cx} = \frac{1 - 0.278}{1 + 0.5 \times 0.278} 1550 \text{ kN} \quad \text{Eq 2.18}$$

$$\therefore F_c \leq \frac{0.722}{1.139} 1550 = 0.634 \times 1550 = 983 \text{ kN} \quad \text{Eq 2.19}$$

Therefore, in cases of double curvature, the column resistance is reduced to 63% of the strut buckling capacity.

Thirdly, find the compression resistance from the **buckling resistance checks** assuming **single curvature** as shown in Figure 2.6

$P_{cx} = 1550 \text{ kN}$ from the Blue Book [SCI 2001]

$M_x = 60.7 \text{ kN-m}$ calculated above

$m = 1.0$ for single curvature

$$\therefore \frac{m_x M_x}{M_{cx}} = \frac{1.0 \times 60.7}{87.3} = 0.695 \quad \text{Eq 2.20}$$

$$\begin{aligned} \therefore F_c &\leq \frac{\left(1 - \frac{m_x M_x}{M_{cx}}\right)}{\left(1 + 0.5 \frac{m_x M_x}{M_{cx}}\right)} P_{cx} = \frac{1 - 0.695}{1 + 0.5 \times 0.695} 1550 \\ &= \frac{0.305}{1.348} 1550 = 0.226 \times 1550 = 350 \text{ kN} \quad \text{Eq 2.21} \end{aligned}$$

Therefore, in cases of single curvature, the column resistance is reduced to 23% of the strut buckling capacity.

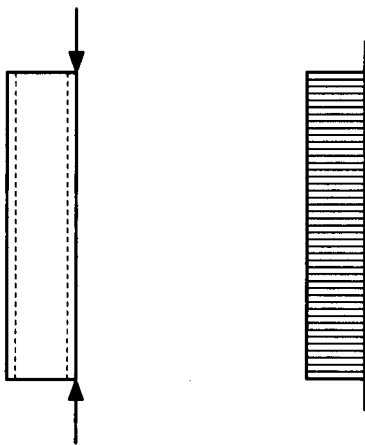


Figure 2.6 Column loading and bending moment diagram for single curvature

The above calculations show that the cap plate method will give low values of calculated column capacities, with only 56% of strut buckling capacity from the cross-sectional resistance check and a possible reduction to 23% for single curvature in the column from the buckling resistance check.

The above calculations have ignored the practical issue of cap-plate stiffness. The England and Wales Building Regulations [ODPM 2004] require vertical tying in all structures of Class 2B and Class 3, as explained in Section 9.6, so the column end plates and bolts must be designed to resist significant tension forces. Being designed to resist these forces, the column end plates will be sufficiently thick to have significant stiffness, so the bending moments in the columns will be increased. The increase could arise from the stiff end plate moving the point of application of the load out beyond the face of the column. It could also arise from the bolts on the “tension” face of the column-beam connection carrying a tensile force, so that the connection is a rigid connection even where the axial compression is low. The deflected form of a typical plate is shown in Figure 2.7. The effect of end plate thickness would have to be included in the calculations.

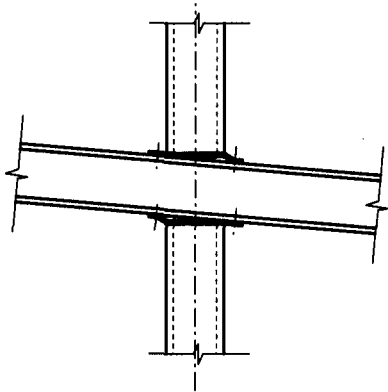


Figure 2.7 Typical end plate deformations

2.3.4 Rigid jointed frame using elastic analysis

It is possible to design the frame as a rigid jointed frame. Elastic analysis predicts large bending moments in the columns. These are caused by the end rotation of the columns enforced by the rotation of the beams at the beam-column connections. Using current steel design codes, large bending moments reduce the axial compression resistance of the columns, making it undesirable to have rigid joints. In fact, the bending moments will be less than those calculated by the commercial software commonly used in design offices. This is because commercial software assumes elastic behaviour of the members but, in reality, the members will yield in some zones. This yielding reduces the bending moments in the columns in braced frames because it reduces the stiffness of the members. (This is not the same for the sway moments in un-braced frames because the sway moments are resisting applied horizontal loads.)

It is seen in the calculations for the cap plate method in Section 2.3.3 above that for double curvature bending in the columns, which means the beams above and below the column deflect in the same way, the column capacity is reduced to 56% of the strut buckling capacity for beam rotations as little as 0.0104 radians (0.6 degrees). This shows that rigid frame design with elastic analysis will often give big reductions in calculated column capacity.

Designs with large bending moments in the columns are also undesirable because transmitting large bending moments between the columns and the beams is expensive. This is because they are transmitted by local bending of the beam flanges. These may need extensive stiffening, depending on their thickness and the geometry of the end-plates on the columns.

2.3.5 Flexibly jointed frame using elastic analysis

To reduce the bending moments in the columns calculated by elastic analysis methods, the end-rotations of the column must be reduced. This is possible if the analysis can account for the flexibility of the beam-column connections explicitly.

The moment transmitted through a simple end plate of a column is not simply a function of the stiffness of the column and the stiffness of the end plate. The purpose of flexible end plates is to avoid transmitting the full rotation of the beam to the column. However, the difference between the rotation of the beam and the rotation of the column opens a gap between the members as shown in Figure 2.8. This makes the connection similar to the cap plate connection shown in Figure 2.4, but with some additional moment caused by the bending of the end plate from the bolts through the plate.

Therefore, the bending moment transmitted is a function of both the axial load and the width of the column, and the stiffness of the end plate, making analysis with flexible end-plates complicated. The moment from the load at the face of the column is largely unaffected by the magnitude of any difference of rotation of the beam and the column, but it is directly affected by the direction of the rotation. The moment from the end plate stiffness is directly affected by the difference of rotation of the beam and the column. At small beam rotations or large column axial forces, the axial force in the column will be sufficient to press the column and the beam together, so the joint will act as a rigid joint. It requires relatively sophisticated software to model this because it needs capabilities like “gap” elements. Without “gap” elements, the designer would need to calculate the stiffness after making a preliminary calculation of the axial forces and the beam rotations and then re-analyse the

structure. Even then, it is possible that the stiffnesses and bending moments would be found to be only approximately consistent. Such approximations are not rare in elastic global analysis in which section sizes are modified as a result of the analysis, but they sometimes add to the burden of the designer to demonstrate to the checking engineer that the analysis and design are adequate.

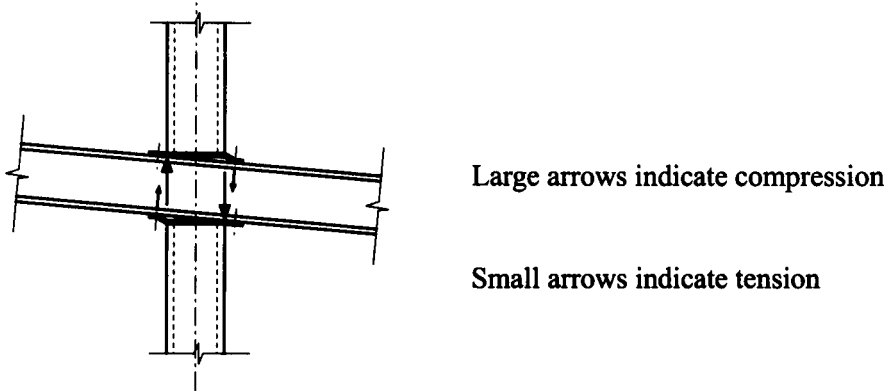


Figure 2.8 Force distribution at a flexible column end plate

2.3.6 Rigid jointed frame using plastic analysis

Braced frames may be designed as rigidly jointed frames using plastic analysis together with member checks from design codes. BS 5950-1:2000 [BSI 2000a] Clause 5.7.2 *Independently braced frames* is applicable to the design of such frames because they fulfil the bracing requirements. The ASCE manual *Plastic Design in Steel* [ASCE 1971] includes the plastic design of rigidly jointed braced frames and EN 1993-1-1 includes provisions for plastic design.

Where either the slope of the beams is large or the columns are stocky, the moment in the columns will reach the plastic moment of resistance. Where the axial compression is low, the load path on the tension side of the beam-column connections would need to be strong to transmit this moment to the column. However, where the axial compression is large, the columns will yield extensively so that the ends will rotate until they bear against the beam across the whole of the column cross-section. This will occur because the column load will act at the face of the column if there is a difference in the end rotation of the column and the rotation of the beam, as shown in Figure 2.4. This induces a bending moment that will cause the end of the column to rotate.

Plastic design is a very attractive design philosophy for this type of frame because it does not regard the formation of a plastic hinge as “failure” of the frame. The potential advantage of

this in the design of a braced frame is that as the axial compression increases, the plastic moment of resistance is reduced. Potentially, this allows the column to be efficient at resisting axial compression by not being required to resist high coincident moments.

The potential improvement in calculated column capacity using plastic analysis is shown below for the case of a $140 \times 140 \times 10$ SHS. In this example the plastic section properties are calculated not using the centre-line assumption of Annex A. This alternative method is used so that this method is demonstrated.

Firstly, the reduced plastic moment is calculated.

The axial compression is 1095 kN, which is less than the squash load of 1807 kN. The area not used to resist axial compression has a squash load of $1807 - 1095 = 712$ kN. In classic theory of plastic cross-sections, this is represented by a strip, with depth d_s , either side of the section, as shown in Figure 2.9 for bending about the yy axis. Therefore the depth of each strip either side of the area resisting compression is:

$$d_s = \frac{1}{2} \left(\frac{712 \times 10^3}{355 \times 140} \right) = 7.16 \text{ mm} \quad \text{Eq 2.22}$$

and the plastic moment of resistance reduced by coexistent axial compression is:

$$\frac{712}{2} (0.140 - 0.00716) = 356 \times 0.13284 = 47.29 \text{ kN-m} \quad \text{Eq 2.23}$$

(Alternatively, the stress blocks in Figure A.2 might be used.)

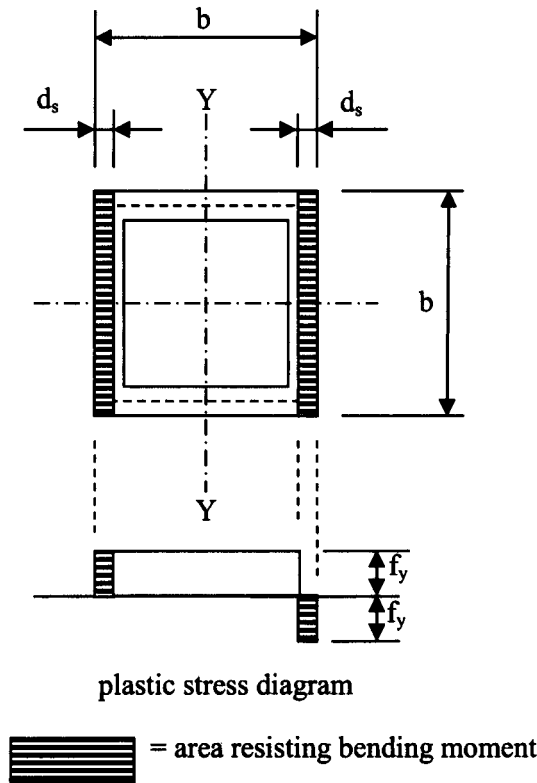


Figure 2.9 Plastic cross-section showing strips resisting bending moment

Secondly the buckling resistance is checked.

The check is made to BS 5950-1:2000 [BSI 2000a] Clause 4.8.3.3.3(a). Only the first of the three checks in 4.8.3.3.3(a) is needed, the check for major axis in-plane buckling, because the section is an SHS. The equation in 4.8.3.3.3(a) is

$$\frac{F_c}{P_{cx}} + \frac{m_x M_x}{M_{cx}} \left(1 + 0.5 \frac{F_c}{P_{cx}} \right) \leq 1 \quad \text{Eq 2.24}$$

$P_{cx} = 1550$ kN from the “Blue Book” [SCI 2001]

$M_x = 47.29$ kN-m calculated above

For double curvature with equal and opposite end moments, $m = 0.4$

$$\begin{aligned} & \frac{1095}{1550} + \frac{0.4 \times 47.29}{87.3} \left(1 + 0.5 \frac{1095}{1550} \right) \\ & = 0.7065 + 0.2167(1 + 0.3532) = 0.7065 + 0.2932 = 1.00 \quad \text{Eq 2.25} \end{aligned}$$

In this case, the column resistance is reduced to $1095/1550 = 71\%$ of the strut buckling capacity. This is a higher calculated resistance than found by the other methods. It is higher

than the cap plate method firstly because that method assumes that the load is applied at the face of the column, so the cap plate method gives a higher calculated applied moment for a given axial load, and secondly because the interaction formula accounts for combined axial compression and bending more accurately than the simpler formula.

The above calculations conform to BS 5950-1, but calculations to Eurocode 3 follow the same principles.

2.3.7 Sensitivity of plastic design to moment gradient

Plastic design checks are sensitive to the bending moment gradient. Because the section is allowed to have extensive plasticity, even small additional bending moments from strut action may be sufficient to cause the member to buckle. This is shown below for the same $140 \times 140 \times 10$ SHS. In this example, the applied axial load is assumed to be 910 kN. This is just above 50% of the squash load of 1807 kN. Therefore the area resisting the bending moment remains in the flanges of the section.

Firstly, the reduced plastic moment is calculated.

The axial compression is 910 kN, which is less than the squash load of 1807 kN. The area not used to resist axial compression has a squash load of:

$$1807 - 910 = 897 \text{ kN}$$

Therefore the depth of each strip either side of the area resisting compression as shown in Figure 2.9 is:

$$d_s = \frac{1}{2} \left(\frac{897 \times 10^3}{355 \times 140} \right) = 9.02 \text{ mm} \quad \text{Eq 2.26}$$

Therefore the bending resistance is:

$$\frac{897}{2} (0.140 - 0.00902) = 448.5 \times 0.13089 = 58.70 \text{ kN-m} \quad \text{Eq 2.27}$$

Secondly the maximum moment gradient factor, m , is found.

Checking the buckling resistance to BS 5950-1:2000 Clause 4.8.3.3(a):

$P_{cx} = 1550 \text{ kN}$ from the “Blue Book” [SCI 2001]

$F_c = 910 \text{ kN}$ defined above

$M_x = 58.70 \text{ kN-m}$ calculated above

$$\frac{F_c}{P_{cx}} + \frac{m_x M_x}{M_{cx}} \left(1 + 0.5 \frac{F_c}{P_{cx}} \right) \leq 1 \quad \text{Eq 2.28}$$

$$\begin{aligned} \therefore m_x &\leq \frac{\left(1 - \frac{F_c}{P_{cx}} \right) M_{cx}}{\left(1 + 0.5 \frac{F_c}{P_{cx}} \right) M_x} \\ &= \frac{\left(1 - \frac{910}{1550} \right) 87.3}{\left(1 + 0.5 \frac{910}{1550} \right) 58.7} = \frac{0.413}{1.294} 1.487 = 0.475 \end{aligned} \quad \text{Eq 2.29}$$

This demonstrates how the calculated column capacity is reduced from 1095 kN = 71% of strut capacity to 910 kN = 59% of strut capacity by a change of moment gradient factor from 0.4 to 0.475. This is the moment gradient factor for the end moment ratio, β , of -0.625 according to BS 5950-1:2000 Table 26. This means that the end moments are opposite (so the column is in double curvature) and the lesser end moment has a magnitude of 62.5% of the greater end moment. The sensitivity to bending moment gradient means that the method gives inefficient designs for columns in single curvature.

A problem arises using this design approach in the case of uniform single curvature. Uniform single curvature is not a common design case in traditional UK simple construction, but only because BS 5950-1 Clause 4.7.7 says that it is not necessary to consider pattern loading. This is because traditional simple construction uses beams that are effectively simply supported, spanning between the column faces. However, in rigidly jointed frames, pattern loading is required by both BS 5950-1:2000 (see Clause 5.7.2) and by the ASCE manual [ASCE 1971]. A member that has equal and opposite moments at the ends is in uniform single curvature. If the end moments were the plastic moment of resistance, even if that is the plastic moment reduced by coexistent axial load, it is not possible to resist axial compression. This is because the member is fully plastified over its entire length, so that there is no resistance remaining to resist the strut action bending moments. The inability of the method to accept single curvature bending moments of nearly constant magnitude means that the method cannot be applied successfully to all frames.

2.3.8 Summary of orthodox methods

The advantages and disadvantages of the orthodox methods are:

Simple buildings using the method for a beam supported on a cap plate.

The method is simple to understand. The application is complicated by the practical effects of end plates of sufficient thickness to provide tying capacity to satisfy building regulations. This necessitates the addition of a moment from the end plate bending arising from the difference between the beam slope and the column end-slope. The calculated column capacities are relatively low.

Rigid jointed frame using elastic analysis.

The method is simple to understand and simple to apply through normal commercial frame analysis software. Where column end moments are large, the calculated column capacities are relatively low and there may need to be relatively expensive connection details to be consistent with the analysis model.

Flexibly jointed frame using elastic analysis.

To analyse such frames rigorously requires considerable effort, making them economically unattractive to design offices. To analyse them approximately may lead either to underestimate of the column moments, giving unconservative design, or to overestimating the column moments, giving design like a rigidly jointed frame. Because the method lies somewhere between the cap plate method and the rigid jointed method, it is expected that the calculated column capacities will be relatively low.

Rigid jointed frame with plastic analysis.

BS 5950-1:2000 [BS 2000a] Clause 5.7.2 *Independently braced frames* allows plastic design of such frames because they fulfil the bracing requirements. This clause allows the plastic hinges to develop in the columns because the frames are braced against sway. Where the columns are in double curvature with almost total reversal of moment, the method is more efficient than other methods. However, where the columns are in single curvature, or nearly single curvature, the method predicts low resistance to axial load.

2.4 Unorthodox design methods for braced frames

2.4.1 Unorthodox methods that might be used

There are other design methods that might be considered for braced frames with discontinuous columns. These are:

1. Gent & Milner's 1966 & 1968 column research
2. Wood's 1973 plastic design method
3. Alpha-pin from the University of Sheffield
4. AD 283 from the SCI

These methods are discussed below.

2.4.2 Gent & Milner's 1966 & 1968 column research

Gent published a paper [Gent 1966] in 1966, followed by a second with Milner [Gent & Milner 1968] in 1968, describing tests on small scale steel I-section columns subject to an initial end-rotation and then to increasing axial compression while the end-rotation remained applied.

In the tests, end rotations were imposed at the two ends of the columns by moments applied to a spring system which simulated the action of beams in a frame and applied end moments. This system allowed the moment to reduce as the column ends rotated, just as the end moments of a fixed-ended beam reduce if the end restraints are allowed to rotate. Initially the column had no axial load applied. The axial load was then increased and the end moment resisted was measured. The experiments showed that as the axial load was increased, the yielding of the column allowed such large end rotations that that the columns "shed" the moments, as shown in Figure 2.10.

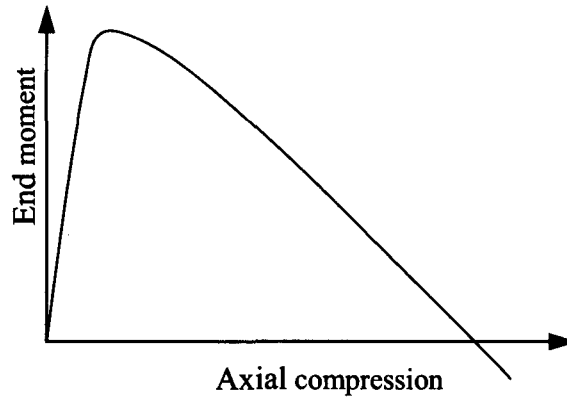


Figure 2.10 Moment shedding from increasing axial load

As the axial compression was increased the end moments reduced to zero and then changed to acting in the opposite direction to some small amount before the member failed by flexural buckling in the plane orthogonal to the plane of the web of the column, even when the end rotations were applied in the plane of the web.

It is important to understand that the end moment was applied by the spring system simulating the behaviour of a beam in a frame. It was not applied as an eccentric load on the column. Application as an eccentric load does not allow the moment to reduce as the column ends rotate and this is the design case assumed in codified checks of resistance to combined axial compression and bending.

Gent and Milner's tests showed that, at Ultimate Limit State in braced frames with rigid beam-column connections, the column behaviour is significantly different from elastic behaviour. The reason is simply that, by definition, the effects of plasticity are not included in elastic analysis. In reality, the stiffness of the members is modified by the extent of the plasticity. The reduced column stiffness limits the bending moment in the columns and also allows more severe curvature in the columns. When moments are applied to the columns by the beams, the reduced column stiffness allows increased rotation of the column ends, tending to shed the applied moments provided that the beams can resist the moments shed by the columns. Gent and Milner observed "that even under biaxial bending restrained columns have a remarkable capacity to sustain high axial loads by shedding end moments".

In Gent 1966 *Part II: An approach towards a rational and economic design method for office type structures*, Gent wrote that "By considering limiting cases in this way, the design

of the beams and the columns could largely be divorced”. The papers propose a possible approach to design, but it is not developed into a complete method. The design approach uses the elastic critical buckling load of the part of the column that remains elastic, but does not consider residual stresses. The papers refer to the issue of geometrical imperfections arising from the curvature induced by the imposed end-rotations and the effect on the compression resistance, but a method to consider different magnitudes of imperfections is not given. Therefore, this research gives very important insights into the behaviour of columns in braced frames, but it does not give the designer a complete procedure.

2.4.3 Wood’s 1973 plastic design method

Wood published a method [Wood 1973] devised for frames in which the columns are assumed to be connected at each floor level by rigid connections to both major and minor axis beams. The beams on the major axis of the columns are designed plastically and the beams on the minor axis of the columns are designed to remain elastic. In columns resisting a large bending moment, the column has an extensive plastic zone which has zero stiffness because of the plasticity. The compression resistance of the column is calculated by finding the portion of the cross-section that remains elastic and calculating the Euler buckling load of this elastic section. This is the same philosophy as used by Gent to estimate the resistance of columns.

There are problems in using this method.

1. The method uses a calculation of column resistance that is not connected to any other codes that designers or checkers might recognise. This is a great disadvantage for a design method because those asked to authorise the design do not have the comfort of extensive use of the method. Instead, it conflicts with the normal code design methods.
2. The method has not been verified against many types of columns, so there is a question of confidence in the results. The columns tested by Gent were I-sections but were small laboratory test specimen with flange and web breadth to thickness ratios far less than in common structural sections. This gave them unusually high torsional stiffness and unusually high resistance to local buckling.
3. Imperfections are recognised in normal modern codes by using a buckling curve appropriate to the type of member. Wood’s method does not explicitly recognise the effects of imperfections. This might be because the method is suitable for even the worst level of imperfections, but it is not clear.

2.4.4 Alpha-pin from the University of Sheffield

The Alpha-pin Method [Gibbons 1990, Kirby et al 1992, Gibbons et al. 1993, 1993a,] was developed at the University of Sheffield with extensive analytical studies and full scale tests.

The method was developed for braced frames in which

1. The columns are continuous and the beams are connected between the columns as shown in Figure 1.2 and
2. There is some stiffness in the beam-column connections

The method allows the columns to be designed for the axial compression alone, taking the effective length of columns as 1.0 times the height between floors. The design moments on the column are taken as zero even where the beam column connections are stiff. The explanation for the neglect of the applied moments is that the detrimental effects of the transmitted moments resulting from connection stiffness are outweighed by the beneficial effect of the restraint afforded by the beam. The method is very attractive because designers often need to have beam column connections with significant stiffness. The connection stiffness may be explicitly desired either to reduce the risk of instability during erection or to benefit from some continuity of the beams for greater strength and stiffness. In other cases, the connection stiffness may result from the geometry of the connections, either where the connections must be designed to resist large tying forces to avoid disproportionate collapse, or where diagonal bracing is connected into the beam-column connection, resulting in a large beam-column connection.

For internal columns of buildings with a regular column grid, the Alpha-pin method is identical in its effect to the UK “simple construction” method given in BS 5950-1:2000 [BSI 2000a] because in these cases the nominal moments are equal and opposite, giving the same results.

The Alpha-pin method was developed for frames with continuous columns as used in frames of traditional simple construction and the analysis and physical testing were conducted on this type of frame. Therefore this method is not immediately applicable to frames with discontinuous columns.

2.4.5 AD 283 from the SCI

The construction of large frames with discontinuous columns of up to 14 storeys in height attracted interest and concern. The Steel Construction Institute published a series of

Advisory Desk articles in the magazine *New Steel Construction*, AD 281, AD 283, AD 285, AD 288 and AD 292 [SCI 2005a, 2005b, 2005c, 2005d and 2005e], to give guidance on the use of discontinuous columns in residential construction. The following issues needed to be addressed:

1. Application of the method needs to be as simple to apply as possible, because complex methods either dissuade designers from using the method or encourages designers to do something simpler that might not be safe.
2. The method needs to lead to member sizes that can be seen to be reasonably economic. If they do not, either the structures will never be built or designers will devise their own methods that give more economical members but might not be safe.
3. The method ought to agree with other design methods where possible, or ought to be similar in philosophy.

In preparing guidance, the following information was reviewed:

1. Some discontinuous columns were reported to be designed assuming that beam-column connections acted like “nominally pinned” bases. This means that they were designed with a low connection stiffness and without the eccentricity of forces shown in Figure 2.4. This would lead to underestimating any bending moments on the columns.
2. The Alpha-pin method suggests that the columns might be designed for the axial load alone, neglecting any bending moments.
3. Gent and Milner, [Gent and Milner 1968], contain some comments on rotation values that suggested caution in adopting Alpha-pin completely, especially as the experience of application of the method is limited. For example, Paragraph 21 includes the comment, “The primary factors emerging as controlling performance under these conditions are the minor axis elastic critical load of one flange and the joint rotation ϕ_R to relax the end moments. Provided the ϕ_R values are not extreme the effect of bending actions is secondary, rather analogous to imperfections in an axially loaded column, and the type of performance and ultimate axial load capacity is primarily controlled by the minor axis stability of one flange.”
4. BS 5950-1 [BSI 2000a] gives guidance for designing beams on cap-plates and it is desirable to produce guidance that is in harmony with the code.
5. Designers expect to have some reduction in column capacity due to bending moment, especially in a frame that is almost a rigid jointed frame.

6. Designers are accustomed to having to apply a nominal moment which is recognised to be approximate, as in the “simple construction” method shown in Figure 2.2 and Figure 2.3.

The resulting method of column design, given in AD 283 [SCI 2005b] uses a nominal moment, but derived differently from the traditional methods used in the design of columns in traditional “simple construction”. In the AD, the moment is calculated from the total reaction from the beam (ie the sum of the shears from the beam extending both sides of the column) acting at the face of the column. This differs from traditional “simple construction” in which equal spans, equally loaded, give zero net moment on the column. It also differs because the moment calculated is applied to the column without sharing between the column above and the column below. However, as in the traditional method, the moment is not expected to be an accurate description of the structural behaviour. Rather, it may be viewed as a reduction in column resistance to allow for applied moments and/or imposed curvatures that might occur and that might reduce the capacity of the column.

The AD was written for use in buildings in which the columns are partially restrained by the floor slab against rotation about the axis along the floor beams. This restraint arises from the stiffness of the floor slab which is constructed so that it occupies the full depth of the beams. This is often the case in modern residential construction and this is the type of construction which had provoked the interest in discontinuous columns. The design rules in AD 283 require that the designer uses an effective length of the columns that is the centre to centre height from floor to floor. This means that the effective length factor for the columns is taken as 1.0. This contrasts with conventional design in which the effective length factor in this case would normally taken as 0.85 or even 0.7 following either the guidance in BS5950-1 [BSI 2000a] Table 22 “Nominal effective length L_E for a compression member” or similar guidance in BS 449 [BSI 1969] . The AD uses 1.0 because the extensive plasticity required to allow moment shedding reduces the stability of the column. Therefore, AD 283 method allows design using the nominal moment, which is less than the moment calculated in conventional rigid frame analysis, but this can only be done if the buckling resistance of the column, P_c , is calculated using the effective length factor of 1.0 to allow for the extensive plasticity. This needs to be remembered when comparing the results of design to the AD with the results of other methods.

The AD uses the column check in BS 5950-1:2000 [BSI 2000a] Clause 4.7.7, which is the clause for the design of columns in traditional simple construction. This check was chosen

both because of its simplicity and because it is this check that designers expect to use when checking columns in braced frames. The method is demonstrated in the following calculations.

Firstly, for a typical exterior column in residential construction

Exterior column, beam span = 6.0 m, column spacing = 5.0 m

Assuming	4.0 kN/m ² for self-weight	× 1.4 =	5.6 kN/m ²
	1.5 kN/m ² for partitions	× 1.4 =	2.1 kN/m ²
	2.0 kN/m ² for live load	× 1.6 =	<u>3.2 kN/m²</u>
	Total	=	10.9 kN/m ²

$$\text{Reaction on column from beam} = 10.9 \times 5.0 \times 6.0/2 = 327/2 = 164 \text{ kN}$$

$$\text{Load from external wall} = 2.5 \times 5.0 \times 1.5 = 19 \text{ kN}$$

$$\text{Total} = 183 \text{ kN}$$

Using the assumption of a nominal design moment,

$$\text{Design moment} = \text{reaction at floor} \times \text{half-width of column}$$

$$= 183 \text{ kN} \times 0.070 = 12.8 \text{ kN-m} \quad \text{Eq 2.30}$$

$$\text{Using the equation from 4.7.7, } \frac{F_c}{P_c} + \frac{M_x}{M_{bs}} + \frac{M_y}{p_y Z_y} \leq 1 \quad \text{Eq 2.31}$$

$$M_y = 0, \text{ so } \frac{F_c}{P_c} \leq 1 - \frac{M_x}{M_{bs}} = 1 - \frac{12.8}{87.3} = 1 - 0.147 = 0.853 \quad \text{Eq 2.32}$$

$$\text{Therefore the maximum value of } F_c = 0.853 \times 1550 = 1322 \text{ kN} \quad \text{Eq 2.33}$$

Secondly, for a typical interior column in residential construction

Assuming the same floor loading as above and that the beam is continuous across the column,

The reaction on the column from the beam is:

$$(5/8) \times 10.9 \times 5.0 \times 12.0 = (5/8) \times 654 = 409 \text{ kN} \quad \text{Eq 2.34}$$

Using the assumption of a nominal design moment,

$$\text{Design moment} = \text{reaction at floor} \times \text{half-width of column}$$

$$= 409 \text{ kN} \times 0.070 = 28.6 \text{ kN-m} \quad \text{Eq 2.35}$$

$$\text{Using the equation from 4.7.7, } \frac{F_c}{P_c} + \frac{M_x}{M_{bs}} + \frac{M_y}{p_y Z_y} \leq 1 \quad \text{Eq 2.36}$$

$$M_y = 0, \text{ so } \frac{F_c}{P_c} \leq 1 - \frac{M_x}{M_{bs}} = 1 - \frac{26.8}{87.3} = 1 - 0.307 = 0.693 \quad \text{Eq 2.37}$$

Therefore the maximum value of $F_c = 0.693 \times 1550 = 1074 \text{ kN}$ Eq 2.38

To find the reduction in capacity below the capacity of a pin-ended strut as above
 $P_c = 1550 \text{ kN}$

Therefore 1322 kN above is a reduction to $1322/1550 = 85\%$ strut capacity
and 1074 kN above is a reduction to $1074/1550 = 69\%$ strut capacity

The method is known by the authors to be conservative in many cases (such as for internal columns with symmetrical beam arrangement and good fit-up between the columns and the beams). However, given the simplicity of the method, this is necessary so that it is safe when used for highly asymmetric cases (the worst of which are exterior columns) or in cases where the lack-of-fit between columns and beams may cause unexpected moments.

2.4.6 Summary of unorthodox methods

The advantages and disadvantages of the unorthodox methods are:

1. Gent & Milner's 1966 & 1968 column research is not a complete design method, even though it provides a very good explanation of the behaviour of columns in braced frames. The approach to checking column resistance used is that of the critical buckling of the member with the stiffness reduced by plasticity. This is a good method for understanding trends and was the best approach available at that time. However, calculation of the critical buckling load of a member with its stiffness reduced by the plasticity developed in a column with end rotations is a complex task. In addition, the method is very different from current codes, neither considering initial imperfections explicitly nor benefiting from extensive calibration. Therefore it is not sufficient as a design method.
2. Wood's 1973 plastic design method is interesting because it is a method that broke away from elastic analysis of columns in braced frames. It suffers the same major disadvantage as Gent and Milner's work in that the approach to checking column resistance used is that of the critical buckling of the member with the stiffness reduced by plasticity. With the limited test justification of the factors used, the absence of explicit treatment of imperfection and a method that is not clearly related to modern codes, few designers and fewer checkers could agree to use of the method.
3. Alpha-pin from the University of Sheffield offers outstanding simplicity and economy, but it was developed on frames in which the columns are continuous and has not been

demonstrated on frames with discontinuous columns. There is some concern that where discontinuous columns are used with long spans of shallow beams, the method might be optimistic because of the end slope induced by the beams.

4. AD 283 from the SCI gives a simple method, but it is clearly conservative in many cases. In the case of internal columns at the internal support of continuous beams, it is very conservative. The method is also imperfect because the nominal moment used to reduce the capacity of the column is only loosely related to the end-rotation induced by the slope of the beams.

2.5 Summary of design methods, orthodox and unorthodox

None of the methods currently available are ideal for the design of discontinuous columns in braced frames. A new design method is required because, firstly, frame analysis with varying joint stiffness is too complex and, secondly, methods based on nominal moments are uncertain and often give very conservative approximations. The Alpha-pin method and the research by Gent and Milner make it clear that much greater economy of material is possible. The Alpha-pin method suggests that this should be possible with a simple method that would make the design process more economical also. The studies presented in this thesis develop such a new design method for discontinuous columns in braced frames.

3 THE NEW DESIGN APPROACH

3.1 Introduction

Braced frames with discontinuous columns are attractive in residential construction because the columns are small in section and can be concealed within the thickness of the walls without losing considerable floor area by using unreasonably thick walls. Because the intention is to minimise the column section, the design process will not try to use moments in the columns to relieve the bending moments in the beams, so the beams will be designed to carry all the bending moments from the floor loading. Therefore, an acceptable process of design would be to:

1. design the beams independently from the columns
2. design the columns to suit the beams, without iterations of analysis and without relying on the beams for restraint

Such a design process would be very simple for designers. The beams would be designed either as simply supported single spans or as continuous beams on knife edge supports. Then the columns would be designed for the axial compression and end slopes equal to the slopes of the beams.

In braced frames, sway effects (storey shears) are resisted by a “bracing system” which may be one of many systems such as cross-bracings, stiff portals or a concrete core. The columns that are braced are not required to resist any bending moments other than those arising from gravity loads on the beams.

The new design method is developed using the symbols from Eurocode 3 because the Eurocodes are to become the main design code in the UK and throughout the European Union during the next decade.

3.2 Behaviour of columns in reality

The starting point for the new design approach is that behaviour of columns in reality is different from the behaviour commonly assumed by designers using elastic analysis techniques. This is reported in Gent [Gent 1966] and Gent and Milner [Gent & Milner 1968] and is presented below.

The behaviour was investigated by non-linear finite element analysis as described in Chapter 4. Examples of the behaviour are shown in Figure 3.1 and Figure 3.2. These show the axial force and coincident end moments resisted by hot-finished square hollow sections (SHS) subject to an increasing load combination of axial compression and end rotations. The graphs are for 140×140×10 sections 3.0 metres long with equal and opposite end rotation (single curvature) and are for load cases in which the axial compression and the end-rotations are increased linearly until the maximum axial compression is reached. The horizontal axis is the end-rotation in radians. The vertical axis is the proportion of the strut buckling resistance (for axial load) and the proportion of the plastic moment (for bending moment).

At lower levels of load, the bending moments increase almost linearly. The increase is not entirely linear because second-order effects reduce the effective stiffness of the member. At higher levels of load, the end moments reduce because of increasing plasticity. These graphs show:

1. The columns need not be designed to resist the bending moments calculated by elastic analysis, provided that the beam design is not relying on the moments in the columns to resist the loads on the beam (for example at stiff external columns resisting hogging moments in the beam).
2. The end moment might not reduce to zero before overall buckling occurs, as in Figure 3.1. This shows the load case in which the maximum load of the column occurs at 1404 kN with end rotations of 0.013 radians.
3. The end moment might change to the opposite sign as in Figure 3.2. This shows the load case in which the maximum load of the column occurs at 1109 kN with end rotations of 0.041 radians. In this case the end moments are increasing the stability of the column. Given that the design approach proposed in Section 3.1 is to separate the column design from the beam design, the increase in axial resistance beyond the point of zero end moment will not be employed. This might be seen as uneconomic, but reliance on reversed end-moments requires that the beam-column connections have sufficient strength and stiffness to mobilise the end moment. Such strong and stiff connections are relatively expensive, so not using end-moments is economic.

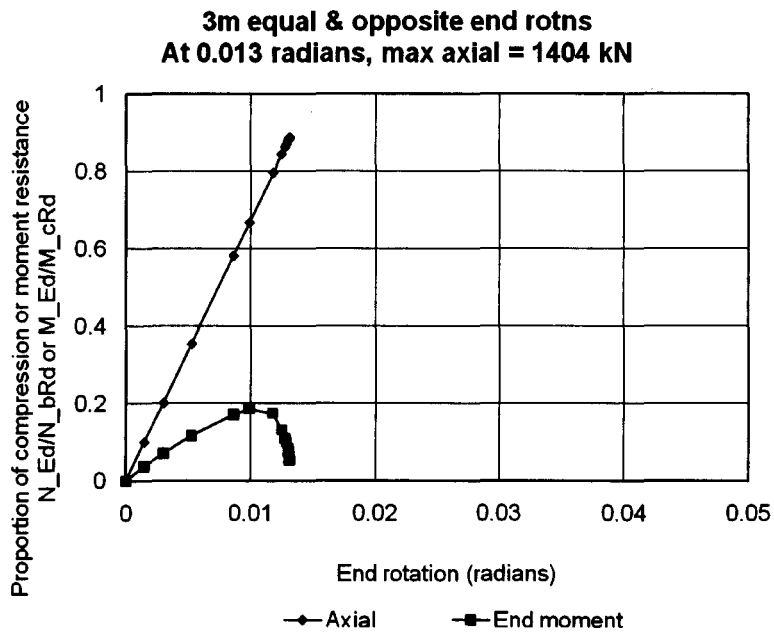


Figure 3.1 Single curvature with small end-rotation

Plot of proportion of compression resistance and moment resistance with increasing end-rotations

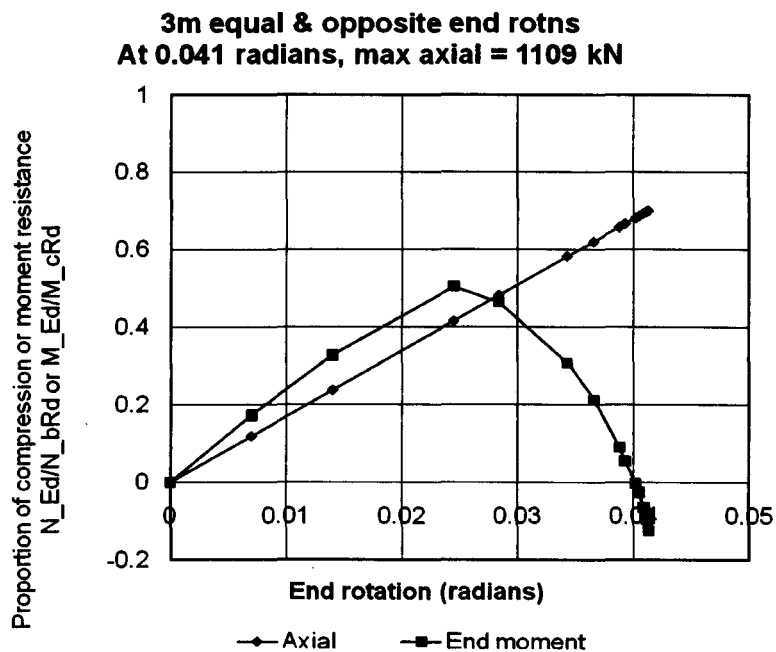


Figure 3.2 Single curvature with large end-rotation

Plot of proportion of compression resistance and moment resistance with increasing end-rotations

3.3 New column design approach

After studying the work by Gent and Milner [Gent 1966], [Gent & Milner 1968], and the development of Alpha-pin [Carr 1993] it was decided that a new design philosophy could be adopted for braced frames with discontinuous columns. This new design philosophy exploits this phenomenon of “moment shedding” demonstrated by Gent.

This new design approach is radically different from current approaches to column design. It uses column behaviour that is very different from that at “working loads” because at working loads there is little or no plasticity in the columns.

Step 1

The beams are designed independently of the columns. Single span beams are designed as simply-supported beams. Multiple-span beams are designed as beams on knife-edge supports. The beam slopes at the supports must be calculated for use in the column design. If the design is to BS 5950-1 [BSI 2000a] or to the ASCE manual [ASCE 1971], the designer should use “pattern loading” to find the worst loading condition for column buckling, as specified in Clause 5.6.2. However, if the design is to the Eurocodes and the structure is a building, the designer would be free to ignore “pattern loading” from the provisions of EN 1991-1-1 [BSI 2002b, CEN2002b] Clause 6.2.2(1).

Step 2

The columns are designed to suit the beams and are assumed to have no effect on the beam design. Therefore the columns are designed to resist the design axial compression while satisfying the following criteria:

1. The rotation at each end of the column is equal to or greater than the rotation of the beam to which it is connected.
2. The column does not require bending moments in the beams to maintain the equilibrium of the column. For example, however slender the column, it is designed assuming single curvature bending, as Figure 3.3, and not double curvature bending, as Figure 3.4, so that the design process remains as simple as possible. The assumption of single curvature will not be consistent with the actual column deflections, but the assumption is convenient and is conservative for calculating the overall buckling resistance.

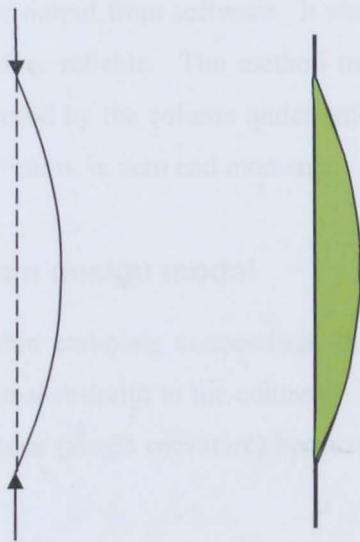


Figure 3.3 Single curvature bending in the column

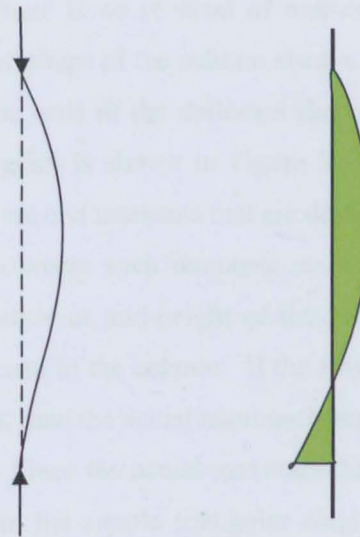


Figure 3.4 Double curvature bending in the column

3.4 Development of a method to apply the new design approach

3.4.1 Introduction

The new design philosophy needs a new design method that is simple to apply either by pencil and paper or by coding into software. It is always desirable to have a method that can

be applied by pencil and paper because it enables designers to make checks independently from software to confirm the output from software. It also means that coding into software should be simple and therefore reliable. The method must be able to calculate the axial compression that can be resisted by the column under enforced rotation at its ends but with no restraint provided by the beams, ie zero end moments.

3.4.2 The new column design model

To allow fabrication with thin end-plate connections, the design model assumes that the beams do not provide rotational restraint to the columns. For simplicity, the model assumes equal but opposite end rotations (single curvature) because this is both the weakest case and the simplest case to consider.

Numerous cases of end rotation were studied using non-linear elastic-plastic analysis as reported by King [King 2006]. In the course of the study, three points became clear.

Firstly, the bending moment diagram in the column is defined by the deflected shape of the column. Therefore, where there is no reversal of moment at the ends and the column is initially straight, the deflected shape of the column always lies between the original unloaded shape and the tangents to the ends of the deflected shape as shown in Figure 3.5 (a). The actual bending moment diagram is shown in Figure 3.5 (b) if the end moments are zero. There are cases where there are end moments that are destabilising (ie of the same sign as the maximum end moment) but where such moments occur, the curvature at the ends of the columns result in less curvature at mid-height of the column for a given end rotation, so reducing the maximum moment in the column. If the maximum deflection of the column is e , as shown in Figure 3.5 (a), then the actual maximum bending moment in the column is Ne as shown in Figure 3.5 (b). Since the actual maximum bending moment diagram is always less than the maximum from the simple triangular diagram shown in Figure 3.5 (c), the maximum applied moment is not greater than $M = N\{\theta(h/2)\}$.

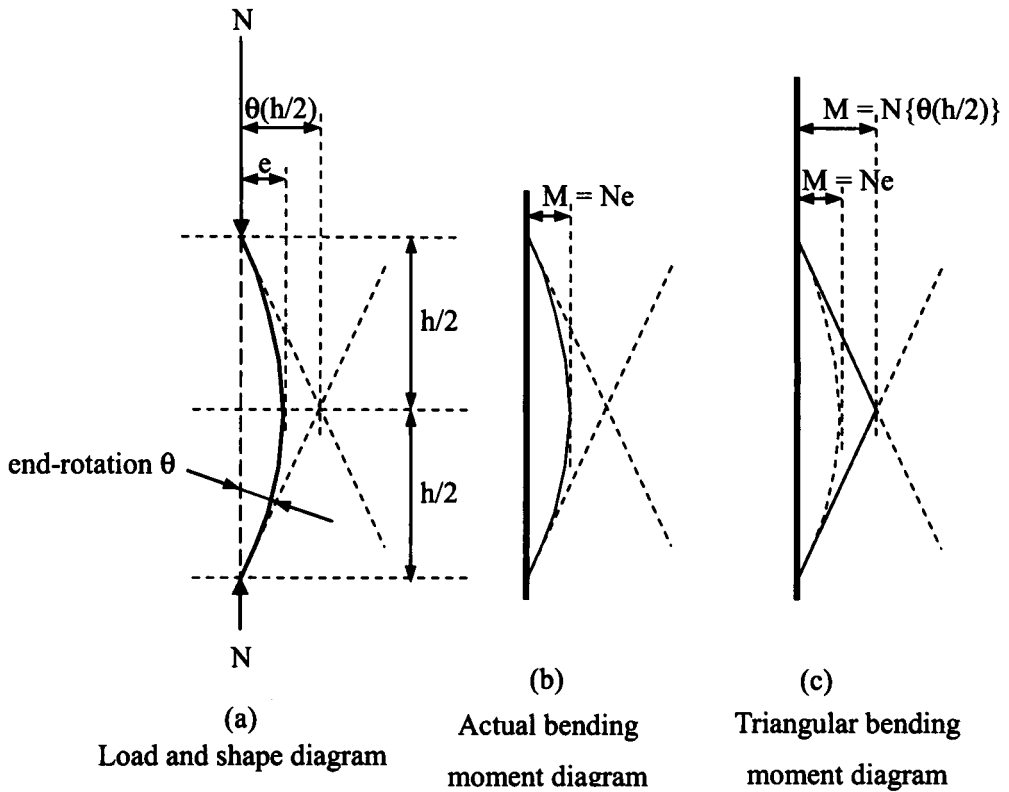


Figure 3.5 Triangular approximation to the bending in the column

Secondly, the shape of the column changes as the magnitude of the imposed end rotation increases. The shape becomes less like a sine curve because much sharper curvatures develop at mid-height as a result of plasticity. Above and below mid-height, the deformed shape of the column approaches the tangents to the end-slopes. Figure 3.6 shows the deformed shape and tangents to the ends for both small end rotations and large end rotations. The small end rotation case in Figure 3.6 (a) corresponds to the column behaviour near the maximum strut compression resistance. The large end rotation case in Figure 3.6 (b) corresponds to the column behaviour in the post buckling range, at deformations greater than at the maximum strut compression resistance. Figure 3.6 (b) uses a solid line for the actual shape and uses a dotted line to show the shape in (a) but amplified to give the same end rotations to show the difference in shape arising from the tighter curvature at mid-height in the case of large end-rotations.

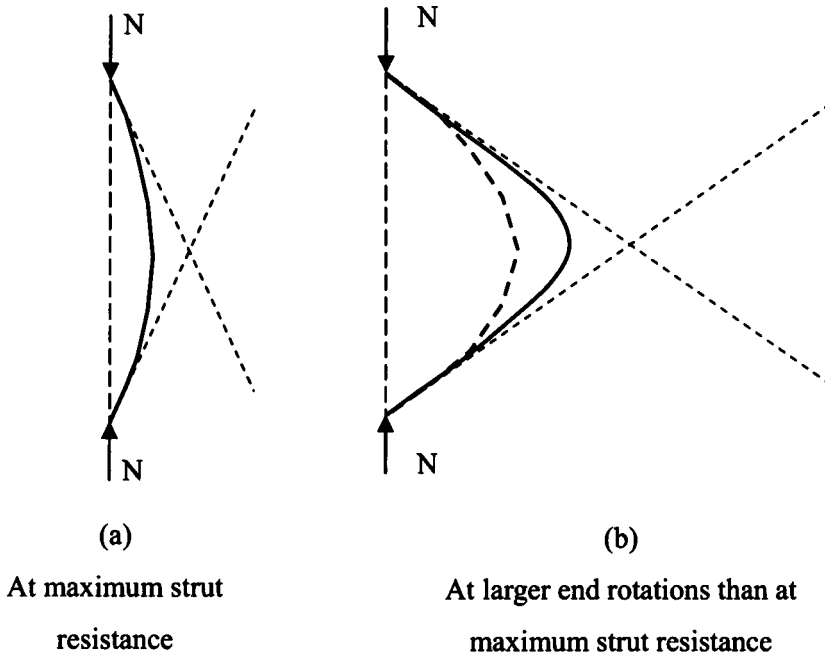


Figure 3.6 Deformation with increasing end rotation

Thirdly, at higher end rotations, there is extensive plasticity across the section. In these cases, the stress distribution mid-height of the column approaches a classic rectangular plastic stress distribution, but the stress-blocks are not entirely rectangular due to the finite rotation, as shown in Figure 3.7 (a). For a given axial compression, N , the classic plastic stress distribution shown in Figure 3.7 (b) gives a larger moment of resistance than the actual stress distribution in (a). This is shown in Figure 3.7 (c) as the difference between the typical actual and plastic stress diagrams.

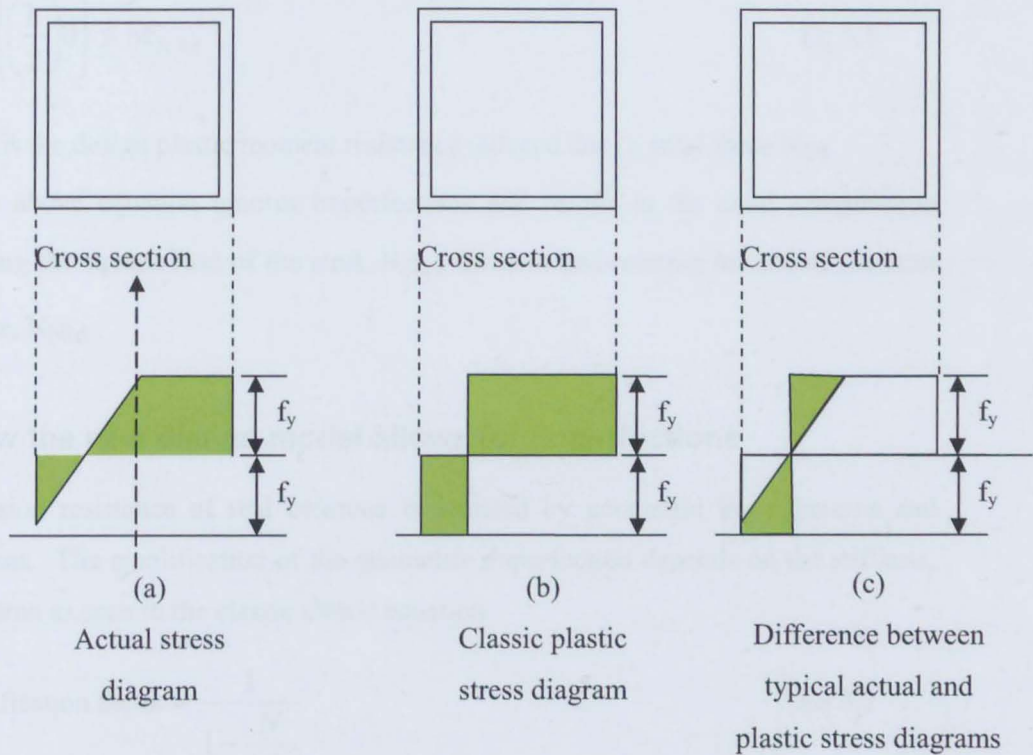


Figure 3.7 Comparison of typical actual v plastic stress distributions

The simplified triangular bending moment diagram in Figure 3.5 (c) over-estimates the bending moment applied to the column. The classic plastic stress diagram in Figure 3.7 (b) over-estimates the bending moment resisted by the column. The two over-estimates tend to cancel each other, providing a possible a design model which is investigated by a parametric study in Chapter 8.

UNIVERSITY
OF SHEFFIELD
LIBRARY

The combination of the triangular bending moment shown in Figure 3.5 (c) and the classic plastic stress distribution shown in Figure 3.7 (b) provide the basis for a simple design model which predicts the column resistance by equating the plastic moment of resistance at mid-height to the applied bending moment at mid-height. In the new design model, only single curvature is used, so the shape of the column is always within the tangents to the ends of the column. Therefore the upper bound of the deformed shape is limited to this, as shown in Figure 3.6. Therefore the approach is similar to classic second-order rigid-plastic [Horne 1963] analysis.

If the effect of imperfections is ignored, this gives a design equation derived from moment equilibrium at mid-height:

$$N_{Ed} \left\{ \left(\frac{h}{2} \right) \theta \right\} \leq M_{N,Rd} \quad \text{Eq 3.1}$$

where $M_{N,Rd}$ is the design plastic moment resistance reduced due to axial force N_{Ed} .

However, the above equation ignores imperfections and results in the axial compression resistance being the squash load of the strut, N_{cRd} , for zero end-rotation instead of the strut buckling value, N_{bRd} .

3.4.3 How the new design model allows for imperfections

The compression resistance of real columns is affected by geometric imperfections and residual stresses. The amplification of the geometric imperfection depends on the stiffness, EI , of the column as seen in the classic elastic equation

$$\text{amplification factor} = \frac{1}{1 - \frac{N}{N_{cr}}} \quad \text{Eq 3.2}$$

which, for a pin-ended strut, is

$$\text{amplification factor} = \frac{1}{1 - \left(\frac{\pi^2 EI}{L^2} \right)} \quad \text{Eq 3.3}$$

The stiffness is reduced by the extent of the zones of yielding, which is affected by the residual stresses. Calculation of the resistance of columns is complicated because it must allow for these effects. Design codes include the effects of imperfections in the calculated design resistances. Most codes rely on formulae that give a “best fit” to test results.

Both geometric and residual stresses can be treated by a design value of geometrical imperfection greater than the geometrical tolerance, as Perry-Robertson in Annex G of BS 5400-3 [BSI 2000b]. This approach calculates the bending moment in the strut arising from the deflection which is calculated from the amplification of the design value of the initial imperfection. The BS 5400-3 formula is derived from first principles in Appendix D.

The effect of imperfections is most pronounced in columns with high axial compression and small bending moments. This is because cross-sectional bending resistance is not affected by residual stresses provided the elements of the cross-section are not affected by local buckling. In cases where the bending moments induced in a column are higher than the

strut-action bending moment that occurs at maximum strut resistance, the bending moment caused by the initial geometrical imperfection and amplification is only a proportion of the total bending moment. Therefore, the effects of initial geometrical imperfections and residual stresses are of lesser importance in cases of higher bending moments than the strut-action bending moment that occurs at maximum strut resistance. This means that at higher column end-rotations, the column resistance becomes less sensitive to initial imperfections.

The design model can be adjusted by use of an appropriate additional moment to represent the effect of initial imperfections. Figure 3.8 (a) shows the same column as in Figure 3.5 (a) and Figure 3.8 (b) shows the design bending moment diagram taken as uniform over the entire height of the column with the maximum value from the triangular construction in Figure 3.5 (c). Figure 3.8 (c) shows a second curved dotted line, to represent initial imperfection of the column, and straight dotted lines describing an additional bending moment of magnitude Ne_i resulting from the initial imperfection. The design bending moment is drawn as if it is uniform over the entire height of the column. This will not occur, but it is shown like this to discourage designers from using non-uniform sections because only uniform members will be considered in this report. The design simplification of single curvature is safe for uniform members, but might not be safe for varying cross-sections, because any cases of double curvature might result in high moments applied to sections that are weaker than the section at mid-height.

The compression resistance, N_b , may be found from the classic rectangular plastic stress distribution, so the approach is similar to classic second-order rigid-plastic [Horne 1963] analysis but with the important additions of actual end-rotations and an initial imperfection to give the correct failure load rather than the over-estimate calculated by classic second-order rigid-plastic analysis. The initial imperfection of a column may be either in the same plane as the column end-rotations or in another plane, so both possibilities have been investigated in the parametric studies in Chapter 8.

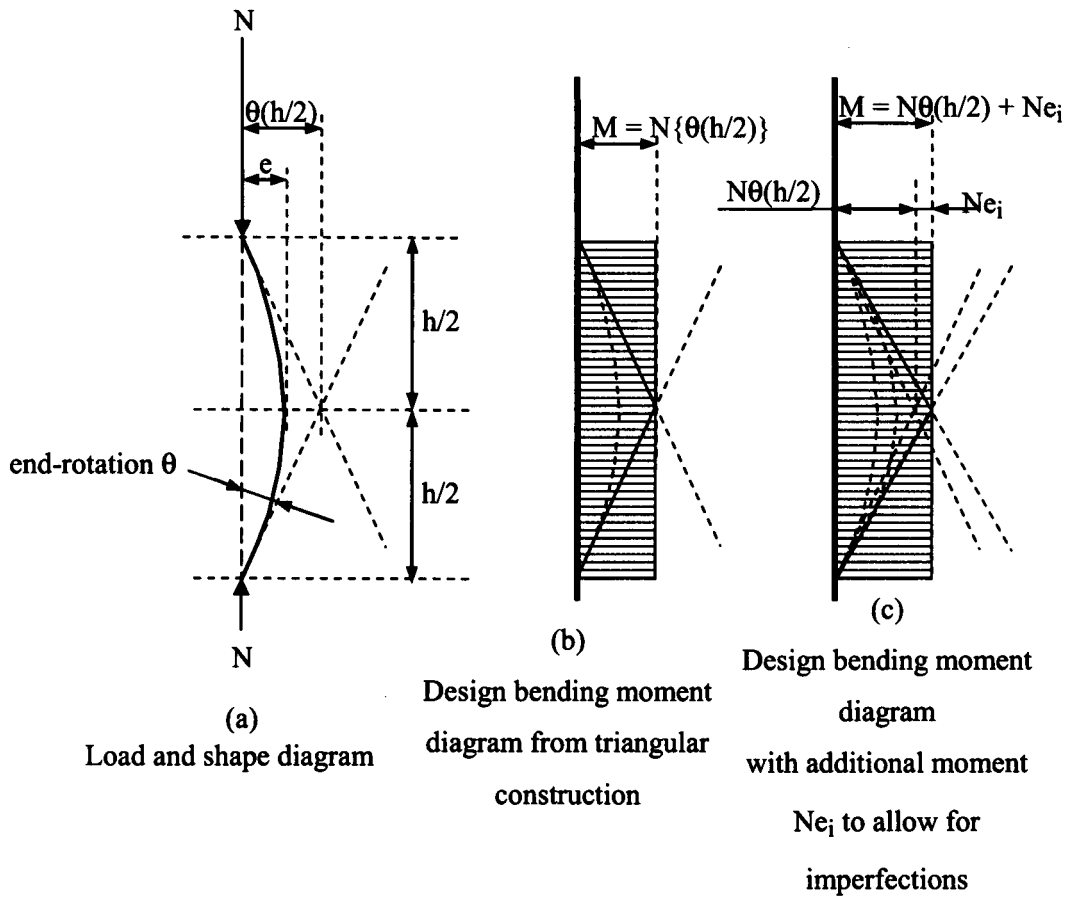


Figure 3.8 Design bending moment in the column including imperfection

The new column design model derives the initial imperfection from the code strut resistance, so the design model will agree with whatever code is specified for the design of the structure.

Therefore, when the effect of imperfections is included, the design equation (derived from moment equilibrium at mid-height) becomes:

$$N_{Ed} \left\{ \left(\frac{h}{2} \right) \theta + e_i \right\} \leq M_{N,Rd} \quad \text{Eq 3.4}$$

where $M_{N,Rd}$ is the design plastic moment resistance reduced due to axial force N_{Ed}
 and e_i is the design value of imperfection.

3.4.4 Defining the design value of the initial imperfection

The model is demonstrably most in need of correction by additional imperfections in the case of very low curvature, as shown in Figure 3.9. In this case, the difference between the actual stress diagram and the classic plastic stress diagram is large.

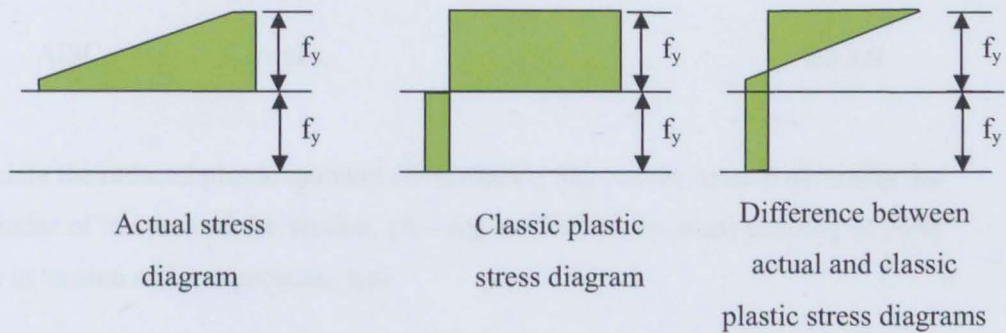


Figure 3.9 Comparison of actual v plastic stress distributions at low end rotations

Where a column is between beams that have no rotation, the resistance of the column can be expected to be not less than the buckling resistance of a pin-ended strut. A pin ended strut has some end-rotation at maximum resistance, but this end-rotation is small and may or may not be in the plane of the rotation of the beam. It may be taken as zero for simplicity. It is necessary that the new design model can be applied to struts with any magnitude of end rotation. Therefore the additional imperfection must be such that the calculated resistance at zero end-rotation is equal to the strut resistance. This allows the new design method to be calibrated to whatever design code is specified by the calculation of an imperfection, e_s , that makes the column resistance at zero end-rotation equal to the pin-ended strut resistance of the specified code.

For a strut with a gross cross-sectional area, A , the imperfection, e_s , may be calculated as follows:

1. Calculate the buckling load of the column, N_b , as if it were a pin-ended strut using the specified design code.
2. Calculate the area, A_b , stressed to the factored yield stress, f_{yd} , required to resist the pin-ended strut load, N_b , so

$$A_b = N_b / f_{yd}, \quad \text{Eq 3.5}$$

where the factored yield stress, f_{yd} , is the minimum specified yield stress reduced by the appropriate material factor for cross-sectional resistance in the specified design code, for example using

$$\text{EN 1993-1-1, } f_{yd} = f_y/\gamma_{M0}, \quad \text{Eq 3.6}$$

$$\text{BS 5950-1, } f_{yd} = p_y, \quad \text{Eq 3.7}$$

$$\text{AISC, } f_{yd} = \phi F_y, \quad \text{Eq 3.8}$$

3. Calculate the reduced plastic moment of resistance, M_{pr} , of the section assuming the remainder of the area of the section, $(A - A_b)$ is available to resist bending at yield stress in tension and compression, and

4. Calculate the imperfection, e_s , at axial load N_b from the assumption that

$$N_b e_s = M_{pr}, \quad \text{Eq 3.9}$$

$$\text{so } e_s = M_{pr} / N_b. \quad \text{Eq 3.10}$$

It is clear that this imperfection e_s is the appropriate value for e_i of Figure 3.8 (c) at zero end-rotation. As explained above, for larger end rotations, the actual stress diagram becomes more like the classic plastic stress diagram, so it is expected that the imperfection will be reduced at higher end rotations. This is investigated in the parametric studies reported in Chapter 8 and confirmed by the data plotted in Section 8.5.

Therefore, when the effect of imperfections is included so as to give the pin-ended strut buckling resistance at zero applied end-rotation, the design equation (derived from moment equilibrium at mid-height) becomes:

$$N_{Ed} \left\{ \left(\frac{h}{2} \right) \theta + e_s \right\} \leq M_{N,Rd} \quad \text{Eq 3.11}$$

where $M_{N,Rd}$ is the design plastic moment resistance reduced due to axial force N_{Ed} .

and e_s is the design value of imperfection derived from the buckling of a pin-ended strut using the design code specified for the particular structure.

3.4.5 Different planes of end rotation

The design model has been proposed in Sections 3.4.2 and 3.4.3 without defining the plane of the column end-rotations.

Examples are shown in Figure 3.10 and Figure 3.11 in which the areas resisting axial compression are shown by single diagonal shading and the two areas resisting bending moment (one in compression and the other in tension) are shown, one with double shading and the other without shading. Figure 3.10 shows the case of a section with bending about the X axis alone resisting an axial load slightly greater than half of the squash load. Figure 3.11 shows a section with bending about both the X axis and the Y axis and resisting an axial load of about half the squash load.

Without detailed examination of the deformations of the column, it appeared logical that the bending resistance should be calculated from the properties of the section bending in the plane of the end-rotations. For example, for column end-rotations in the Y-plane, a rectangular plane, the stress blocks would be as in Figure 3.10 but for end-rotations in the X = Y plane, the stress blocks would be close to those shown in Figure 3.11.

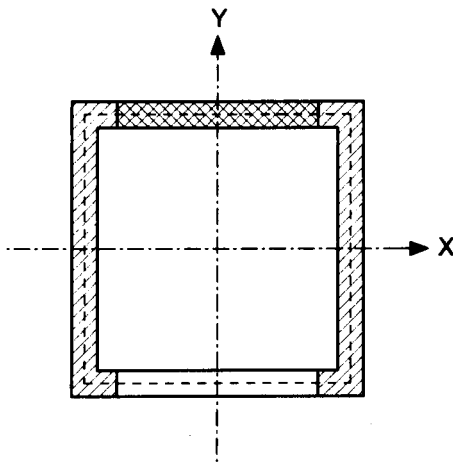


Figure 3.10 Plastic cross-section to calculate N_b from M_x only

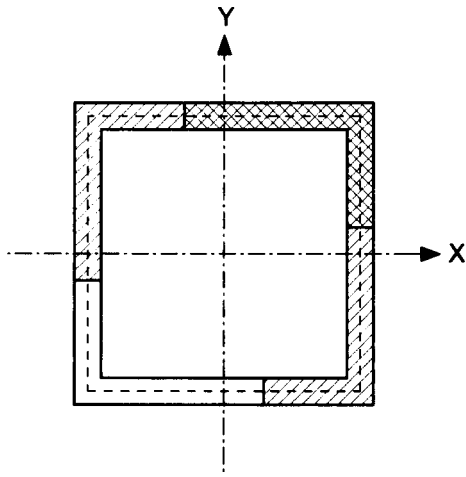


Figure 3.11 Plastic cross-section to calculate N_b from M_x and M_y

A study was made of the deformations of the column using the Abaqus model described in Section 4.3 and this showed that application of the moment in the plane of the end-rotations is not necessarily appropriate. This is because the behaviour is governed by the loss of stiffness of the section due to plasticity and the direction of the initial imperfection so that the direction of the initial imperfection dominates the displacements at mid-height of the column when extensive plasticity has developed.

In an SHS column, where the initial imperfection is in one of the rectangular planes of the column and the applied rotations in the same plane, the mid-height displacement of the column is also in that rectangular plane. This is shown by the plots of “0 away” and “0 towards” in Figure 3.12 in which the initial imperfection is in the $X=0$ plane (ie in direction $+Y$). When the rotation is in the rectangular plane perpendicular to the initial imperfection, the mid-height displacement is between the rectangular planes, but close to the rectangular plane. This is shown by the plots “90 left” and “90 right” in Figure 3.12.

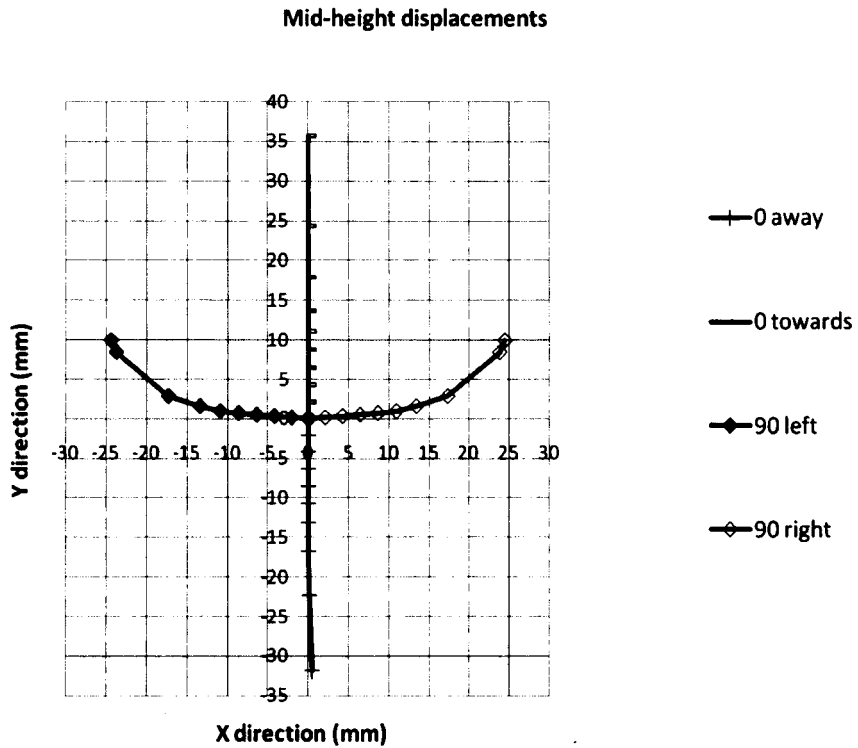


Figure 3.12 Mid-height displacements – rotations applied about rectangular axes from Abaqus analysis

Where the initial imperfection is in a plane at 45° to the rectangular planes of the column, referred to later as the $X=Y$ plane, and the applied rotations are in the same plane (ie in the $X=Y$ plane), the displacements are in the $X=Y$ plane. However, where the initial imperfection is in one of the rectangular planes of the column and the applied rotations are in the $X=Y$ plane, the initial displacements are in the $X=Y$ plane, but then the displacements develop out of the $X=Y$ plane, approaching a locus perpendicular to the $X=Y$ plane. This can be seen in Figure 3.13 which shows the locus of the mid-height when the applied rotation is towards the initial imperfection (in the $X=0$ plane) and also when it is away from the initial imperfection.

Midheight displacements, 1.5m column

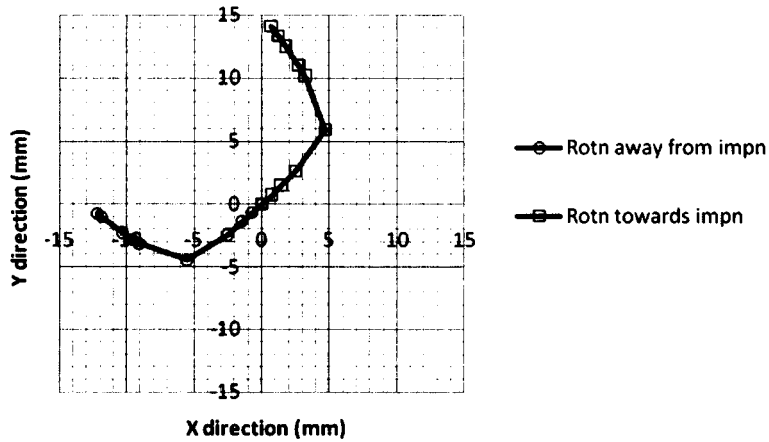


Figure 3.13 Mid-height displacements – rotation applied at 45 to rectangular axis from Abaqus analysis

The reason for this behaviour was seen in the stress contour plots of Abaqus which showed that the displacements remain in the $X=Y$ plane while the plastic zone remained less than 30% to 40% of the area of the section, but became out of plane when the plastic zones became more extensive. This is shown diagrammatically in Figure 3.14 which shows the cross-section of a column at mid-height. The cross-section is shown with an initial imperfection in the $Y=0$ plane, firstly with a small plastic zone and secondly with the plastic zone exceeding 50% of the area including the corners at A and B.

While the plastic zone is small, there is little reduction in stiffness to resist displacements in the $X=-Y$ plane, so the deflections remain in the $X=Y$ plane. As the plastic zone increases, it spreads across the corners at A and B so the stiffness to resist displacements in the $X=-Y$ plane is greatly reduced and the displacements increase in the direction of the initial imperfection.

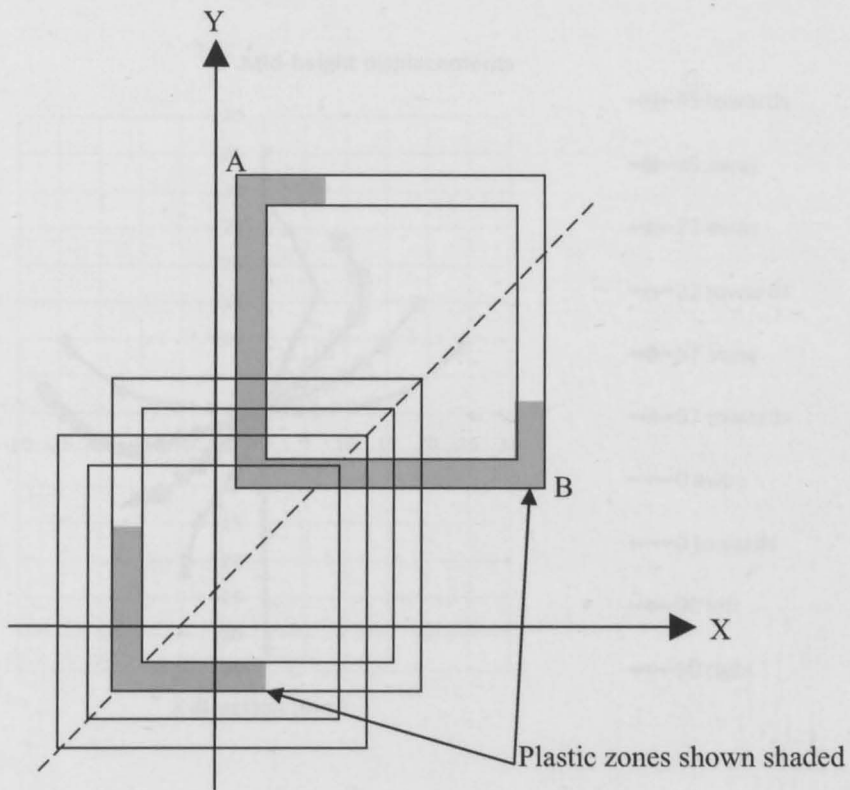


Figure 3.14 Spread of plasticity – column displacements in $X=Y$ plane

Where the initial imperfection is in a rectangular plane and the rotations are applied in other planes, similar behaviour is observed, as shown in Figure 3.15. This observation is important because it shows that the behaviour of the column at mid-height is not a simple function of the planes of the applied end rotations.

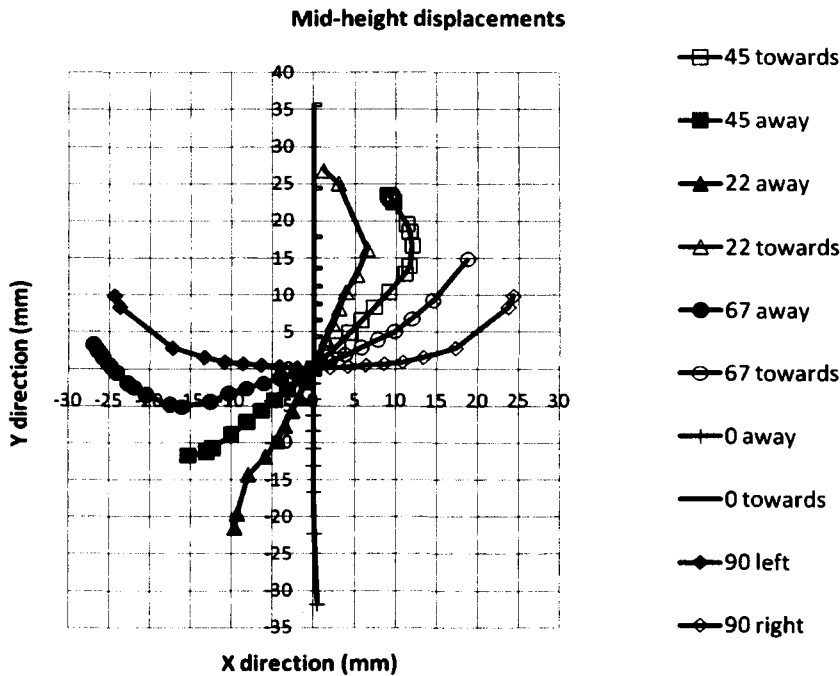


Figure 3.15 Mid-height displacements – rotation at 22.5° intervals

applied at 0°, 22.5°, 45°, 67.5° and 90° to Y=0 plane with imperfection in Y=0 plane.

Having seen that the column displacements might not remain in the plane of the applied end-rotations, it was observed that the design model might be kept simple by using bending about one rectangular axis only. This is verified by the parametric study in Chapter 8.

For simplicity the properties may be calculated assuming that they are concentrated along the mid-plane of the walls. An example is shown in Figure 3.10 in which the areas resisting axial compression are shown by single diagonal shading and the two areas resisting bending moment (one in compression and the other in tension) are shown, one with double shading and the other without shading.

3.4.6 Different end rotations at top and bottom

The design model proposed above assumes equal but opposite end rotations at the top and bottom of the column. In most structures and under most load cases, this will not occur. End rotations are generally not equal and opposite, but a design model allowing for this requires

uneconomic beam-column connection details and undesirable complexity of calculation to justify it, as explained below.

Connection details

One of the goals of this design approach is to allow simple beam-column connections made with thin column end-plates. Where columns are in double curvature, the end moments are usually too big to be resisted by thin end-plates, so the exploitation of the double curvature is in conflict with this goal.

Complexity of calculation

If the reversal of end moment is exploited to reduce the column deflections, the effect of the column end moment must be calculated both for the beams and for the columns. Another goal of this design approach is to allow the simplest possible analysis of the beams by making the analysis separate from the column behaviour, so incorporating the lesser end-rotation is undesirable.

Defining a simple column design model of the column in the elasto-plastic domain becomes extremely difficult for deformed shapes other than the symmetrical shape arising from equal and opposite end-rotations. This is especially difficult because the effects of plasticity so alter the stiffness of the member along its length that the behaviour is far from simple to predict.

Using the assumption of single curvature with end-slopes equal to the greatest slope at either end is always conservative. The conservatism might be questioned as uneconomic, but, the design method has the potential to allow much more economical columns than traditional methods available in columns with significant end-slopes.

The issue that does need to be considered for cases of double curvature is the issue of wall stability. Double curvature gives greater curvature for the same end rotation, so the wall stability is of greatest concern under double curvature.

3.4.7 Effect of lateral loads

Lateral load on the column increases the bending moment applied to the column. Because the design model assumes that the beams do not provide resistance to end-moments in the columns, the axial compression resistance cannot exceed the resistance of a pin-ended strut with lateral loading. This must always be checked.

Therefore the design equation derived from moment equilibrium at mid-height becomes:

$$N_{Ed} \left\{ \left(\frac{h}{2} \right) \theta + e_s \right\} + M_{Ed} \leq M_{N,Rd} \quad \text{Eq 3.12}$$

but $N_{Ed} \leq$ resistance of a pin-ended strut with the the same lateral loading

where M_{Ed} is the applied moment due to lateral loads on the column,

$M_{N,Rd}$ is the design plastic moment resistance reduced due to axial force N_{Ed} .

and e_s is the design value of imperfection derived from the buckling of a pin-ended strut using the design code specified for the particular structure.

3.5 Effects of breadth to thickness ratios of the walls of the members

Local deformations may reduce the buckling resistance of columns of either “open sections”, such as I-sections or H-sections, or hollow sections. The deformations might be caused

1. by local buckling of the parts in compression,
2. by radial loads caused by curvature of the member, or
3. by a combination of both 1 and 2 above.

This is recognised in most steel design codes by limiting the breadth to thickness ratios of the elements through a procedure commonly called “classification” of the cross-section.

The breadth-to-thickness ratios required for the new design method were investigated both in the full-scale laboratory tests (see Section 5.8) and in a parametric study (see Section 7.2). The laboratory test results were compared with the Abaqus analysis (see Section 7.3) and this comparison was used to define a calibration function (see Figure 7.9) which was used in Section 7 to define design limits for the breadth to thickness ratio shown in Figure 7.10.

3.6 Range of column end-rotations

It is important that the range of column end-rotations considered covers the range that might occur in practice. The maximum column end-rotations are caused by the maximum slopes of

the beams and these occur at the ends of simply supported beams rather than continuous beams. It must be remembered that the design method checks the columns at Ultimate Limit State, so the column end-rotations must be calculated at Ultimate Limit State also, not at Serviceability Limit State.

The calculations below are to the Eurocodes, following the guidance of SCI P 365 [SCI 2009]. Therefore the governing loading equation is 6.10(b) of EN 1990 [BSI 2002a, CEN 2002a], which gives the reduced partial safety factor on permanent loads of 1.25 together with the partial safety factor on variable loads of 1.50.

For a typical simply supported beam of longer span in residential construction

Beam span = 7.5 m, column spacing = 5.0 m

Assume

4.0 kN/m ²	for dead	× 1.25	=	5.00	kN/m ²
1.5 kN/m ²	for partition walls	× 1.25	=	1.88	kN/m ²
2.0 kN/m ²	for live	× 1.5	=	<u>3.00</u>	kN/m ²
Total			=	9.88	kN/m ²

Total load/m on beam = 5.0 × 9.88 = 49.4 kN

Firstly, find the beam size:

The bending moment in the beam is

$$wL^2/8 = 49.4 \times 7.5^2/8 = 347 \text{ kN-m} \quad \text{Eq 3.13}$$

The resistance of a 280 ASB 74 is

$$f_y W_{pl}/\gamma_{M0} = 355 \times 979 \times 10^{-3}/1.0 = 348 \text{ kN-m} \quad \text{Eq 3.14}$$

Therefore use a 280 ASB 74

Secondly calculate the end slope at Ultimate Limit State

The end slope assuming elastic behaviour is

$$\frac{1}{24} \frac{wL^3}{EI} = \frac{1}{24} \frac{49.4 \times 10^3 \times 7500^3}{210000 \times 121.9 \times 10^6} = 0.0339 \quad \text{Eq 3.15}$$

Therefore slopes of around 0.034 radians can be expected.

The above is only one example, but the order of magnitude remains valid for most practical cases because as the span increases, the beam size must be increased to provide sufficient bending resistance and the increased beam size provides greater stiffness. There also two other limitations that arise from code limits on deflections and from floor stiffness requirements to avoid unsatisfactory vibrations of the floor.

Deflection related limitations arise from the relationship between end slope and deflection under elastic conditions. Taking the case of a simply supported beam, the deflection is given by

$$\delta = \frac{5}{384} \frac{WL^3}{EI} \quad \text{Eq 3.16}$$

The end-slope is given by

$$\theta = \frac{1}{24} \frac{WL^2}{EI} = \frac{1}{24} \frac{384}{5} \frac{5}{384} \frac{WL^3}{EI} \frac{1}{L} = \frac{1}{24} \frac{384}{5} \delta \frac{1}{L} = \frac{16}{5} \frac{\delta}{L} \quad \text{Eq 3.17}$$

For brittle finishes, a common case for shallow floors in domestic construction, the deflection limit in BS 5950-1:2000 is L/360 under un-factored live load alone. If the live load is approximately 1/3rd of the total load, which is possible for domestic loading with concrete floors, and the factored load is 1.5 times the working load, then the end-slope at ULS is:

$$\theta = \frac{16}{5} \frac{L/360}{L} \times \frac{3}{1} \times 1.5 = \frac{16}{5} \frac{1}{360} \times 3 \times 1.5 = 0.040 \text{ radians} \quad \text{Eq 3.18}$$

This suggests that the range of end-rotations needs to extend to about 0.040 radians.

Vibration related limitations arise from the need to avoid very low natural frequencies in floor so that the dynamic response is limited to acceptable levels. Although it is now recognised that the dynamic response of floors depends on more than the natural frequency alone, it is advisable to design a floor to have a natural frequency above 3 Hz so that the natural frequency is separated from the frequency of walking activity. The natural frequency depends on the second moment of inertia of the beams, I, the span and spacing of the beams and the self-weight of the floor. A numerical investigation of this effect was conducted for both domestic and commercial floor loadings with floors designed with ASB beams and concrete slabs. The beam design was checked both for cross-sectional resistance and for natural frequency and showed that the beams have end slopes of about 0.034 radians when the natural frequency is limited to 3 Hz, whatever span of beam is used. This appears to give

a limit of beam slope even lower than the limit from deflections of brittle finishes described above and applies to beams without brittle finishes.

In addition to the slopes of the beams, the column end-slope is affected by sway of the building, so some allowance for a relatively small inclination from sway must also be made, probably of the order of 0.005 to 0.010 radians. This can be deduced from the SLS limit of $h/300$ limit on sway. Taking $ULS\ wind = 1.5 \times SLS\ wind$, then $ULS\ sway = 1.5 \times (h/300) = h/200 = 0.005h$, so the inclination of the columns = 0.005 radians. However, this has ignored second-order effects that must be considered at ULS, so the inclination might be greater than 0.005 radians, but not greater than 0.010 radians.

It should be noted that where continuous beams are used, the beam slopes can be expected to be less than calculated above for simply supported beams. Therefore it was concluded that the design method must allow for column end-rotations up to 0.040 to 0.050 radians and so the laboratory testing and parametric studies should cover this range.

3.7 Summary

A design model has been proposed for square hollow sections (SHS) that uses the moment shedding behaviour recorded by Gent [Gent 1966]. The model uses classic plastic cross-sectional resistance calculations with rectangular stress-blocks together with rigid-plastic behaviour modified by application of an imperfection. The imperfection is derived so that at zero applied end-rotation, the resistance to axial compression is equal to the resistance of a pin-ended strut.

The model assumes that the beams behave as beams on knife-edge supports without any affect from the columns. The columns are designed with equal and opposite end-rotations top and bottom (ie single curvature), taking the end-rotation equal to the greater of the beam rotations at the top or bottom of the column. The model assumes no stabilizing action is provided by floor construction (beams and/or slabs).

The breadth to thickness ratio of the wall of the SHS has been identified as an issue that should be studied to avoid local instability. Initial calculations show that the limits in current codes are not sufficient for columns with higher end-rotations designed with the new method.

Parametric studies are required to confirm two aspects of the new design model:

1. To confirm that the design value of the initial imperfection can be reliably taken as the strut imperfection, e_s , proposed in Section 3.4.4.
2. To establish what breadth-to-thickness ratio is required for different column end-rotations.

These parametric studies were conducted using Abaqus finite element software calibrated with the results of laboratory tests conducted with full-size columns, as described in the following chapters.

The bending moment calculated in the design model comprises two components. The first is the moment due to end rotation caused by the beam rotations. The second is the component to allow both for imperfections (geometrical and residual stresses) and the difference between the actual stress distribution and the classic rectangular plastic stress blocks used in the model. The first is always conservative because it assumes that the column is rigid between the beams and the hinge at mid-height. The second is always conservative because the actual stress distribution becomes closer to the rectangular plastic stress distribution at end-rotations higher than occur at the pin-ended strut buckling condition at which the imperfection is calibrated. Therefore the design model is expected to be conservative.

4 ANALYSIS TOOLS

4.1 Introduction

4.1.1 General

The analytical studies reported in this thesis were performed in two phases. The first phase used a finite slice model (developed by the author and described in Appendix F) to confirm the general principles of the design approach which led to the initial version of the design model [King 2006]. The second phase included both a programme of testing of full-scale columns, reported in Chapter 5, and a parametric study using ABAQUS finite element software that was used to confirm and refine the design model. The results of the full scale tests were compared with ABAQUS analysis of the test specimen as reported in Chapter 6. The results of these comparisons were used to refine the design model by applying an appropriate calibration factor to the results of the parametric study.

The analyses included the effects of non-linearity of both geometry and material behaviour and also the effects of residual stresses and of initial geometrical imperfection. Throughout the analyses, it has been assumed that the values of resistance calculated from the appropriate structural code are correct when the straightness tolerance is as defined in Section 4.1.2. This assumption was used to derive the appropriate magnitude of residual stress. The effect of initial imperfection in a plane that is not a rectangular plane was investigated for a few cases.

4.1.2 Initial geometrical imperfections

The initial geometrical imperfection is taken as a half sine curve. Imperfections are taken as acting in only one plane at a time for frame analysis in both BS 5950-1 [BSI 2000a] and EN1993-1-1 [BSI 2005a, CEN 2005a]. Therefore, in these analyses, the initial imperfection was generally applied in one plane at a time. Figure 4.1 shows the case when the initial imperfection is in the same rectangular plane as the deflection due to the end-rotations of the column imposed by the rotations of the beams. This results in deflections in only one plane.

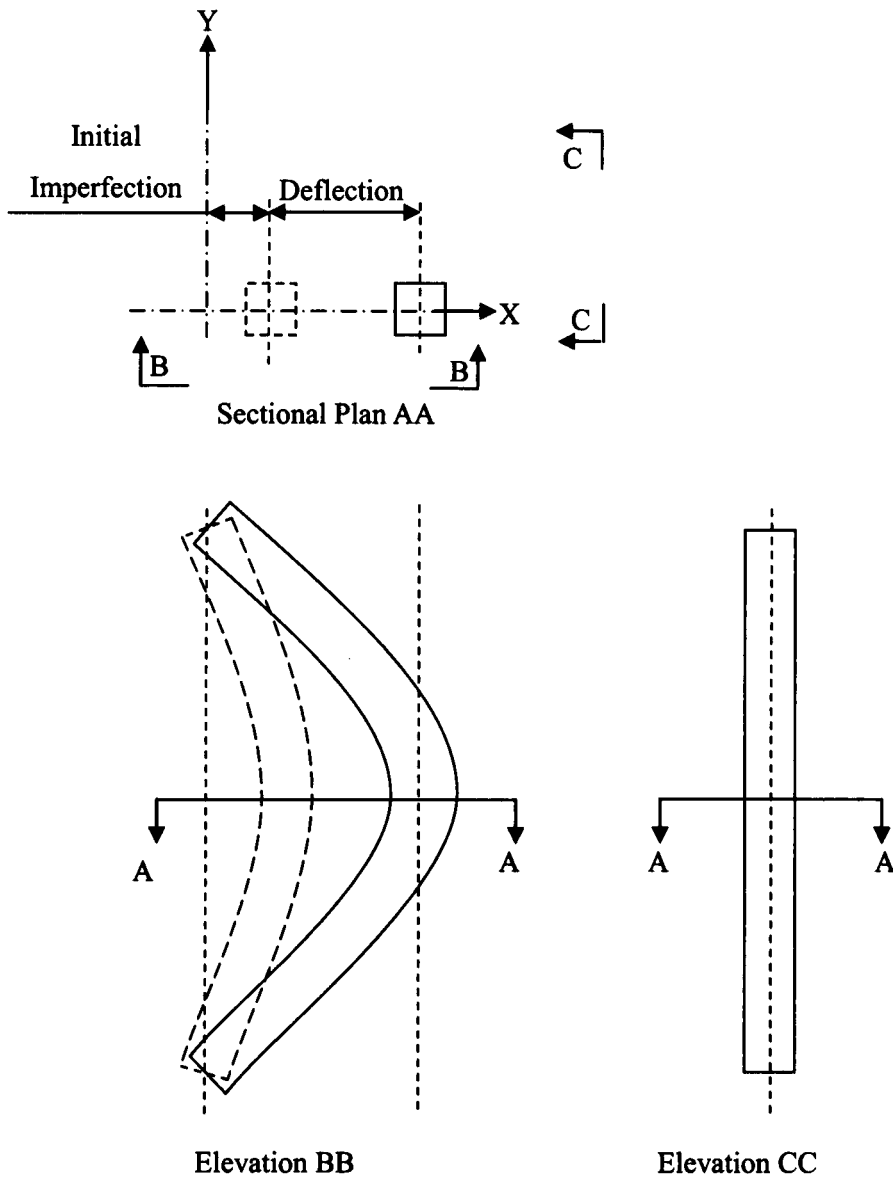


Figure 4.1 Imperfection and deflections in one plane only

Figure 4.2 shows the case when the initial imperfection is in the rectangular plane orthogonal to the deflection due to the end-rotations of the column imposed by the rotations of the beams. This results in deflections in the two rectangular planes.

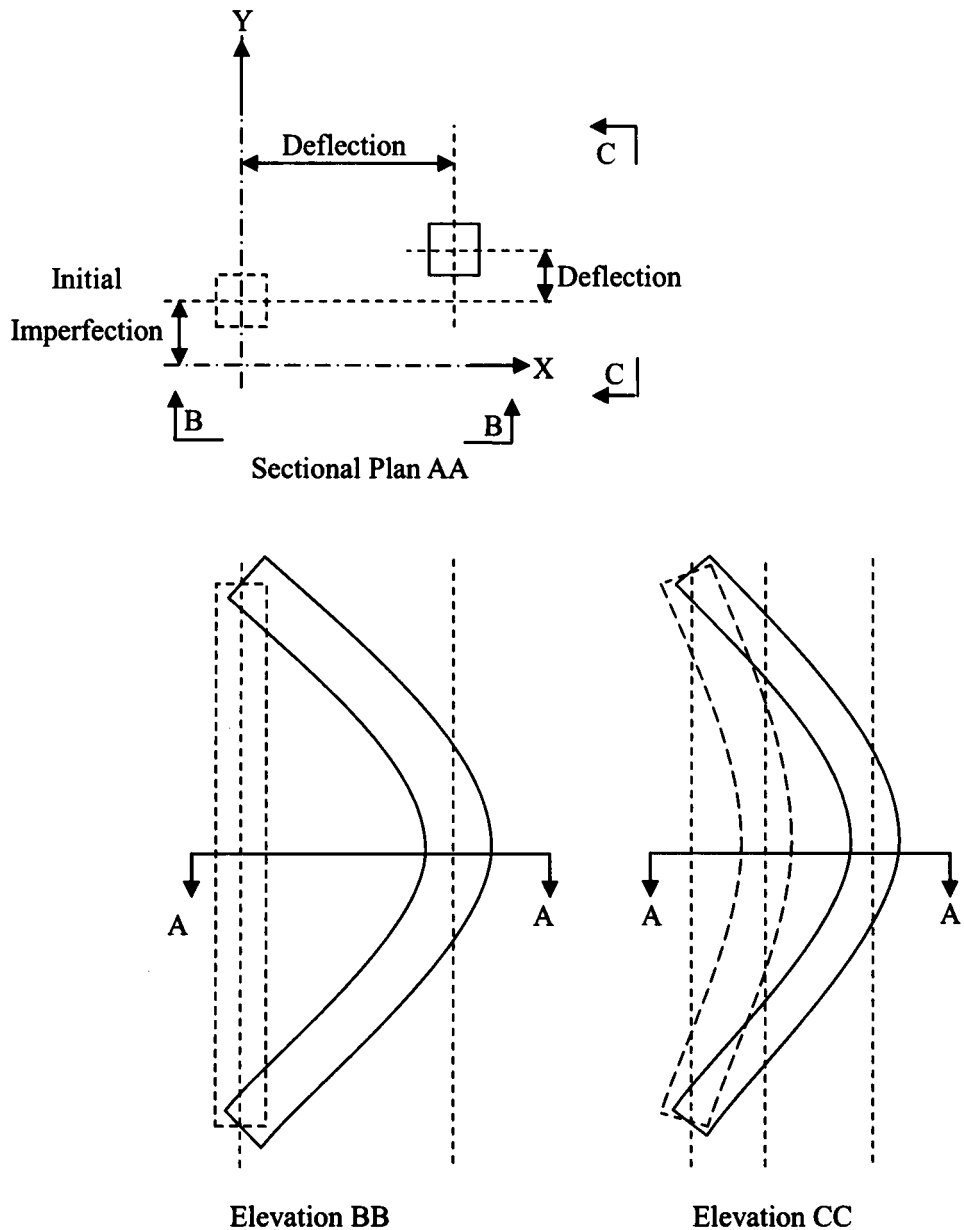


Figure 4.2 Deflections in two planes

The magnitude of initial imperfection used is $length/1000$. This magnitude corresponds to the principal manufacturing tolerance in BS 5950-2 [BSI 2001] and in the National Structural Steelwork Specification [BCSA 2002]. The manufacturing tolerance allows a 6mm deviation from straight in all members. In a 3 metre long member, this is $length/500$ which is much greater than $length/1000$. However, this 6mm deviation would result in column resistances significantly below the buckling curve for hot-finished SHS. Therefore, a choice has to be made between:

1. analysis with the worst tolerance (in addition to residual stresses), or

- analysis with a tolerance (in addition to residual stresses) that agrees with the strut buckling curves in the design code.

It was decided to conduct the analysis to agree with the strut buckling curves in the design code BS 5950-1 [BSI 2000a] so that the design method converges with the code method for columns which have no imposed end rotation.

The effect of an initial imperfection not in a rectangular plane was investigated for a few cases in the Abaqus parametric study reported in Chapter 8 by using an imperfection in the $X = Y$ plane and end-rotations in the $X = Y$ plane resulting in deflections in $X = Y$ plane as shown in Figure 4.3.

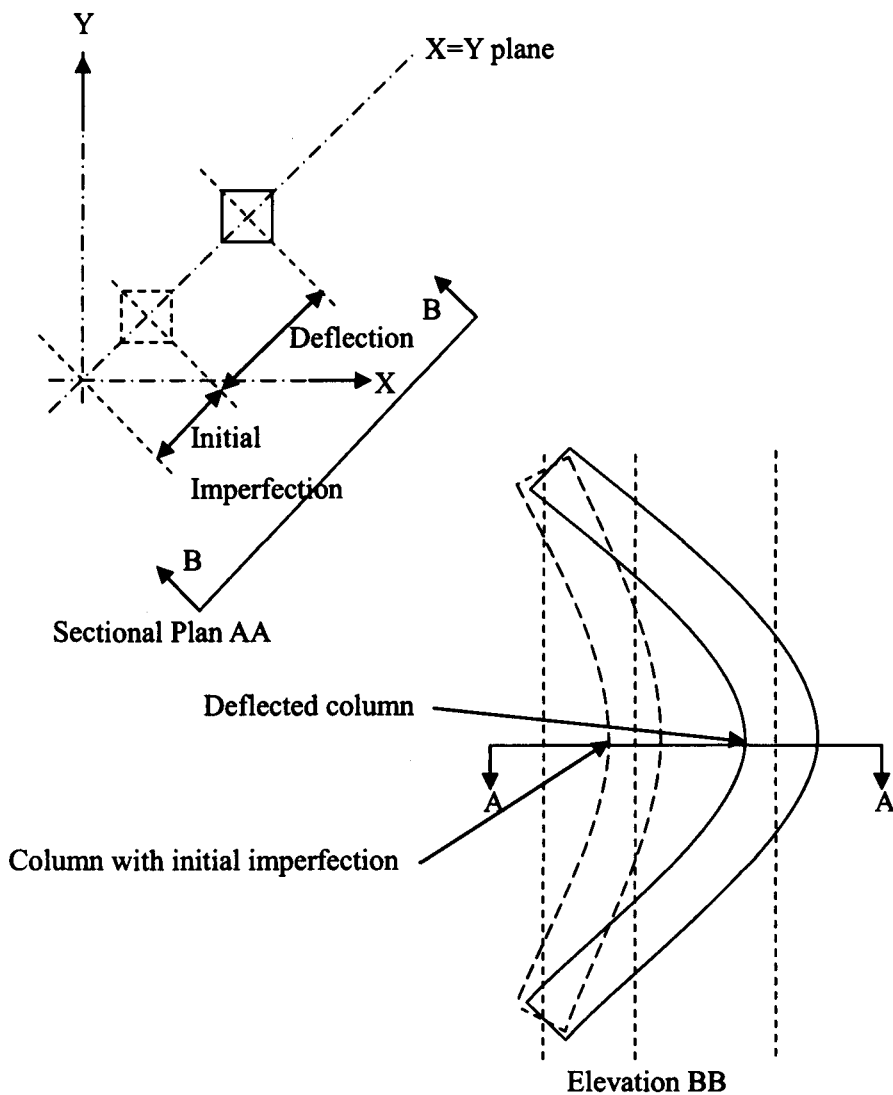


Figure 4.3 Imperfection and deflections in the $X = Y$ plane

The finite element model used the same residual stress as previously derived and the magnitude of the initial imperfection was chosen so that the resistance of a pin-ended column with the imperfection in the $X = Y$ plane was equal to the resistance of the same column with the imperfection of length/1000 in one rectangular plane. This magnitude was found to be $0.75 \times \text{length}/1000$ in both rectangular planes, which in the $X = Y$ plane is $\sqrt{2} \times 0.75 \times \text{length} / 1000$, which is $1.06 \times \text{length} / 1000$ in the $X = Y$ plane.

4.2 Finite slice model

4.2.1 Description of analysis tool

The first step in developing the new design model was to find an analysis tool that can analyse columns at different end rotations very accurately over a wide range of members and end rotations. Study of the results from these analyses stimulates ideas for possible simple design models and shows potential complications. An analysis tool was developed for Square Hollow Sections which are the column sections most commonly used in frames with discontinuous columns. The tool is a multiple-page Excel spreadsheet which finds the compression resistance by a series of iterations. This considers flexural buckling about both principal planes. It does not consider any torsional deformations, but these do not affect normal hollow sections. The analysis divides the length of the member into 30 sections, so that there are 31 cross-sections at which analysis is made. The input data includes the length, the yield stress, the section properties, residual stresses and the geometrical imperfection taken as a half-sine curve along the length of the member in either of the principal planes, or in both principal planes if required. The section properties are applied in the form of wall width and thickness that give the area and inertia of the specified SHS but allows the cross-section to be simplified to four walls of constant thickness with perfectly square corners. The model and the analysis spreadsheets are described in Appendix F.

At each analysis cross-section, the stress distribution is found for equilibrium with the applied axial compression, N , at the deformation arising from the current curvature. To date, the stress distribution includes the effects of plasticity in compression only. Therefore, the equilibrium stress distribution currently must be checked to ensure it does not exceed yield in tension.

4.2.2 Residual stresses

The residual stress distribution used was parabolic as shown in Figure 4.4. The parabolic distribution was used because the finite slice had been developed originally for I-sections and parabolic distributions have been used for these sections by various researchers [ECCS 1976, Galambos 1998]. For the preliminary investigation of this design method using structural hollow sections, it was decided to use the finite slice analysis software using the same form of distribution as I-sections to avoid delay. This distribution was assumed to exist in all four sides of the SHS. The magnitude of the maximum compressive residual stress, f_{rmax} , is 10% yield stress. This magnitude was chosen because it gave the best agreement between calculated column resistance and the column resistance calculated using BS 5950-1:2000 for hot-finished SHS when using the initial geometrical imperfection of length/1000.

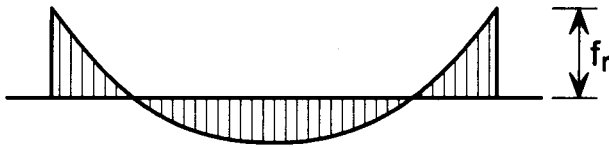


Figure 4.4 Parabolic residual stress pattern (on all sides)

4.2.3 Validation of the column analyses

Validation of the analyses was done by the following steps:

1. Validation of elastic range by checking the elastic critical buckling load for known modes with Sine curve displacements.
2. Validation of elastic behaviour by comparison with the BS 5950-1 strut buckling curve using the code value of the Perry-Robertson imperfection and with the residual stress set to zero.
3. Validation of the elastic-plastic range for a column in single curvature with severe end-slopes by pencil and paper checks. Firstly, the input curvature was taken from the second-order elasto-plastic analysis spreadsheet and used to calculate the deflected form. Secondly, the equilibrium of the sections was checked by drawing the strain and stress diagrams on graph paper and calculating the bending moment and axial force resisted. Finally the equilibrium of the axial force at the eccentricity of the deformed shape was compared with the bending moment resisted.

4.3 ABAQUS finite element model

4.3.1 Change from finite slice to Abaqus finite element analysis

The finite slice model was useful as an initial analysis tool. Firstly, creating the finite slice analysis tool required detailed consideration of all aspects of the structural behaviour. Secondly, the simplicity arising from using entire slices helped to identify the design model. However, the finite slice model has disadvantages:

1. It cannot consider the effects of wall thickness and local out-of-plane deformations.
2. It requires a lot of time and attention to converge even in the simplest cases.
3. It is a “custom-made” analysis tool, so it does not have the credibility of an established finite element analysis software package.

Therefore it was decided to change to a well-known finite element analysis software. Abaqus was selected because it is used by the University of Sheffield and was used by Professor Greiner and his co-workers in the derivation of the rules for calculating resistance of columns to combined axial compression and bending for Eurocode 3 Part 1.1 [BSI 2005a, CEN 2005a], described in detail in ECCS No 119 [ECCS 2006].

4.3.2 Analysis method

The analysis method is the finite element method. The analyses used geometric non-linear and material non-linear solutions. The model used shell elements with the nodes and the mid-thickness of the elements in the plane of the centre-line of the walls of the column. This results in a model with square corners, which is slightly different from the tight radius corners of hot-formed SHS sections. The ends of the model are connected to a “spider” of rigid-body elements, whose legs radiate the point of intersection of the centre-line of the column and the plane of the end of the column. Most analysis was conducted using a model of the entire column as described in Section 4.3.3. The effect of mesh refinement was checked by using a half-model that comprised a column cut longitudinally along the centre-line of two opposite sides as described in Section 4.3.4.

4.3.3 Full model

The mesh of the finite element model is shown in Figure 4.5. The same proportions of elements, along the length of the member, and the same number of elements were used for all full models, whatever the member length. The element mesh of the walls divides each wall into 6 elements across the width. Details of the model are given in Appendix C.

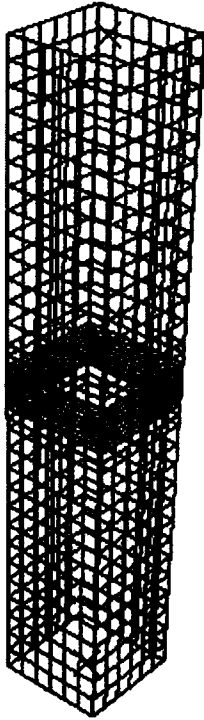


Figure 4.5 Finite element model mesh of full model

4.3.4 Half model

To check the sensitivity of the model to the element dimensions, the length of all the elements was halved to produce a comparison of results. The number of nodes available is limited to 1000 in the student edition of Abaqus being used. Therefore the model had to be reduced to one half, as shown in Figure 4.6.

Because of the 1000 node limitation, the mesh lengths are halved except at the bottom slice which remains at the original length because there are not enough nodes available. The model was made full length but half width to allow the tests to be modelled with the different eccentricity at each end. Details of the model are shown in Appendix C.

The output from the half-model showed no significant difference from the output from the full model.

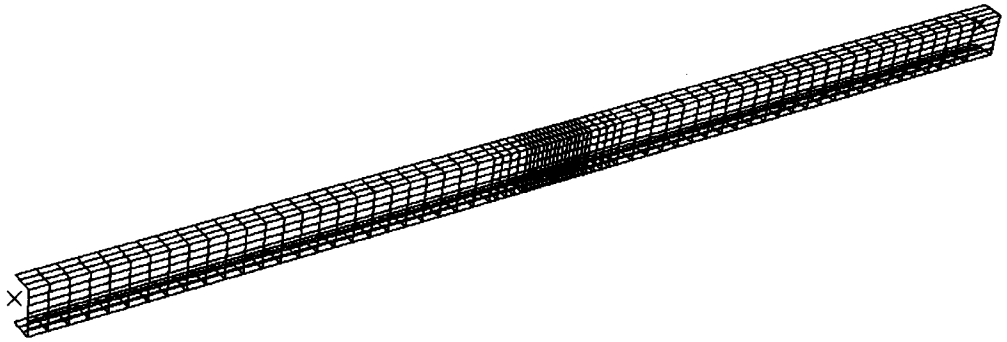


Figure 4.6 Finite element model mesh of half model

4.3.5 Residual stresses

For the finite element analysis, the pattern of residual stresses applied was slightly different from that used in the finite slice model. The stress pattern was taken as straight lines as shown in Figure 4.7. Straight line residual stress patterns were used by the authors of the rules for axial and bending in EN 1993-1-1 [BSI 2005a, CEN 2005a] as may be seen in Greiner et al [Greiner et al 1998]. The residual stress pattern used for structural hollow sections in the development of the rules for Eurocode 3 was chosen to reproduce the behaviour of cold formed sections, which is the method of manufacture used for the majority of hollow sections in Europe. The cold forming of the corners necessitates high residual stresses in the model. In contrast, this report considers hot-finished hollow sections, which are designed with compressive strength from higher buckling curves because the hot-finishing reduces the residual stresses. Having established that a residual stress of 10% yield stress gave strut buckling results very close to BS 5950-1 in the first phase of the analysis, it was decided to try this magnitude with a simple straight line stress distribution as used by the authors of the rules for axial and bending in EN 1993-1-1 [BSI 2005a, CEN 2005a] for the webs of hot-rolled I and H sections. This pattern was assumed to exist in all four sides of the SHS. The value of 10% yield stress was adopted because it gave the best agreement between calculated column resistance and the column resistance calculated using BS 5950-1:2000 for hot-finished SHS when using the initial geometrical imperfection of length/1000. The residual stresses were introduced by the technique of applying a temperature to the walls such that the intended residual stresses result.

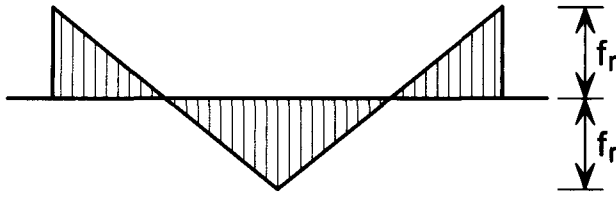


Figure 4.7 Bi-triangular residual stress pattern (on all sides)

4.3.6 Comparison with design codes

The maximum load for a 140×140×10 SHS with yield stress of 355 N/mm², pin-ended and 3.0m long, calculated to BS 5950-1 is 1550 kN according to the SCI Blue Book (SCI 2001).

The section in Abaqus that is used to model a 140×140×10 SHS is a square section with the dimensions from mid-plane to mid-plane of the walls of 130mm×130mm. The walls modelled with shell elements of thickness 10mm and no radii at the corners. This section has an area of 4×130×10 = 5200 mm². The maximum load from the model when analysing with the yield stress of 355 N/mm², initial geometrical imperfection of L/1000 and residual stresses of 10% yield as Figure 4.7 is 1582 kN. When this load is multiplied by the ratio of the model area to the nominal SHS area, it is reduced to (5090/5200)×1582 = 1549 kN. This is almost exactly the resistance calculated from BS 5950-1 showing that the use of an initial geometrical imperfection of L/1000 and a residual stresses of 10% yield as Figure 4.7 is appropriate.

Calculated to EN 1993-1-1, the pin-ended strut resistance is 1492 kN:

$$\bar{\lambda} = \frac{\lambda}{\lambda_1} = \frac{\left(\frac{L_{cr}}{i}\right)}{\left(\pi\sqrt{\frac{E}{f_y}}\right)} = \frac{\left(\frac{3000}{52.7}\right)}{\left(\pi\sqrt{\frac{210000}{355}}\right)} = \frac{56.9}{76.4} = 0.745 \quad \text{Eq 4.1}$$

$$\phi = 0.5\left[1 + \alpha(\bar{\lambda} - 0.2) + \bar{\lambda}^2\right] = 0.5\left[1 + 0.21(0.745 - 0.2) + 0.745^2\right] \quad \text{Eq 4.2}$$

$$= 0.5\left[1 + 0.114 + 0.555\right] = 0.835$$

$$\chi = \frac{1}{\left[\phi + \sqrt{\phi^2 - \bar{\lambda}^2} \right]} = \frac{1}{\left[0.835 + \sqrt{(0.835^2 - 0.745^2)} \right]} = 0.826 \quad \text{Eq 4.3}$$

$$\therefore N_{b,Rd} = \frac{A\chi f_y}{\gamma_{M1}} = \frac{5090 \times 0.826 \times 355}{1.0} = 1492 \text{ kN} \quad \text{Eq 4.4}$$

There are differences in calculated resistance between design codes, for example BS 5950 and EN 1993-1-1, but this is not important because the design method adjusts the resistance according to the pin-ended strut resistance of the specified design code, as shown in Sections 9.2.3 and 9.2.4.

4.4 Summary

The analysis of columns was initially performed using a custom-made finite slice analysis. After the initial analyses, Abaqus finite element software was used with a finite element model of the entire column section. The sensitivity of the element shapes used was checked with a model of half of a column but with double the number of elements along the length of the model.

All the analyses incorporate initial geometrical imperfections and residual stresses which gave buckling resistance equal to that from BS 5950-1. The design model in Section 9.2 adjusts the resistance to agree with whatever design code is specified.

5 FULL SCALE LABORATORY TESTS

5.1 Introduction

Tests were conducted on full scale columns

1. To validate the analysis used to develop the design model
2. To investigate the effects of wall slenderness
3. To give confidence in the design method

As reported in Chapter 4, the analysis was done both by an iterative finite slice model, and also by Abaqus finite element analysis software using non-linear geometry with non-linear material properties. While Abaqus is regarded as a generally reliable software package, there is always scope for any analysis system to be applied in such a way that it does not model the structural behaviour correctly. This is particularly true in models considering instability where practical variations along a member of thickness, flatness, residual stress, yield stress and stress-strain relationship might cause behaviour not foreseen in the model. While the design model is broadly logical in its form, it required validation and calibration.

Early studies using elementary theory of plastic flow and simple slice models, as reported in Appendix E, had identified that the curvatures in the columns would cause major out-of-plane deformations in thinner walled columns. The proposed design model is based on the gross section of the column, so these deformations might make the proposed design model unsafe for columns with slender walls. These deformations are simulated by Abaqus, but such effects might be affected by aspects of the member that are not included accurately in the model, such as local geometric imperfections, variations in residual stresses or even variation of the stress/strain characteristics of the material. Therefore it is wise to assess the behaviour both by analysis and by full-scale testing.

The philosophy used in the proposed design method is entirely different to the philosophy to which most structural engineers are accustomed. Historically, designers regarded the onset of yield as defining the failure load. Since the development and application of plastic methods of design in the 1950s, many designers are accustomed to designing with plastic cross-sectional resistance, but many are not comfortable with plastic frame design. The proposed design method is only an extension of the fundamental principle of plastic design, that the designer is free to proportion a structure so that it develops the bending moment

diagram that is desired. However, the method is likely to be greeted with suspicion because plastic design has not been applied in this way in design offices for members sensitive to buckling. Therefore it was decided that laboratory testing of full scale columns was desirable to give designers the confidence to use the method.

5.2 The test programme

The test programme is shown in Table 5.1. All specimen were Celsius 355 120×120 Square Hollow Sections (SHS). Celsius is the brand name for structural grade hot-finished hollow sections produced by Corus to EN 10210 in steel grade S355J2H.

As one of the reasons for the testing was to validate the modelling and analysis, it was desirable to have more than one test so that repeatability could be investigated. The most common application of this column design philosophy is expected to be with thick wall columns to reduce the column section size to the minimum. Therefore there are more tests on sections with 10mm wall thickness.

Another reason for full scale testing was to study the effect of slender walls. To allow the wall slenderness effect to be compared with thick walled behaviour, the same size section was used but with thinner walls. Two wall thicknesses were chosen. Two tests on each wall thickness were conducted which was considered the minimum number of tests. More tests are always desirable, but testing budgets are limited.

Test no.	Specimen	
kc1	120 SHS × 5mm	pilot test
kc2	120 SHS × 5mm	pilot test continuation
kc3	120 SHS × 10mm	stable wall thickness
kc4	120 SHS × 10mm	stable wall thickness
kc5	120 SHS × 6.3mm	possible sensitivity to wall slenderness
kc6	120 SHS × 5mm wall	expect sensitivity to wall slenderness
kc7	120 SHS × 10mm wall	stable wall thickness
kc8	120 SHS × 10mm wall	stable wall thickness
kc9	120 SHS × 6.3mm wall	possible sensitivity to wall slenderness
kc10	120 SHS × 5mm wall	expect sensitivity to wall slenderness

5.3 Test rig

The test rig was defined by the need to have full-scale tests and to be able to conduct numerous tests for the budget available. The University of Sheffield laboratories have numerous test rigs available. The tests required full-scale specimens, so the hydraulic two-post rig, shown in Figure 5.1, was chosen because of the height of column that can be tested and the load that can be applied. The laboratory staff have extensive experience in testing with this rig. Although the rig is normally operated under load control rather than displacement control, with skill the displacement can be controlled by limiting the flow of oil from the pump to the jack. Using this control technique, very smooth curves were recorded on the falling branch of the plot of load versus displacement.



Figure 5.1 Test rig with column in position

The section size of SHS 120 was chosen because the failure load was well within the capacity of the jack in this rig. Therefore, even if the steel in the specimen was at the upper end of the yield range of S355 steel, the tests would still be successful.

The laboratory staff manufactured end-fittings or “shoes” to fit to the ends of the specimen without fastening. That avoided the expense of work on the specimen themselves, so the plane SHS sections supplied could be used directly. The shoe at the bottom of the test column is shown in Figure 5.2 and the shoe at the top of the column was similar. They articulated about a cylindrical pin. These shoes ensured that the deformation of the column was in one predetermined plane. The use of these shoes introduced some friction which was evaluated by the unload/re-load cycles. The shoes added 75mm to each end of the column ie the overall length of the strut is 2650mm from centre of roller to centre of roller.



Figure 5.2 Shoe at bottom of test column

5.4 Instrumentation

The instrumentation on each specimen was as listed in Table 5.2.

Table 5.2 Instrumentation on the specimen	
Note: In-plane and out-of-plane are defined with reference to the intended plane of displacement which is determined by the orientation of pins in the end shoes.	
Top	1 in-plane inclinometer 1 out-of-plane inclinometer
Middle	2 LVDTs in-plane, one on each side 1 LVDT out-plane
Bottom	1 in-plane inclinometer 1 out-of-plane inclinometer

The LVDTs were connected by wires to a spring-grip frame, known as the “thing”, shaped to avoid displacements arising from local deformations of the walls. It is shown in Figure 5.3 at the end of a column to show how it fits the section at all 4 corners.

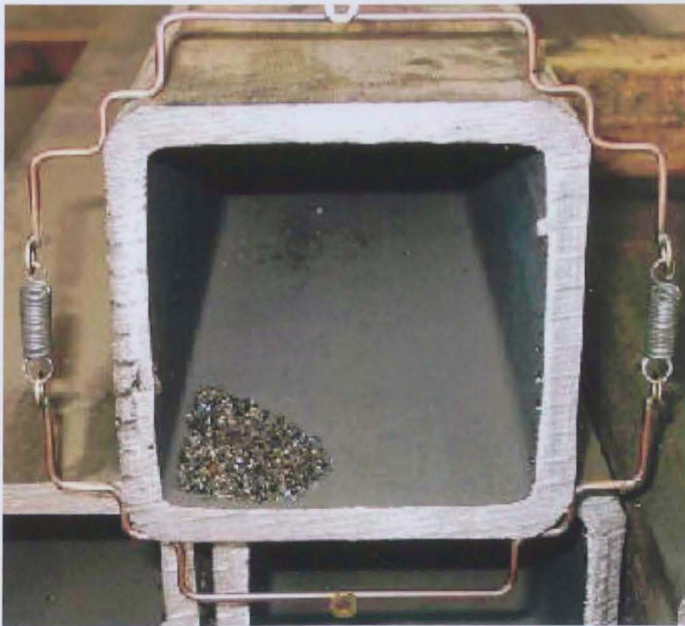


Figure 5.3 Spring grip frame, the “thing”, for LVDT connections

The inclinometers were attached directly to the specimen at 200mm from the centres of the pins. Only in-plane rotations were measured in the pilot tests, kc1 and kc2, and tests kc8, 9 and 10.

The axial shortening was measured by the ram movement. Therefore these measurements include the extension of the posts of the rig. The ram displacement within the jack was measured by an externally mounted LVDT on the lower loading platten and the jack force was determined by a pressure transducer fitted to the hydraulic circuit of the machine.

The test data was recorded to spreadsheets. The columns titled P were zeroed at the start. The channel numbers in tests kc3 to kc10 were as follows, though P 8 and P 9 were not recorded for tests kc 8, 9 and 10.

P 1 is the applied load in kN

P 2 is the in-plane rotation at the top (milliradians)

P 3 is the in-plane rotation at the bottom (milliradians)

P 4 mid height out-of-plane displacement (mm)

P 5 mid height in-plane displacement, rear (mm)

P 6 mid height in-plane displacement, front (mm)

P 7 ram movement (axial shortening), (mm)

P 8 is the out-of-plane rotation at the top (milliradians)

P 9 is the out-of-plane rotation at the bottom (milliradians)

5.5 Test duration

The duration of the tests is listed in Table 5.3. The strain rate was as slow as reasonably practical with the test equipment used.

Time	start to maximum load (mins)	maximum load to end (mins)	Total time (mins)
Test			
kc3	9.4	3.3	12.7
kc4	13.8	5.0	18.8
kc5	10.5	4.3	14.8
kc6	10.5	3.6	14.1
kc7	11.7	14.7	26.4
kc8	9.9	7.4	17.3
kc9	10.2	6.7	16.9
kc10	7.7	2.4	10.1

5.6 Material properties

The yield stress of the test columns were measured from coupons cut from most of the specimen after the tests were completed. The results were as follows:

Specimen	Thickness (mm)	Yield (N/mm ²)	UTS (N/mm ²)	Elongation %
kc1/2	5	396	548	27.5
kc3	10	375	530	35.0
kc4	10	390	530	35.0
kc5	6.3	428	561	25.0
kc6	5	389	540	24.0
kc7	10	not known	not known	not known
kc8	10	375	514	36.5
kc9	6.3	431	549	32.0
kc10	5	402	533	32.0

5.7 Test results

5.7.1 General

The test results proved to be broadly as predicted with all the tests showing a long falling branch after maximum resistance.

Different aspects of the results are discussed below. The general form of the results was very similar for all the tests, as shown by Figure 5.12, Figure 5.18 and Figure 5.19, except for the loss of strength due to local buckling in the thinnest wall sections at end rotations greater than 40 milliradians.

The tests on the 10mm, the 6.3mm and one 5mm wall thickness specimen included an unloading and re-loading cycle. This forms a hysteresis loop as described below.

5.7.2 The unloading/re-loading cycle

If the test were conducted at an infinitely slow strain rate and if there were no friction in the bearings, the unloading plot would be as shown in Figure 5.4. Under the same conditions plus the condition of no Bauschinger effect, the unloading/re-loading cycle would be as Figure 5.5. The Bauschinger effect causes a transition curve from the elastic reloading line to the line of the falling branch as shown in Figure 5.6.

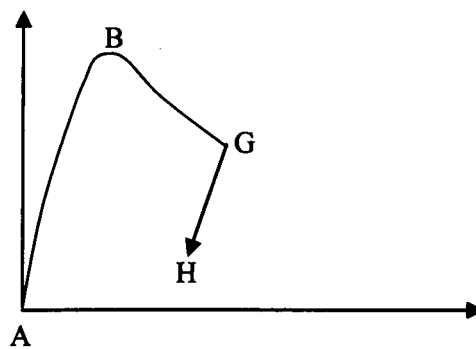


Figure 5.4 Unloading cycle with no friction in the bearings

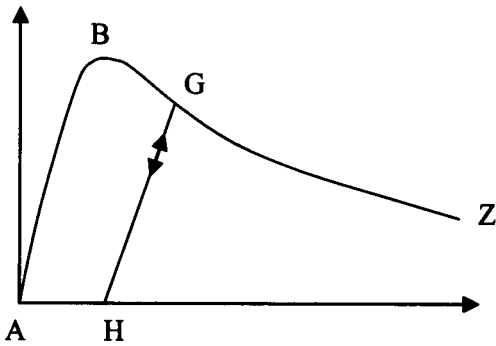


Figure 5.5 Unloading/re-loading cycle with no friction and no Bauschinger effect

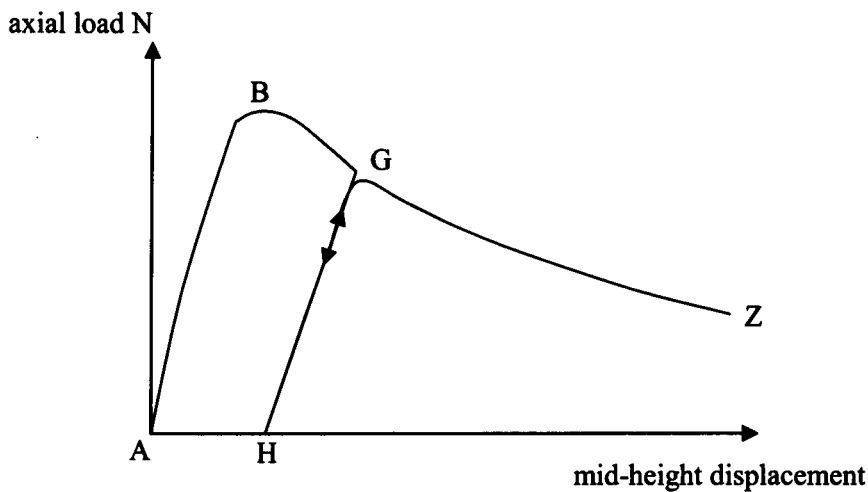


Figure 5.6 Unloading/re-loading cycle with no friction in the end fittings

The friction in the bearings at the two ends of the specimen causes moments that affect the plots because the friction always opposes the rotation of the ends. This effect can be seen in Figure 5.7 which shows the load v displacement plot of the unloading/re-loading cycle from test kc7 which had the widest loop. The total width of the loop is 1.2 mm at its widest between the unloading and loading paths, so the friction moment is equal to 0.6 mm times the axial compression. At the maximum axial load of 1290 kN, this gives a moment of 0.77 kN-m which is very small compared with the plastic moment of resistance of 87.3 kN-m.

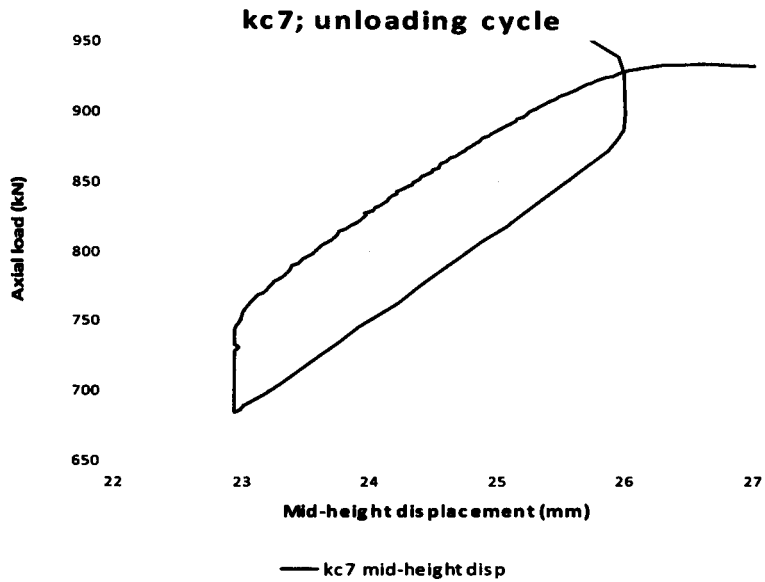


Figure 5.7 Unloading/re-loading cycle test kc3

The effect of the friction moments on the bending moment diagram in the column is determined by the movement of the ram. If there is no unloading cycle, in Figure 5.8, the ram is extending throughout the test from zero load at A through the point of maximum load at B and along the falling branch to Z.

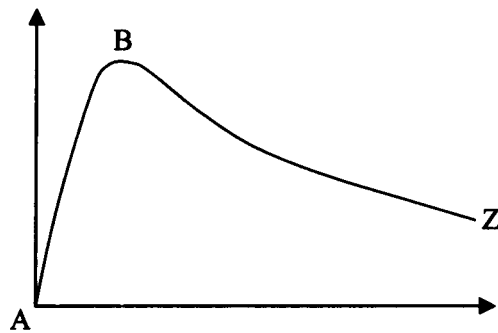


Figure 5.8 Rising and falling branches

The friction in the end fittings resists the extension of the ram and the increasing deformation of the column, so the bending moment in the column is of the form in Figure 5.9. This may be understood as the sum of the bending moment from [the axial compression \times the displacement of the column] minus the bending moment from the friction moment = μNr as shown in Figure 5.9.

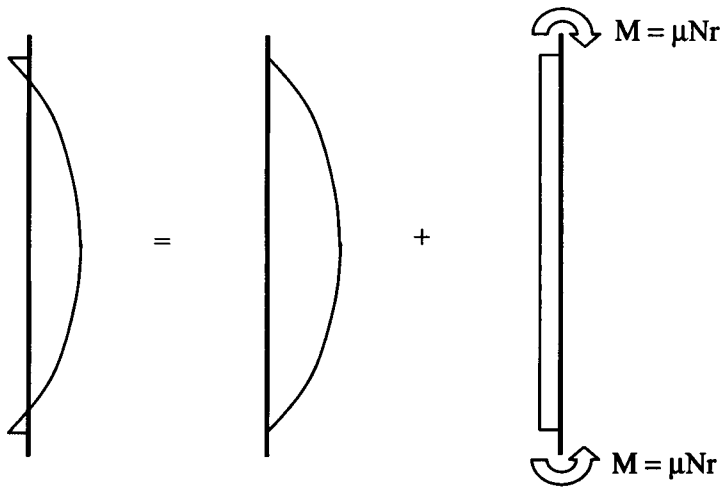


Figure 5.9 Bending moment for ram extension

The test curve including the unloading/re-loading cycle including the effect of friction is shown in Figure 5.10. The un-loading path is shown vertical from C to D as the friction moment reduces from opposing the buckling of the column to opposing the unloading. The unloading path is then inclined to represent the elastic behaviour from D to E. The reloading path starts vertically from E as the friction moment changes direction until at F the limiting friction moment is reached and the reloading path commences linearly towards F, with some small elasto-plastic effect expected due to the Bauschinger effect as the loading approaches the path CZ.

On the unloading path from C to D, the friction moments at the end fittings prevent the ends from rotating as the bending moment diagram changes from that in Figure 5.9 to that in Figure 5.11. On the re-loading path from E to F, the friction moments again prevent the ends from rotating as the bending moment diagram changes from that in Figure 5.11 to that in Figure 5.9.

On the unloading path from D to E, the friction in the end fittings resists the decreasing deformation of the column, so the bending moment in the column is of the form in Figure 5.11. This may be understood as the sum of the bending moment from [the axial compression \times the displacement of the column] plus the bending moment from the friction moment = μNr as shown in Figure 5.11.

On the reloading path from F to C, the bending moment diagram is again as shown in Figure 5.9.

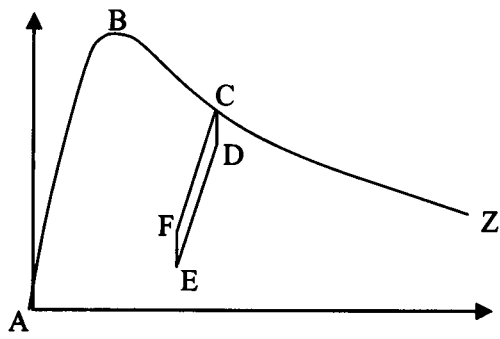


Figure 5.10 Rising and falling branches with unloading/re-loading cycle

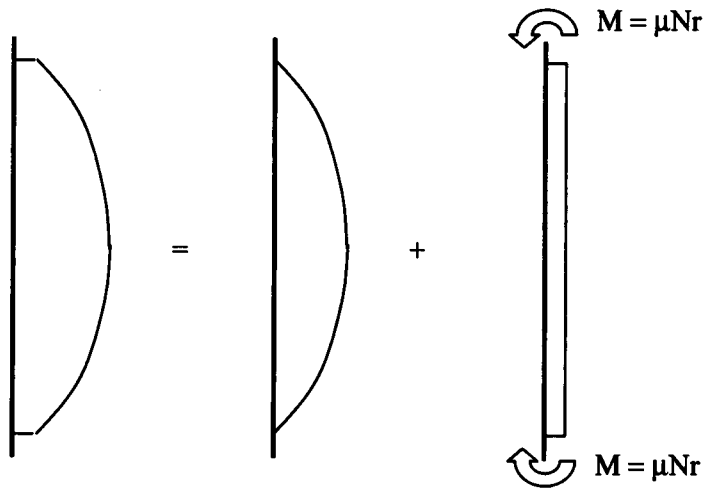
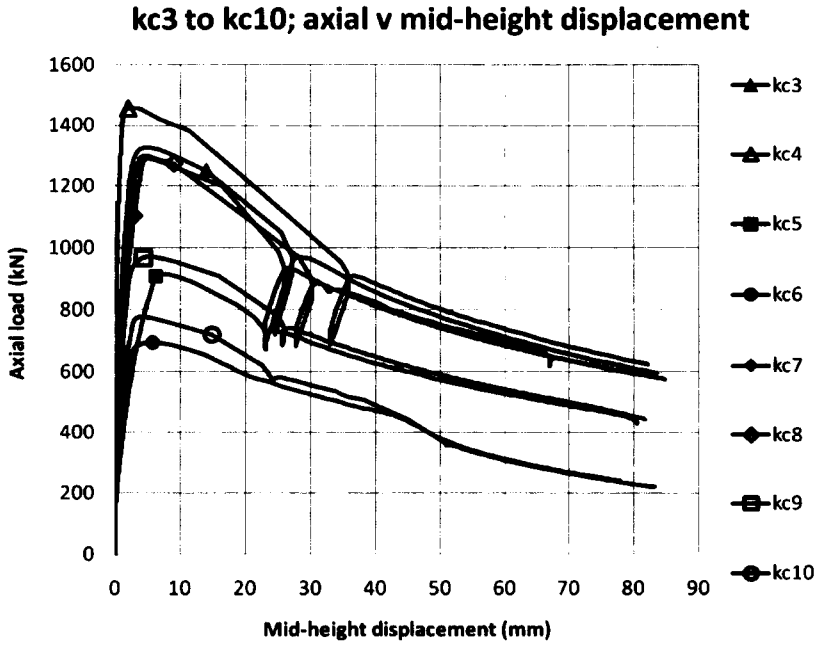


Figure 5.11 Bending moment for ram retraction

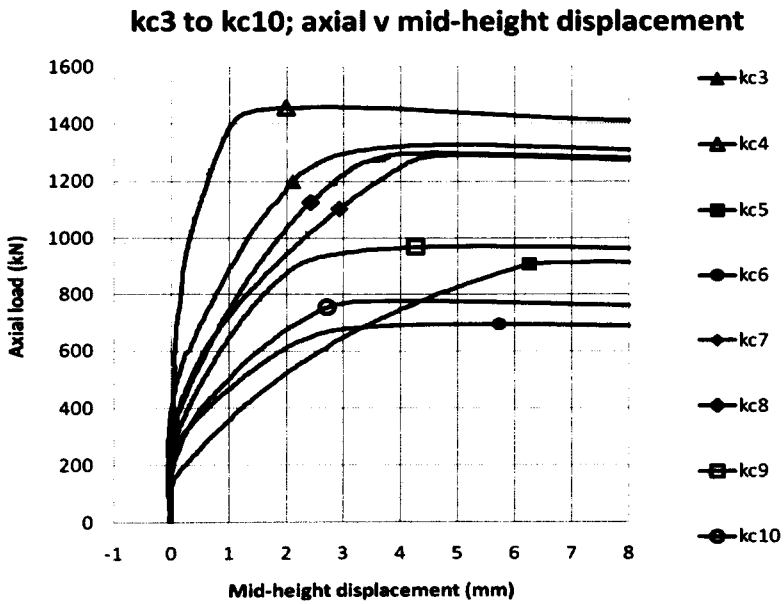
On the unload/re-load cycle CDEFC, the difference in the displacement arises from the difference in the bending moment diagrams in Figure 5.9 and Figure 5.11 which depends on the friction moment acting in opposite directions.

5.7.3 In-plane displacements

Plots of load versus mid-height displacement in the plane of buckling are shown in Figure 5.12.



The mid-height displacements differ between tests during the initial loading up to the maximum load. This is shown more clearly in Figure 5.13 which shows the displacements at a larger scale. This shows that the tests cover a wide range of imperfections as might be expected in practical construction.



The target initial imperfection for the tests was length/750 which is the maximum geometric imperfection expected to be permitted for hot-finished hollow sections in EN 1090-2 [BSI 2008, CEN 2008], the Standard giving straightness tolerances for the execution of structural steelwork to Eurocode 3, in Tables D.1.11, D.1.12 and D.1.15.

The straightness of each specimen was measured against a straight edge. The longest available straight edge was 1.5m long, so only the central half-length could be checked in detail. These checks showed that the straightness was better than the limit in EN 1090-2 [BSI 2008, CEN 2008] which would be 2mm over a length of 1.5m using length/750 as the limit or 1.5mm over 1.5m using length/1000. Generally the deviation from straight was found to be much smaller than 2mm, with values recorded from less than 0.05mm in 1.5m to 0.95mm in 1.5m on kc8.

The end-fittings used for the tests were designed to allow some adjustment of the position of the column with respect to the pivots which are the points of application of load. This was controlled by the horizontal screws that are visible in Figure 5.2. However, it is not easy to control the position precisely.

It is possible to estimate the actual position of the columns in the rig from the plots of end rotation versus load in the elastic range of loading. The estimates are approximate because the end-rotation depends on the shape of the initial imperfection along the entire length of the column. However, if the column were perfectly straight, the end positions are simply calculated from the end rotations. It is also possible to estimate the initial bow of the column from the change of end-rotations and the change of mid-height displacement with change of axial load.

The mid-height displacements are plotted in Figure 5.14 for 10mm wall thickness, in Figure 5.15 for 6.3mm wall thickness and in Figure 5.16 for 5.0mm wall thickness. In these figures, the test displacements are compared with the mid-height displacement expected from a 3.0mm half-sine curve initial imperfection assuming entirely elastic behaviour. The 3.0mm value is used simply to give a comparison against an imperfection of the appropriate order of magnitude. (A tolerance of length/750 on a length of 2650mm is 3.5mm, but friction would reduce the expected deflections below those arising from the imperfection, making 3.0mm a reasonable comparator.) From these figures, it can be seen that the test behaviour varies significantly from that of a half-sine imperfection.

10mm wall SHS; mid-height displacement comparison with 3mm half-sine impn

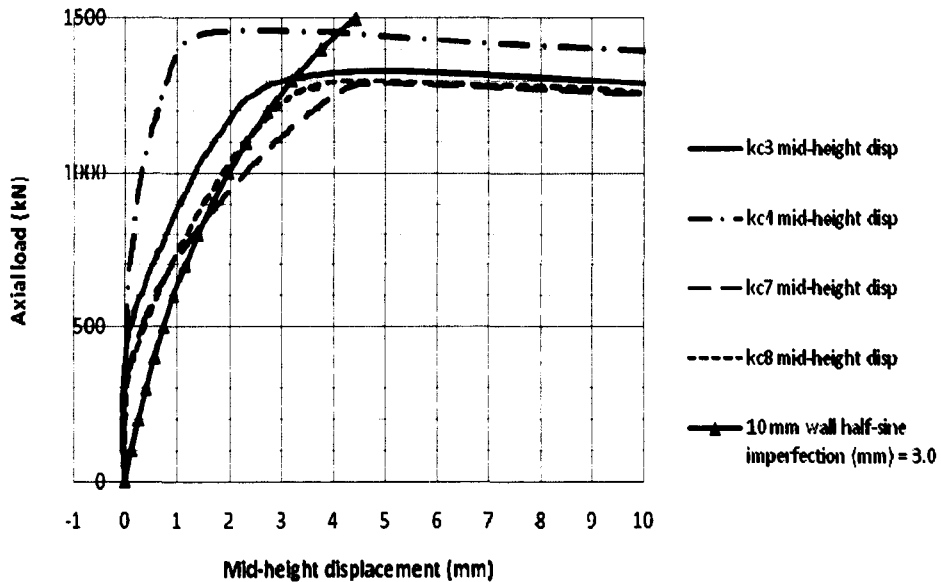


Figure 5.14 10mm wall SHS, mid-height displacements v 3mm half-sine

6.3mm wall SHS; mid-height displacement comparison with 3mm half-sine imperfection

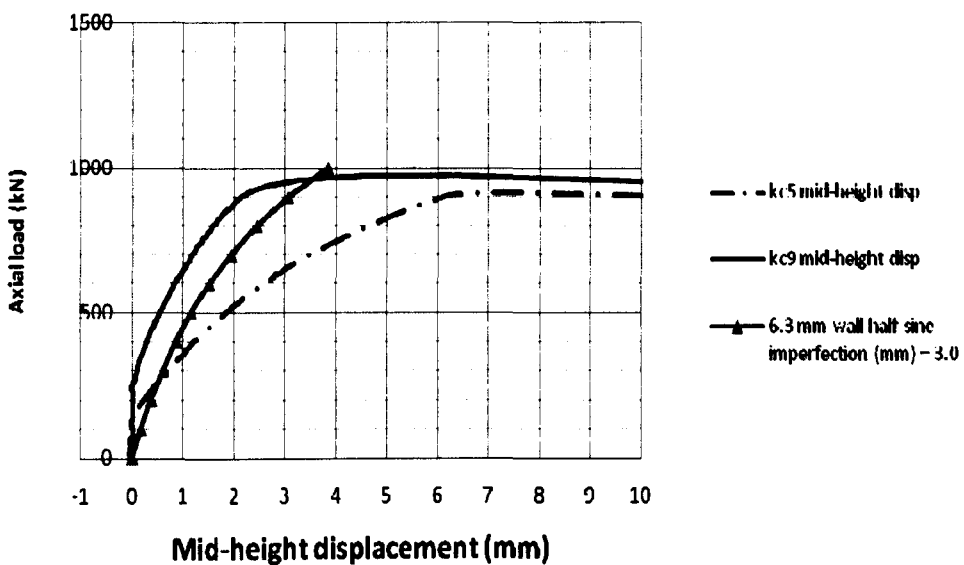


Figure 5.15 6.3mm wall SHS, mid-height displacements v 3mm half-sine

5mm wall SHS; mid-height displacement comparison with 3mm half-sine imperfection

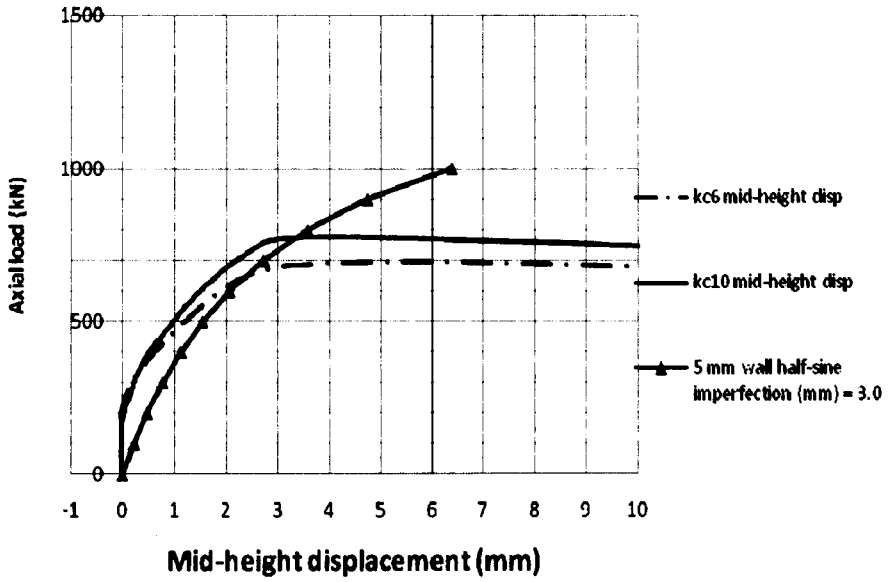


Figure 5.16 5mm wall SHS, mid-height displacements v 3mm half-sine

5.7.4 Out-of-plane displacements

It was intended that the out-of-plane displacements should be limited to small values relative to the in-plane displacement by the design of the end fittings. The plots in Figure 5.17 show that this was achieved for the large in-plane displacements along the falling branch. At the point of maximum load, both the range of out-of-plane displacements and the range of ratios of out-of-plane displacement to in-plane displacement was considerable, as shown in Figure 5.17 and Table 5.5 .

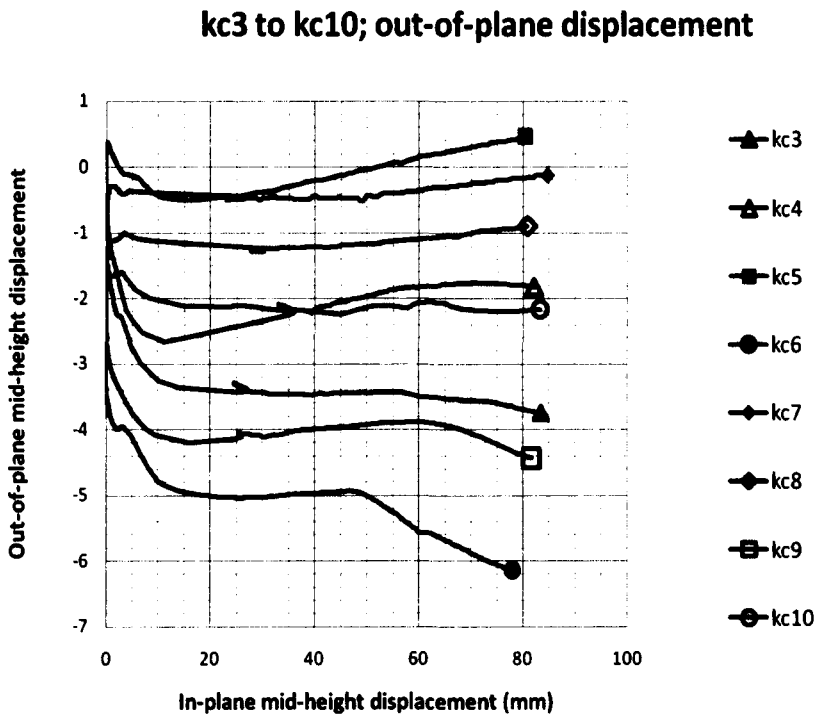


Figure 5.17 Load v mid-height displacement (out-of-plane)

Table 5.5 Ratio of out-of-plane to in-plane displacements at maximum load								
Test	kc3	kc4	kc5	kc6	kc7	kc8	kc9	kc10
Ratio	0.55	0.71	0.04	0.74	0.07	0.23	0.69	0.41

5.7.5 In-plane end rotations

Plots of load versus mean end-rotation are shown in Figure 5.18. This shows that the load/end-rotation from all the tests have long falling branches as expected. The figure also shows the design values of resistance of the sections when calculated to EN 1993-1-1 as pin-ended struts.

The plots for the two tests on specimen with 5mm wall thickness show marked reductions in resistance below the general trend due to local wall buckling. This was predicted, as discussed in Chapter 7 and Appendix E. It is interesting to note that kc10 has a higher maximum resistance than kc6 but has a lower rotation capacity before the dramatic loss of resistance at about 50 milliradians. This suggests that the lower yield of kc6 produced a more uniform curvature which was lower than the curvature of kc10.

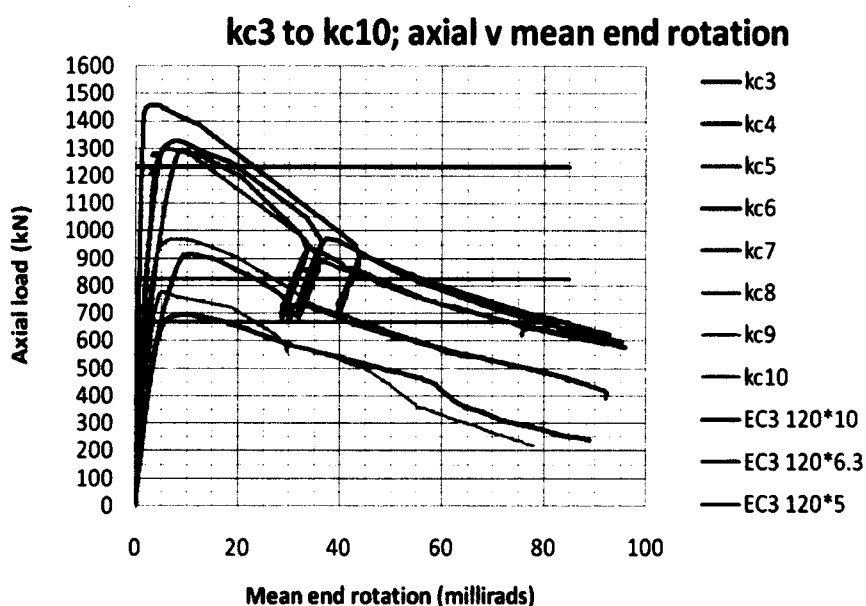


Figure 5.18 Load v mean end-rotation

Plots with the maximum load normalised to 1000kN are shown in Figure 5.19. These plots show how similar the behaviour is up to the rotation at which local instability of the wall precipitates a drastic loss of resistance. It is difficult to identify the individual tests in Figure 5.19, but the important point is that all the tests are similar except the 5mm wall tests drop significantly from about 40 milliradians.

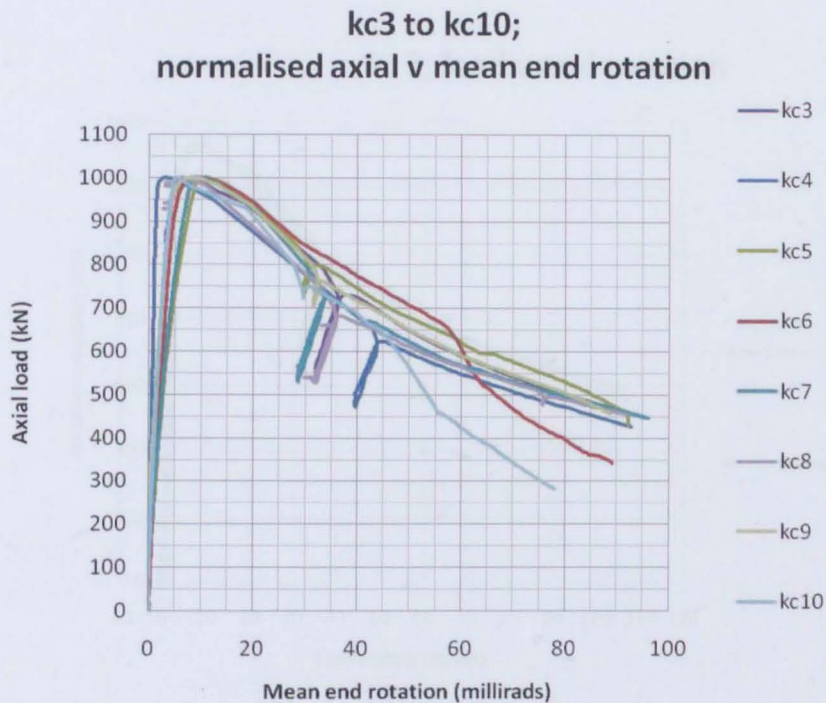


Figure 5.19 Normalised load v mean end-rotation

5.7.6 Difference in rotations at each end

The least welcome observation was that the end rotations at top and bottom of the specimen were different as shown below in Figure 5.20 to Figure 5.31. These figures show the end-rotations at top and bottom of each test with a plot of the difference between the end-rotation and the mean of the end rotations.

The comparison of the tests with the analyses reported in Chapter 6 indicates that the primary reason for the difference in the zone from zero to maximum load almost certainly is sway of the rig, as discussed in that chapter. The stability of the column is governed by the bending moment at mid-height, so the most reliable measure of end-rotation is the mean end-rotation. In the zone beyond maximum load, the proportion of the member that is strained beyond yield is very large, so there is little elastic stiffness remaining. Therefore, normal expectations of structural behaviour are not fulfilled. With such extensive plasticity, the probable reasons for the difference in end rotations are either the slight variation of stress-strain curve or the slight variation of wall thickness along the member. Even slight variations could cause asymmetry of the curvature about the mid-height of the member, resulting in asymmetry of end-rotations. As a result of these observations, the analysis of the results was made using the mean value of the end-rotations.

kc 3; load v end rotation

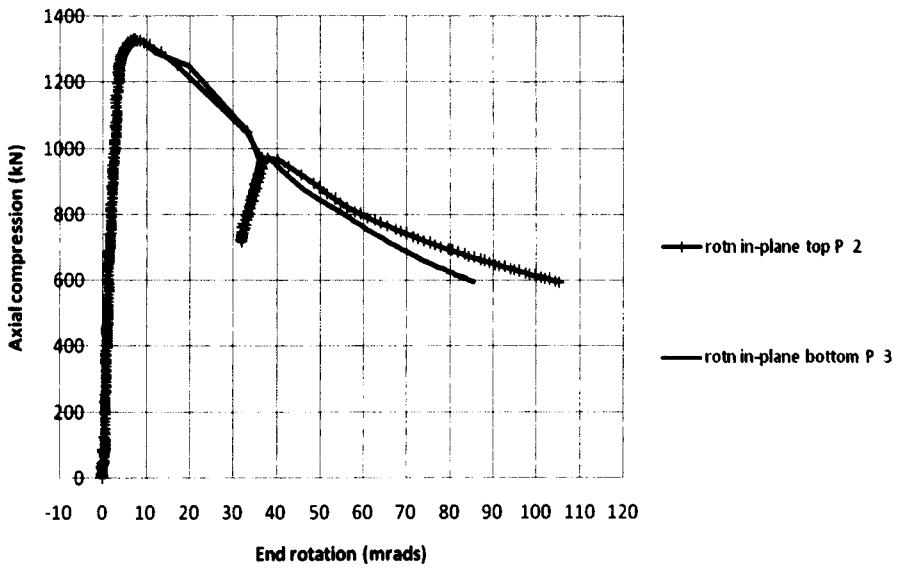


Figure 5.20 kc3 end rotations

kc 3; difference from mean end rotation



Figure 5.21 kc3difference from mean end rotation

kc 4; load v end rotation

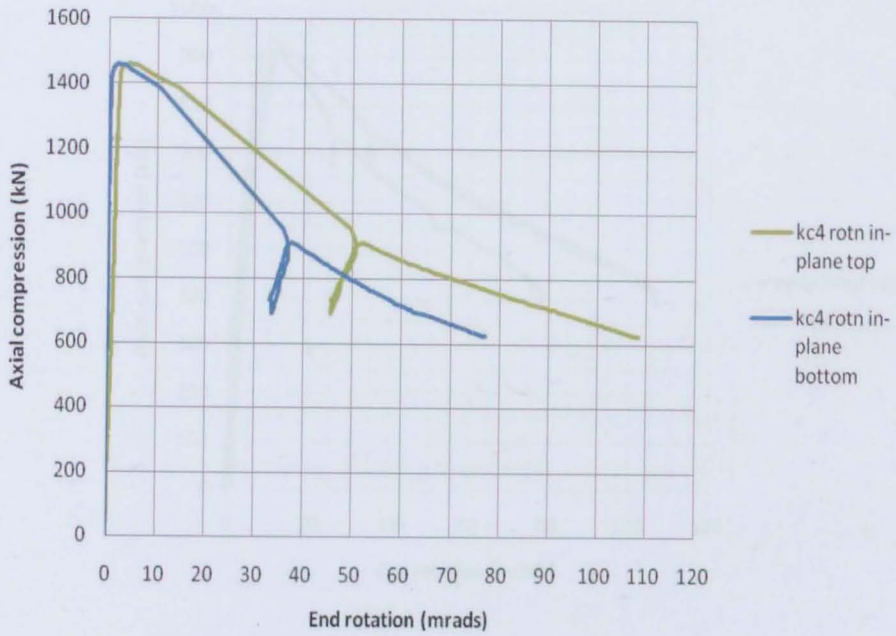


Figure 5.22 kc4 end rotations

kc 4; difference from mean end rotation

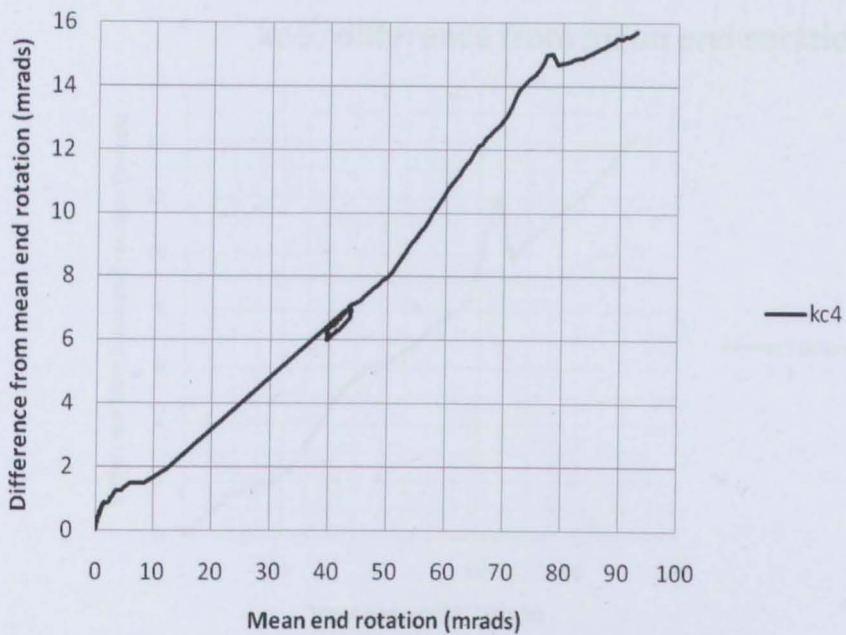


Figure 5.23 kc4 difference from mean end rotation

kc5; load v end rotation

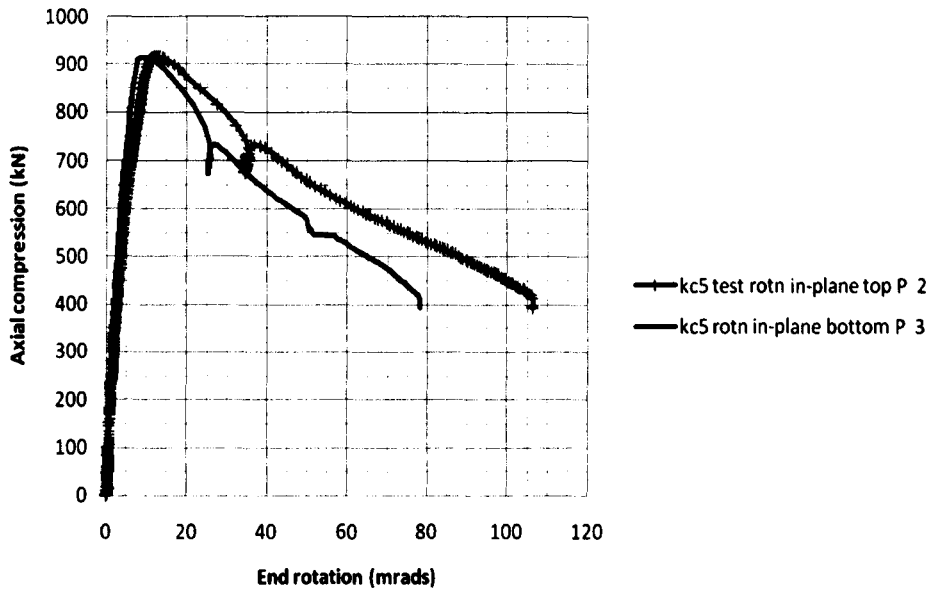


Figure 5.24 kc5 end rotations

kc 5; difference from mean end rotation

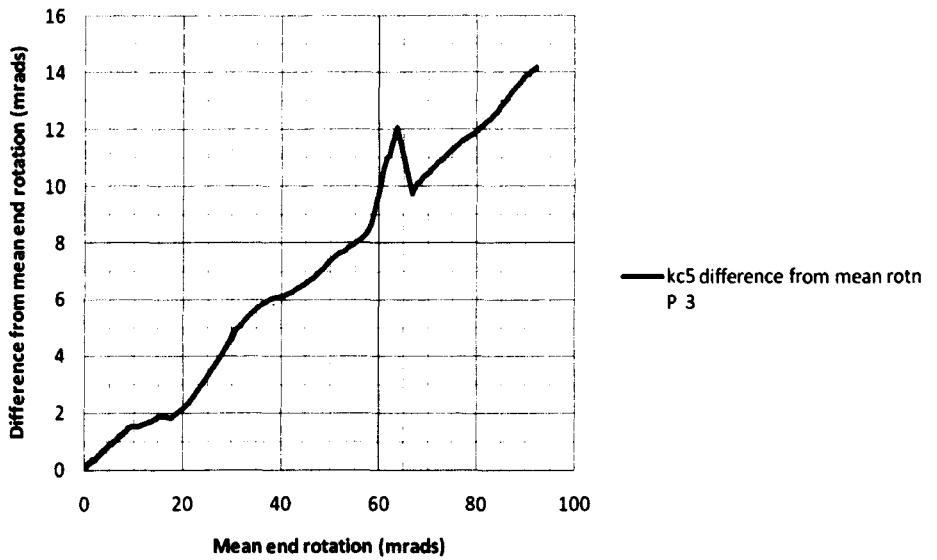


Figure 5.25 kc5difference from mean end rotation

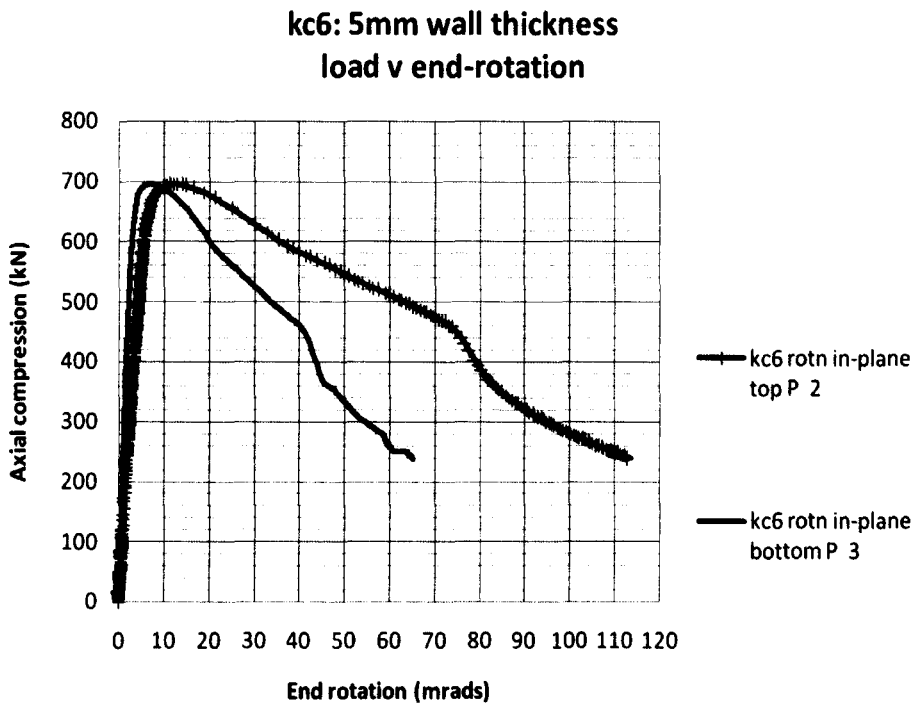


Figure 5.26 kc6 end rotations

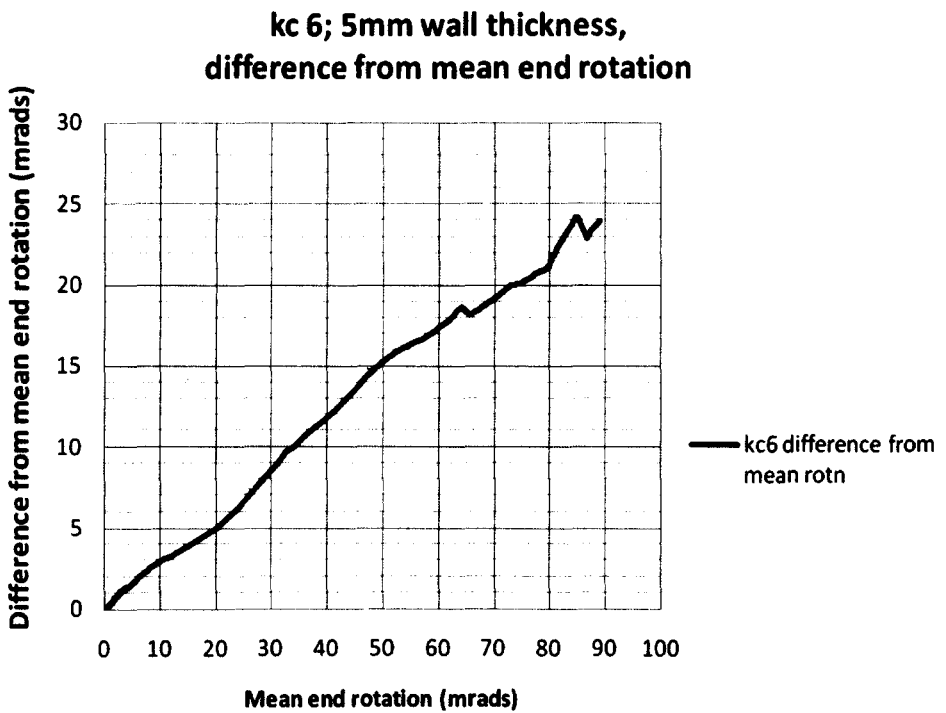


Figure 5.27 kc6 difference from mean end rotation

kc 7: load v end rotation

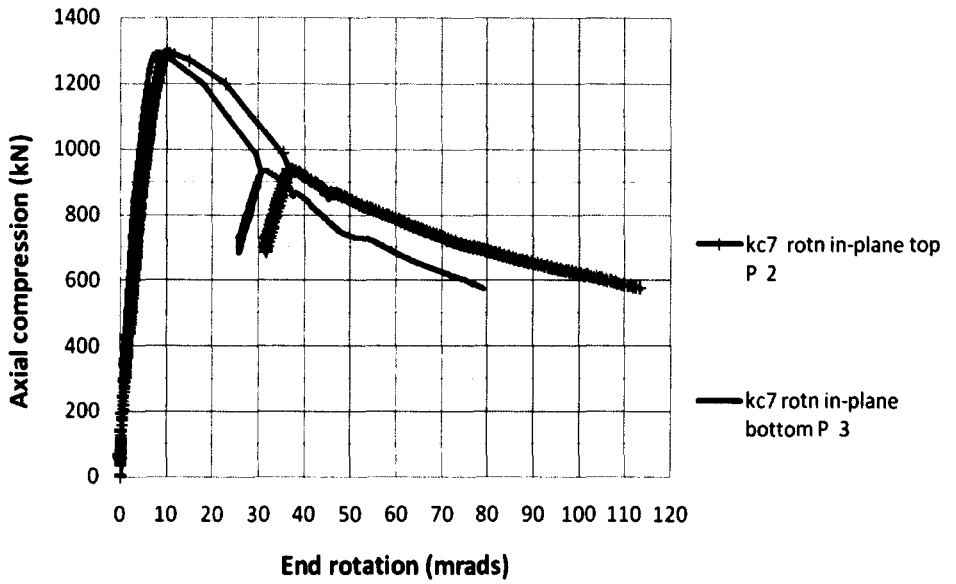


Figure 5.28 kc7 end rotations

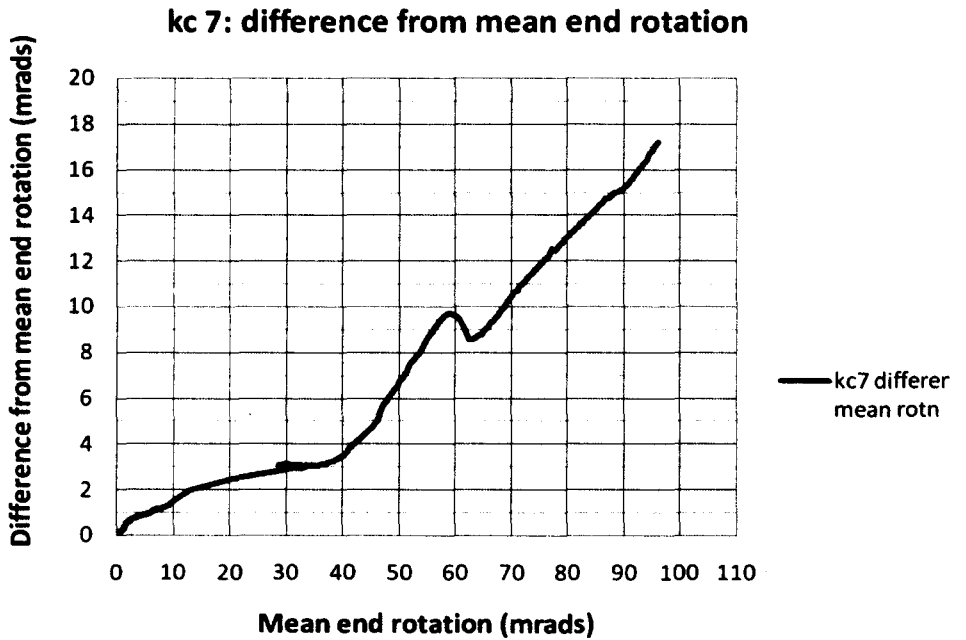


Figure 5.29 kc7difference from mean end rotation

kc 8: load v end rotation

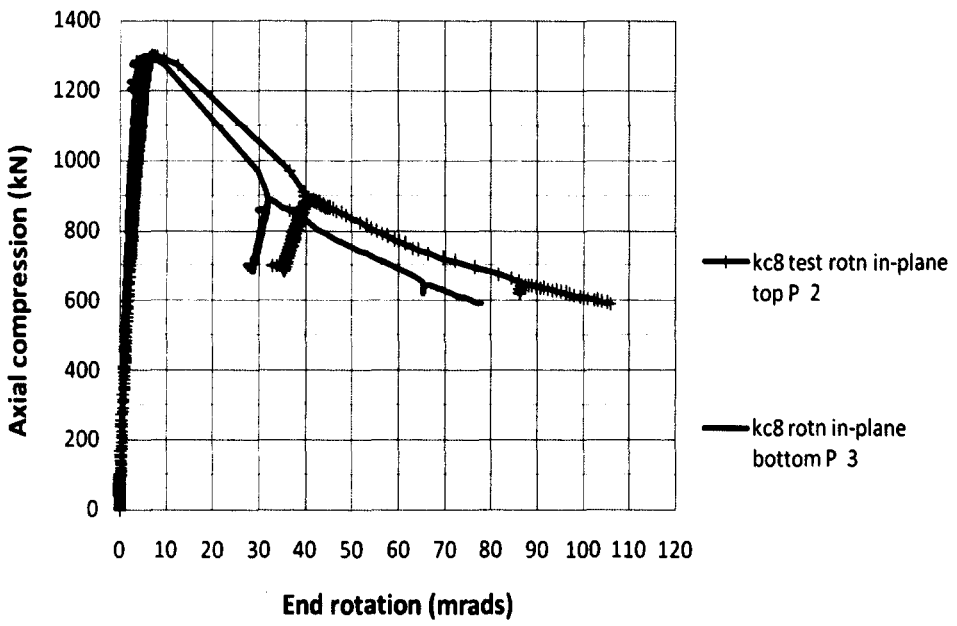


Figure 5.30 kc8 end rotations

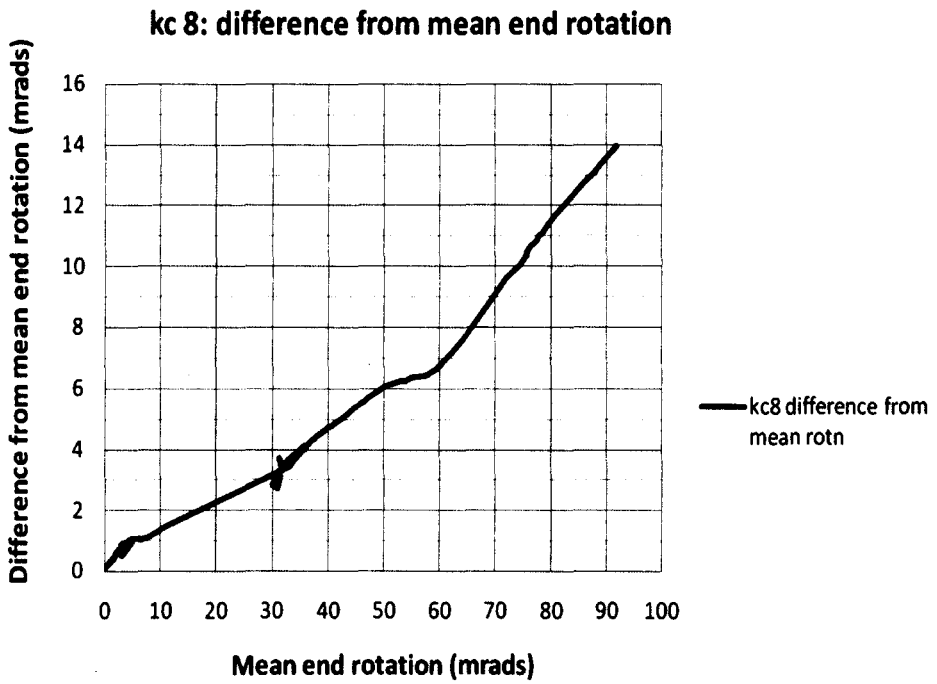


Figure 5.31 kc8 difference from mean kc8 end rotation

kc 9: load v end rotation

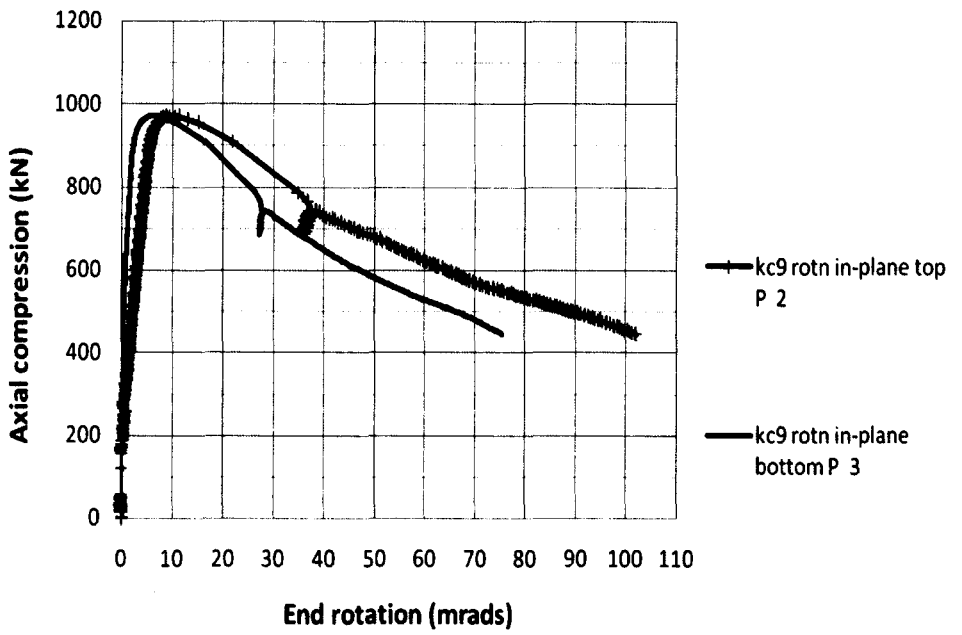


Figure 5.32 kc9 end rotations

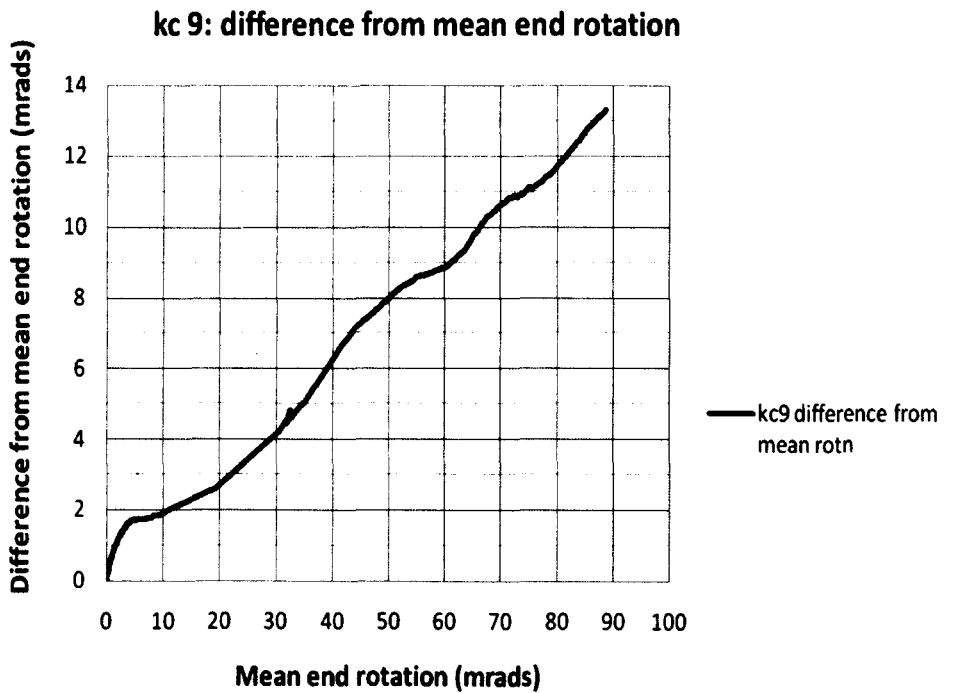


Figure 5.33 kc9 difference from mean end rotation

kc 10: load v end rotation

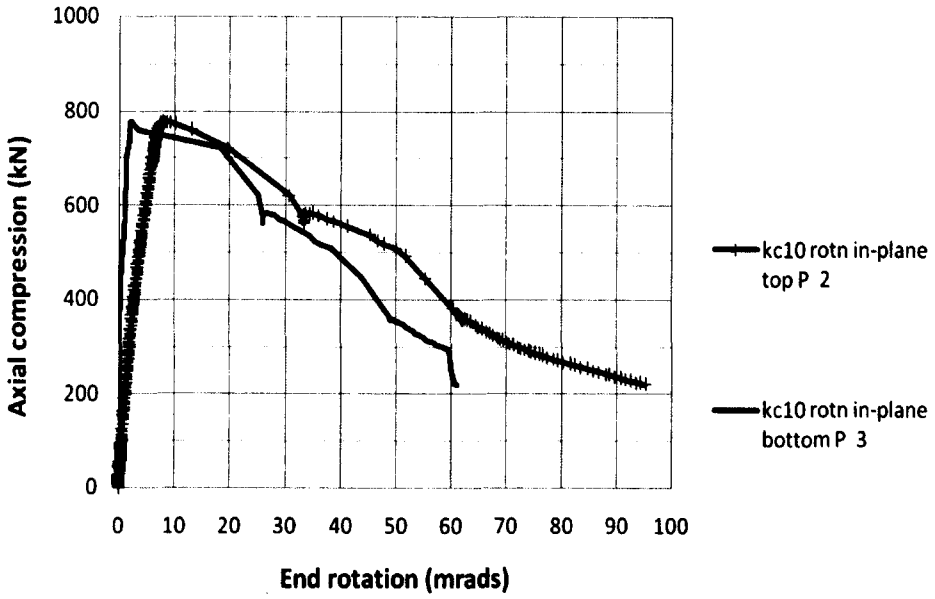


Figure 5.34 kc10 end rotations

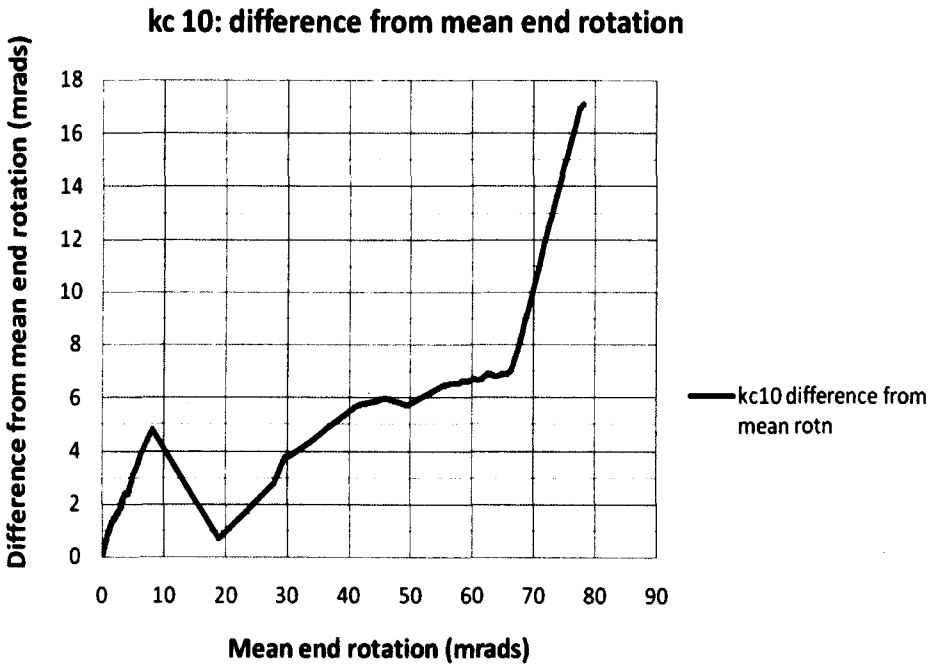


Figure 5.35 kc10 difference from mean end rotation

5.8 Effect of wall thickness

The two columns with 5mm wall thickness, kc6 and kc10, show a clear drop in axial load arising from buckling of the wall. This is seen in terms of end-rotations in Figure 5.36. The mid-height displacement is approximately 40 to 50 mm as seen in Figure 5.12.

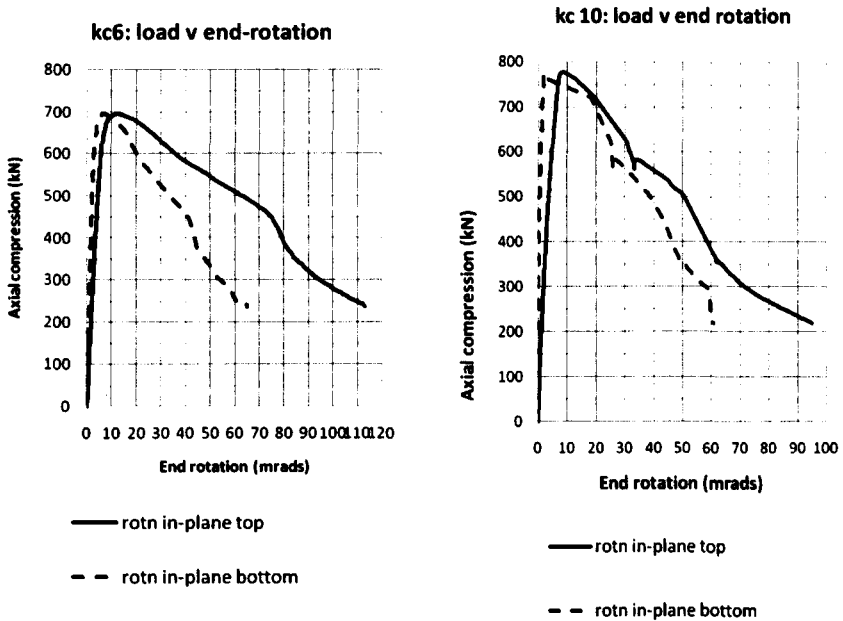


Figure 5.36 kc6 and kc10 end rotations

The two columns with 6.3mm wall thickness, kc5 and kc9, show only a very slight reduction in axial resistance in the tests. There is a small increase in the downward slope of the axial load versus mid-span displacement curve at a mid-height displacement from about 70 mm as seen in Figure 5.12. This is seen in terms of end-rotations in Figure 5.24 and Figure 5.32.

These observations and analysis contribute to the formulation of a design limitation on wall thickness later in this report.

5.9 Summary

Tests have been performed on full-scale columns with different wall thicknesses, using 120×120 SHS sections. The column behaviour was generally as predicted both by analysis including non-linear geometry and material properties and by the proposed design model. Sections with 10mm wall thickness showed no wall instability over the full range of the tests, whereas sections with thinner walls displayed wall instability.

6 COMPARISON OF TESTS WITH ANALYSIS

6.1 Introduction

6.1.1 General

The reason for the comparison of the tests with the Abaqus finite element model is to confirm the structural behaviour assumed by the design method and to calibrate the results of the parametric study made using Abaqus analysis so that the behaviour of the tests is included in the design model.

The test specification required the columns to be installed into the rig with eccentricities such that the mid-height bending moment would be similar to that occurring in columns with the worst out-of-straightness allowed by current Standards. The test columns were found to be very nearly perfectly straight, so the columns were installed in the rig with equal eccentricity top and bottom of $L/750$ which was the value of out-of-straightness being discussed by European standardisation committee CEN/TC250/SC3 at the time of the test program.

6.1.2 Summary of method

The general form of the load-displacement curve measured in the tests is broadly similar to the results generated by Abaqus if the initial imperfection is applied as either a straight member at a uniform offset from the line of thrust between the rig bearings or a member curved throughout as a half-sine curve. However, the test curves are slightly different, especially in that many of them show distinct asymmetry of end-rotations even in the elastic range. To achieve Abaqus analyses that are closer to the test curves, initially it was decided to alter the initial imperfection to arrive at close agreement in the elastic range. The imperfections required to make the Abaqus analysis agree with the test results can be calculated with reasonable accuracy from simple structural mechanics for a first analysis. The imperfections can then be refined from the results of this first analysis.

Because the measurements of the straightness of the specimen showed such small deviations from straight, the Abaqus model was made straight. Some investigation of different initial geometry was made, but the out-of-straightness observed before the tests was so small compared with the eccentricity deliberately applied at the ends that it was decided to model

the members as straight. Compared with the effects of possible variations of friction in the bearings, yield stress and section properties, the assumption of a perfectly straight member has only a modest effect. The sensitivity to member curvature between the ends was investigated, as reported in Section 6.4.4.

Abaqus was used to reproduce the maximum resistances found in the tests, assuming that

1. the stress-strain was the simple elastic/perfectly-plastic stress strain diagram as used in the Abaqus parametric study,
2. the yield stress in the steel was equal to the test coupon 0.2% proof stress,
3. the residual stress is 10% of the nominal yield of 355 MPa with the same stress distribution as used in the Abaqus parametric study,
4. the Young's modulus of the steel is 210000 MPa as in Eurocode 3 [BSI 2005a, CEN 2005a],
5. the behaviour of the test column was similar to a pin-ended member with the friction effect equivalent to a reduction in the eccentricity of application of load.

The results of analyses using these asymmetric eccentricities are shown in Section 6.3 and the key test and analysis data are shown in Table 6.2. The Abaqus analyses showed that the eccentricities were far in excess of what is credible with such carefully made end-fittings which allowed fine adjustment and in a laboratory with such long experience of testing.

On reflection, it was realised that the finite stiffness of the relatively tall test rig must allow some small amount of side-sway. This could be initiated by the axial load because it is impossible to achieve perfect vertical alignment. The inclinometers use gravity as the datum, so sway of the test rig will increase the inclination at one end of the column while it gives an equal decrease in the inclination of the other end. Therefore, even if the bearings were perfectly friction-free and the end-rotations of the column were equal relative to the line of thrust between the centres of the bearings, the inclinometer output would indicate unequal end-rotations. After this was noticed, the analyses of the tests were then conducted with equal eccentricities top and bottom with the eccentricity chosen to give reasonable agreement between the test and analysis for both the maximum load and the mean end rotation. The results of analyses using these asymmetric eccentricities are shown in Section 6.4 and the key test and analysis data are shown in Table 6.3.

In an ideal world, differences between the Abaqus behaviour and the test results might be resolved by adjusting the Abaqus model until the Abaqus results exactly mirror all the test data including

1. maximum load
2. end-rotation at each load
3. in-plane deflection at mid-height at each load.

However, this requires a precise knowledge of the test specimen, including

1. stress/strain curve at all points including dynamic effects,
2. geometry including all irregularities,
3. distribution of residual stresses, and
4. a precise knowledge of the behaviour in the rig, including
 - what friction is acting at what time,
 - what is the position of the bearing components relative to the specimen,
 - any inclination of the specimen or the line of thrust (from centre to centre of the bearings)
 - the sway behaviour of the rig
 - the flexural behaviour of the columns of the rig when loaded because the transducer recording the in-plane deflection at mid-height was attached to one of these.

Very high precision is NOT required on these points for the falling branch of the tests (the region of interest for these tests) because the deformations of the specimen are large in this region.

The Abaqus output is from analyses in which the specimen is assumed to be perfectly straight and offset by a constant eccentricity from a line between the centres of the bearings, except in the analyses investigating the sensitivity of the analysis to curvature in the specimen in Section 6.4.4.

The eccentricity is chosen so that the maximum resistance of the Abaqus analysis is close to the maximum load recorded in the test, ideally within 1%. The yield stress was generally taken as the yield stress from the coupon test.

6.1.3 Estimating the offset of the column ends from line of load

The effect of an offset from the line of load is to induce a moment in the member. This causes curvature in the member which results in end rotations. The axial compression

increases the moments according to the deflected shape. The behaviour is non-linear, but the non-linearity is small at low levels of load.

When the non-linear effects are small, which is the case when the axial load is small at the beginning of the test, the end-rotations approach the end-rotations of beams with end moments calculated by elastic small-deflection theory. The bending moments and end-rotations, assuming the effect of axial load is negligible, are shown in Figure 6.1 for a pinned column with an eccentric load applied at the top. The bending moments and end-rotations, assuming the effect of axial load is negligible, are shown in Figure 6.2 for a pinned column with an eccentric load applied at the bottom.

In some tests, the curves of end rotation and mid-height displacement exhibited steps at low levels of load, making it difficult to calculate the initial imperfection accurately.

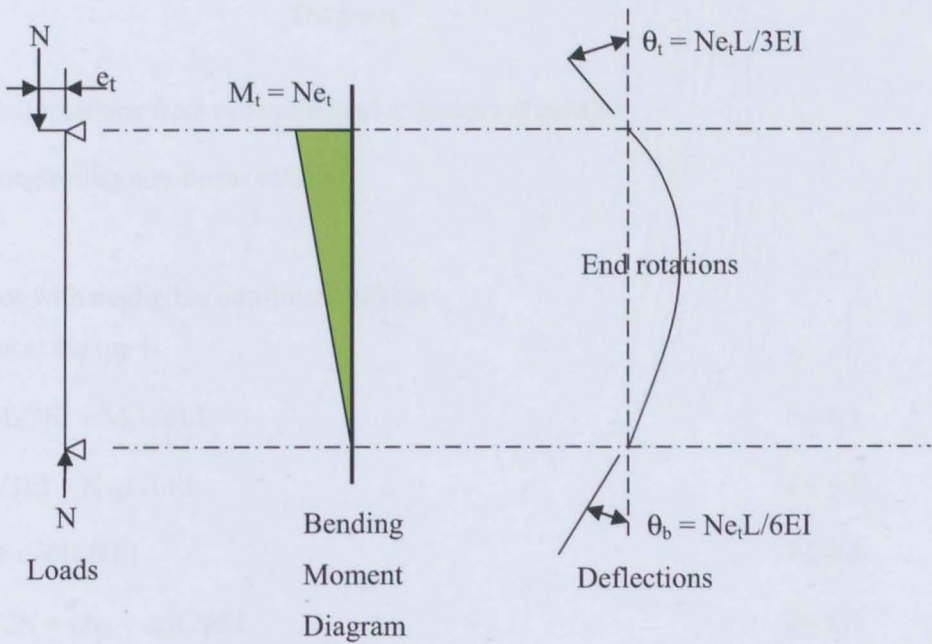


Figure 6.1 End rotations from eccentric load at top of column
(neglecting non-linear effects)

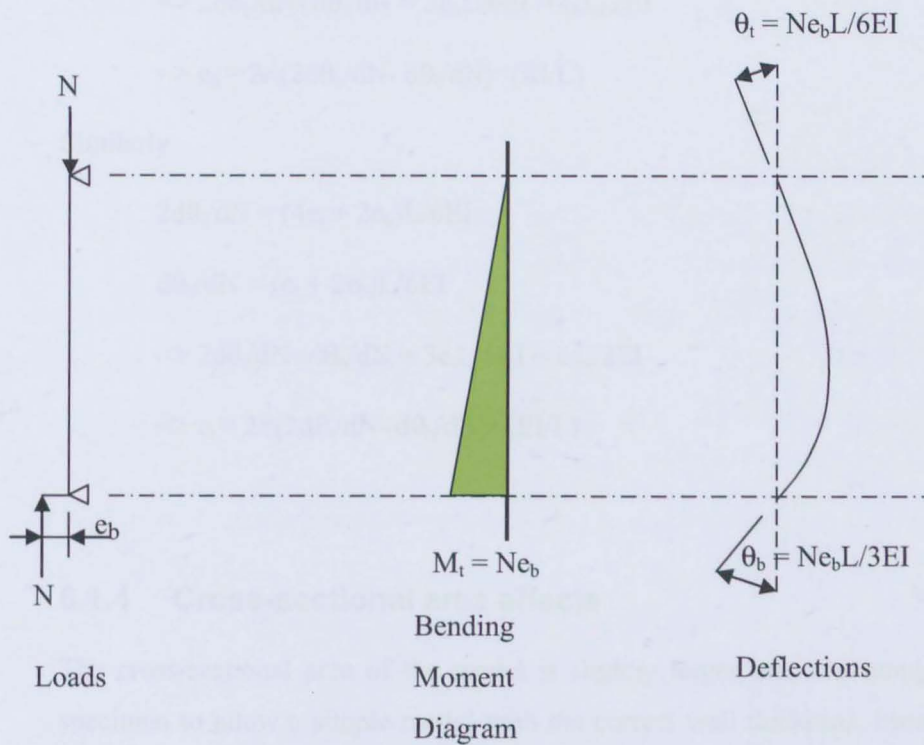


Figure 6.2 End rotations from eccentric load at bottom of column
(neglecting non-linear effects)

For a straight bar with negligible non-linear effects,
The end rotation at the top is

$$\theta_t = M_t L / 3EI + M_b L / 6EI \quad \text{Eq 6.1}$$

$$= N e_t L / 3EI + N e_b L / 6EI \quad \text{Eq 6.2}$$

$$= (2e_t + e_b)NL / 6EI \quad \text{Eq 6.3}$$

$$\Rightarrow d\theta_t/dN = (2e_t + e_b)L / 6EI \quad \text{Eq 6.4}$$

Similarly, the end rotation at the bottom is

$$\theta_b = (e_t + 2e_b)NL / 6EI \quad \text{Eq 6.5}$$

$$\Rightarrow d\theta_b/dN = (e_t + 2e_b)L / 6EI \quad \text{Eq 6.6}$$

The end rotations can be found in terms of $d\theta/dN$ from

$$2d\theta_b/dN = (2e_t + 4e_b)L / 6EI \quad \text{Eq 6.7}$$

$$d\theta_t/dN = (2e_t + e_b)L / 6EI \quad \text{Eq 6.8}$$

$$\Rightarrow 2d\theta_b/dN - d\theta_t/dN = 3e_bL/6EI = e_bL/2EI \quad \text{Eq 6.9}$$

$$\Rightarrow e_b = 2 \times (2d\theta_b/dN - d\theta_t/dN) \times (EI/L) \quad \text{Eq 6.10}$$

Similarly

$$2d\theta_t/dN = (4e_t + 2e_b)L/6EI \quad \text{Eq 6.11}$$

$$d\theta_b/dN = (e_t + 2e_b)L/6EI \quad \text{Eq 6.12}$$

$$\Rightarrow 2d\theta_t/dN - d\theta_b/dN = 3e_tL/6EI = e_tL/2EI \quad \text{Eq 6.13}$$

$$\Rightarrow e_t = 2 \times (2d\theta_t/dN - d\theta_b/dN) \times (EI/L) \quad \text{Eq 6.14}$$

6.1.4 Cross-sectional area effects

The cross-sectional area of the model is slightly larger than the nominal area of the test specimen to allow a simple model with the correct wall thickness, because the models use the nominal wall thickness and assume square corners. The test columns, being hot-finished sections, have curved corners with very tight external radii. The exact area of the specimen was not measured, so the nominal area of the section is assumed. The analysis results were multiplied by a reduction factor of 'nom/model', the ratio of the nominal area to model area, from Table 6.1 before making comparisons with the test results either by plotting or by calculations. Steel producers are very careful not to give away steel in their cross-sections and there is an area tolerance on sectional area in the product specification. It is very unlikely that the areas were greater than the nominal area.

Table 6.1 Cross-sectional areas				
test	wall thickness	model area (mm ²)	nominal area (mm ²)	nom/model
kc3, 4, 7, 8	10.0 mm	4×10×(120-10) = 4400	4290	0.975
kc5, 9	6.3 mm	4×6.3×(120-6.3) = 2865	2820	0.984
kc6, 10	5.0 mm	4×5×(120-5) = 2300	2270	0.987

6.2 Correlation factor for test v Abaqus

6.2.1 Introduction

As shown in Figure 6.10 to Figure 6.17, the Abaqus analysis predicts behaviour close to that measured in the tests, but not identical. The relationship between the Abaqus analysis and the test results is expressed as a correlation factor on the end-rotations. This factor is calculated from the top of the unloading/reloading cycle and is the ratio of the end-rotation measured in the tests to the end-rotation predicted by Abaqus. The correlation factors are used to adjust the results of the Abaqus parametric study when defining the design model.

The top of the unloading/reloading cycle can be found from the plot of the mean end-rotation v load. A typical test plot of is shown in Figure 6.3. The maximum load is at B. The top of the unloading/reloading cycle is at C. This point C is the point at which the test operator began to unload the specimen, so the end-rotation ceases to increase while the load is decreasing. At this point, referred to later as the “static” point, the strain rate is zero and the friction moment is about to decrease. The load at this point is designated N_u , the load at the point of unloading.

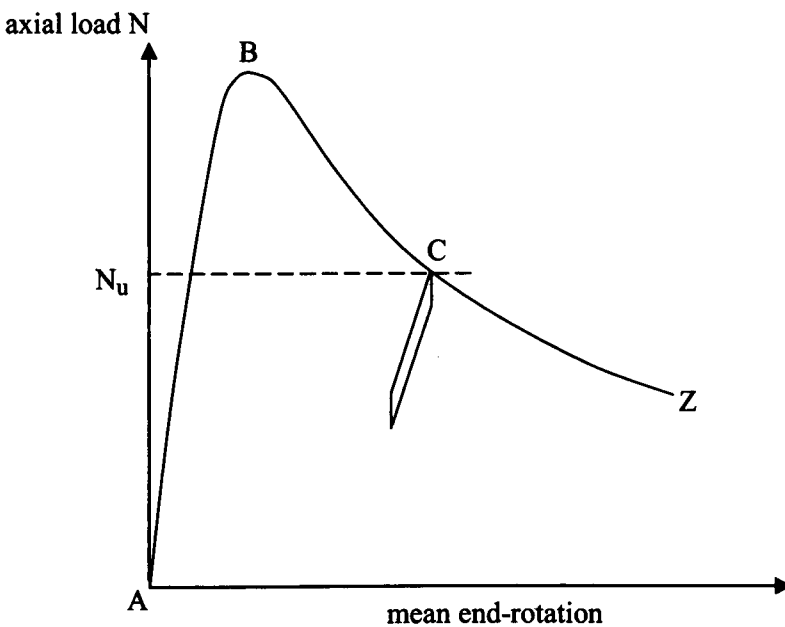


Figure 6.3 Typical end-rotation v load from tests

6.2.2 Calculating the correlation factor c_f

The unloading/reloading cycle, described in Chapter 5, provides a point at which the test results can be compared with the Abaqus results. The method used to calculate the correction factor is to compare the mean value of the end-rotations at the top of the unloading/reloading cycle with the end-rotation predicted by Abaqus at the same load.

The mean value of end-rotation in the laboratory tests at the point of unloading, designated θ_{Ct} , is shown in Figure 6.4. The value of θ_{Ct} is found from the test results at the load N_u . The value of mean end-rotation predicted by Abaqus, designated θ_{CA} , is found by interpolation to N_u from the adjacent points from the Abaqus output.

The correlation factor, c_f , is the ratio of the rotations,

$$c_f = \theta_{Ct} / \theta_{CA} \quad \text{Eq 6.15}$$

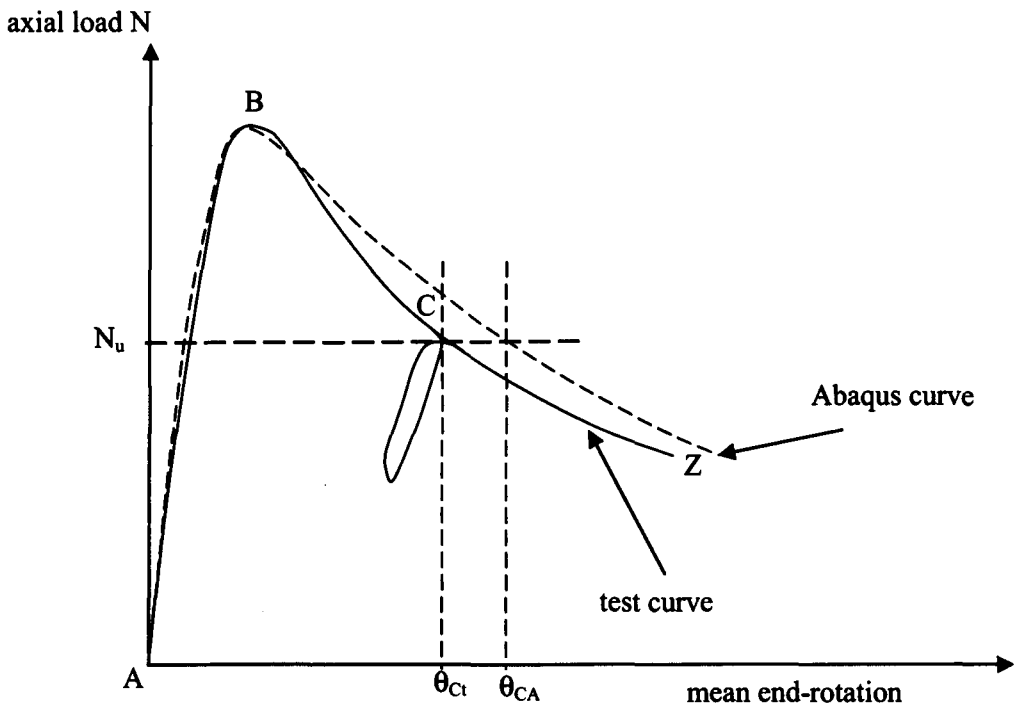


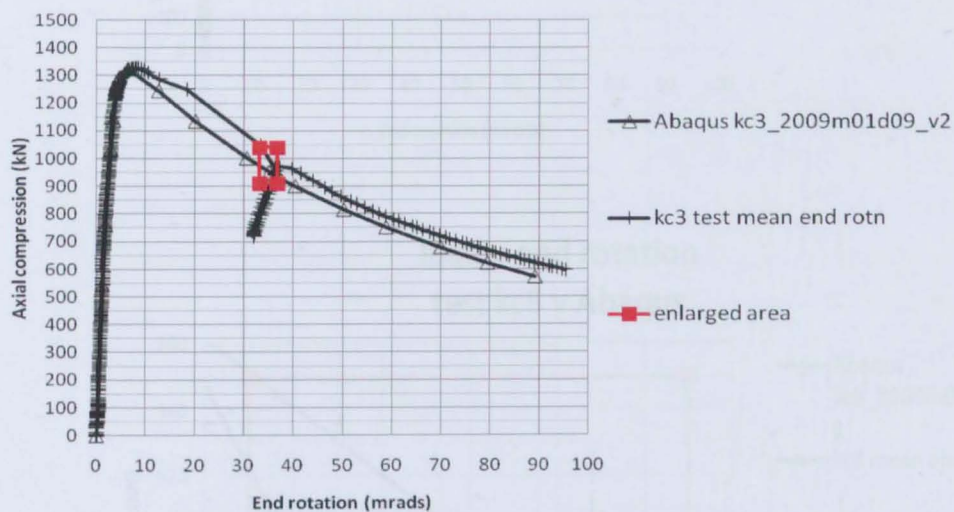
Figure 6.4 Mean end-rotation v load: test v Abaqus

The key points of test kc3 are shown in Figure 6.5. The point of maximum end-rotation is easily seen and can be verified by inspecting the tabulated test results. The difference between the test rotation and Abaqus rotation at this load is also seen in Figure 6.5. It can be

seen that for kc3, the Abaqus prediction of rotation is very slightly less than the test result at that load. The opposite is seen in Figure 6.6 which shows that for kc8 the Abaqus prediction of rotation is greater than found in the tests.

The values of c_f are given in Table 6.2 for asymmetric eccentricities and in Table 6.3 for symmetric eccentricities. The effect from partly curved imperfections on c_f is investigated in Section 6.4.4 and the effect of residual stresses on c_f is investigated in Section 6.4.5. The choice of value of c_f used to modify the parametric study is given in Section 6.6.

load v end rotation; test kc3 v Abaqus



load v end rotation; test kc3 v Abaqus enlarged area

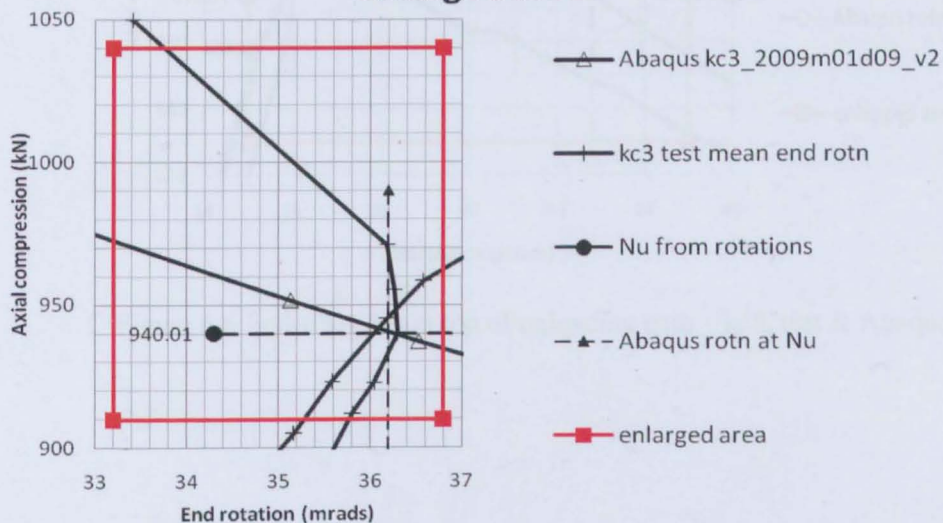
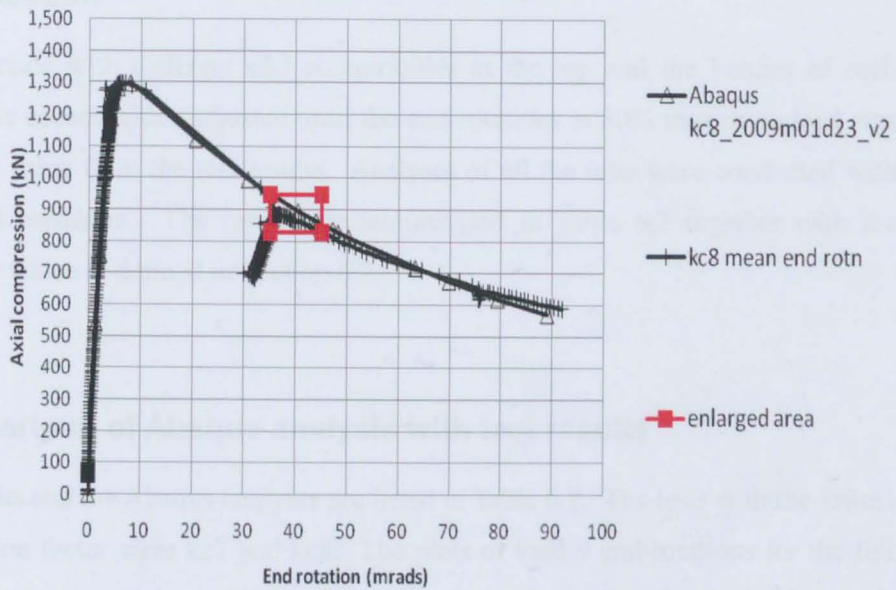


Figure 6.5 Top of the unloading/reloading cycle – kc3, test & Abaqus

load v end rotation test kc8 v Abaqus



load v end rotation test kc8 v Abaqus

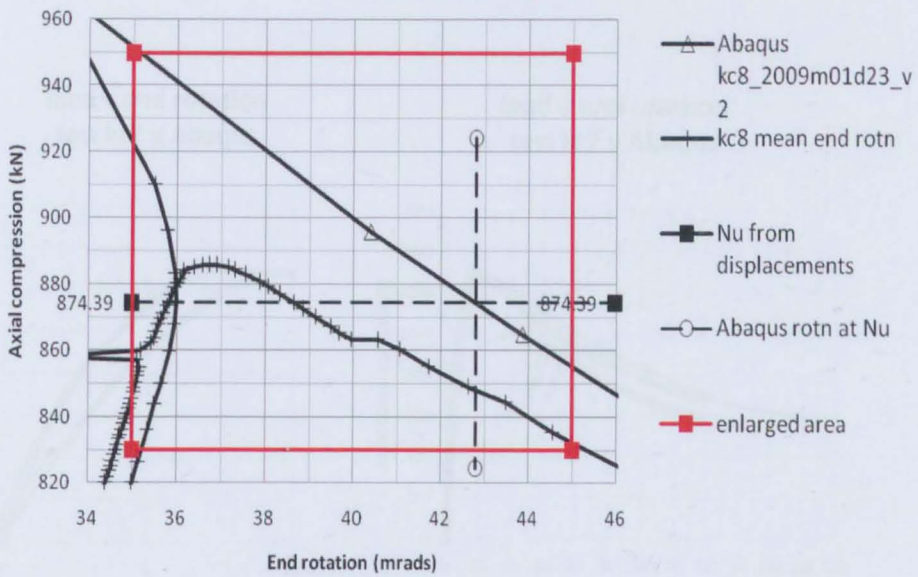


Figure 6.6 End-rotations at top of unloading path – kc8, test & Abaqus

6.3 Straight members with asymmetrical eccentricities

6.3.1 Introduction

Analyses were made with different end eccentricities at the top and the bottom of each specimen with the eccentricities adjusted until the end-rotations at 80% maximum load was very close to the value from the test results. Analyses of all the tests were conducted with perfectly straight members. The results are summarised in Table 6.2 together with the correlation factor which is defined in Section 6.2.

6.3.2 Comparison of Abaqus analysis with test results

The key test results and the Abaqus analyses are listed in Table 6.2. The tests with the lowest value of correlation factor were kc7 and kc8. The plots of load v end-rotations for the full range of these two tests, together with the plots of load v end-rotations for the loading path shown to a larger scale, are shown in Figure 6.7 and Figure 6.8. The plots of load v end-rotations for the loading path show that the imperfections in the analysis give end-rotations close to the test results.

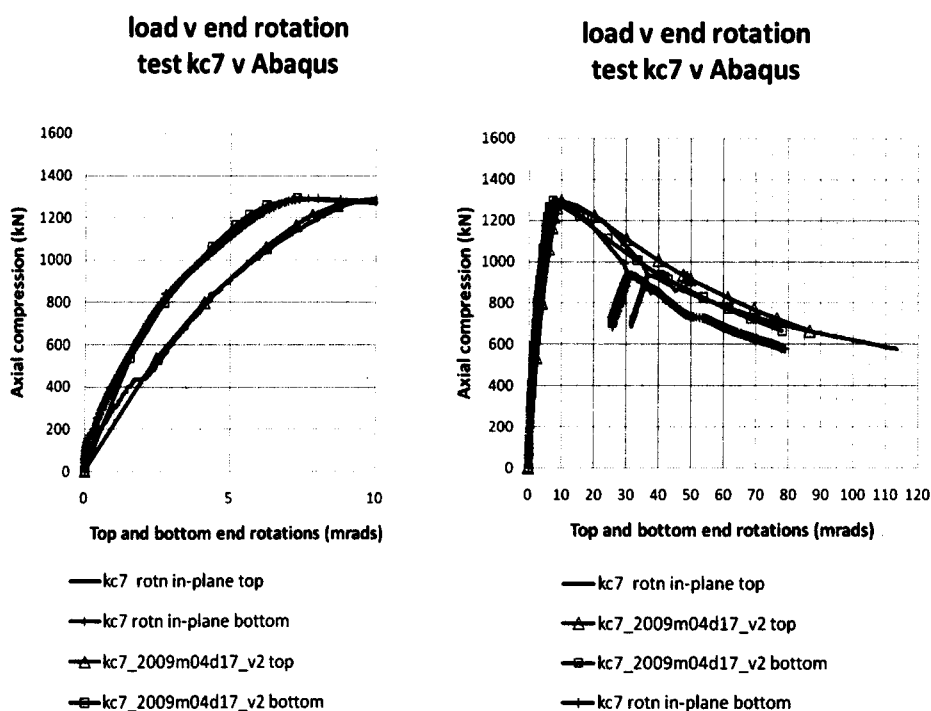
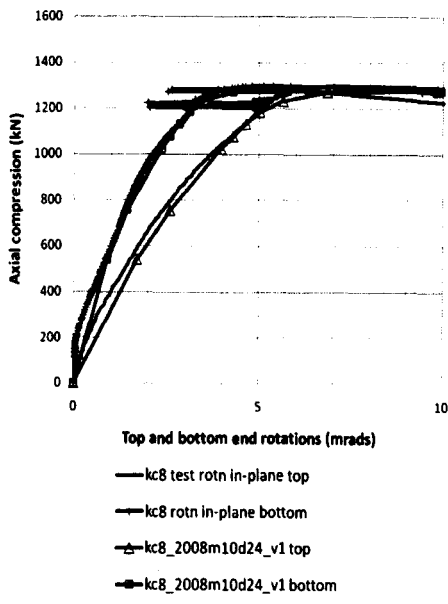


Figure 6.7 End-rotations – kc7, test & Abaqus

load v end rotation
test kc8 v Abaqus 2650mm



load v end rotation
test kc8 v Abaqus 2650mm

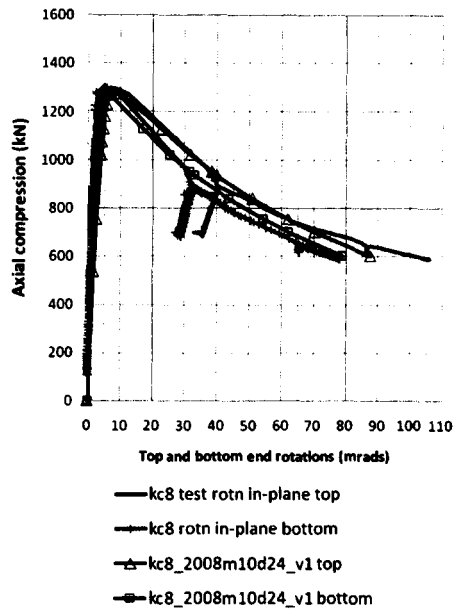


Figure 6.8 End-rotations – kc8, test & Abaqus

Table 6.2 Abaqus with asymmetric eccentricities				
Comparison of tests with asymmetrical model				
Abaqus analysis with the classic elastic/perfectly-plastic stress/strain curve.				
Test	kc3	kc4	kc7	kc8
Wall thickness (mm)	10	10	10	10
Max test load (kN)	1328	1458	1290	1298
0.2% proof stress (MPa)	375	390	not known	375
area factor	0.975	0.975	0.975	0.975
yield stress (MPa) used in Abaqus analysis	375	375 note1	413	375
residual stress (MPa)	35.5	35.5	35.5	35.5
Abaqus max load	1361	1458	1327	1310
area reduced Abaqus max load (kN)	1327	1422	1293	1277
difference in max loads (kN)	-1	-36	+3	-21
Abaqus reduced N – test N				
Abaqus e_t (mm)	2.25	3.20	10.39	7.92
Abaqus e_b (mm)	2.87	-1.34	-0.59	-1.99
Abaqus mean e (mm)	2.56	0.93	4.90	2.97
Abaqus deviation from mean e (mm)	+/- 0.31	+/-2.27	+/-5.49	+/- 4.96
Correlation factor for mean end-rotation, $c_f = \theta_{Ct}/\theta_{CA}$	0.991	1.018	0.749	0.829
note 1	Using the coupon stress as the yield stress with the classic elastic/perfectly-plastic stress/strain curve, the analysis model could not continue beyond the maximum load			
note 2	Abaqus input files: kc3: kc3_2008m10d19_v2 kc4: kc4_2008m10d22_v3 kc7: kc7_2009m04d17_v2 kc8: kc8_2008m10d24_v1			

The results for tests for kc5, kc6, kc9 and kc10 were not calculated because it was concluded from the results of kc3, kc4, kc7 and kc8 that the tests had been affected by sway of the test-rig, see Section 6.3.3, before these tests had been analyzed. Therefore there was no benefit

in completing the analysis of the other four tests using the assumption of asymmetric behaviour. The low values of correlation factor, c_f , found for tests kc7 and kc8 are similar to those reported in Table 6.3 and discussed in Section 6.4.2.

6.3.3 Asymmetry of specimen or of rig

Adjusting the Abaqus model to reproduce the end-rotations recorded leads to the eccentricities e_b and e_t given in Table 6.2. In the tests with the greatest differences between end-rotations at the top and the bottom, tests kc7 and kc8, the eccentricities are not believable considering the care taken in the assembly of the tests. The eccentricities for kc7 are shown in Figure 6.9.

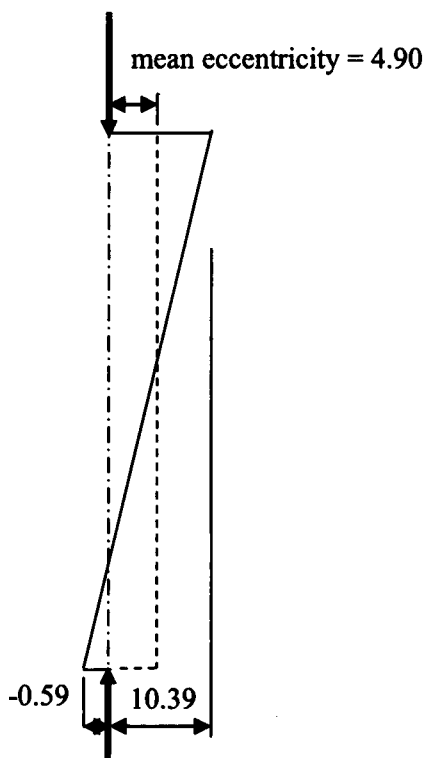


Figure 6.9 Asymmetric eccentricity of loading for test kc7

It should be noted that a significant eccentricity is required to cause only a very small difference of end rotations. This is demonstrated by comparing Table 6.3 with Table 6.2. At 80% load, the end-rotations differ from the mean value by only ± 0.9 mrad, but the difference in end eccentricity needed to generate this is ± 5.49 mm. However, 0.9 mrad rotation from vertical would be generated in a rig height of 3.0 metres by a sway of only

$0.9 \times 10^{-3} \times 3000 = 2.7$ mm. This supports the theory that the rig swayed slightly, so the rotations recorded relative to the vertical were not the end-rotations relative to the line of thrust through the bearings.

Because of the high probability that sway of the rig had made the end-rotation test output differ from the end-rotations relative to the specimen, it was decided to re-analyse based on the assumption of equal end-rotations. The probable sway of the rig limited the use of the mid-height deflection values because the LVDT was fixed to a leg of the rig. If the sway involved a different stiffness between the top and bottom of the rig columns, which is likely, the reading of the LVDT would be affected by the rig sway.

6.4 Straight members with symmetrical eccentricities

6.4.1 Introduction

Analyses were made with equal end eccentricities with the eccentricity adjusted until the mean end-rotation at 80% maximum load was very close to the value from the test results. Initially, the analyses of all the tests were conducted with perfectly straight members so that correlation factors between analysis and test could be calculated. The results are summarised in Table 6.3 together with the correlation factor, c_f , which is defined in Section 6.2. Then the sensitivity of the results to effects of

1. out-of-plane deflections,
2. partly-curved initial imperfections,
3. residual stresses

were investigated to find the effect on the correlation factor.

6.4.2 Comparison of Abaqus analysis with test results

The plots of the Abaqus analyses listed in Table 6.3 are shown in Figure 6.10 to Figure 6.25. Although in general the correspondence between test and analysis was very good, there were some difficulties encountered in the analysis. Test kc4, for example, proved very difficult to analyse. The minimum imperfection possible that would allow the analysis to pass the peak load was 0.73mm with 375 MPa yield despite changing solution time-step parameters from 10^{-5} to 10^{-9} . It can be seen from Figure 6.19 that the Abaqus plot is very close to the test plot, so the results are acceptable. However no improvement was found possible. The analysis would not run with yield at 390 MPa, the coupon 0.2% proof stress. Analysis runs

kc4_2009m03d06_v1 to _v10 were devoted to using a stress/strain curve that had an elastic limit at or below 375 MPa and a reduced modulus beyond, with a stress/strain graph passing through 390 MPa, but a higher load and an analysis continuing beyond the peak load was not achieved.

Analysis of tests kc3, kc4, kc8 and kc10 show analysis that is very close to the tests plots, showing that the eccentricity in the analysis must be very close to the eccentricities in the tests.

Test kc5 shows good agreement at 50% maximum load. Test kc6 did not have an unloading cycle to allow a correlation factor to be calculated. The analysis of kc7 is not so close. Regrettably the coupon test result for kc7 was not available, so the comparison with analysis is uncertain. Test kc9 analysis is offset from the test results, but the analysis plot is 'parallel' with the test plot. This effect might arise from a friction effect in the test rig or from the stress/strain curve of the material being different from elastic/perfectly-plastic.

test 3; load v end rotation v Abaqus 2650mm

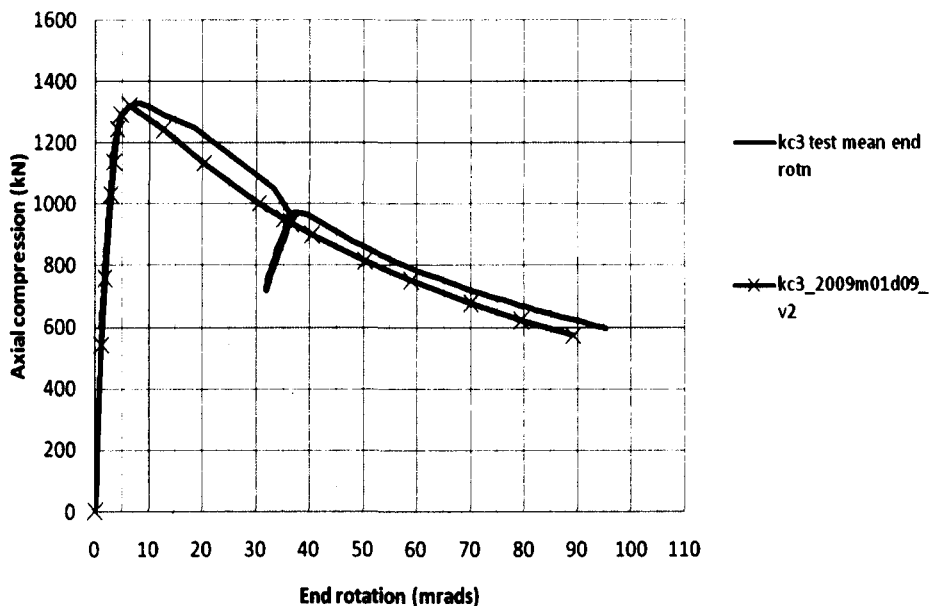


Figure 6.10 End-rotations – kc3, test mean & Abaqus

load v end rotation test 4 & Abaqus

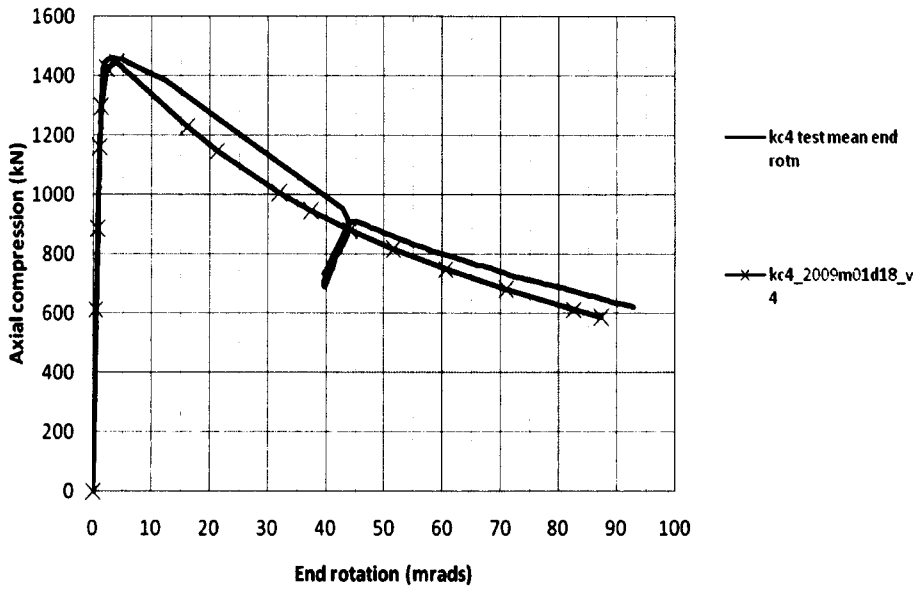


Figure 6.11 End-rotations – kc4, test mean & Abaqus

load v end rotation test 5 & Abaqus

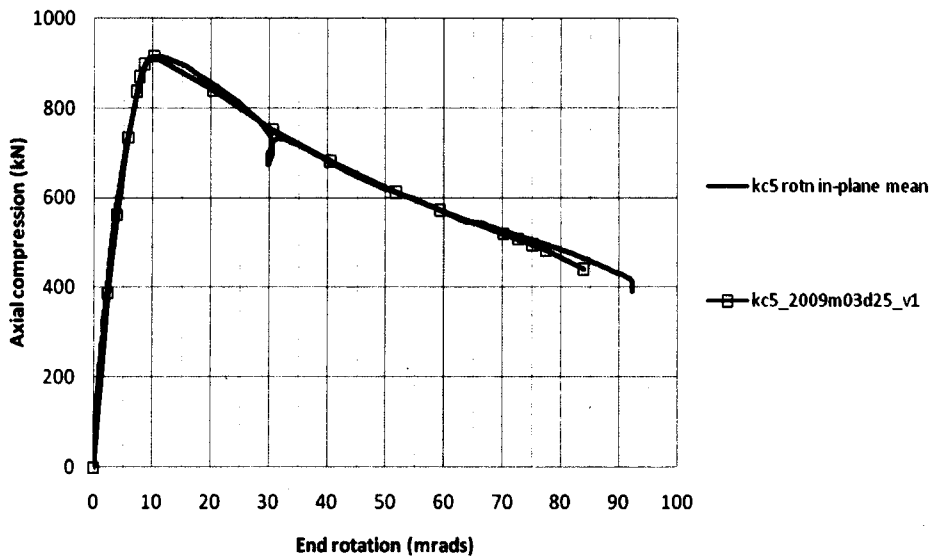


Figure 6.12 End-rotations – kc5, test mean & Abaqus

**load v end rotation
test 6 v Abaqus**

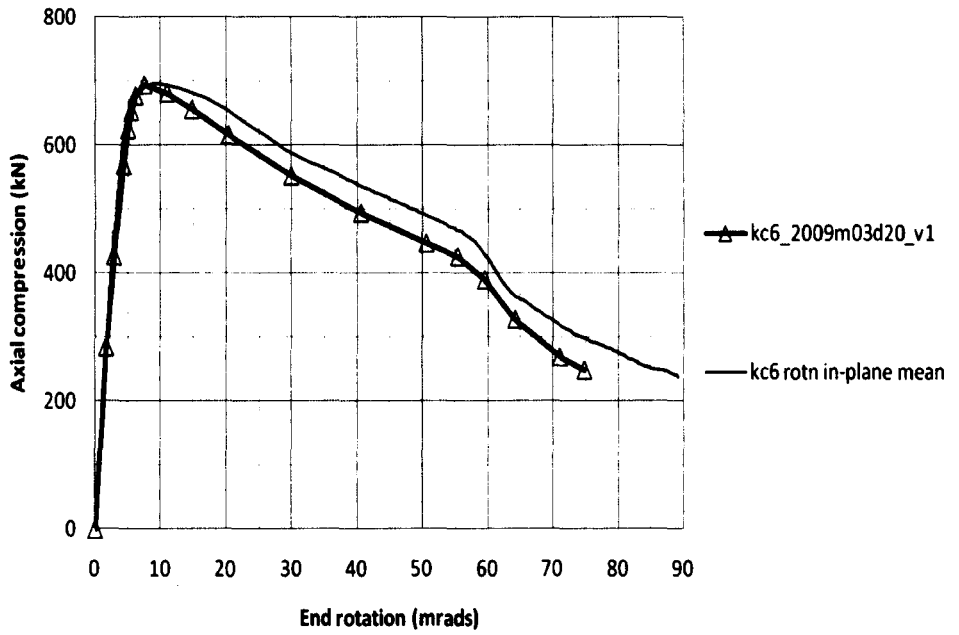


Figure 6.13 End-rotations – kc6, test mean & Abaqus

**load v end rotation
test 7 v Abaqus**

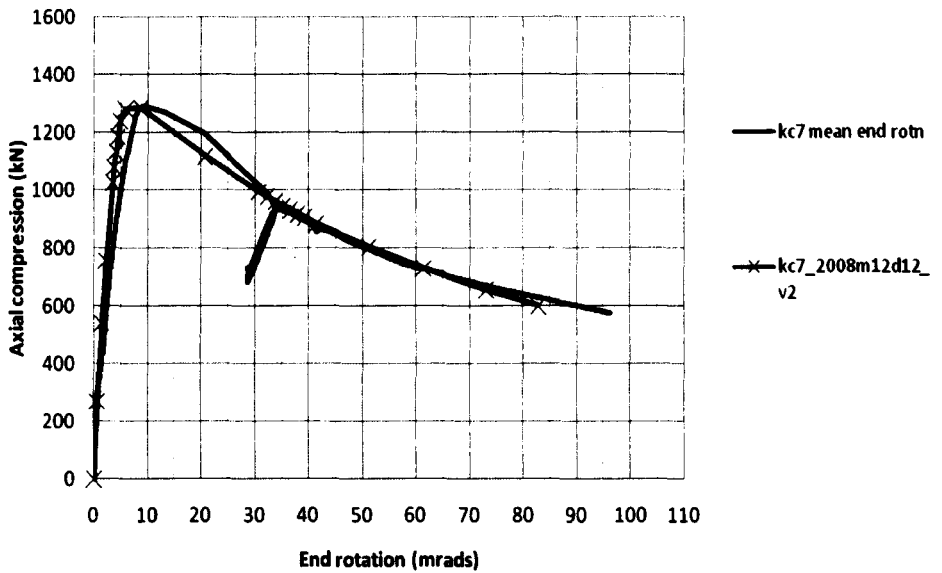


Figure 6.14 End-rotations – kc7, test mean & Abaqus

load v end rotation test 8 v Abaqus

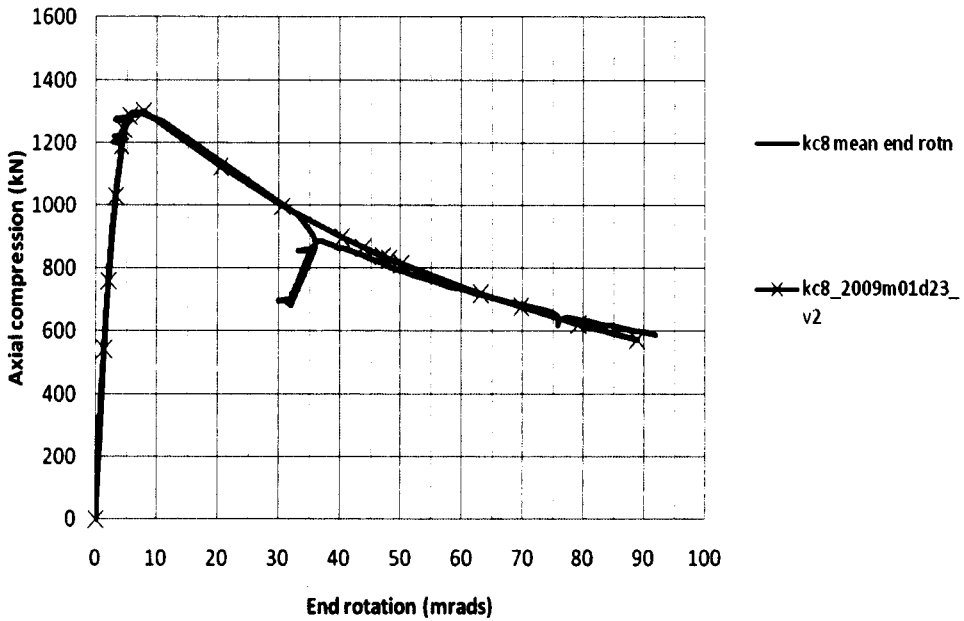


Figure 6.15 End-rotations – kc8, test mean & Abaqus

load v end rotation test 9 v Abaqus

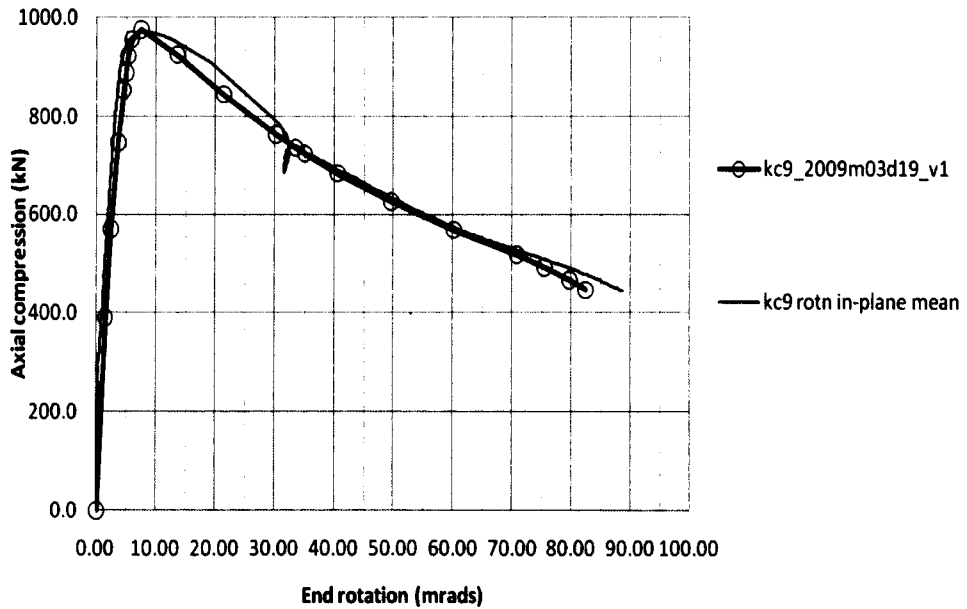


Figure 6.16 End-rotations – kc9, test mean & Abaqus

**load v end rotation
test 10 v Abaqus**

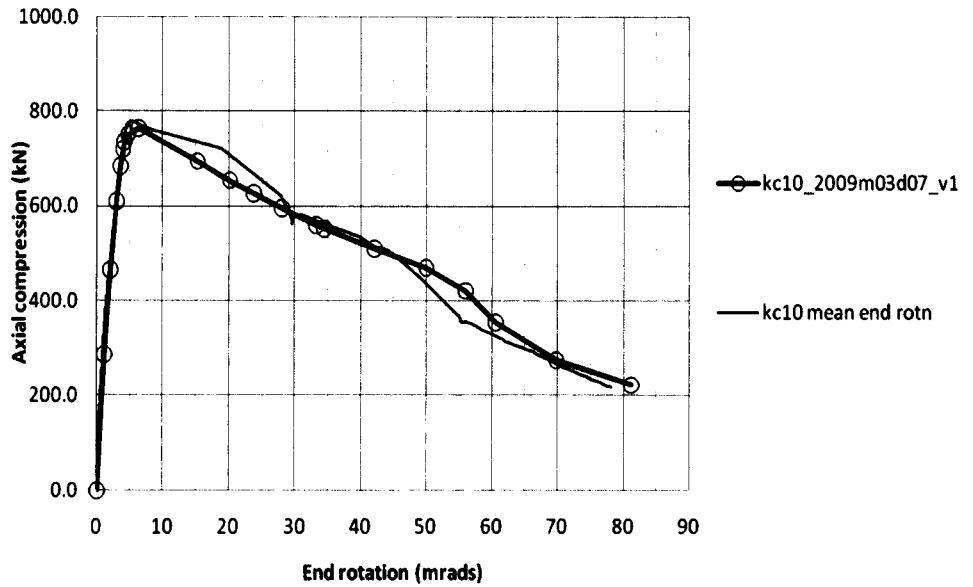


Figure 6.17 End-rotations – kc10, test mean & Abaqus

**test 3; load v end rotation
v Abaqus 2650mm**

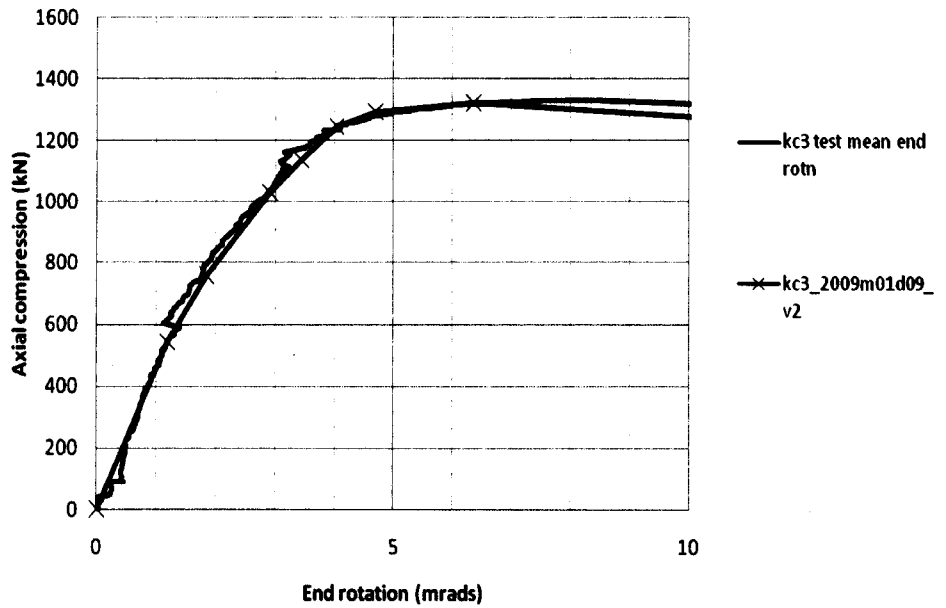


Figure 6.18 Initial end-rotations – kc3, test mean & Abaqus

load v end rotation test 4 & Abaqus

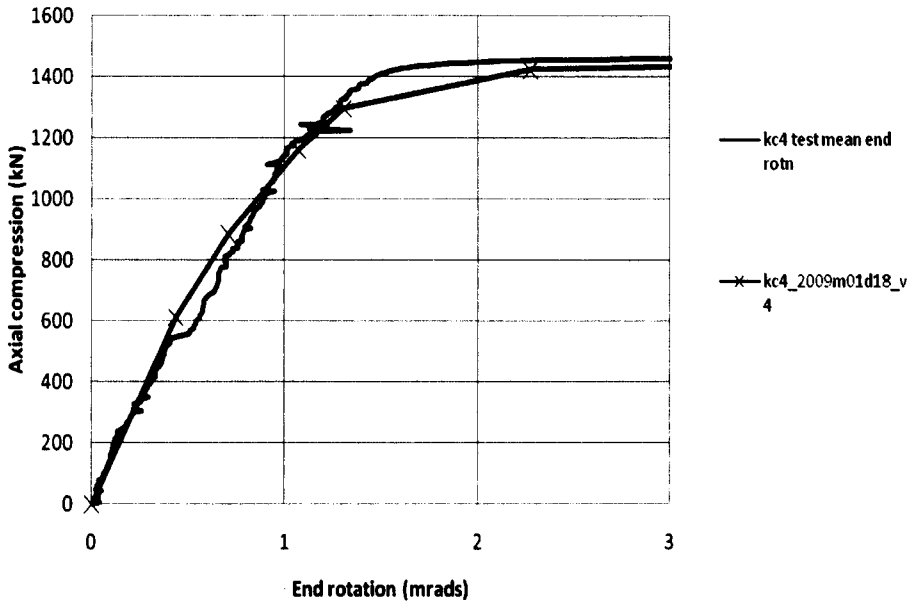


Figure 6.19 Initial end-rotations – kc4, test mean & Abaqus

load v end rotation test 5 & Abaqus

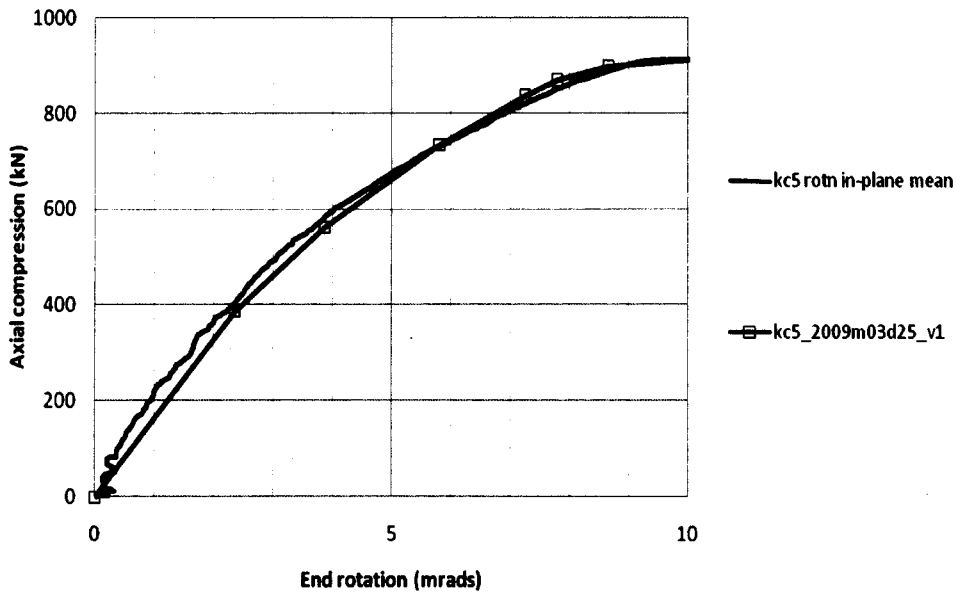


Figure 6.20 Initial end-rotations – kc5, test mean & Abaqus

**load v end rotation
test 6 v Abaqus**

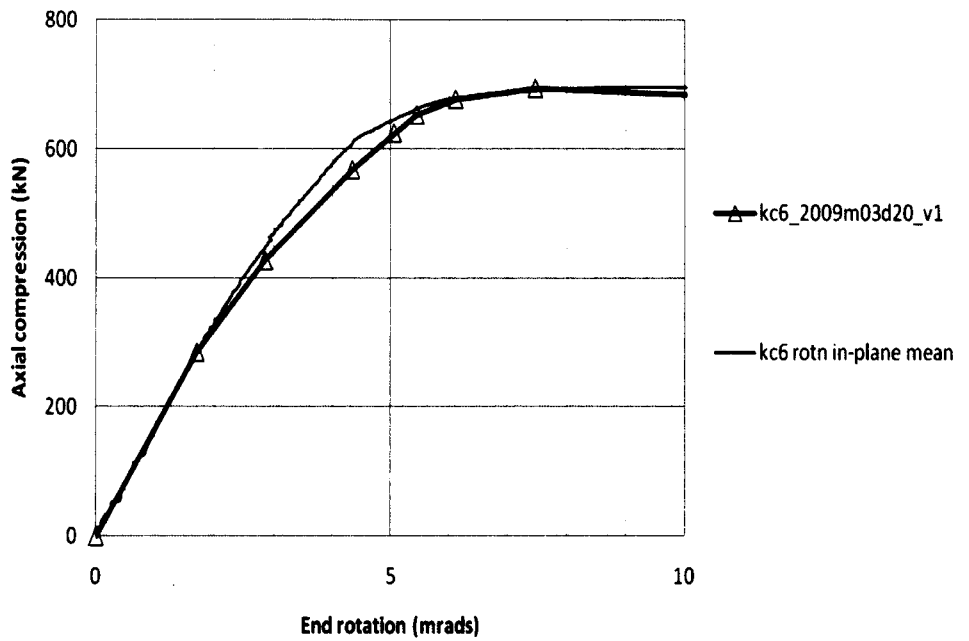


Figure 6.21 Initial end-rotations – kc6, test mean & Abaqus

**load v end rotation
test 7 v Abaqus**

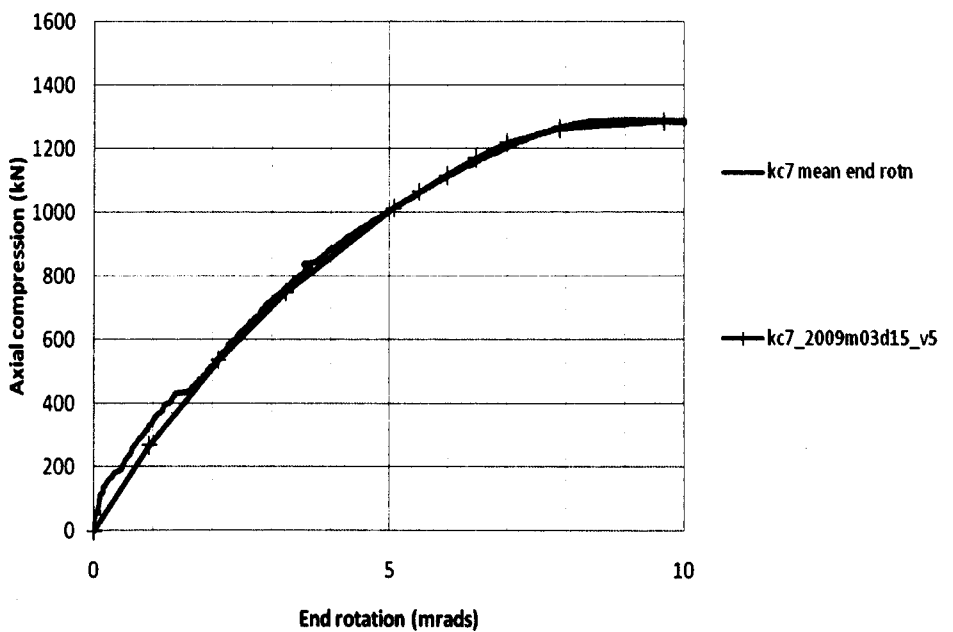


Figure 6.22 Initial end-rotations – kc7, test mean & Abaqus

load v end rotation test 8 v Abaqus

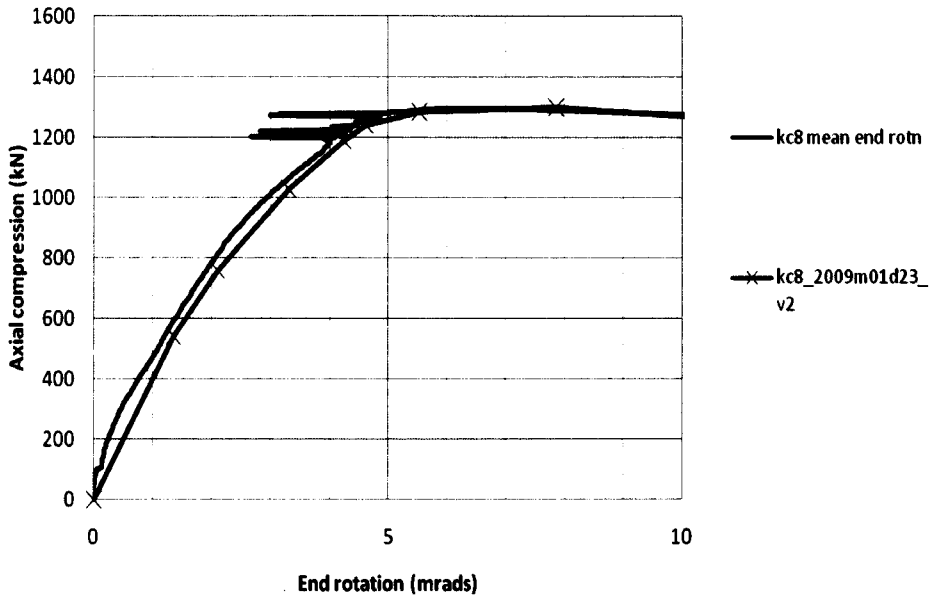


Figure 6.23 Initial end-rotations – kc8, test mean & Abaqus

load v end rotation test 9 v Abaqus

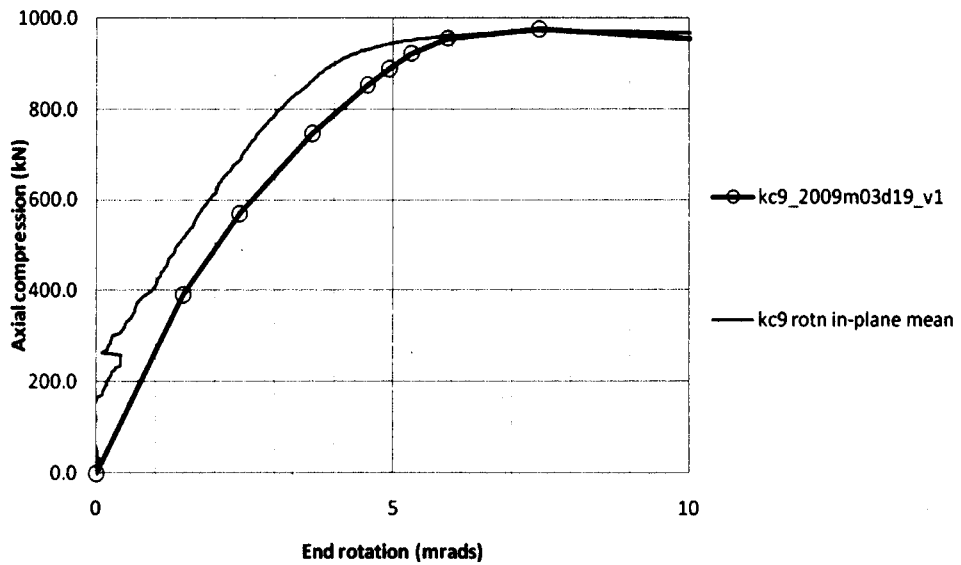


Figure 6.24 Initial end-rotations – kc9, test mean & Abaqus

load v end rotation test 10 v Abaqus

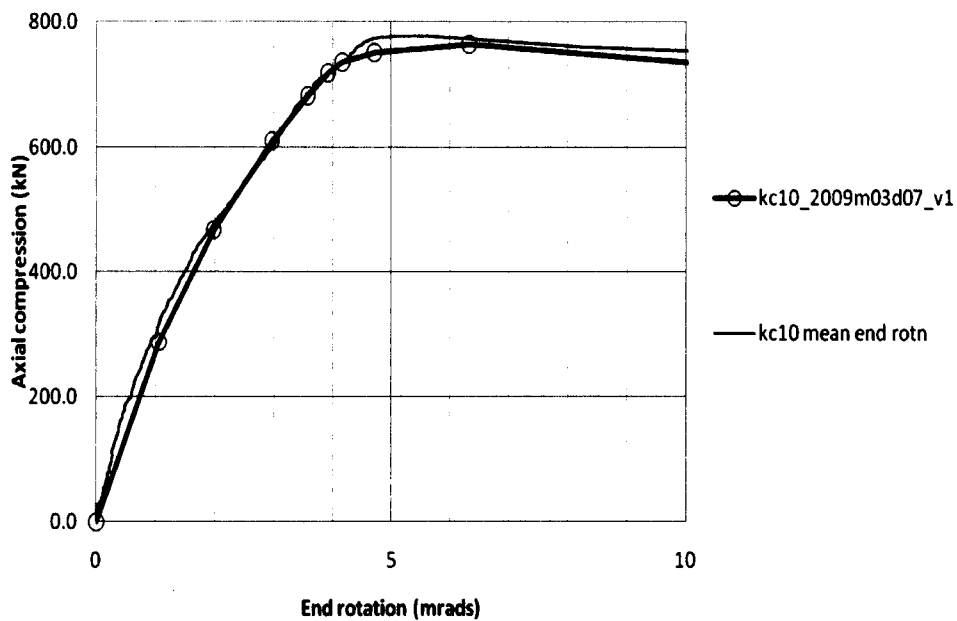


Figure 6.25 Initial end-rotations – kc10, test mean & Abaqus

Table 6.3 Abaqus with symmetric eccentricities - Comparison of tests and model.

Abaqus analysis using the standard elastic/perfectly-plastic stress/strain curve.

Test	kc3	kc4	kc5	kc6	kc7	kc8	kc9	kc10
Wall thickness (mm)	10	10	6.3	5	10	10	6.3	5
Max test load (kN)	1328	1458	915	695	1290	1298	971	777
0.2% proof stress (MPa)	375	390	428	389	note5	375	431	402
area factor	0.975	0.975	0.984	0.987	0.975	0.975	0.984	0.987
yield stress (MPa) used in Abaqus analysis	375	375 note1	437 note2	389	400	375	431	402
residual stress (MPa)	35.5	35.5	35.5	35.5	35.5	35.5	35.5	35.5
Abaqus max load	1356	1481	930	703	1320	1333	991	773
area reduced Abaqus max load (kN)	1322	1444	915	694	1287	1300	975	763
Abaqus red'd N – test N (kN)	-6 0.5%	-14 1.0%	+0 0.0%	-1 0.1%	-3 0.2%	+2 0.2%	+4 0.4%	-14 1.8% note4
Abaqus e_t (mm)	2.68	0.73	5.27	4.3	4.9	3.08	3.15	2.55
Abaqus e_b (mm)	2.68	0.73	5.27	4.3	4.9	3.08	3.15	2.55
Correlation factor $C_f = \theta_{CI}/\theta_{CA}$	1.003	1.021	0.831	see note3	0.804	0.841	0.941	0.918
note1	Using the coupon stress of 390 MPa as yield with the elastic/perfectly-plastic stress/strain curve, Abaqus could not continue beyond the maximum load.							
note2	A yield of 428 MPa, higher than the 0.2% proof stress, was used in the analysis because the maximum load was not achieved with an initial imperfection sufficient to make the analysis rotations agree with the test rotations.							
note3	No unloading cycle in tests so no point at which to calculate correlation							
note4	Using the coupon stress as the yield stress with the standard elastic/perfectly-plastic stress/strain curve, the test maximum could not be achieved							
note5	0.2% proof stress not known							
Abaqus input files	kc3_2009m01d09_v2 kc4_2009m01d18_v4 kc5_2009m01d27_v1	kc6_2009m03d20_v1 kc7_2009m03d15_v5 kc8_2009m01d23_v2	kc9_2009m03d19_v1 kc10_2009m03d07_v1					

The correlation factors, which are correlation factors on end-rotation at a given axial load, are shown in Figure 6.26. The mean value is 0.91, the maximum is 1.042 and the minimum is 0.804.

The reason for these differences between the test results and the Abaqus analysis is not known. Possibilities are:

1. Cross-sectional area of some sections might be less than nominal. The standard for hot-finished hollow sections, BS EN 10210-2:2006 [BSI 2006b], allows the weight/metre to vary by +/- 6% and individual wall thickness to vary by as much as -10%. This could explain some deficiency in measured resistance versus predicted.
2. Stress/strain characteristics at strains greater than yield strain cannot be expected to be as simple as the bi-linear stress-strain characteristics used in the model. It is probable that the actual stress at 1.0 yield strain yield is below the 0.2% proof stress, so the resistance is less than the Abaqus analysis predicts simply because it assumes the yield stress is equal to the 0.2% proof stress when the strain is equal to 1.0 yield strain.
3. The lack of yield stress coupon data for kc7 causes some uncertainty. The lowest value of correlation factor was calculated for test kc7 for which even the yield stress was not available, so the yield was deduced from the load and deflection output from the loading range of the test and the maximum load.

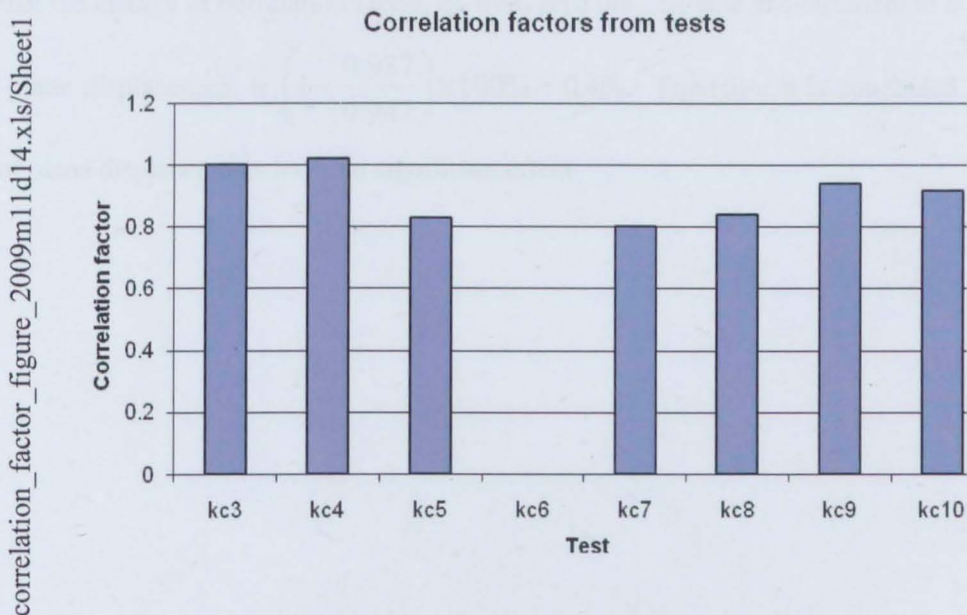


Figure 6.26 Correlation factors for rotation

6.4.3 Effect on the correlation factor of out-of-plane deflections

The tests were designed to study the columns deflecting in only one plane. There were also some modest out-of-plane deflections. These were not expected to make a significant difference to the results because the simple plastic model gives no difference in in-plane bending resistance for small out-of-plane bending moments. However, to quantify the effect of these on the correlation factor, it was investigated by analysis of the test case with the greatest out-of-plane deflection. This test was kc9 which had out of plane deflections of the order of 4mm. The out-of-plane deflection was induced in the Abaqus analysis by imposing equal and opposite end rotations. This might not induce the same deflected shape as in the test, but the magnitude of deflection at mid-height was similar. The sensitivity to out-of-plane deflection was then assessed by comparing the correlation factor calculated without out-of-plane deflection with the correlation factor calculated with out-of-plane deflection.

The out-of-plane displacements from the test and from the analysis are plotted in Figure 6.27. The mean in-plane end-rotations are plotted in Figure 6.28, showing that the effect of the out-of-plane displacement is very small.

The values are as follows:

Abaqus zero out-of-plane displacement gives $c_f = 0.941$

Abaqus with out of-plane-displacements gives $c_f = 0.937$

This shows that the change of correlation factor, c_f , from zero out-of-plane displacement to a 4mm out-of-plane displacement is $\left(1 - \frac{0.937}{0.941}\right) \times 100\% = 0.4\%$. Therefore it is concluded that the out of plane displacements have no significant effect.

**out-of-plane mid-height displacement
v mean end-rotation
test 9 v Abaqus**

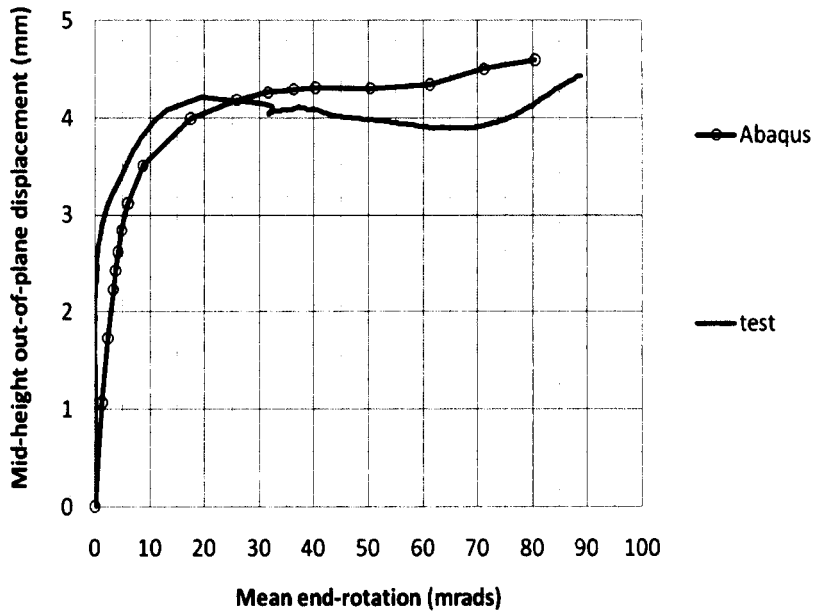


Figure 6.27 Effect of out-of-plane displacements – kc9, test & Abaqus

**load v end rotation
test 9 v Abaqus**

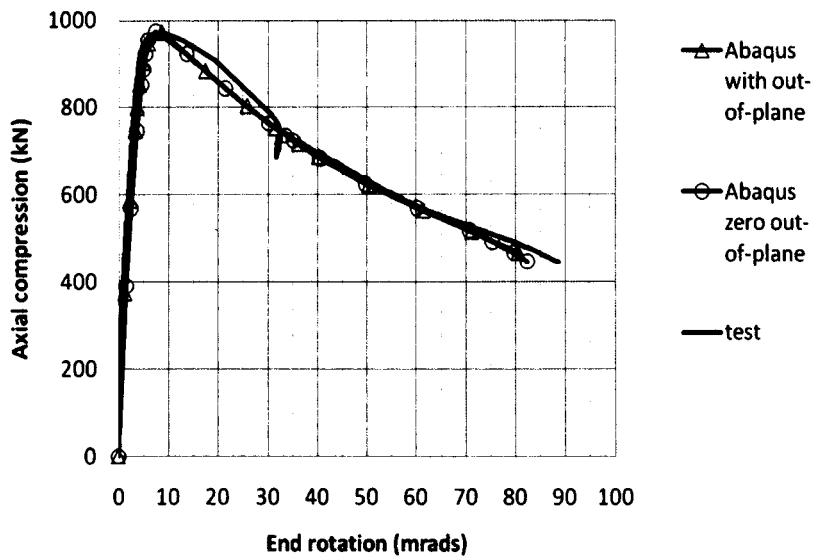


Figure 6.28 End-rotations – kc9, test mean & Abaqus

6.4.4 Effect on the correlation factor of a partly curved initial imperfection

The effect on the correlation factor of an initial imperfection that is partly curved was studied using test kc7. The test was to investigate if the value of the correlation factor is significantly affected by the choice either of the imperfection being a uniform eccentricity or a varying eccentricity as in a curved member. Test kc7 was selected because

1. it has the lowest correlation factor
2. the eccentricity is greater than the target eccentricity of 3.5mm

The end eccentricity was taken as equal top and bottom. The magnitude was taken as the target eccentricity less the eccentricity equivalent to the friction in the test rig bearings. The eccentricity equivalent to the friction was found from the plot of mid-height displacement v load for unloading/reloading cycle shown in Figure 6.30. At 800 kN, the displacement is 24.8 mm on the unloading path and 23.6 mm on the reloading path giving a range of 1.2 mm. The friction is equivalent to half the range so the magnitude is 0.6 mm. Therefore the end eccentricity was taken as:

$$\text{target eccentricity} - \text{friction eccentricity} = 3.5 - 0.6 = 2.9 \text{ mm} \quad \text{Eq 6.16}$$

The remainder of the imperfection was modelled as a sine curve as shown in Figure 6.29. This component of the imperfection needs to be 3.01 mm to give the same value of mean end-rotation at 80% maximum load as measured in the the test kc7. This makes a maximum initial imperfection of $2.9 + 3.01 = 5.91$ mm compared with 4.90 mm for the case of a uniform imperfection (equal to a uniform initial eccentricity of a perfectly straight column). Given the partly sinusoidal imperfection of 5.91 mm, the yield stress needs to be 411 MPa to achieve the maximum load measured in test kc7. The plots of test kc7 and the Abaqus analyses are shown in Figure 6.31 and Figure 6.32.

The correlation factors calculated for the two cases are

Uniform imperfection = 4.90 mm, $c_f = 0.804$,
(from Sheet "cf(2)" of kc7_Abaqus_factor_2010m03d05.xls)

Part curved imperfection = 5.91 mm, $c_f = 0.781$,
(from Sheet "cf(3)" of kc7_Abaqus_factor_2010m03d05.xls)

This shows the sensitivity is $0.804 - 0.781 = 0.023$ from 3.01 mm Sine curve

The measurement of the test specimen prior to testing found that the out-of-straight over the central 1.5 metres (the length of the longest available straight-edge) was only 0.1 mm to 0.2 mm in both the XX and YY planes. If the sinusoidal component of imperfection had been 3.01 mm as in the analysis, the out-of-straightness would have been $3.01(1-\text{Sin}(\pi(0.575/2.65))) = 1.11$ mm instead of the 0.1 to 0.2 mm measured.

Therefore, the reduction in c_f from the out-of-straightness of, say 0.15 mm, is only $0.023 (0.15/3.01) = 0.0011$, giving $c_f = 0.804 - 0.0011 = 0.803$. This is an insignificant difference from $c_f = 0.804$. This leads to the conclusion that the value of the correlation factor is not significantly affected by the choice either of the imperfection being a uniform eccentricity or a varying eccentricity as in a curved member.

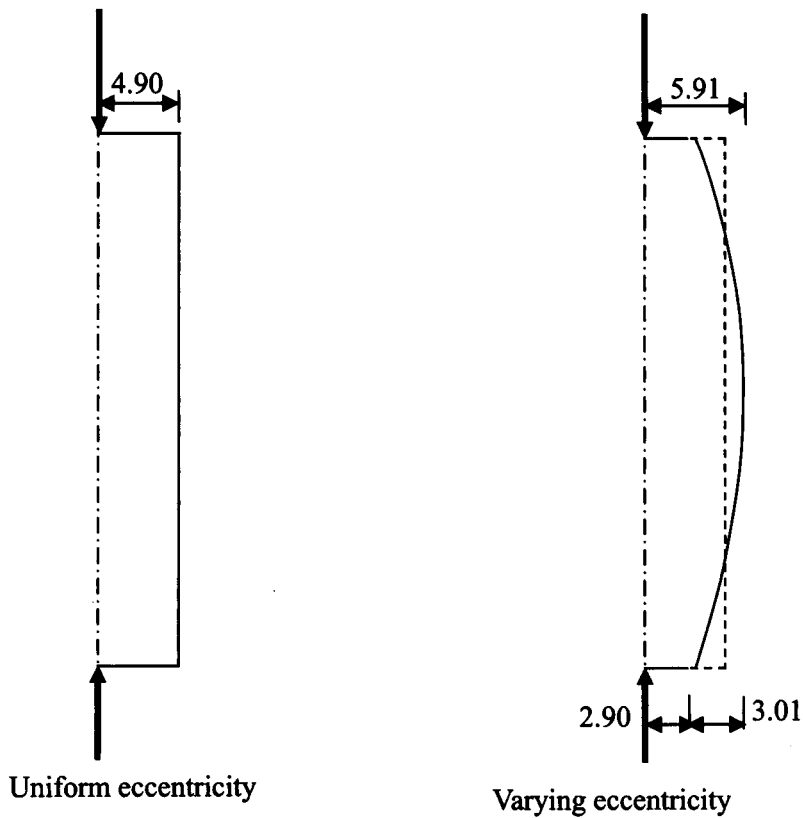


Figure 6.29 possible initial imperfections – kc7

**test 7 v Abaqus 2650mm
load v mid-height displacement**

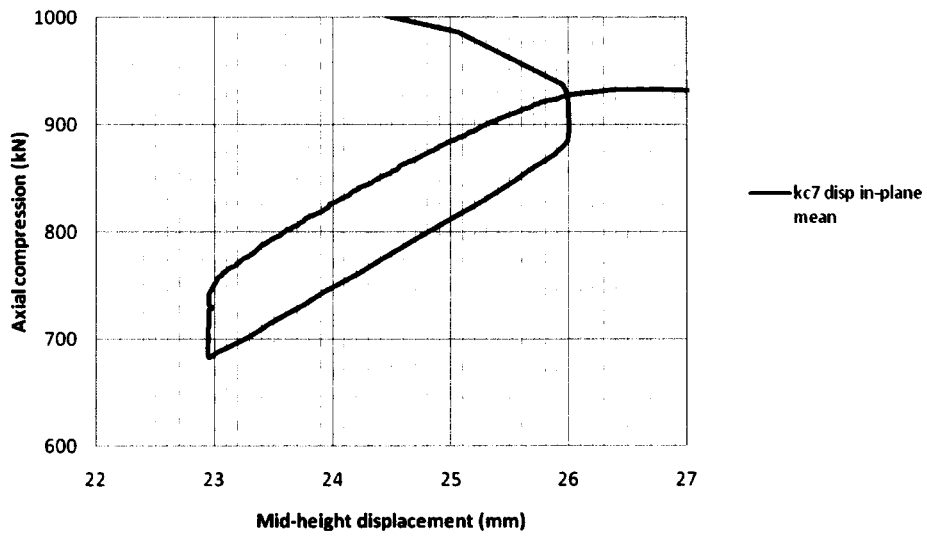


Figure 6.30 Unloading/reloading cycle – kc7, test

**load v end rotation
test 7 v Abaqus**

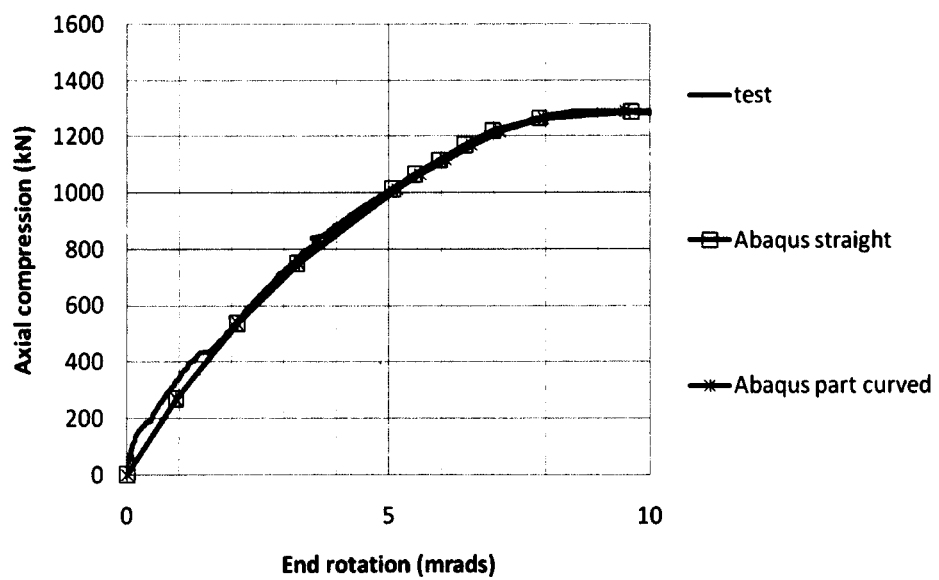


Figure 6.31 Initial end-rotations – kc7, test mean & Abaqus

load v end rotation test 7 v Abaqus

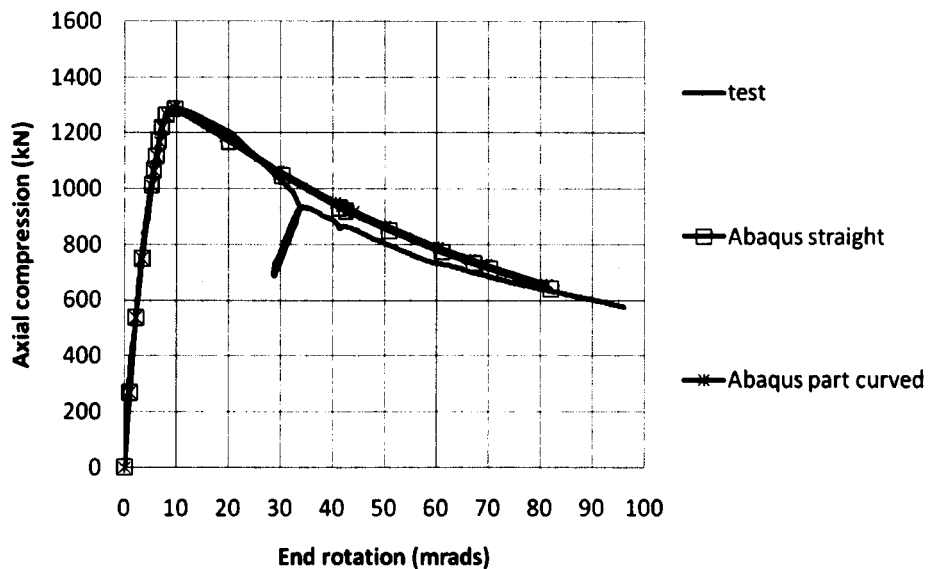


Figure 6.32 End-rotations – kc7, test mean & Abaqus

6.4.5 Effect on the correlation factor of residual stresses

The effect on the correlation factor of residual stresses was studied using test kc7 using the partly curved initial imperfection as shown in Figure 6.33. Test kc7 was selected because it has the lowest correlation factor. The partially curved initial imperfection was chosen because the effect of imperfections is least where the length of the yielded zone is least and this occurs where the initial imperfection is curved. The initial imperfection was the same as use in Section 6.4.4 so that the loading curve was as recorded in the test.

To achieve the same maximum load as in test kc7, the yield stress had to be reduced to 400MPa. The correlation factors for the two cases are:

With residual stress 10% nom yield , $c_f = 0.781$,

(from Sheet “cf(3)” of kc7_Abaqus_factor_2010m03d05.xls)

Zero residual stresses, $c_f = 0.837$,

(from Sheet “cf(4)” of kc7_Abaqus_factor_2009m03d05.xls)

This shows the sensitivity of the correlation factor is $0.837 - 0.781 = 0.056$ from residual stress of 10% nominal.

The actual residual stresses in the specimen are not known. However, assuming the actual residual stress was between 50% and 100% of the 10% nominal yield assumed in the parametric studies, the correlation factor is higher than shown in Table 6.3 by somewhere by up to 50% of $0.056 = 0.023$. This shows that the correlation factors deduced in the table are slightly conservative, but it was decided to use the values in the table because conservatism helps to give confidence in new structural models.



Figure 6.33 Initial imperfections – effect of residual stresses kc7

6.5 Effects of breadth to thickness ratios of wall

The effect of the breadth to thickness ratios of was originally investigated by the theory and formulae in Appendix E. These predicted that a 140×140 SHS with a 6.8mm wall thickness would be stable with equal and opposite end-rotations (single curvature) of 40 milliradians.

The range of wall thicknesses of the test columns was chosen to study the effect of the breadth to thickness ratio. Scaling from the predictions for 140×140 SHS to a 120×120 SHS, the wall thickness for stability at 40 milliradians would be $6.8 \times 120 / 140 = 5.8$ mm. Therefore the walls of the $120 \times 120 \times 6.3$ SHS in tests kc5 and kc9 were expected to be stable at end-

rotations greater than 40 milliradians but the walls of the 120×120×5.0 SHS in tests kc6 and kc10 were expected to be unstable at 40 milliradians.

The load v end-rotation curves together with the Abaqus analysis results for tests kc5 and kc9 are shown in Figure 6.35 and Figure 6.36. The tests kc5 show a very slight and gentle reduction of load from about 70 milliradians. Examination of the deformed plots of the Abaqus models showed that Abaqus predicts that local buckling develops from 78 milliradians in test kc5 and from 75 milliradians in test kc9.

The load v end-rotation curves together with the Abaqus analysis results for tests kc6 and kc10 are shown in Figure 6.37 and Figure 6.38. The tests show a major reduction of load from about 55 and 40 milliradians. The Abaqus plots predict that the reduction should not appear until near 55 milliradians, showing that the actual stability might be less than predicted by the Abaqus analysis but greater than that predicted by the finite slice model and simplified application of plastic flow theory in Appendix E. The rotation capacity from the tests is shown as a bar chart in Figure 6.34. The minimum rotation achieved without reduction of resistance due to local buckling is shown for the three wall slendernesses tested. The wall slenderness is calculated as the distance between mid-planes of the walls divided by the wall thickness, so for a 120×120×10 SHS, $b/t = (120-10)/10 = 11$. It should be noted that for the 10mm wall columns (wall slenderness $b/t = 11$), there was no drop of resistance due to local buckling even at the maximum test rotation.

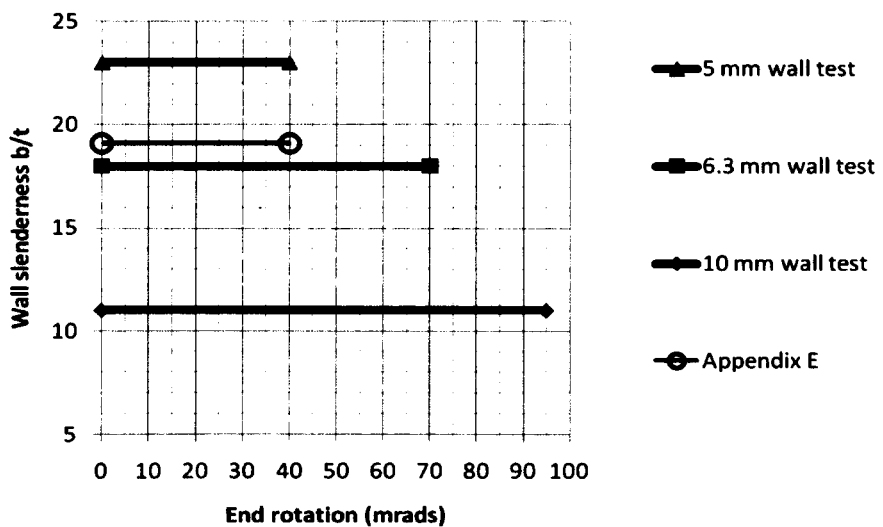


Figure 6.34 Effect of local buckling – rotation capacity from tests

**load v mid-height displacement
test 5 v Abaqus**

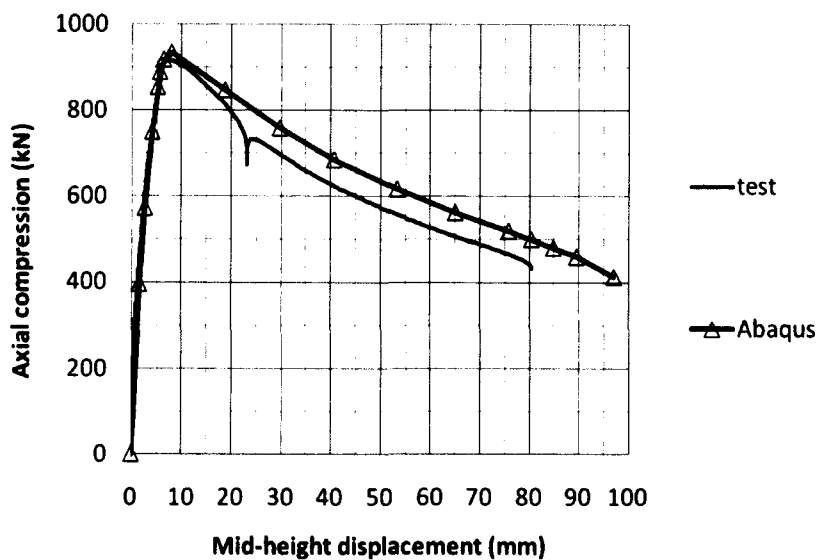


Figure 6.35 Effect of local buckling – kc5, test & Abaqus

**load v mid-height displacement
test 9 v Abaqus**

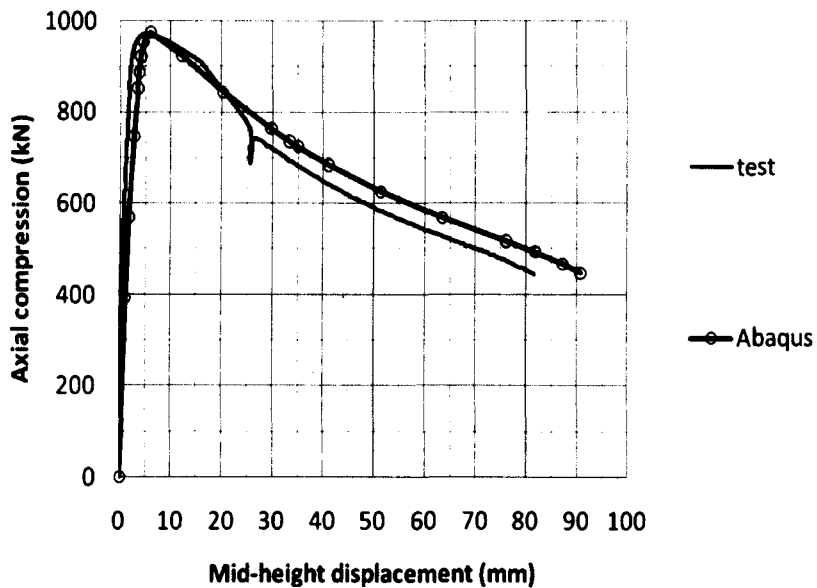


Figure 6.36 Effect of local buckling – kc9, test & Abaqus

**load v end rotation
test 6 v Abaqus**

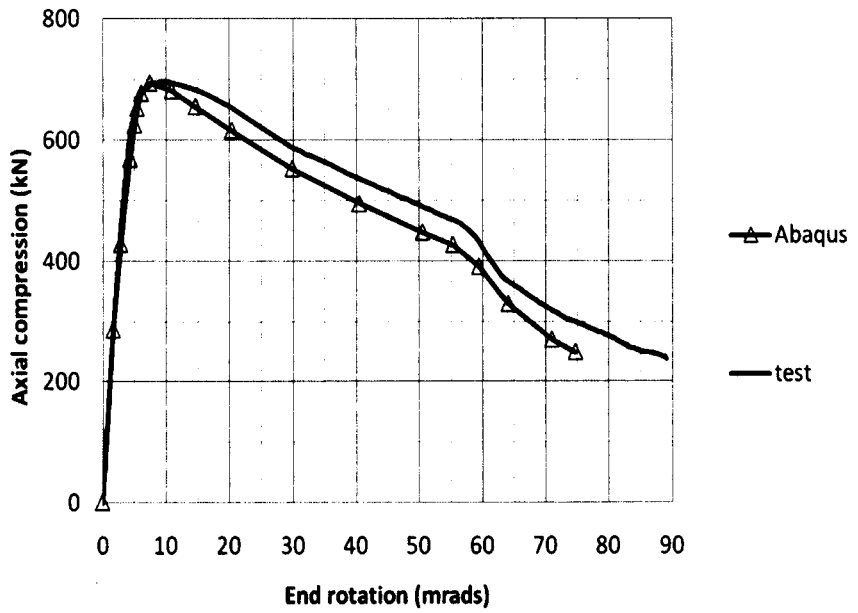


Figure 6.37 Effect of local buckling – kc6, test mean & Abaqus

**load v end rotation
test 10 v Abaqus**

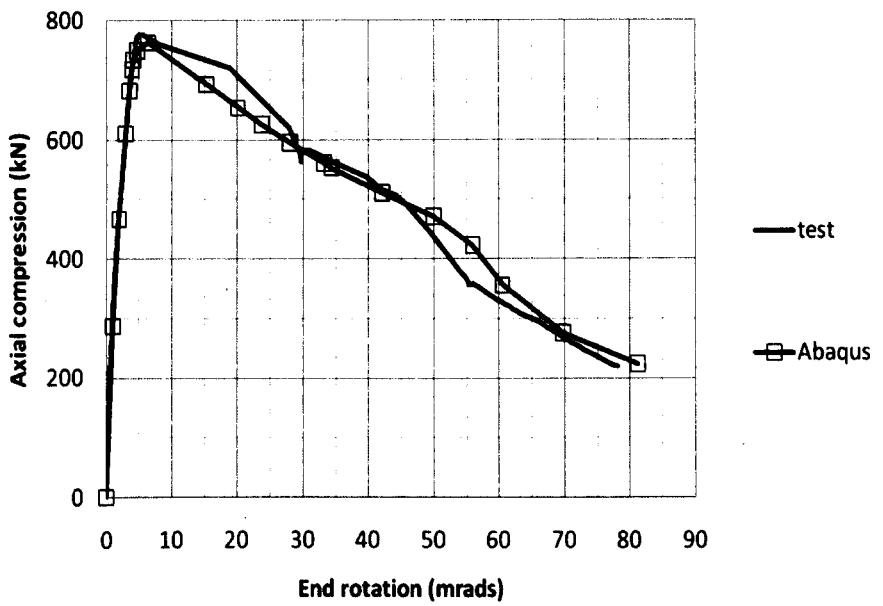


Figure 6.38 Effect of local buckling – kc10, test mean & Abaqus

6.6 Correlation factor, c_f , used for the design model

The values of the correlation factor, c_f , from Table 6.2 and Table 6.3 are shown in Table 6.4.

Table 6.4 Abaqus with symmetric eccentricities								
Comparison of tests and symmetrical model.								
Abaqus analysis using the standard elastic/perfectly-plastic stress/strain curve.								
Test	kc3	kc4	kc5	kc6	kc7	kc8	kc9	kc10
Wall thickness (mm)	10	10	6.3	5	10	10	6.3	5
Asymmetric eccentricities								
Abaqus e_t (mm)	2.25	3.20	note1	note1	10.39	7.92	note1	note1
Abaqus e_b (mm)	2.87	-1.34			-0.59	-1.99		
Abaqus $e_t - e_b$ (mm)	0.62	4.54			10.98	9.91		
Correlation factor (rotns) $c_f = \theta_t / \theta_A$	0.991	1.018			0.749	0.829		
Symmetric eccentricities								
Abaqus e_t (mm)	2.68	0.73	5.27	4.3	4.9	3.08	3.15	2.55
Abaqus e_b (mm)	2.68	0.73	5.27	4.3	4.9	3.08	3.15	2.55
Correlation factor (rotns) $c_f = \theta_t / \theta_A$	1.003	1.021	0.831	note2	0.804	0.841	0.941	0.918
note1	Not analysed with asymmetric eccentricities							
note2	No unloading cycle in tests so no defined point at which to calculate correlation							

The misalignment between the lines of application of load, ($e_t - e_b$), in the asymmetric analysis of kc7 and kc8 (in Table 6.2) are not credible given the quality of the test laboratory and the care taken to align the column correctly. Therefore it must be concluded that the majority of the difference of end rotation, at least in the loading part of the test, was caused by sway of the test rig. In the critical case of test kc7, 11 mm eccentricity reduced the correlation factor c_f from 0.804 to 0.741, a reduction of 0.063. Given the special adjustable shoes used, the maximum credible misalignment is around 1 mm.

Therefore the worst credible correlation factor is $0.804 - 0.063/11 = 0.798$. This gives the range of credible values of correlation factor from 1.042 for test kc3 (symmetric) to 0.798 for kc7 (worst credible asymmetric). These were all deduced with a residual stress of 10% of nominal yield stress, which is a likely maximum value, so it is improbable that this was the value in the test columns. If the test columns had lower residual stresses, the actual yield stress would be lower than applied in Abaqus to achieve the predicted maximum load. From Section 6.4.5 it can be seen that if the residual stress were 8% nominal yield instead of 10%, the correlation factor would be raised by $0.2 \times 0.056 = 0.011$, giving a likely minimum value of correlation factor of $0.798 + 0.011 = 0.809$.

Therefore, the value of correlation factor selected for the calibration of the design model was taken as 0.80, giving a small margin below the lowest value and a significant margin below the median of the range from 1.042 and $0.809 = 0.926$.

6.7 Summary

The Abaqus model described in Chapter 4 was used to simulate the full-scale laboratory tests. A correlation factor, c_f , was obtained using an elastic/perfectly-plastic bi-linear model for the stress-strain characteristics. For each test, the model was correlated to the test both by using the “yield” test coupon 0.2% proof stress as the yield stress of the model (wherever it was available and the Abaqus model could complete the analysis with it) and by adjusting the initial imperfection in the model to reproduce the test behaviour of the test from zero to near maximum load (the “elastic” range of the test).

The load v end-rotation curves from the models were close to the load v mean-end-rotation curves of the tests. The difference between the end-rotations from the tests and from the analyses was established from the “static” point on the unloading cycle and a correlation factor, c_f , was calculated as rotation-from-test/rotation-from-model at the load of the “static” point in each of the tests. The mean value of the correlation factors was 0.914 with the minimum of 0.804.

While 0.8 might be considered disappointing as a correlation of end-rotations from a finite element analysis of a structure in which considerable elastic zones remain, it is considered acceptable for the falling branch of a compression member which has been almost completely plastified. The correlation between test and analysis looks much better when examined from the more common point of view of loads. The lowest correlation factor for

end rotation was found from test kc7 which gave an axial load of 927 kN at the “static” point compared with 1011 kN predicted by Abaqus at the same rotation. This gives a ratio of 0.92, which is good for a falling branch in a test which plastified almost the entire cross-section of the column over a considerable length.

The lowest credible value of end-rotation correlation factor, $c_f = 0.8$, was selected for calibration of the design model.

7 BREADTH TO THICKNESS LIMITS

7.1 Introduction

7.1.1 Overview

The structural mechanics of the effects of curvature are shown in Figure 7.1, Figure 7.2 and Figure 7.3. Figure 7.1 shows a section of an SHS that is curved. On the compression face, a longitudinal slice of the wall is marked. On the right of Figure 7.1, this longitudinal slice is shown in elevation. The longitudinal force on this section causes a radial component as indicated by the radial arrows. The radial component is most easily considered as a radial pressure, $p_{RC} = t\sigma_C/R$, where σ_C is the longitudinal compressive stress in the wall of the SHS at that longitudinal slice, t is the wall thickness and R is the radius of curvature of the deflected member at the section under consideration.

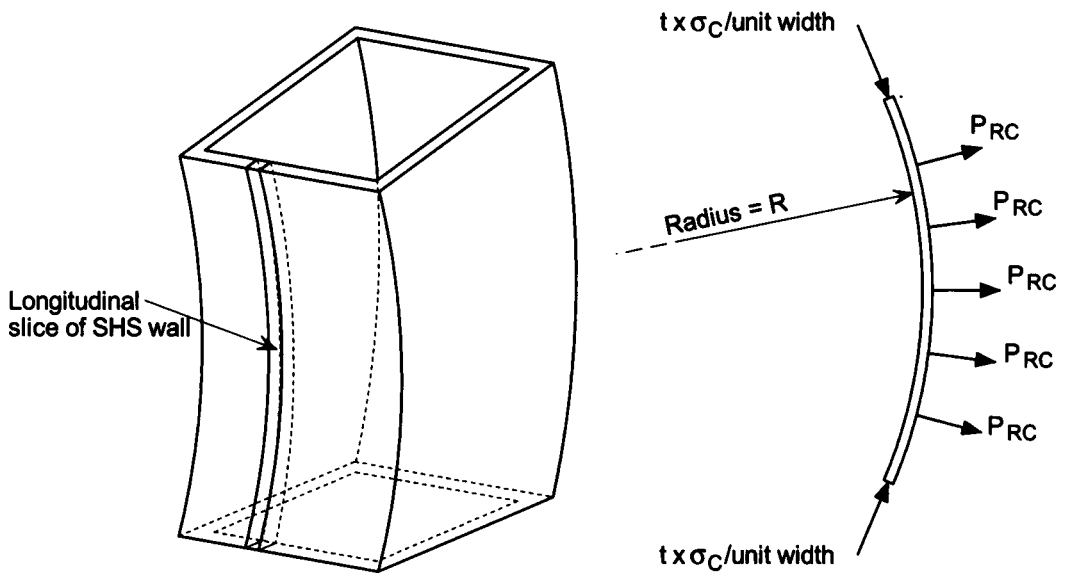


Figure 7.1 Out-of-plane loads on curved walls

The radial pressure, p_{RC} , can only be resisted by transverse bending of the wall of the SHS, as shown in Figure 7.2 and Figure 7.3. Figure 7.2 shows the radial pressures and the transverse bending moment diagram from longitudinal compression in both curved walls. Figure 7.3 shows the radial pressures and the transverse bending moment diagram from longitudinal compression in the wall on the inside of the curve and longitudinal tension in the wall on the outside of the curve. A special limitation on the breadth to thickness ratios is needed, similar to the need for a special limitation for seismic design in cases with high ductility demand.

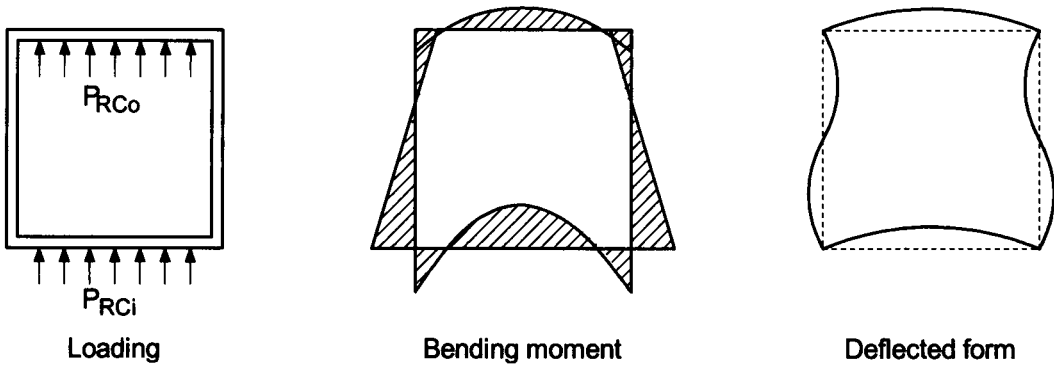


Figure 7.2 Transverse bending of walls, both sides in compression

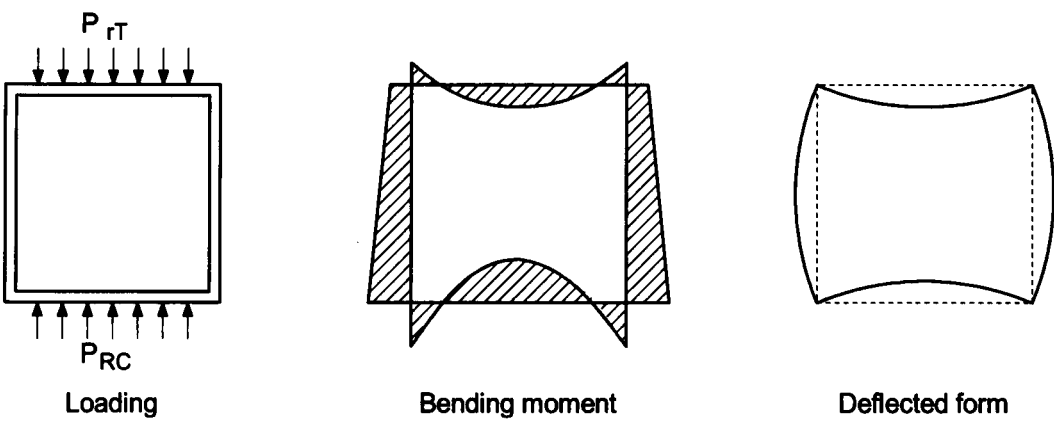


Figure 7.3 Transverse bending of walls, one side compression, one in tension

7.1.2 Non-linear geometrical effects (second-order effects)

The deflected forms shown in Figure 7.2 and Figure 7.3 cannot be calculated accurately by first-order analysis of the transverse bending, because the deflections induced by the transverse pressure cause an increase in local curvature along the centreline of the wall, thus causing an increase in transverse pressure. This is shown in Figure 7.4. If the wall remains in the elastic range, this magnification can be calculated approximately using classic magnification approaches.

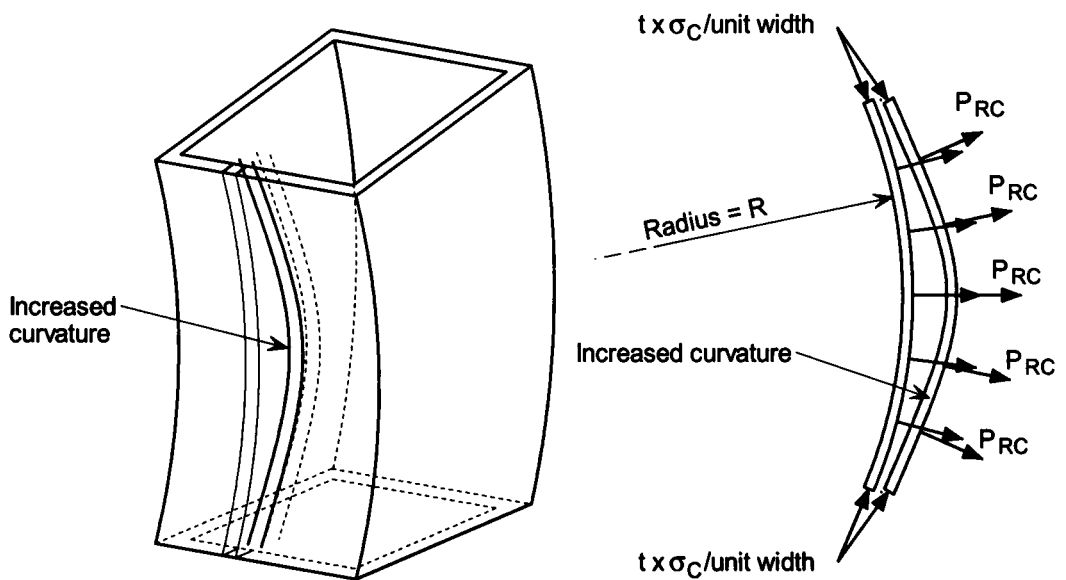


Figure 7.4 Increased curvature of wall towards the middle of the wall

7.1.3 Yield and non-linear material effects

In all common structural steel columns at maximum load, the most compressed elements are at yield stress. In columns of modest slenderness with significant end rotations, the strains are in excess of yield strain. For example, for a $140 \times 140 \times 10$ SHS 3.0 metres long in single curvature with a 0.040 radian end rotation, the most severe curvature is $2 \times 10^{-4} \text{ mm}^{-1}$ and the maximum compressive strain is approximately $(5000/355) \times \text{yield strain} = 14 \times \text{yield strain}$.

Where a material exceeds yield, there will be plastic flow. The extent of the plastic flow will depend on the strain beyond the yield strain. The effect of plastic flow is to increase the local deflections of the walls beyond the elastic deflections. This will increase local curvatures caused by transverse bending of the walls and might precipitate failure of the column. Plastic flow is explained with elegant simplicity by Calladine [Calladine 1969]. Detailed calculations are given in Appendix E, showing that the breadth-to-thickness ratios need to be limited.

The issue was studied in the laboratory test program reported in Chapters 5 and 6 by testing a variety of wall thicknesses for the same nominal size of square hollow section and also by a parametric study by Abaqus reported in Section 7.2.

7.1.4 Breadth to thickness limits in codes

BS 5950-1:2000 and Eurocode 3 use similar classifications, from Class 1 to Class 4, where Class 4 have the most slender component parts. Class 4 sections have parts that are so slender that these sections would not be suitable for the structures considered in this project firstly because these structures need the smallest possible sections (to allow the sections to be hidden in the wall thickness) and secondly because the design method requires plasticity to allow “moment shedding”. Therefore, Class 4 sections will not be considered further.

The classification systems in BS 5950-1:2000 and Eurocode 3 are as follows:

- a member resisting compression alone needs to be Class 3,
- a member that is designed to develop the plastic moment of resistance must be Class 2
- a member that is designed to develop a plastic hinge and rotate must be Class 1.

Because the classification rules are intended for application in relatively simple design models, there is some ambiguity about the range of application of Class 2 and Class 1. This arises because most global analysis routines in design offices do not consider local plastic strains, so do not calculate rigorously the curvature at points at which the plastic moment of resistance has been attained. Instead, the curvature for Class 2 is limited to use with elastic global analysis with a redistribution allowance of 10% - 15% and the curvature of Class 1 sections (or the rotation of the plastic hinge) is generally not limited in codes.

Because codes do not give explicit curvature limits appropriate to each Class of element slenderness, it is not possible to decide whether the columns may be Class 2 or need to be Class 1 if designed with the methods developed in these studies. There is even the possibility that the breadth to thickness ratios need to be more severe than Class 1. There is concern that common Class 1 limitations are not adequate for earthquake design due to the severe curvatures developed. The issue is recognised in design guidance for earthquake resistant design, such as Dowrick, [Dowrick 1977]. The AISC Seismic Provisions for Structural Steel Buildings [AISC 2005a] contains Table I-8-1 which gives more severe breadth to thickness ratios for certain members than required for normal design.

A similar condition to the case of single curvature arises in earthquake resistant design in certain types of structures. Three of these types of structure are included in the AISC Seismic Provisions for Structural Steel Buildings [AISC 2005a]. These are Special Truss Moment Frames, Special Concentrically Braced Frames and Ordinary Concentrically Braced Frames. In these frames, compression members with high demand for ductility have to satisfy the Limiting Width-Thickness Ratios for Compression Elements given in Table I-8-1.

For rectangular hollow sections, this gives the b/t limit of $0.64\sqrt{(E/F_y)}$. Structures in the USA without seismic loading would be designed to the AISC Specification [AISC 2005] which has a slenderness limit of $1.12\sqrt{(E/F_y)}$. Therefore, for S355 steel, $b/t \leq 0.64\sqrt{(205000/355)} = 15.4$ for the flat segment of the wall for these types of seismic resistant structures compared with $1.12\sqrt{(205000/355)} = 29.9$ in the AISC Specification [AISC 2005] and $28\epsilon = 28\sqrt{(275/355)} = 24.6$ required for Class 1 in BS 5950-1:2000.

Taking $B = b + 3t$, as given in BS 5950-1:2000 Table 12, and using $b/t = 15.4$ gives the overall breadth $B = 15.4t + 3t = 18.4t$. Therefore the minimum thickness for a 140×140 SHS is $140/18.4 = 7.6$ mm to satisfy the AISC Seismic Provisions. By comparison, to satisfy BS 5950-1:2000 Table 12, Class 1 allows $B = b + 3t = (24.6 + 3)t = 27.6t$. Therefore the minimum thickness for a 140×140 SHS is $140/27.6 = 5.1$ mm, demonstrating that more severe b/t ratios may be required than found in BS 5950-1 and EN 1993-1-1. The initial studies of this issue made as part of this project, reported in Appendix E, confirmed that much more onerous limits are required than appear in the BS and the EN.

7.2 Parametric study

The reduction of resistance of high breadth to thickness ratios is most pronounced when the curvature is high. The design model assumes that the column is in single curvature for calculation of overall buckling resistance, but many columns will be in double curvature as shown in Figure 7.5.

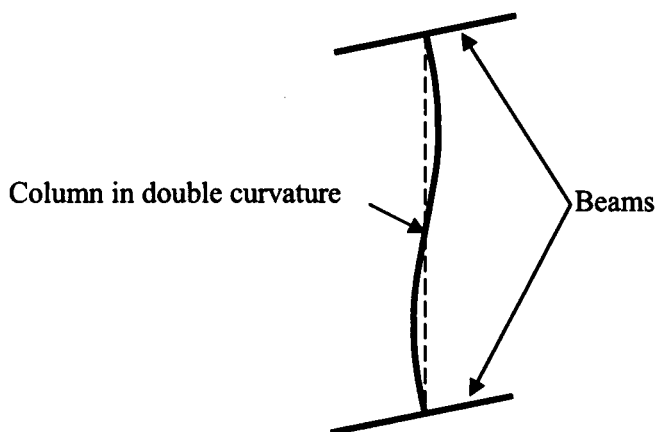


Figure 7.5 Column in double curvature

This effect was investigated by a parametric study using 140×140 SHS sections of different thicknesses. The analyses were made using enforced shortening of pin-ended columns with the initial imperfection in the plane of the end-rotations. The effects with end-rotations in a rectangular plane were investigated for columns of in single curvature of lengths 750mm and 1500mm to reproduce the behaviour of columns in double curvature of 1500mm and 3000mm length. The results are shown in Figure 7.6. From these it can be seen that the wall stability is more demanding for 750mm than for 1500mm, but not enormously so.

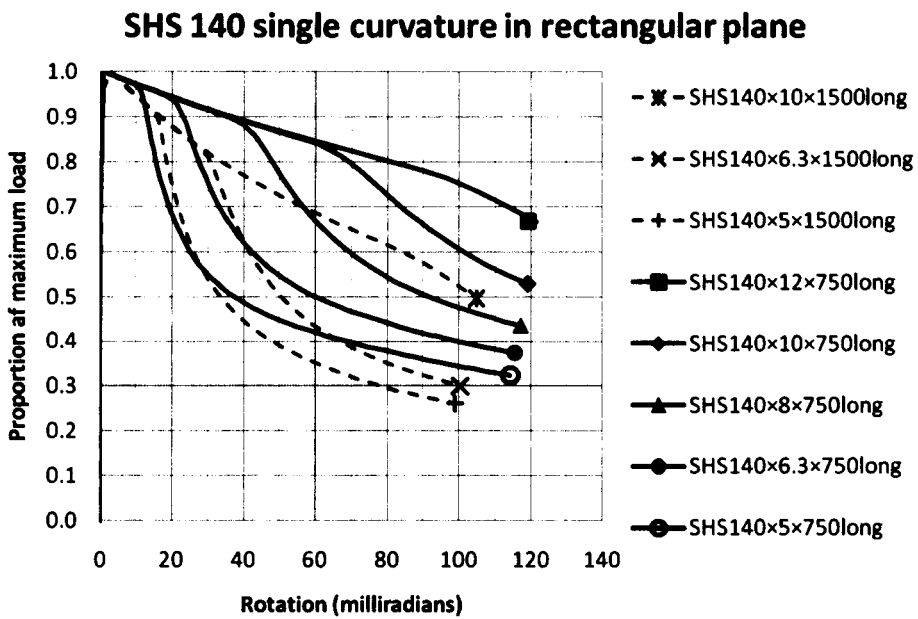


Figure 7.6 140×140 SHS in single curvature in rectangular plane

Similar analyses were conducted for end-rotation in a plane at 45° to the rectangular planes as shown in Figure 7.7. From these it can be seen that the wall stability requirements for end-rotations at 45° are almost identical to those for end-rotations in a rectangular plane.

SHS140×750mm single curvature in 45° plane

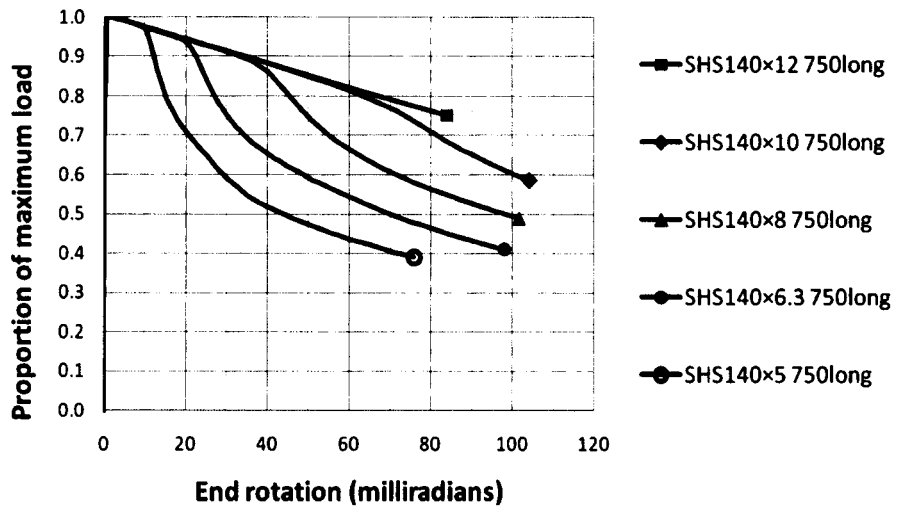


Figure 7.7 140×140 SHS in single curvature at 45° to rectangular plane

The breadth to thickness ratio at which the column resistance falls below the stable wall behaviour is shown in Figure 7.8.

design limits 750mm single curvature

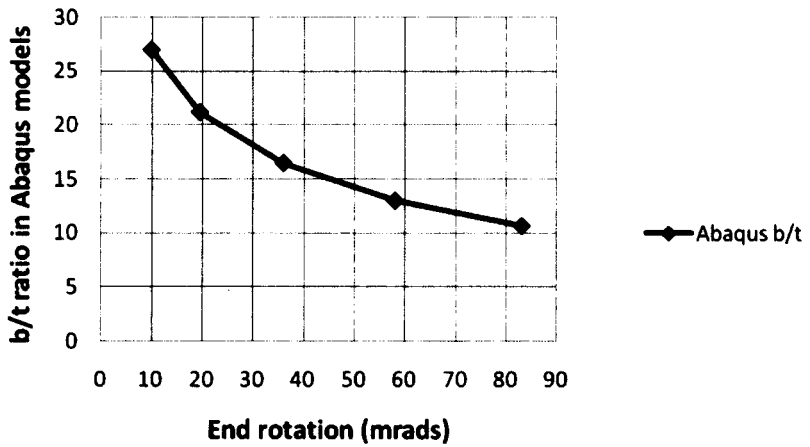


Figure 7.8 Limiting wall breadth to thickness ratio from Abaqus

7.3 Calibration of Abaqus with laboratory test results

In Chapter 6, the comparison of the laboratory tests with Abaqus analysis shows that Abaqus may overestimate the end-rotations at which the walls remain stable. The ratio of worst test result to Abaqus analysis result is 40mrads/55mrads for 120×120×5 SHS and 70mrads/78mrads for 120×120×6.3 SHS. The points are plotted in Figure 7.9 and the equation of the straight line through these points is used as a reduction factor on the results of the Abaqus parametric study to allow for the differences between real SHS sections and the Abaqus finite element models. The reduction factor is $1.5175 - 0.03436(b/t)$, but it cannot be greater than 1.0.

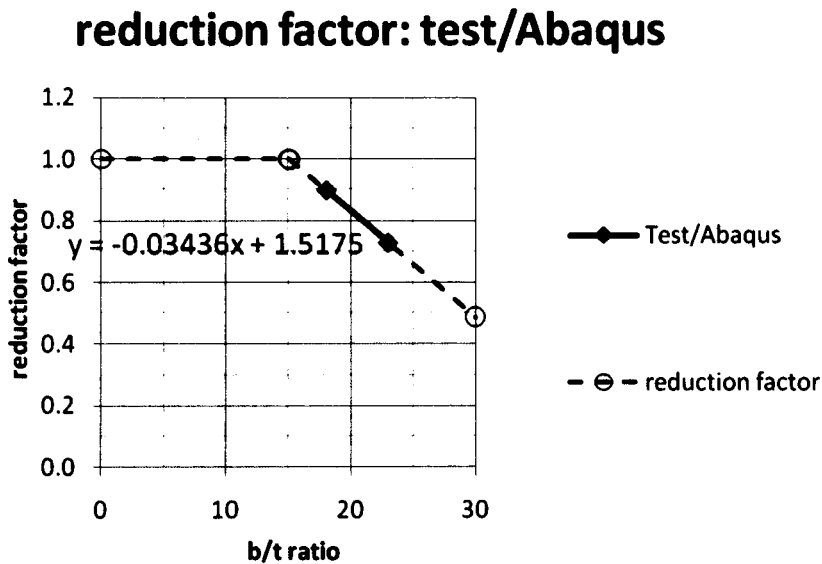


Figure 7.9 Wall slenderness limitations, test v Abaqus

7.4 Design limits

The design limits are defined using the results of the Abaqus parametric study shown in Figure 7.8 together with the reduction factor of test/Abaqus shown in Figure 7.9. Another factor in defining design limits is the relationship between calculated values of column end-rotations and the values that may occur in real structures. In design offices, the deflections of beams are commonly calculated by elastic analysis. Where a plastic hinge occurs in a beam, the hinge would be assumed to occur at a point and the deflections would be calculated assuming elastic behaviour between the points of the hinges. The effects of

spread of plasticity along the beam would not normally be considered. This produces some slight underestimate of deflections. Therefore it is helpful for designers to have design values of wall slenderness versus end-rotation that can be used with the end rotations calculated by the common design office techniques.

While b/t is a useful ratio for theoretical studies of wall slenderness, it is not so helpful for designers because section sizes are given in terms of the overall width, B , not the distance between mid-planes of walls, b . Therefore, the design limits in this report are given in terms of B/t .

To ensure that the columns can sustain the end-rotation, the slenderness should not exceed the limit defined by the “ B/t limit” line shown in Figure 7.10. This is derived from the parametric study in Section 7.2 with the allowable rotations reduced

1. by the reduction factor derived from the ratio of limiting end-rotation in the tests to the limiting end-rotation from the Abaqus analysis of tests from Chapter 6, shown in Figure 7.9 and
2. by a factor of 0.8 to allow for both the uncertainties of manufacture (eg wall thickness) and of analysis.

This curve has been derived for columns of length/breadth = 10.7 in double curvature. Columns that have smaller ratio of length/breadth can be expected to need thicker walls, but it is considered unlikely that such stocky columns would ever be desired in structures designed using this design model. The curve is

$$B/t = -14\text{Log}_{10}(\theta/1000) + 38.5 \quad \text{Eq 7.1}$$

where θ is in radians (not milliradians).

design limits: $L/B \geq 10.7$

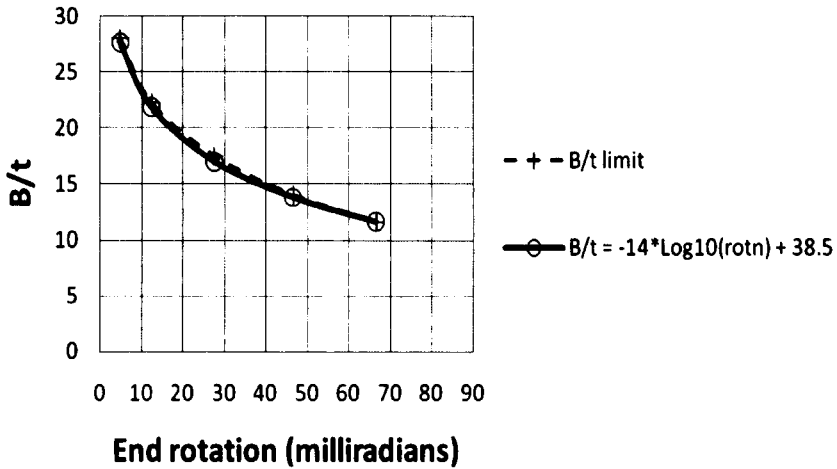


Figure 7.10 Wall slenderness limitations, overall breadth/thickness, B/t

These requirements are more demanding than common code limits as demonstrated for BS 5950-1 and Eurocode 3 below.

Requirements of BS5950-1

For a hot-finished square hollow section designed to BS 5950-1 [BSI 2000a], the slenderness limits for sections is expressed as $b/t = 28\epsilon$ for Class 1 and $b/t = 32\epsilon$ for Class 2, where b is the width of the external flat face and $\epsilon = (275/\text{yield})^{0.5} = (275/355)^{0.5} = 0.880$.

Therefore, for the flat face, $b/t = 28 \times 0.880 = 24.6$ for Class 1 and $b/t = 32 \times 0.880 = 28.2$ for Class 2.

According to Annex A3 of EN 10210-2 [BSI 2006b, CEN 2006b], the external corner radius may be taken as 1.5 times the wall thickness. Writing the slenderness limits in terms of the overall width, B , of the section, these limits are:

$B/t = 1.5 + 24.6 + 1.5 = 27.6$ for Class 1 and $B/t = 1.5 + 28.2 + 1.5 = 31.2$ for Class 2.

Requirements of Eurocode 3

For a hot-finished square hollow section designed to Eurocode 3 [BSI 2005a, CEN 2005a], the slenderness limits for sections is expressed as $c/t = 33\epsilon$ for Class 1 and $c/t = 38\epsilon$ for Class 2, where c is the width of the internal flat face and $\epsilon = (235/\text{yield})^{0.5} = (235/355)^{0.5} = 0.814$.

Therefore, for the flat face, $c/t = 33 \times 0.814 = 26.9$ for Class 1 and $c/t = 38 \times 0.814 = 30.9$ for Class 2.

According to Annex A3 of EN 10210-2 [CEN 2006b, BSI 2006b], the internal corner radius may be taken as 1.0 times the wall thickness. Writing the slenderness limits in terms of the overall width, B, of the section, these limits are:

$B/t = 1 + 1 + 26.8 + 1 + 1 = 30.8$ for Class 1 and $B/t = 1 + 1 + 30.9 + 1 + 1 = 34.9$ for Class 2.

8 VALIDATION OF THE DESIGN MODEL BY A PARAMETRIC STUDY AND CALIBRATION

8.1 Introduction

The new design model is described in Section 3.4. A parametric study was conducted to show the reliability of the model as a design tool over a wide range of slenderness and end-rotations.

The study needed to investigate:

1. end-rotations in different planes
2. a range of slendernesses representing practical construction

The study did not need to investigate:

1. different imperfections and residual stresses because the design model is calibrated to the specified design code, whichever that might be,
2. difference in end-rotations at the two ends of the column because the design model uses the worst rotation at either end and assumes single curvature, which is the worst case,
3. different wall thicknesses because the test results in Chapter 5 from columns with different wall thickness and the analysis of the results in Chapter 6 shows that the column behaviour is essentially the same for all thicknesses up to the point of local wall buckling. This is confirmed by the parametric study of breadth to thickness limits in Chapter 7,
4. the design limits the wall breadth to thickness ratio to avoid local buckling because these were investigated by the study reported in Section 7.

The study was conducted using Abaqus finite element software as described in Section 4. The section chosen was 140×140×10 SHS in S355 steel. This section was chosen for the following reasons.

1. The size 140×140 was reported to be one of the largest used in the multi-storey buildings with discontinuous columns described in Section 1. The extent of plasticity caused by end-rotations is more pronounced in larger sections because the end-rotations in the elastic range are less.
2. 10mm wall thickness in a 140×140 SHS is thick enough not to suffer significant deformations even at high plastic rotations.

S355 steel was chosen because this is the commonest grade of steel used for structural hollow sections in Europe.

The 140×140×10 SHS was analysed for lengths of 3.0m, a representative length for typical domestic construction, and also for lengths of 1.5m and 6.0m to give a wide range of slenderness.

End rotations were applied as equal and opposite because that is both the worst design case and the design case assumed in the design model.

8.2 Load-rotation path sensitivity

Because the columns become partially plastic, the resistance is expected to depend on the sequence of load application. The Eurocode proposes that incremental loading should be applied in the proportions of the ULS loads. For example, if a column is subject to coexistent loading at ULS of 1000kN axial compression and 50kN-m bending moment, the load might be applied in 10 increments of 100kN combined with 5kN-m. In Figure 8.1, this is shown by the straight line OA.

There is an infinite range of alternative load increments. One possible path would be to apply increments of axial load alone up to the maximum applied axial compression, 1000kN in the example, and then apply increments of bending moment until the maximum applied moment, 50kN-m in the example, has also been applied to the column. This is shown in Figure 8.1 by the lines OBA. Another possible path would be to apply increments of bending moment alone up to the maximum applied moment, 50kN-m in the example, and then apply increments of axial load until the maximum applied axial compression, 1000kN in the example, has also been applied to the column. This is shown in Figure 8.1 by the line OCA.

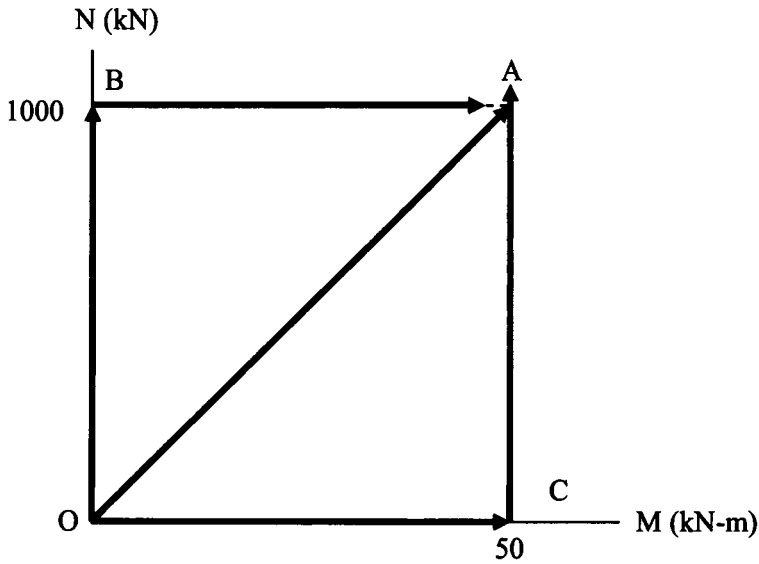


Figure 8.1 Load paths for a column resisting axial and bending

Loading a column subject to axial compression and end-rotation presents the same possibilities. However, the imposition of large end-rotations causes more extensive plasticity than traditional column design for axial and moments, so the effect of the load-path might be more pronounced. This could result in a different resistance to axial load depending on the load path. Possible load paths for a column subject to 1000kN axial compression and 50 milliradians end-rotation are shown in Figure 8.2.

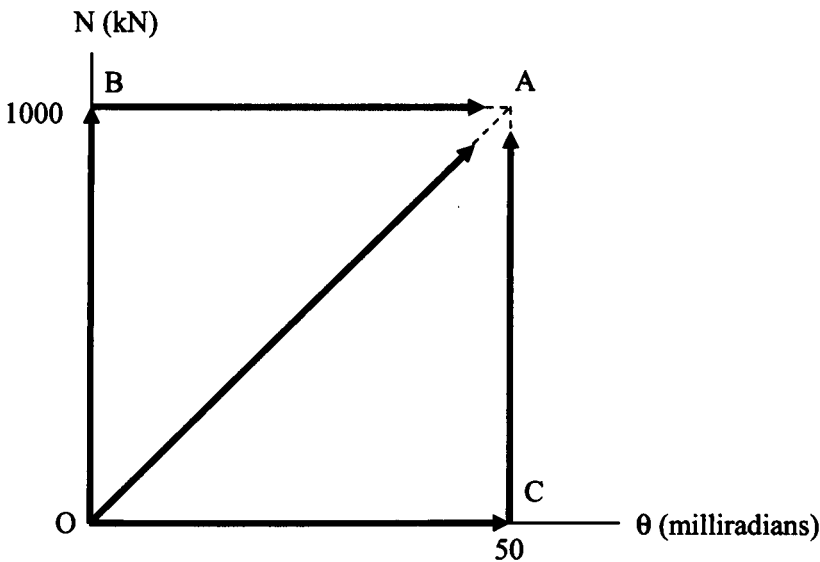


Figure 8.2 Load paths for a column subject to axial and end-rotation

For the initial imperfection in a rectangular plane of the section and imposed rotations in the plane of the initial imperfection, the load-rotation path used in the analysis is the case of a column unloading as the distance between the ends is reduced by an imposed shortening. The path is shown in Figure 8.3 as ODA. This is a slightly conservative case because the extent of plasticity is expected to be greater at the load at D than at B, which marks the maximum axial load in Figure 8.2

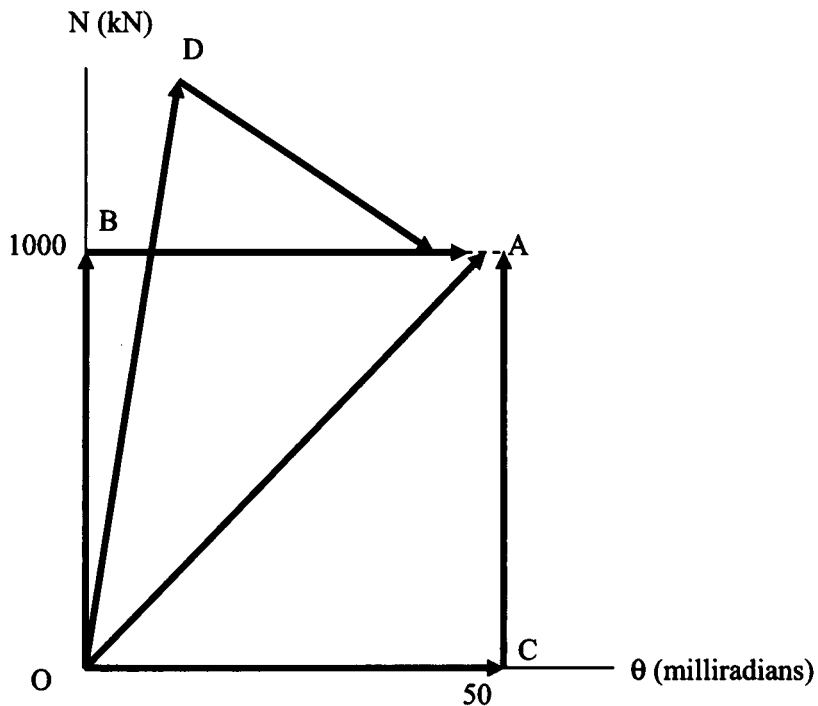


Figure 8.3 Load paths for imposed rotation in the plane of the initial imperfection

The effects of the load paths OBA and ODA shown in Figure 8.3 were investigated for of the initial imperfection in a rectangular plane and end-rotations in the same plane. The case of 140×140×10 SHS columns of 3.0m length was calculated at one of the points generated in the parametric study. The point chosen was at approximately 30 milliradians firstly because this is the range where the critical case is end-rotation in the plane of the initial imperfection and secondly because this is expected to be a relatively common magnitude of end-rotation for columns at the ends of beams. Analysis following the path OBA (applying axial load alone up to the maximum and then imposing rotation) gives the end-rotation as 31.60 milliradians at the point at which the end-moment changes from destabilising to stabilising. Analysis following the path ODA (imposed end shortening) gives the end-rotation of 30.15 milliradians. These results are shown in Table 8.1.

Table 8.1	End-rotn (radians)	Axial compn (kN)
Load path ODA SHS2006m10d10_130by10_v2	0.03105	1158.0
Load path OBA SHS2008m09d05_out140by10_Nthenrotn_v10 Interpolation to zero moment	0.03160	1158.0

The effects of the load paths OA, OBA and OCA were investigated for the initial imperfection in a rectangular plane of the section, but with end-rotations orthogonal to the plane of the initial imperfection as follows. The case of 140×140×10 SHS columns of 3.0m length was calculated at two of the points generated in the parametric study. The points chosen were at 8.6 and 13.1 milliradians firstly because this is in the range where the critical case is end rotation orthogonal to the initial imperfection and secondly because this is expected to be a common magnitude of end-rotation at interior columns. The results are shown in Table 8.2. It can be seen that there is almost no difference, showing that the sensitivity to the load path is very small.

Table 8.2	end rot (radians)	compn (kN)
Point at 13.13 milliradians		
Proportional loading, path OA SHS2006m10d13_130by10_v3	0.01313	1404
Axial alone then end-rotation alone, path OBA SHS2008m09d05_out140by10_Nthenrotn_oplane_v3	0.013068	1404
Rotation alone then axial alone, path OCA SHS2008m09d06_out140by10_rotnthenN_oplane_v2	0.01313	1404.8
Point at 8.6 milliradians		
Proportional loading, path OA SHS2006m10d13_130by10_v5	0.0086058	1483.4
Axial alone then end-rotation alone, path OBA SHS2008m09d08_out140by10_Nthenrotn_oplane_v1	0.0085815	1483.4
Rotation alone then axial alone, path OCA SHS2008m09d08_out140by10_rotnthenN_oplane_v1	0.0086058	1483.5

For the initial imperfection not in the rectangular plane of the section, the initial imperfection was introduced in the $X=Y$ plane with a magnitude that gave the same maximum resistance for a pin-ended strut as for the case with the initial imperfection in the rectangular plane. It was found that the case of a pin-ended column loaded by imposed shortening, as load-path ODA of Figure 8.3, gave significantly lower resistances (at end-rotations greater than at maximum load) than by proportional loading. Therefore further analyses with the initial imperfection in the $X=Y$ plane were made by proportional loading.

8.3 Planes of rotations

The analyses have been conducted to explore the behaviour for the combinations of initial imperfection and imposed end-rotation in about several different axes as shown in Table 8.3.

Table 8.3 Planes of initial imperfections and end-rotations		
Plane of initial imperfection	Plane of end rotation	Case
X=0	X=0	1
	Y=0	2
	Y=X	3
	$Y=X/\tan 22.5^\circ$	4
	$Y=X/\tan 67.5^\circ$	5
Y=X	Y=X	6

Cases 1 and 2 have been analysed for $140 \times 140 \times 10$ SHS columns of 1.5m, 3.0m and 6.0m lengths. From Figure 8.4 and Figure 8.5, it can be seen that the behaviour is very similar. Case 3 has been analysed for $140 \times 140 \times 10$ SHS columns of 3.0m and 1.5m length only because the similarity of behaviour in the Cases 1 and 2 show that the Case 3 will be similar for all lengths of columns. Cases 4, 5 and 6 were performed for the 3.0m columns because 3.0m length of $140 \times 140 \times 10$ SHS columns is expected to be most representative of the proportions of the majority of structures in which discontinuous columns are used.

8.4 Similarity with different slendernesses

The similarity of behaviour at different slendernesses is shown by the plots of all three column lengths in Figure 8.4 and Figure 8.5 for end-rotations in a rectangular plane. Tabulated data giving the analysis file and describing the “failure mode” of each analysis are given in Appendix G.3 for the 1.5 m length, Appendix G.4 for the 3.0 m length and Appendix G.5 for the 6.0 m length.

At higher end-rotations, the resistances for end-rotation in the plane of the imperfection are lower than for end-rotation out of the plane of the imperfection. However, at lower end-rotations, the opposite is found because the imperfection produces an end-rotation in its own plane. This may be seen in Figure 8.5. Considering end-rotation in the plane of the imperfection, the maximum strut load occurs with a slight end-rotation in this plane, which reduces the effect of any imposed end-rotation. Considering end-rotation out of the plane of the imperfection, the maximum strut load occurs without any end-rotation out of the plane of the imperfection, so there is no reduction in the imposed end-rotation.

Results of Abaqus finite element analysis

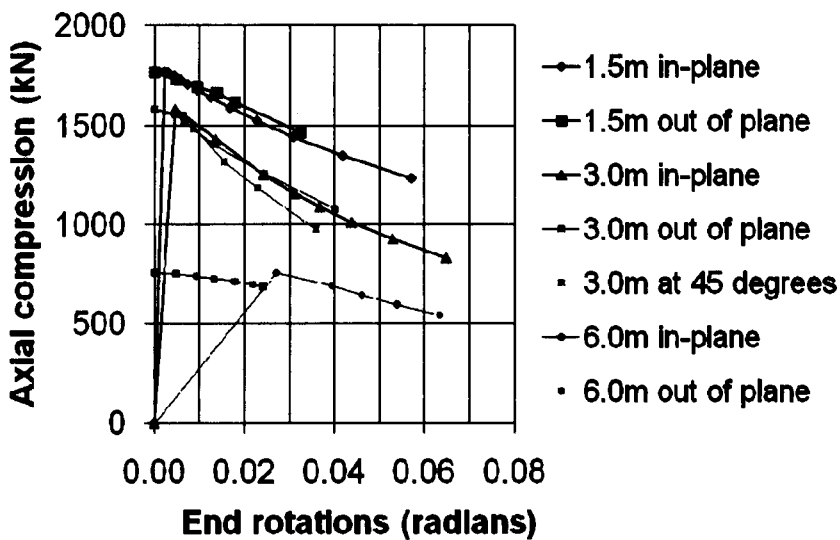


Figure 8.4 All column lengths, end-rotations about a rectangular axis

Results of Abaqus finite element analysis

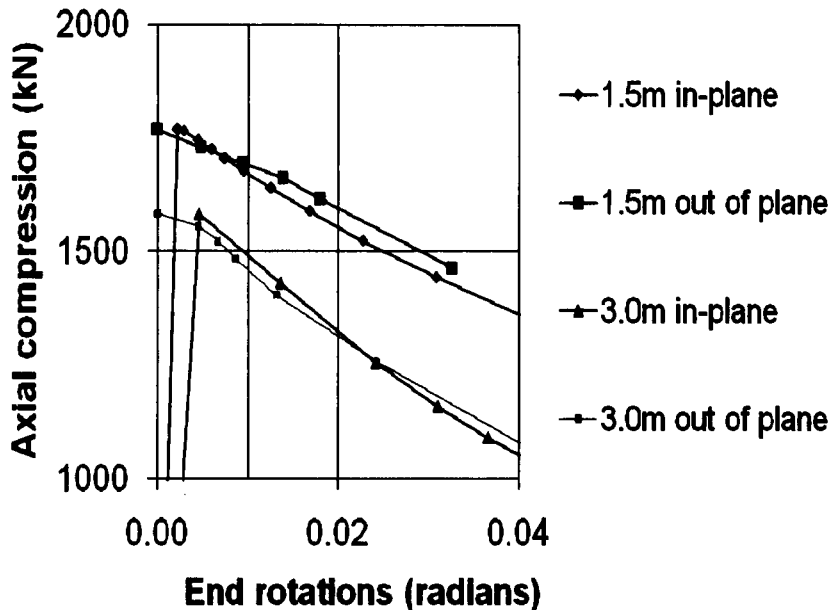


Figure 8.5 Comparison of imperfections “in plane” with “out of plane”

8.5 Confirmation of the proposed design model

8.5.1 Basic design model

The column behaviour described in Section 3.4.5 shows that the behaviour of the column at mid-height, the governing behaviour of the column, is not a simple function of the applied end rotations. This suggests that the resistance model need not include a detailed calculation of the cross-sectional resistance to co-existent moments about both rectangular axes. Instead, it might combine the co-existent moments about both rectangular axes to form a “design moment” about one rectangular axis and apply this to a simpler resistance model which includes only bending about one rectangular axis plus axial compression. This greatly simplifies the equations necessary in the resistance model which makes the method much more attractive to designers.

Study of the results of the parametric study shows that the design model proposed in Section 3 and shown in Figure 8.6 is valid using

1. the resistance properties about a rectangular axis,
2. the end-rotation applied (even when not in a rectangular axis), and
3. the initial imperfection $e_i = e_s$, the imperfection about a rectangular axis that gives the buckling resistance of a pin-ended strut.

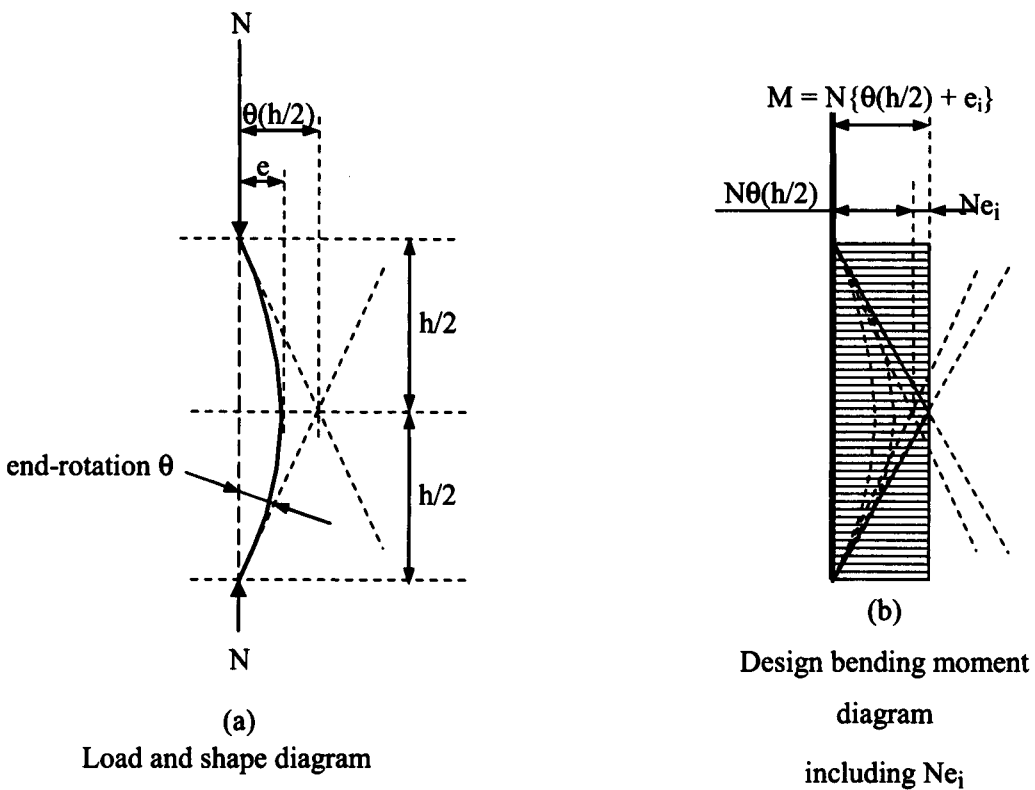


Figure 8.6 Design bending moment in the column including imperfection

The deflection at mid-height of the column caused by the end slopes is shown in Figure 8.6(a). The displacement is calculated from the root of the sum of the squares of the end-rotations in the two rectangular planes and this displacement is applied in the calculation of the resistance as if it is in one of the rectangular planes. The appropriate value of

imperfection, e_i , is added in the same rectangular plane. Therefore the check is made with design deflection:

$$e_d = (h/2)\theta + e_i \quad \text{Eq 8.1}$$

giving the design bending moment:

$$M = Ne_d = N\{(h/2)\theta + e_i\} \quad \text{Eq 8.2}$$

where e_d is the design deflection along one rectangular axis of the SHS

θ is the end-rotation applied to the column (the root of the sum of the squares of the end-rotations in the two rectangular planes)

e_i is the imperfection along a rectangular axis of the SHS. In the design model,

$e_i = e_s$ which is the imperfection along a rectangular axis of the SHS to make the resistance to axial compression equal to the pin-ended strut resistance.

The reliability of this model is easily shown by plotting the difference between (i) the eccentricity at mid-height, $(h/2)\theta$, imposed by the end-rotation θ alone and (ii) the eccentricity at mid-height needed for the design model to give the correct failure load for that end-rotation. This difference is the additional imperfection, e_i . These are shown for hot-finished 140×140×10 SHS in S355 steel in Figure 8.7 for columns 1.5m long, in Figure 8.8 for columns 3.0m long and in Figure 8.9 for columns 6.0m long. These plots are normalised by e_s , which is different for different lengths of column. The values of e_s are:

for 1.5m long, $e_s = 2.80\text{mm}$, so $\theta=40\text{mrads}$ gives $\{(h/2)\theta\}/e_s = 10.7$

for 3.0m long, $e_s = 10.81\text{mm}$, so $\theta=40\text{mrads}$ gives $\{(h/2)\theta\}/e_s = 5.6$

for 6.0m long, $e_s = 92.5\text{mm}$, so $\theta=40\text{mrads}$ gives $\{(h/2)\theta\}/e_s = 1.3$

These plots use the correlation factor, c_f , of 0.8 described in Section 6, to reduce the end rotation so that $\theta = 0.8$ times the rotation predicted by Abaqus. It can be seen that the additional eccentricity required, e_i , is less than e_s in all cases and that the imperfection required in the design model reduces as the end rotation increases, as deduced in Section 3.4.4.

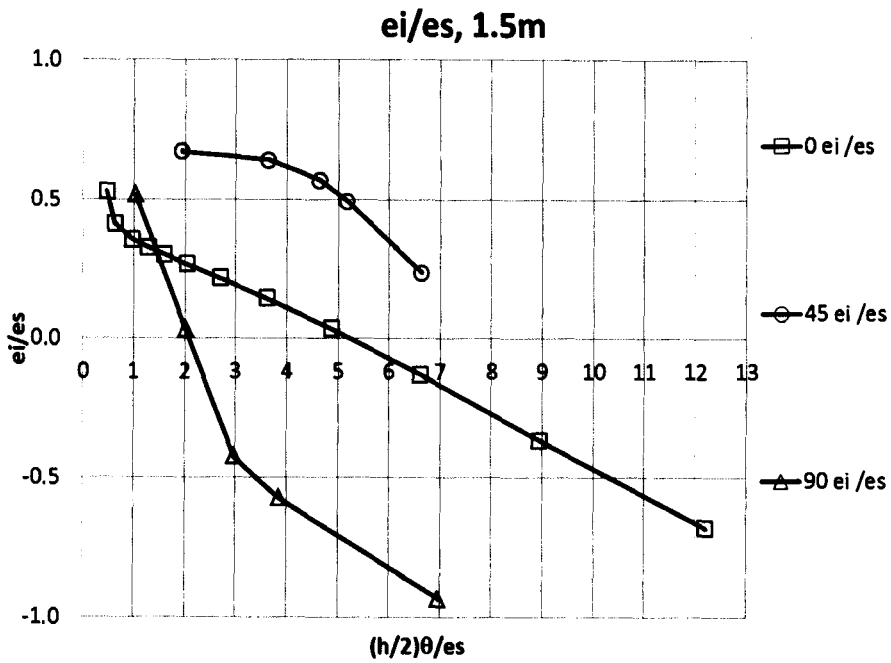


Figure 8.7 1.5 m columns, e_i required

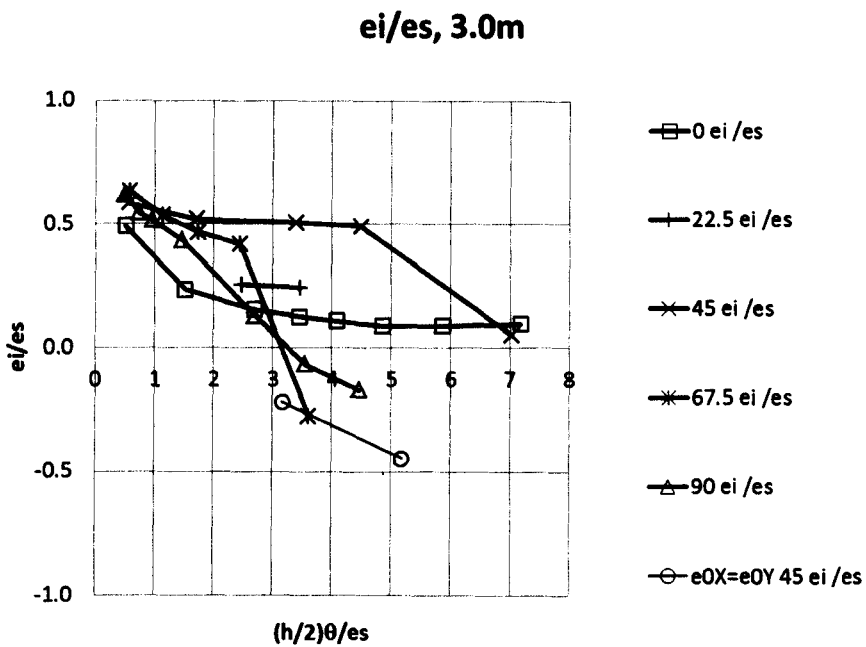


Figure 8.8 3.0 m columns, e_i required

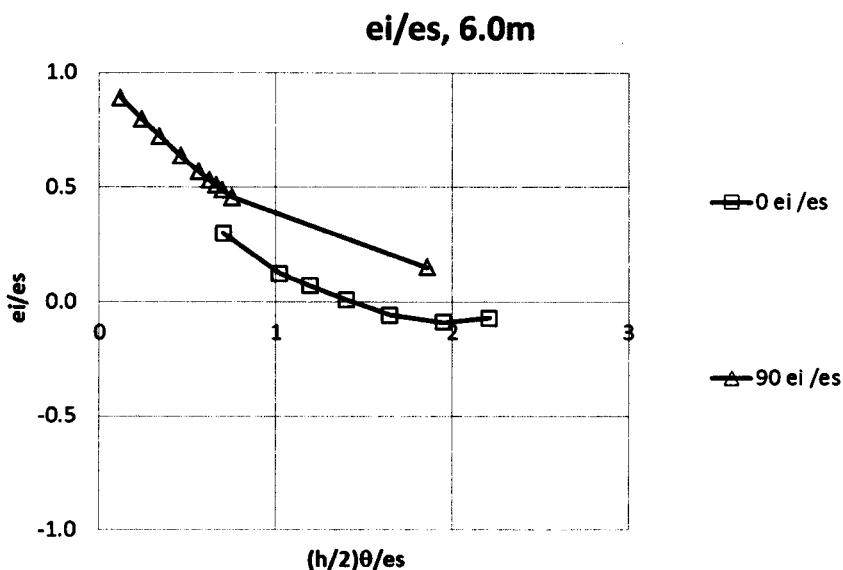


Figure 8.9 6.0m columns, e_i required

8.5.2 Comparison of 2009 basic design model with Abaqus

The resistances from the design model were calculated using a total mid-height eccentricity $= e_s + (h/2)\theta$ where $\theta = c_f \times$ Abaqus end-rotation (with $c_f = 0.8$ as Section 6) to give a design model resistance corresponding to each Abaqus resistance but with the Abaqus rotation reduced by the correlation factor to correct the overestimate of rotation given by Abaqus when compared to the test results, as found in Chapter 6. It can be seen from these plots that the design model always underestimates the resistance of the column.

Results for the 3.0m long columns are plotted with in Figure 8.10, for the 1.5m long columns are plotted in Figure 8.11 and for the 6.0 m long columns in Figure 8.12. The axial resistance v end-rotation calculated using BS 5950 as applied in Appendix B is shown for comparison in Figure 8.10. The label “N max model” is used for two sets of data, one indicated by a triangle having the end rotation in a rectangular plane and the initial imperfection orthogonal to that plane, the other indicated by a square having the end rotation in a rectangular plane and the initial imperfection in that plane. Both are labelled “N max model” because one gives the maximum in one range of end rotations and the other gives the maximum elsewhere.

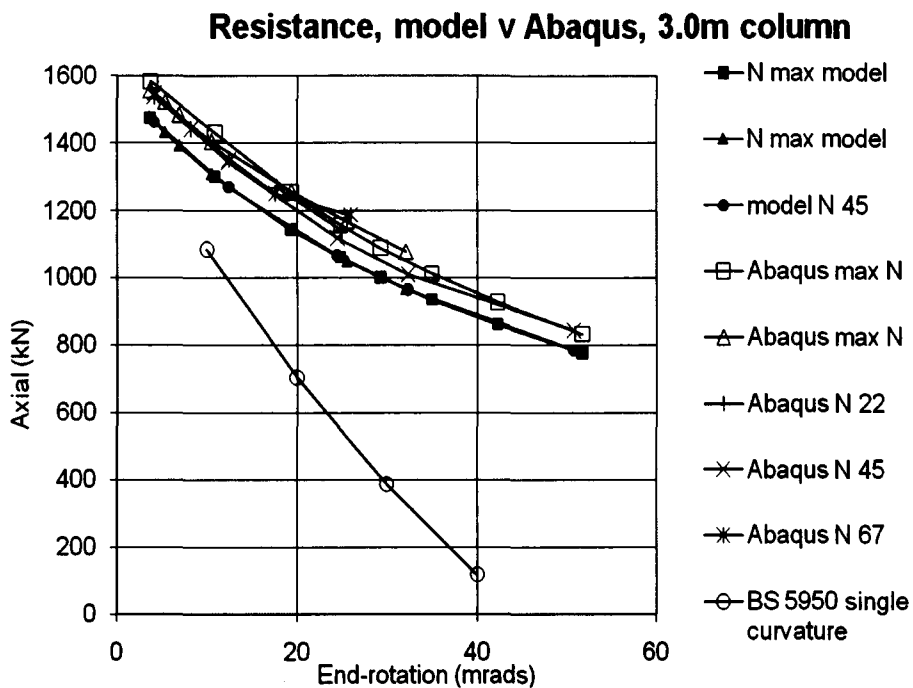


Figure 8.10 Abaqus v CMK 2009 design model, 3.0m height

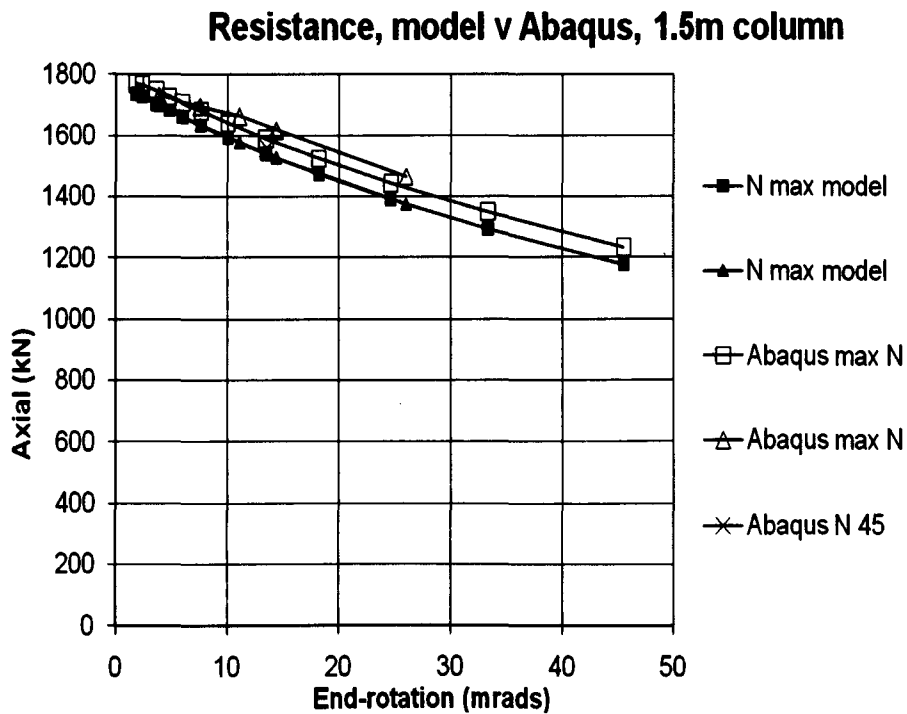


Figure 8.11 Abaqus v CMK 2009 design model, 1.5m height

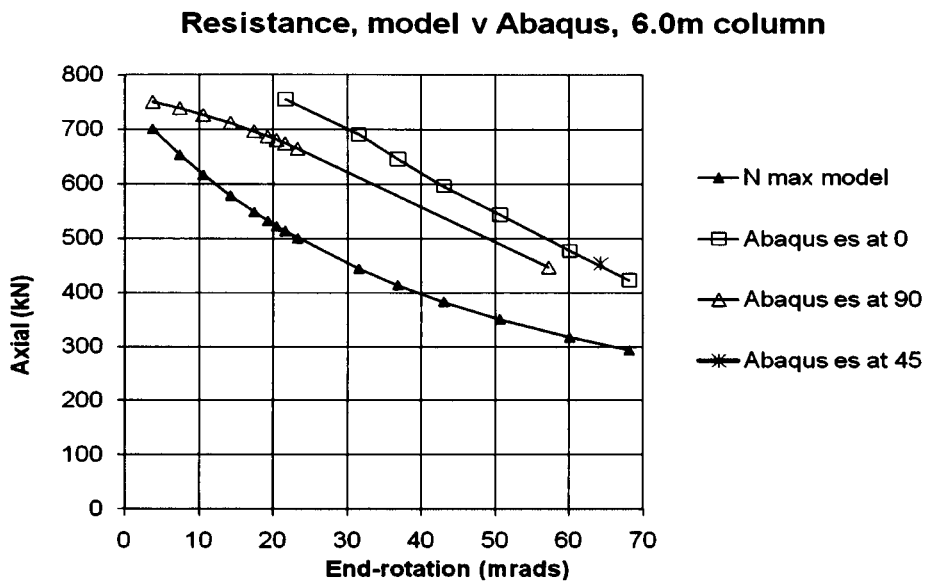


Figure 8.12 Abaqus v CMK 2009 design model, 6.0m height

8.6 Conclusions

The accuracy of the CMK 2009 design model compared with finite element analysis is shown

in Figure 8.10, and for 3.0m columns,

in Figure 8.11 for 1.5m columns and

in Figure 8.12 for 6.0m columns

These figures are graphs of the maximum axial compression v end-rotation when there is no restraint moment provided at the end of the column to increase the buckling resistance.

The figures all show the resistance of a 140×140×10 column which is a typical column size in residential construction. A column height of 3.0 metres is a typical column height in residential construction. The behaviour of stockier and more slender column sections is shown by heights of 1.5 metres and 6.0 metres. The same cross-section has been used in all of the figures to make comparisons easier.

It can be seen that the model gives safe predictions of the column resistance when the proposed value of the imperfection, e_s , is used in the basic design model. This confirms the prediction that the design model is conservative made in Section 3.7

9 DESIGN METHOD

9.1 Scope of application

9.1.1 General

The design model is appropriate for the types of beam and column structures comprising both:

1. Shallow beams (eg Corus ASB) with the floor filling the depth of the beam and fully connected or fully grouted to the beam to provide stability as AD 281 and AD 285 [SCI 2005a, SCI 2005c] and
2. Columns of hot-finished square hollow sections (eg Corus Celsius). The distinction between hot-finished and cold formed structural hollow sections is important. Cold-formed hollow-sections have different residual stresses and have not been calibrated.

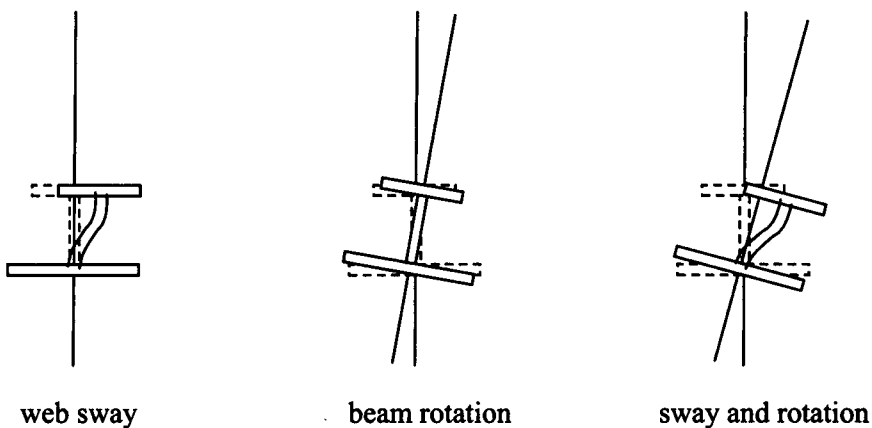


Figure 9.1 Instabilities to be avoided in beams at top and bottom of columns

There is the possibility of using the method with other floor systems, but only if the instabilities shown in Figure 9.1 are avoided. Sway stability of the beam webs can be assured by web stiffeners and torsional stability of the beams can be assured by transverse beams and connections of suitable stiffness spanning at right-angles to the main beams.

9.1.2 Factors affecting the reliability of the design method

There are a number of issues that affect the reliability of the design method.

1. The method assumes that the end-rotations of every column are equal and opposite at the top and bottom. This is improbable. Therefore the column resistance will frequently be higher than predicted by the model.
2. Plastic deformations of beams cause bigger beam rotations than predicted by the normal engineering approach which assumes elastic deformations. Therefore plastic deformations must either be avoided or they must be explicitly included in the calculations.
3. The load factors specified in design codes are calibrated so that there is an acceptable improbability of failure due to the probability distributions of both resistance and load even for single elements (such as a simply supported beam). Therefore the reliability is higher when there are two elements from different statistical populations. It is improbable that the yield stress of both the beam and the column are as low as the specified minimum yield and it is even more improbable that this would happen in a structure that is subject to maximum design load. The column might be stronger or the beam might be stronger, providing increased column resistance because there would be some resistance to column end moments. The design model assumes that the columns cannot derive any resistance from the beams because the beams are designed to be just strong enough to support the applied loads from the floor and do not have any spare resistance to resist column end-moments. However, it is statistically improbable that beams have no spare capacity because of the statistical distribution of both the beam strength and the beam loading. Therefore the column resistance will frequently be higher than predicted by the model because the beams will provide some resistance to column end-moments. (Even though the columns may have flexible base plates and cap-plates, some end moment can be transmitted from the column because the axial compression may act at a small eccentricity from the centre-line of the column.)

9.2 Column design model

9.2.1 The new column design model

The design model allows the beams to be designed independently from the columns. Each floor level can be analysed individually assuming the beams are on knife edge supports.

In this Chapter, the design model is written assuming that it is being applied using EN 1993-1-1 [BSI 2005a, CEN 2005a], but the design model can be used with any design code by using the appropriate value of initial imperfection e_s derived from the strut buckling resistance of the code.

9.2.2 Breath to thickness ratio of wall

The wall breadth to thickness ratio must be sufficient to avoid local deformations of the walls. The required values are derived in Section 7.3 and the design limits are repeated in Figure 9.2. The curve is shown in terms of the overall breadth, B , which is not used in EN 1993-1-1. This is easier for designers to use because the designer is not required to find the internal radius of the section, which has been incorporated into B . The equation of a line that fits the data closely and may be taken as the design limit is:

$$B/t = -14\text{Log}_{10}(\theta/1000) + 38.5 \tag{Eq 9.1}$$

where θ is in radians

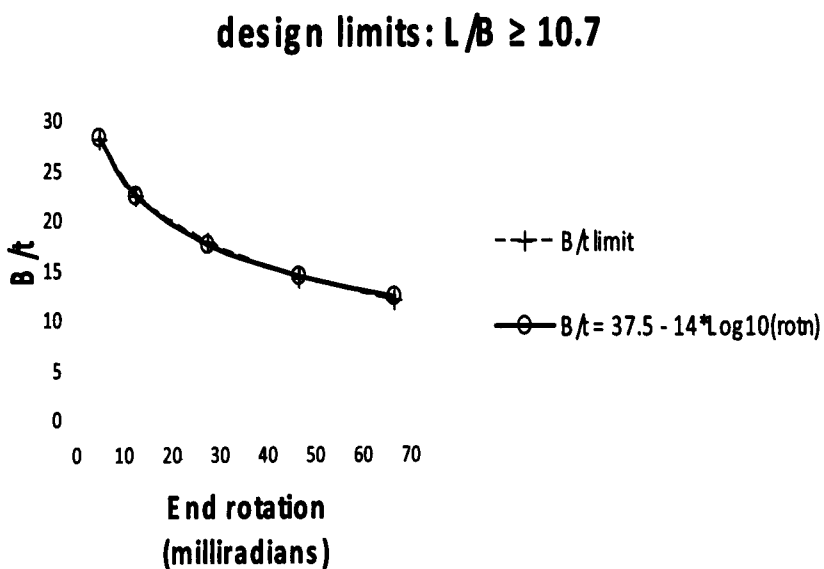


Figure 9.2 Wall slenderness limitations, overall breadth/thickness, B/t

9.2.3 The design process

The design method is applied as follows:

1. Analyse the beam, as if on knife edge supports, carrying the factored floor loading
2. Calculate the slope of the beams carrying the factored floor loading at each column

3. Taking the end slope, θ , of the column equal to the greater of the slopes of the beams above and below the column plus the frame sway, calculate the design deflection at mid-height of the column caused by the end slopes, as shown in Figure 9.3 (b).

$$e_d = (h/2)\theta + e_i \quad \text{Eq 9.2}$$

where e_d is the design deflection along one rectangular axis of the SHS

θ is the end-rotation applied to the column (the root of the sum of the squares of the end-rotations in the two rectangular planes)

e_i is the imperfection along a rectangular axis of the SHS. In this case, the basic design model, $e_i = e_s$ which is the imperfection along a rectangular axis of the SHS to make the resistance to axial compression equal to the pin-ended strut resistance

h is the storey height of the column.

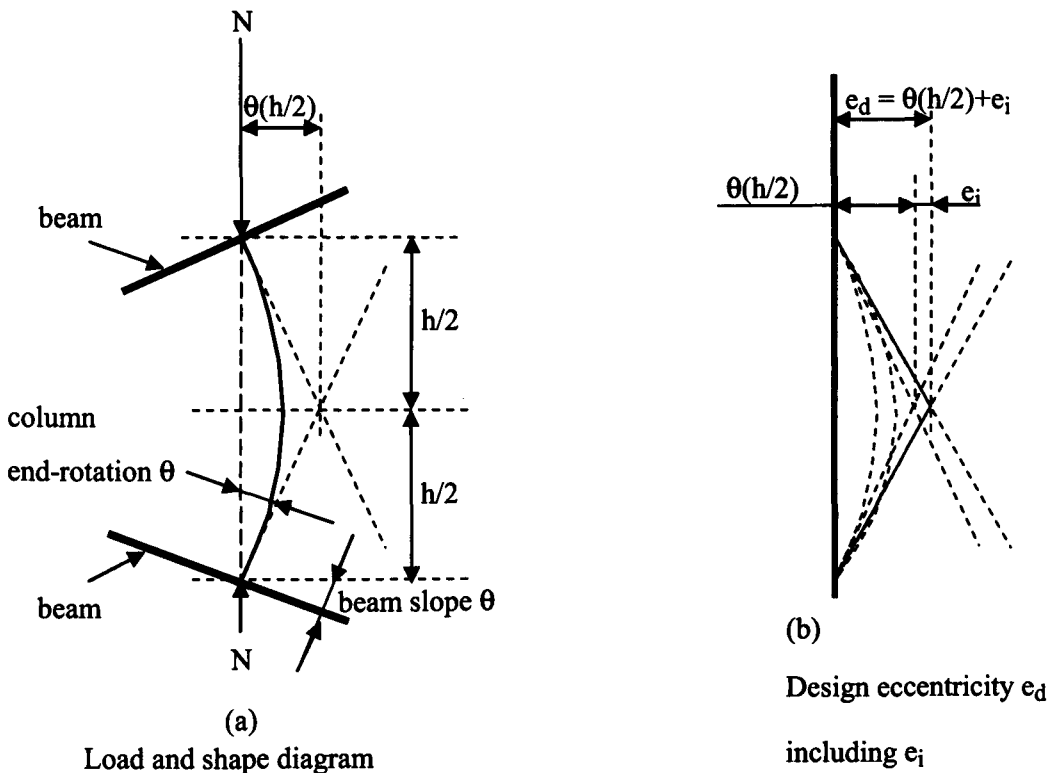


Figure 9.3 Design eccentricity including imperfection

4. Calculate the axial compression resistance $N_{\theta,Rd}$ using the plastic resistance model in Figure 9.4 and (where there are no additional moments applied) the applied bending moment is

$$M_{Ed} = N_{\theta,Rd}e_d = N_{\theta,Rd}\{(h/2)\theta + e_i\} \quad \text{Eq 9.3}$$

Where there is an additional moment M_{ext} from external forces, such as wind load or explosion load as in design for key elements, see Sections 9.6.3 and 9.8.1, the applied bending moment is

$$M_{Ed} = N_{\theta,Rd}e_d + M_{ext} = N_{\theta,Rd}\{(h/2)\theta + e_i\} + M_{ext} \quad \text{Eq 9.4}$$

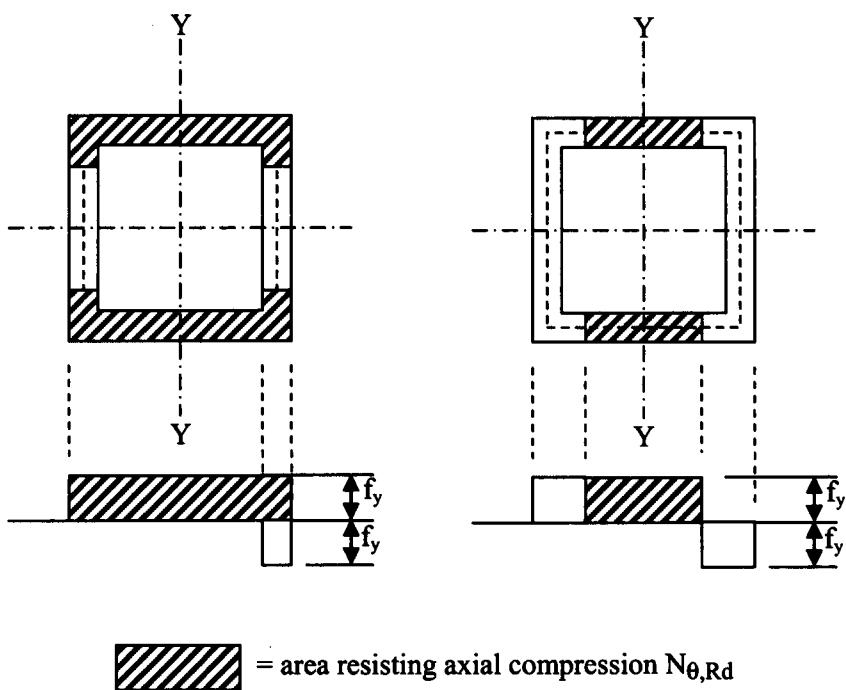


Figure 9.4 Plastic cross-section to calculate N_{θ} from M_y only

This design method is similar to design using EN1993-1-1 [BSI 2005a, CEN 2005a] Section 5.3.2 applied to an individual column using the initial bow imperfection with plastic analysis as in (3)b.

9.2.4 Defining the strut imperfection

The imperfection is defined in terms of the imperfection, e_s , that must be used with the plastic cross-section model in Figure 9.4 to give a resistance equal to that of a pin-ended strut. For a strut with a gross cross-sectional area, A , the imperfection, e_s , may be calculated as follows:

1. Calculate the buckling load of the column, $N_{b,Rd}$, as if it were a pin-ended strut using the specified design code.
2. Calculate the area, A_b , stressed to yield stress, f_y , required to resist the pin-ended strut load, $N_{b,Rd}$,

$$A_b = N_{b,Rd}/f_y \quad \text{Eq 9.5}$$

3. Assume the remainder of the area of the section, $(A - A_b)$ is available to resist bending working at yield stress in tension and compression, and calculate the reduced plastic moment of resistance, $M_{N,Rd}$, of the section
4. Calculate the imperfection, e_s , at axial load $N_{b,Rd}$ from the assumption that

$$N_{b,Rd} \times e_s = M_{N,Rd} \quad \text{Eq 9.6}$$

$$\text{so } e_s = M_{N,Rd}/N_{b,Rd} \quad \text{Eq 9.7}$$

This value of e_s is the value of e_0 that would be derived from EN1993-1-1 [BSI 2005a, CEN 2005a] Section 5.3.2(3)b using the UK National Annex which allows e_0 to be calculated by calibration with the buckling resistance calculated using EN1993-1-1.

9.3 Beam design

9.3.1 General

Beams can be designed as simple beams (statically determinate beams), comprising both simply supported beams and cantilever-and-suspended-spans, or as continuous beams (statically indeterminate beams). Modern design codes allow beams to be designed to resist bending moments equal to the plastic moment of resistance. However, design to the plastic moment of resistance would result in very large deflections if the yield stress were no greater than the design value and the loading reached the factored design value. These large deflections would be accompanied by large slopes of the beams which would cause large

end-rotations of the columns. Therefore the beams must be designed to be elastic except at internal supports of statically indeterminate continuous beams, as described in Section 9.3.3. These limits do not prevent the use of plastic design in the hogging regions, provided the sagging region moments are limited to the first yield moment and the end-rotations are calculated as described below for continuous beams.

A similar problem arises in the design of conventional rigid-jointed multi-storey frames. In BS 5950-1 [BSI 2000a] Annex E, *Effective length of compression members in continuous structures*, beams are considered as pinned where the moments applied to the beams exceed 90% of the reduced plastic moment capacity. The limit of 90% of the reduced plastic moment capacity is used because it is approximately equal to the first yield moment of bi-symmetric hot-rolled I-beams. Where bi-symmetric beams are used, the 90% plastic moment limit may be applied as in Annex E to ensure that the beams remain essentially elastic. Asymmetric beams have a much greater difference between the plastic moment of resistance and the first yield moment, so it is proposed that, where asymmetric beams are used, the sagging moments should be limited to the first yield moment of the section, $= \text{yield} \times \text{lowest elastic modulus}$, to ensure that the beams remain elastic.

In the type of floor construction expected in buildings using the new design method, the floor slab is concrete (precast or composite), at least as deep as the steel beam and fully grouted. In certain cases, as described in SCI P175 [SCI 1997], the slab acts compositely with the beam, increasing the sagging moment of resistance. Where this type of construction is used, it is proposed that should be applied to the plastic moment of resistance of the composite beam. The use of the 90% limit is justified because there is no essential difference between a composite beam made with an asymmetric section and one made with a symmetric section, so what is acceptable for Annex E should equally be acceptable for this design method to ensure that the beams remain essentially elastic.

In this report, the term “essentially elastic” is used to refer to

1. the 90% limit from BS 5950-1 Annex E for bi-symmetric steel I-beams and composite beams, or
2. elastic design for asymmetric steel beams,

whichever is appropriate as discussed above in this Section.

9.3.2 Simple beams

Simply supported beams are shown in Figure 9.5 in which the beam splice resists shear alone and is depicted as a circle. For bi-symmetric beams and composite beams, the beams should be designed to be essentially elastic. The column end rotation is the same as the beam end rotation. For elastic behaviour, the end rotation for a simply supported beam under uniformly distributed loading is $(1/24)(WL^2/EI)$ where W is the total load on the beam, L is the span, E is the young's modulus and I is the second moment of area.

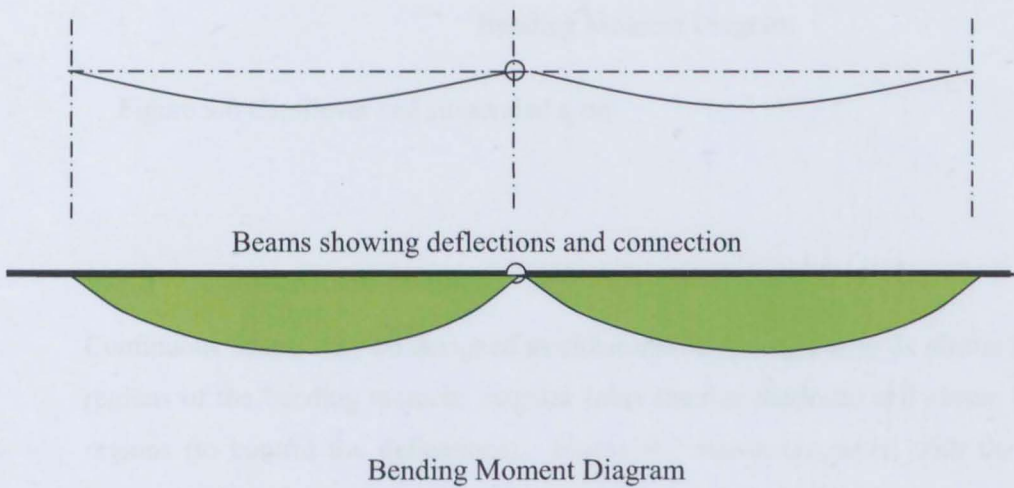


Figure 9.5 Simply supported beams (connections at column face)

Cantilever-and-suspended-span beams are shown in Figure 9.6 in which the beam splice resists shear alone and is depicted as a circle. The beams should be designed to be essentially elastic in both the sagging region and in the hogging region because the beams are statically determinate. The column end rotation is the same as the beam slope at the column. The beam slope at the column is reduced by the cantilever.

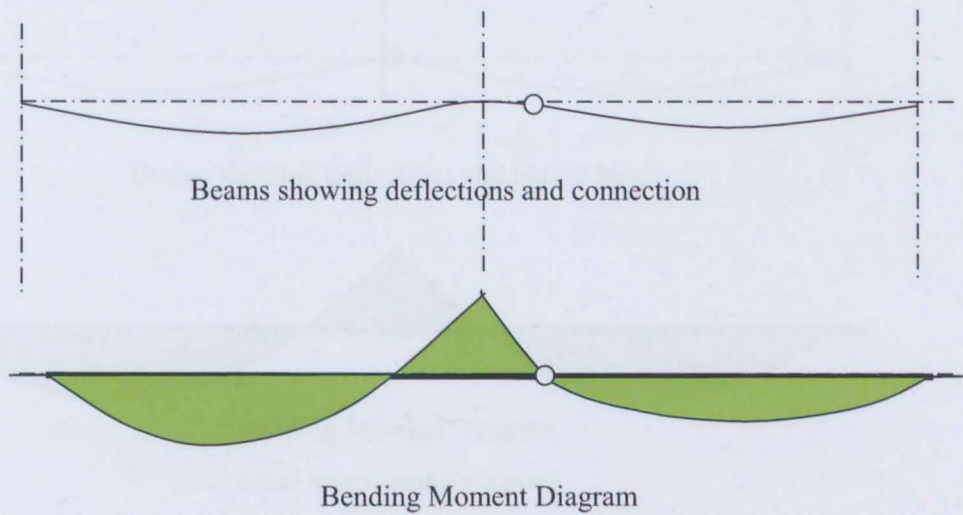


Figure 9.6 Cantilever and suspended span

9.3.3 Continuous beams

Continuous beams may be designed as either elastic throughout or as plastic in the hogging regions of the bending moment diagram (over interior supports) and elastic in the sagging regions (to control the deflections). Figure 9.7 shows the latter, with the plastic hinge location depicted as a black circle. In the sagging region, the bending moments in the beams should be limited so that the beams remain essentially elastic as described in Sections 9.3.1 and 9.3.2. In the hogging region, the beams should be designed so that the applied moments do not exceed the plastic moment capacity reduced by shear (and also reduced by axial if there is axial force in the beam, as would occur in a braced bay).

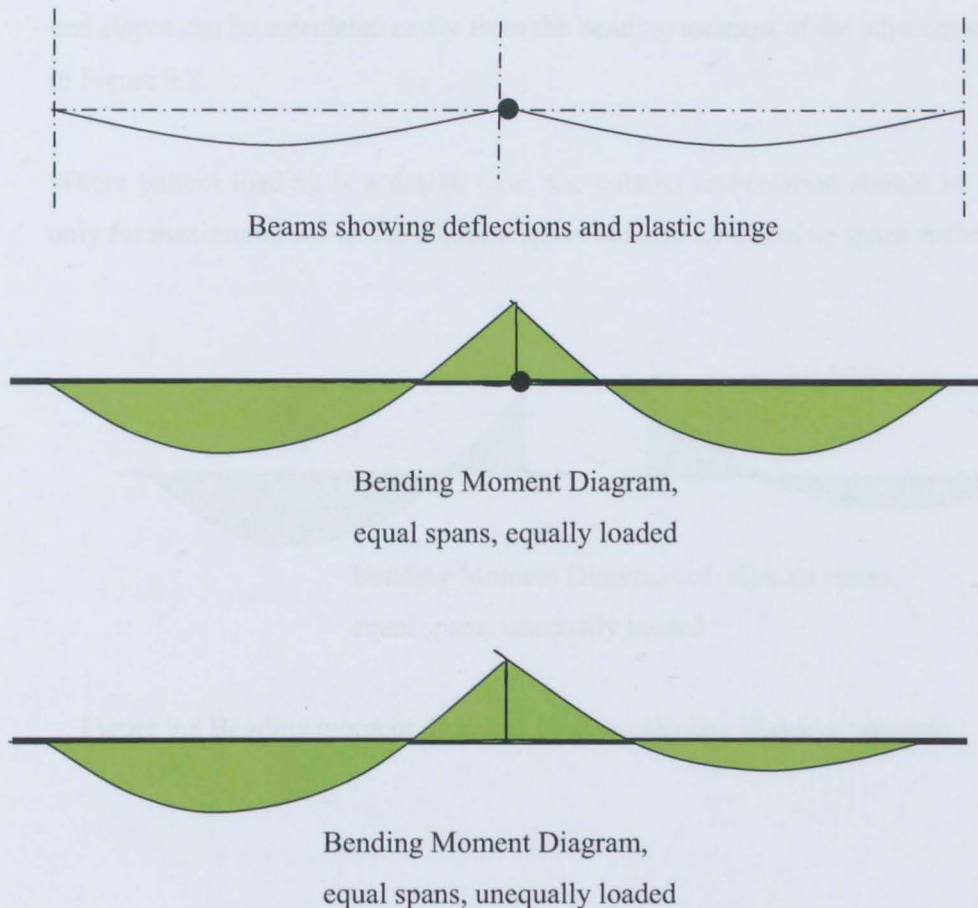


Figure 9.7 Continuous beams

If the beams are designed as elastic, the column end rotation is the same as the beam slope at the column. If the beams are designed as plastic in the hogging region, the beam slopes will be different on either side of the column because of the rotation of the plastic hinge. The end-rotation of the column will be somewhere between these two beam slopes, but the end-rotation is not easily determined because of the range of behaviour from initial plasticity to strain-hardening as described by Horne [Horne 1960] and Davies [Davies 1966]. Initially the plastic hinge rotations will start in the span in which the reduced plastic moment of resistance is lowest, which depends on the coexistent shear force and axial force in the beam. Initially, the end-rotation of the column is governed by the opposite span, the span with the higher value of reduced plastic moment of resistance. However, as the rotation continues, strain hardening may occur and this will increase the moment of resistance at the plastic hinge so much that the other span starts to form a plastic hinge and the end-rotation of the column is now governed by the span that first formed a plastic hinge. This makes it difficult to be sure what the end-rotations of the column will be, so it is recommended that the end-rotation is taken as the greatest end-rotation in the beam on either side of the column. The

end slopes can be calculated easily from the bending moment of the adjacent spans as shown in Figure 9.8.

Where pattern loading is a design case, the column end-rotation should be calculated not only for maximum load on the adjacent spans but also for alternate spans without live load.

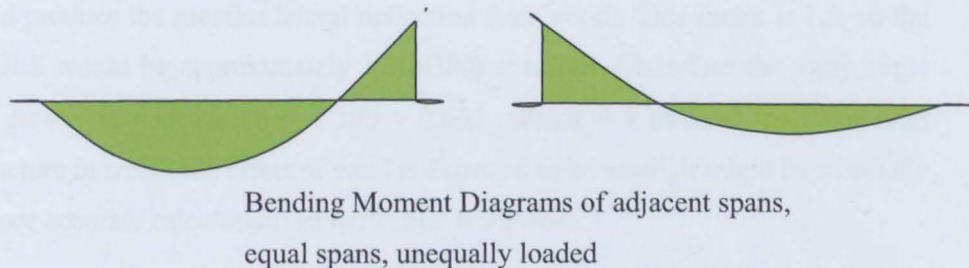


Figure 9.8 Bending moment diagrams used to calculate slopes at columns

9.4 Frame effects

9.4.1 Effects of sway deformations of the frame on column design

All beam and column frames will sway to some extent, even if they are braced frames. The sway deflections have three principal causes:

1. Externally applied horizontal forces, the most common being wind loads
2. The effect of out-of-vertical of the columns, causing a horizontal component of load
3. In rigidly jointed frames, asymmetry of loading or asymmetry of structural stiffness

In designing any steel frame, the effect of sway on the stability of the frame should be considered. Both BS 5950-1 [BSI 2000a], in Section 2.4.2, and EN 1993-1-1 [CEN 2005a, BSI 2005a], in Section 5.3.2, require that the sway effects of frame imperfections should be considered in design. The detailed requirements of these two codes are different, but the broad principles are the same, except that EN 1993-1-1 requires that the sway imperfection is included in all load combinations whereas BS 5950-1 only requires that the sway imperfection is included in Combination 1, which comprises factored dead and vertical imposed loads. Both codes assume a basic value of frame imperfection of 1:200. EN 1993-1-1 allows this to be reduced for increasing column height and greater numbers of

columns. In both codes, the sway effects will be increased in frames with significant second-order effects, but the methods and the limits differ.

Wind loads cause sway of frames even when they are braced frames. For initial design, the effect of sway can be estimated from the Serviceability limit on slope which is set by the UK National Annex to EN 1993-1-1 at $h/300$ similar to traditional UK practice. This is at SLS, so the deflection at ULS can be expected to be $(h/300)$ times the partial safety factor for wind load that would produce the greatest lateral deflection from wind. This factor is 1.5, so the deflection at ULS would be approximately $1.5(h/300) = h/200$. Therefore the sway angle would be not greater than $(h/200)/h = 1/200 = 0.005$ radians = 5 milliradians. For final design in a structure in which the effect of wind is expected to be small, it might be worth the effort to use more accurate calculations of deflection from wind.

The simple design model in a frame with no sway deformation is to calculate the end-rotation of the beam at the top of the column and the end-rotation of the beam at the bottom of the column and design the column assuming that both the top and the bottom of the column have the same rotation as shown in Figure 9.9.

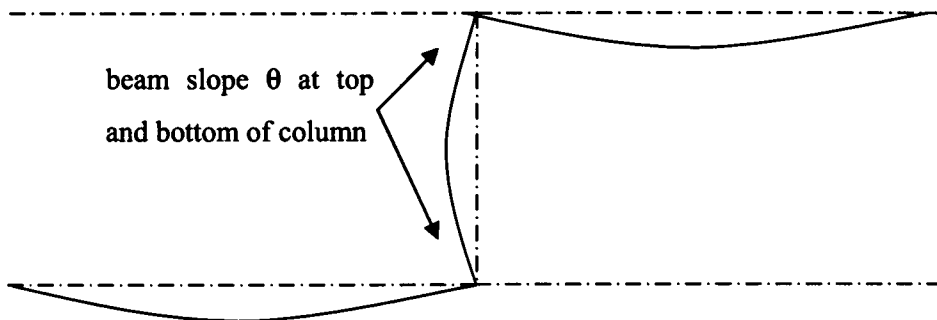


Figure 9.9 End-rotations assumed where there is no sway

Sway deformations affect the angle between the beams and the end-to-end lines of the columns, increasing the angle at one end of the column and decreasing it by an equal amount at the other end. If the column end-rotation were θ without sway, as shown in Figure 9.9, and then the frame were to sway by the angle ϕ , as shown in Figure 9.10, the column end-rotation relative to the line through the column end points (the “end-to-end line”) would be $\theta + \phi$ at the bottom and $\theta - \phi$ at the top as shown in Figure 9.10. Following the simple design model in which the design is made for the greatest end-rotation at top or bottom, the design value of the column end-rotation should be increased to the sum of the beam rotation at the

column plus the sway angle. Therefore, it is recommended that the sway effect should be applied as an additional rotation to the column, in addition to the beam end rotation. The sway effect should be amplified if required according to the code being used, as explained below.

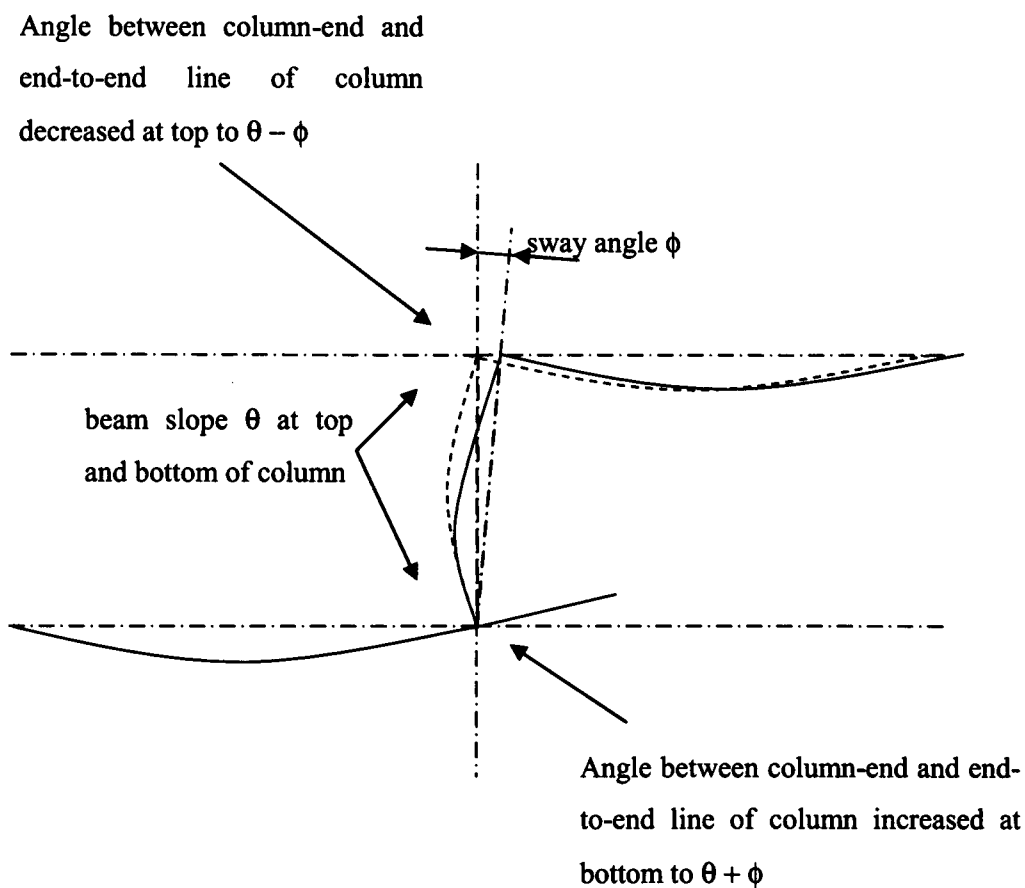


Figure 9.10 End-rotations modified by sway

When using EN 1993-1-1, the amplification factor may be calculated from Section 5.2.2(5) & (6) and the sway angle due to the frame imperfection may be calculated directly from Section 5.3.2, or taken as $1:200 = 5$ milliradians for simplicity. In EN 1993-1-1, the frame imperfection must be considered in all load cases. In addition to the frame imperfection, the wind sway angle must be included in load cases. It may be taken as an additional 5 milliradians for frames with wind deflections limited to height/300 at SLS.

When using BS 5950-1, the amplification factor may be calculated from Section 2.4.2.7.2(b) and the imperfection sway angle may be taken as $1:200 = 5$ milliradians. In BS 5950-1, the sway due to imperfections (represented by the Notional Horizontal Forces of BS 5950-1) is only applied in load cases without wind. In load cases with wind, the sway angle may be taken as 5 milliradians for frames with wind deflections limited to height/300 at SLS.

9.4.2 Additional sway forces on bracing

Bracing needs to be designed to resist

1. Imperfection effects (Sway + Splice)
2. Externally applied lateral loads
3. Additional sway forces from column end-moments as described in Section 9.4.3

The design for imperfection effects and externally applied lateral loads is the same as for the design of conventional simple-construction frames as SCI P334 [SCI 2004], the new SCI guide to the design of braced frames to Eurocode 3.

The addition of sway forces from column end-moments is not part of conventional simple-construction frame design but it is an integral part of the design of a frame that is both braced and rigid jointed.

9.4.3 Additional sway forces from column end-moments

The design method assumes there are no end-moments transferred from the beams to the columns and, therefore, there are no column end-moments. However, because the beams will often have greater strength and stiffness than the minimum required, there might be some end-moments in the columns and these might apply additional shear to the vertical bracing. There are two fundamentally different mechanisms for creating the moments.

The first mechanism is where the column ends do not rotate as much as the beams. This is shown in Figure 9.11. This would occur with small column loads. Assuming the load is applied to the beam at the face of the column, the moment on the column at each end is given by $M_{\text{end}} = N_{\text{Ed}}(B/2)$. The sway shear caused by each column is equal to the sum of the end-moments on the column at the top and bottom divided by the column height. Therefore, for 140×140 SHS columns 3.0 metres high, the shear per column

$$V_H = 2N_{Ed} \frac{\left(\frac{B}{2}\right)}{h} = \frac{B}{h} N_{Ed} = \frac{140}{3000} N_{Ed} = 0.0467N_{Ed} \quad \text{Eq 9.8}$$

There would be some small additional shear from the moment caused by the stiffness of the end-plate, but this would be small if the end-plate were thin. Therefore a reasonable estimate of the additional shear on the bracing is $0.05 = 5\%$ of the column loads. This is a considerable load compared with the Equivalent Horizontal Forces of EN 1993-1-1 Section 5.3, which are of the order of 0.5% of the vertical load, or the Notional Horizontal Forces of BS 5950-1 Section 2.4.2.4, which is 0.5% of the vertical load. However, this force would only occur where the columns are loaded to a low proportion of their compression resistance, so the shear applied to the bracing would not be very large. With high compression in the column, the column would deform, reducing the eccentricity of the load on the column ends and so reduce the sway shear. The two end columns would give opposite directions of shear force which would cancel out and, depending on the positions of the columns with respect to the end of the beam segments, it is possible that some of the other columns would give shears that cancel. The bracing could be designed for 5% of the force in the columns, but it would be more economical to arrange the beam ends and column positions so that as many column shear as possible cancel.

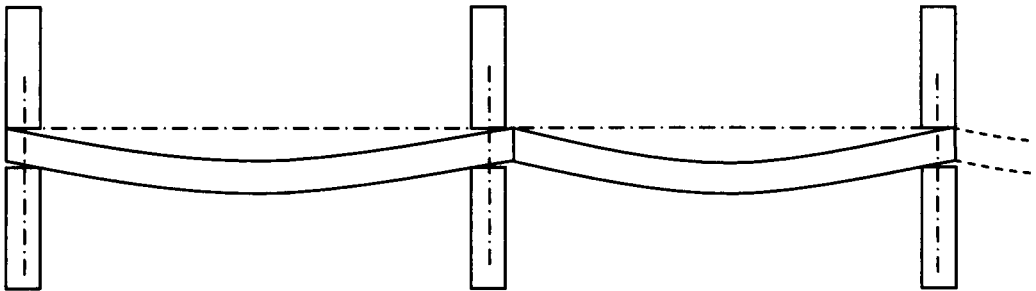


Figure 9.11 Columns not deflected to slope of beams

The second mechanism is when the column is forced to take the slope of the beam by the axial compression. In this case, the column end-moment is dictated by the column stiffness and the beam slope, as shown in Figure 9.12 for simply supported beams and in Figure 9.13 for continuous beams.

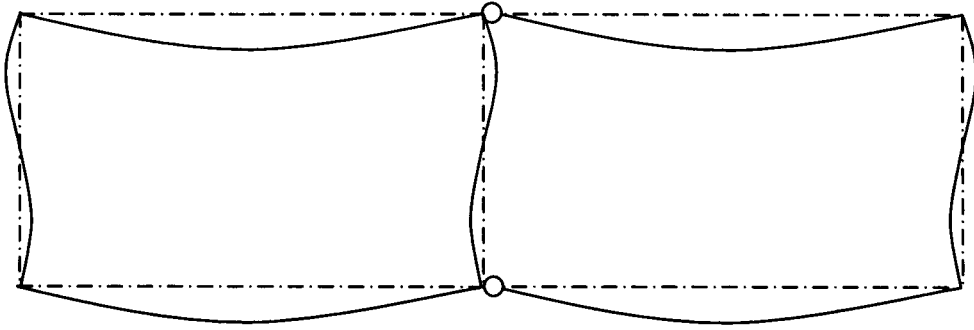


Figure 9.12: Column end-rotation equal to beam slope, simply supported beams

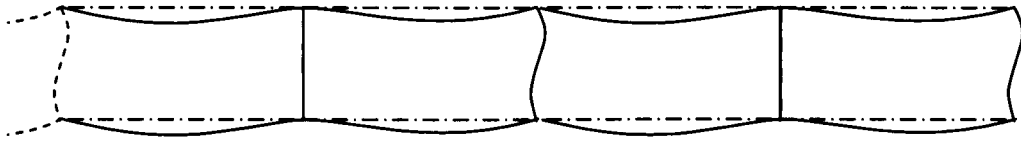


Figure 9.13 Column end-rotation equal to beam slope, continuous beams

Because continuity reduces the beam slope at the interior columns, it is clear that the case of simply supported beams gives the worst case. As an example the beam end-slope of 0.034 radians calculated in Section 3.6 is considered. For a 140×140×10SHS column 3.0 metres high and assuming equal end-rotations at the top and bottom of the column, the end moment induced assuming elastic behaviour would be

$$M = 3EI\theta/(\text{height}/2) = 6EI\theta/(\text{height}) \quad \text{Eq 9.9}$$

$$= 6 \times 210000 \times 14160000 \times 0.034 / 3000 \text{ N-mm} = 202 \text{ kN-m}$$

However, the characteristic value of the plastic moment resistance of the column is

$$f_y W_{pl} = 355 \times 246000 \text{ N-mm} = 87.3 \text{ kN-m} \quad \text{Eq 9.10}$$

Therefore, the end moment will be much less than the moment calculated by elastic analysis. For a column carrying half of its yield force, the reduced plastic moment of resistance is equal to the moment of resistance of the two opposite sides. Therefore, for 140×140×10 SHS columns, the characteristic value is

$$(f_y A/4)(B-t) = (355 \times 5090/4)(140-10) \text{ N-mm} = 58.7 \text{ kN-m} \quad \text{Eq 9.11}$$

Therefore, for a 140×140×10 SHS column 3.0 metres high with equal end-moments of 58.7 kN-m, the characteristic value of sway shear applied from each column is

$$V_H = 2 \times 58.7 / 3.0 = 39.1 \text{ kN} \quad \text{Eq 9.12}$$

The characteristic value of half of the yield force is

$$355 \times 5090 / 2 = 903 \text{ kN} \quad \text{Eq 9.13}$$

Therefore the sway shear expressed as a proportion of column load is

$$V_H = 39.1 / 903 = 0.0433 \quad \text{Eq 9.14}$$

This may be expressed more generally as

$$V_H = \frac{2 \left[\frac{f_y A}{4} (B - t) \right] \frac{1}{h}}{\frac{f_y A}{2}} = \frac{(B - t)}{h} \quad \text{Eq 9.15}$$

Note that for axial compressions that are higher proportions of the squash load, the available moment of resistance is reduced so the sway shear is reduced.

This is close to the value B/h for the case where the column ends do not rotate as much as the beams. As in that mechanism, the bracing could be designed for 5% of the force in the columns, but it would be more economical to arrange the beam ends and column positions so that as many column shear as possible cancel.

In conclusion, for rapid design, a sway shear of 5% vertical could be assumed, but this could be reduced by appropriate arrangement of the beam ends relative to the columns. 5% vertical might be uneconomic, but it might serve to give a frame that is sufficiently stiff to avoid calculation of second-order sway effects for the design of the bracing.

9.5 Connection design fundamentals

9.5.1 General

For discontinuous columns, the connections are different from the beam-column connections in conventional simple construction because the columns are discontinuous and the beams

are continuous. Typical structural arrangements have been published in AD 281 and AD 283 [SCI 2005a, SCI 2005b].

This section develops typical details that could be used to integrate discontinuous columns into a complete frame design. It is not intended to be exhaustive, but to show the range of sizes required for normal buildings

There are five common requirements for the design of beam-column connections for frames with discontinuous columns.

1. The connection must be made so that any moments induced in the column at the ends do not rupture the connection.
2. In frames in which plasticity of the beam is to be used, the top flange of the beam is not adversely affected by the beam-column connection.
3. The building regulation requirement to avoid disproportionate collapse should be observed.
4. The connections should minimise the storey-shears (or sway shears) that might arise from the rigidity of the beam-column connections and will be applied to the vertical bracing of the building.
5. The connections should not be expensive to fabricate.

Design to Eurocode 3 [BSI 2005a, CEN 2005b, BSI 2005a, BSI 2005b] using the UK National Annex gives broadly the same results as design to BS 5950-1 [BSI 2000a]. The calculations in this section are made using Eurocode 3.

9.5.2 Avoiding connection rupture from column end moments

In cases where the column has greater capacity than required, it is likely that the column end-rotations will be less than the beam rotations. This will be a common case when using the design method proposed because it assumes single curvature of the column so that the design method can remain simple. Where the column end-rotation is less than the beam rotation, forces and moments will be induced in the connection. To keep the design method simple, analysis of this effect should be avoided by appropriate detailing of the column-beam connection. This can be achieved by ensuring that the welds and bolts in the connection are so strong that they remain intact while the plates in the connection yield. In simple end plate connections, which are the first choice of connection for hollow section columns, it is easy to select a thickness of plate to yield along plastic hinges at loads lower than the loads that would rupture the bolts and welds. A typical end plate connection is shown in Figure 9.14.

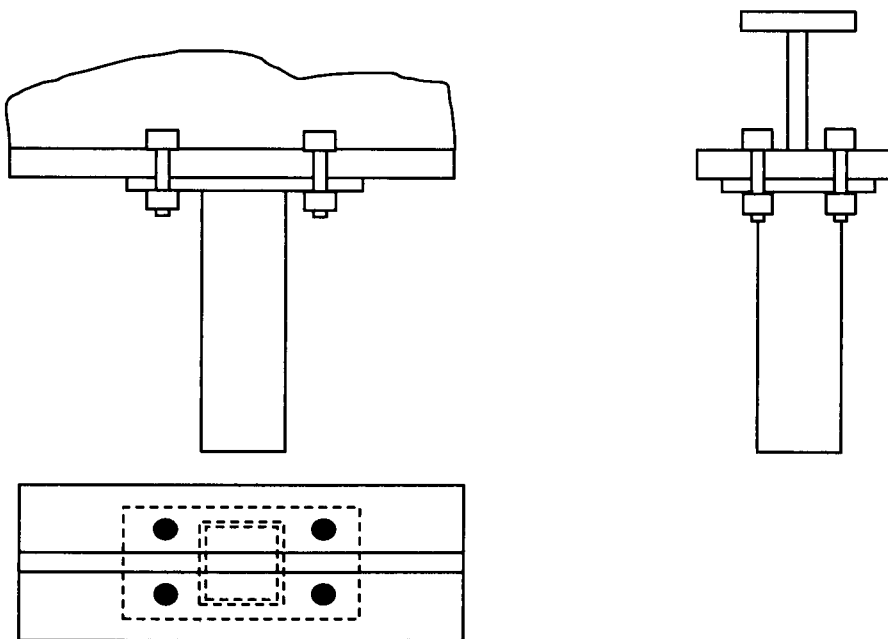


Figure 9.14 Typical thin end-plate connection

If the beam rotation is different from the column end rotation, the end plate will deform with plastic hinges along the lines shown in Figure 9.15, provided that the bolts and the weld between the end-plate and the column do not rupture. The forces on the weld and on the bolts are easily calculated from the plastic moment of resistance of the plate along the hinge lines shown.

From simple statics:

the resistance of the end-plate to vertical shear is given by

$$V = (M_{pl,Rd1} + M_{pl,Rd2})/L_a \quad \text{Eq 9.16}$$

There is a prying force, Q , generated by the moment $M_{pl,Rd1}$ such that

$$Q = M_{pl,Rd1}/e_p \quad \text{Eq 9.17}$$

The total tensile load in the two bolts is

$$2P = V + Q \quad \text{Eq 9.18}$$

The values of $M_{pl,Rd1}$ and $M_{pl,Rd2}$ are commonly calculated as

$$M_{pl,Rd} = (b \times t^2 / 4) \times f_y / \gamma_{M0} \quad \text{Eq 9.19}$$

This ignores issues of reduction of effective yield stress by shear stress, increase in effective yield away from the edges of the plate by Poisson effects, reduction of the section at the bolts by the bolt holes and increase in resistance by strain hardening. However, Eurocode 3 EN 1993-1-8 Table 6.2 [BSI 2005b, CEN 2005b] uses the above simplifications in the formula described as Method 1.

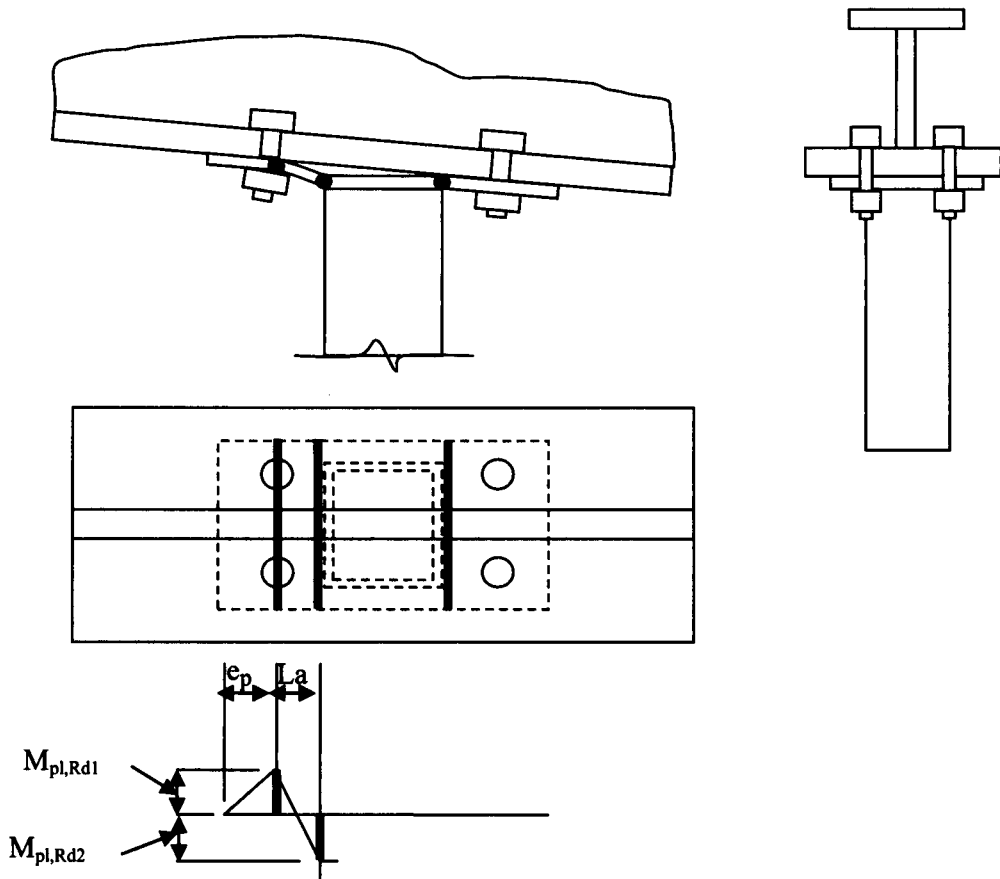


Figure 9.15 Bending moments in end-plate

If a connection has a 120×120 SHS and a 160mm wide by 10mm thick end plate in S275 steel, with 6mm fillet welds and 20mm diameter Grade 8.8 bolts at placed 70mm from the face of the column with 50mm edge distance, the calculations to EN 1993-1-8 [BSI 2005b, CEN 2005b] are as follows:

Weld resistance stress on S275 plate is

$$f_{wvd} = \frac{f_u / \sqrt{3}}{\beta_w \gamma_{M2}} = \frac{430 / \sqrt{3}}{0.85 \times 1.25} = 199 \text{ N/mm}^2 \quad \text{Eq 9.20}$$

Weld resistance along one side of the column (length of weld is 120 mm) is

$$199 \times 120 \times \frac{6}{\sqrt{2}} = 101 \text{ kN} \quad \text{Eq 9.21}$$

Plate plastic moment of resistance of the plate 160 mm wide and 10 mm thick is

$$M_{pl,Rd} = \frac{bt^2}{4} \frac{f_y}{\gamma_{M0}} = \frac{160 \times 10^2}{4} \times \frac{275}{1.0} = 1100 \text{ kN-mm} \quad \text{Eq 9.22}$$

$$L_a = 70 - 0.8 \times 6 = 65.2 \text{ mm} \quad \text{Eq 9.23}$$

$$V = 2M_{pl,Rd}/L_a = 2 \times 1100/65.2 = 33.7 \text{ kN} \quad \text{Eq 9.24}$$

$$Q = M_{pl,Rd}/e_p = 1100/50 = 22.0 \text{ kN} \quad \text{Eq 9.25}$$

$$\text{Force/bolt} = (33.7 + 22.0)/2 = 28 \text{ kN} \quad \text{Eq 9.26}$$

$$\text{Bolt resistance } F_{tRd} = k_2 f_{ub} A_s / \gamma_{M2} = 0.9 \times 800 \times 245 / 1.25 = 141 \text{ kN} \quad \text{Eq 9.27}$$

The bolt resistance and the weld resistance far exceed the plate resistance, so the connection is ductile, allowing end rotation of the column without rupture of the bolts, welds or end-plate. Therefore it is safe to use the proposed column design method without checking the implications of the actual end rotation of the column being less than the rotation of the beam.

9.5.3 Allowing plastic rotations of the beams at the columns

One of the structural benefits of discontinuous columns is that it is relatively inexpensive to have continuity of the beams to increase the load bearing capacity of the beams and/or to reduce the deflections. Therefore it is not desirable to drill large holes through the tension flange of the beams. Because the top flange of a continuous beam at a column is in tension, the vertical tying needs to be designed to pass either side of the top flange. This is especially true for designs in which plastic redistribution of the beam moments is desired. EN 1993-1-1 Section 5.6, *Cross-section requirements for plastic global analysis*, subsection (4) requires that any fastener holes in tension in the area of plastic hinges should satisfy Section 6.2.5(4). This section is to avoid rupture at the holes. It requires that the net cross-sectional area of the tension flange at the fasteners is no smaller than $(f_y/0.9f_u) \times (\gamma_{M2}/\gamma_{M0})$ times the gross cross-sectional area of the flange. For S355 steel and the UK National Annex value of 1.15 for γ_{M2} at holes in tension flanges, $(f_y/0.9f_u) \times (\gamma_{M2}/\gamma_{M0}) = (355/0.9 \times 510) \times (1.15/1.0) = 0.89$, so only very small holes are acceptable. The total width of holes at a section is 11% of the flange width. Given that the top flanges of ASBs vary from 175 mm to 203 mm, the allowable diameter if there were two holes would be from 9 to 11 mm which is impractically small. Therefore the bolts at the level of the top flange need to

pass either side of the top flange. There is no limitation on holes in the compression flange at plastic hinges. A simple detail is shown in Figure 9.16.

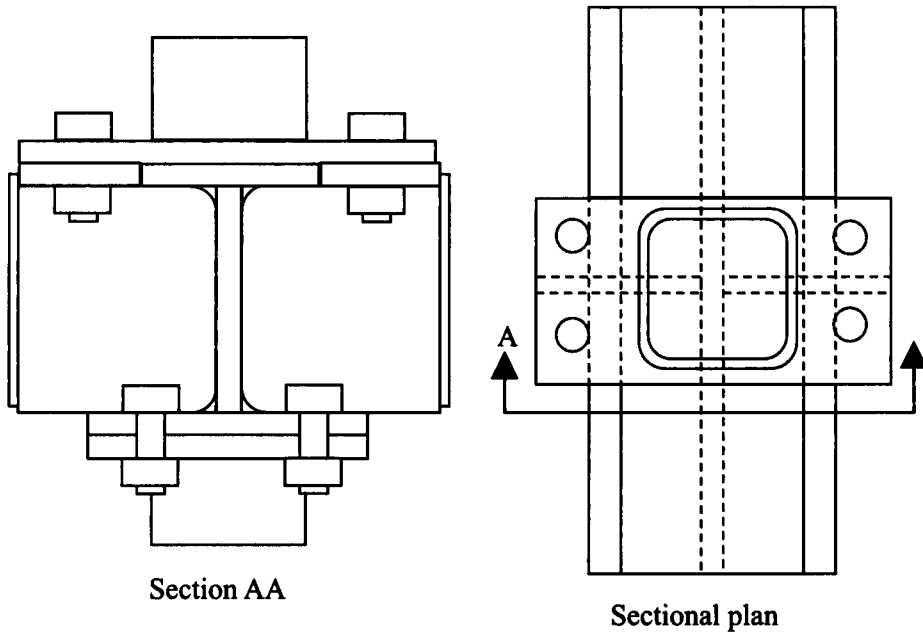


Figure 9.16 Typical beam-column connection for plastic rotations in the beam

9.6 Avoiding disproportionate collapse

9.6.1 Overview of Building Regulation requirements in the UK

Building regulations in the UK require that buildings should not be so sensitive to accidents so that damage is disproportionate to the cause. There are three different domains of regulation in the United Kingdom alone which are:

England and Wales

Scotland

Northern Ireland

The following discussion is in terms of the England and Wales Building Regulations for simplicity. The England and Wales regulations cover the greatest proportion of construction in the UK and the other regulations are similar in intent.

In the England and Wales Building Regulations, the Regulation A3 requirement is:

“The building shall be constructed so that in the event of an accident the building will not suffer collapse to an extent disproportionate to the cause.” Approved Document A gives ways that are deemed to satisfy the regulations. Section A3 divides structures into a variety of Classes. These Classes relate to both the size and the use of the building. The different Classes have different requirements in Approved Document A. Steel frame structures will usually be used for Classes 2A, 2B and 3. The Building Regulations Classes are given in Table 9.1:

Table 9.1 <i>Classes of buildings</i>	
Classes	Building type and occupancy
1	Houses not exceeding 4 storeys Agricultural buildings Buildings into which people rarely go (with limitations)
2A	5 storey single occupancy houses Hotels not exceeding 4 storeys Flats, apartments and other residential buildings not exceeding 4 storeys Offices not exceeding 4 storeys Industrial buildings not exceeding 3 storeys Retailing premises not exceeding 3 storeys of less than 2000m ² floor area in each storey Single-storey educational buildings All buildings not exceeding 2 storeys to which members of the public are admitted and which contain floor areas not exceeding 2000m ² at each storey
2B	Hotels, flats, apartments and other residential buildings greater than 4 storeys but not exceeding 15 storeys Educational buildings greater than 1 storey but not exceeding 15 storeys Retailing premises greater than 3 storeys but not exceeding 15 storeys Hospitals not exceeding 3 storeys Offices greater than 4 storeys but not exceeding 15 storeys All buildings to which members of the public are admitted which contain floor areas exceeding 2000m ² but less than 5000m ² at each storey Car parking not exceeding 6 storeys
3	All buildings defined above as Class 2A and 2B that exceed the limits on area and/or number of storeys Grandstands accommodating more than 5000 spectators Buildings containing hazardous substances and/or processes

The requirements in Approved Document A for hot-rolled steel framed buildings may be summarised as follows.

1. For Class 2A: to provide effective horizontal ties as described in BS 5950-1:2000.
2. For Class 2B: to provide effective horizontal ties together with effective vertical ties in all supporting walls or columns as described in BS 5950-1:2000. Alternatively,

limited areas of collapse following notional removal of individual columns may be used or design of members as “key elements”.

3. For Class 3: following a systematic risk assessment of the building accounting for normal and abnormal hazards, to design the structure to reflect the conditions that can reasonably be foreseen as possible during the life of the building.

9.6.2 Class 2A buildings

For Class 2A buildings, BS 5950-1 requires that the horizontal ties comply with Section 2.4.5.2 *Minimum requirements*. In brief, this requires lines of horizontal ties with a resistance of 75 kN at the perimeter and on the column lines in two directions, approximately at right-angles. The ties can be the steel beams. This requirement is easily achieved with almost any beam-beam and beam-column connections with not less than two 20 mm diameter bolts. With discontinuous columns, tying along the line of main beams is simple because the beams are not interrupted by the beam-column connections and it is easy to provide simple end-plate or web-cleat connections to provide the necessary continuity. Equally, the tying at right-angles is simple to provide with the lateral tie-members recommended in AD 281, AD 283 and AD 285 [SCI 2005a, SCI 2005b and SCI 2005c]. Therefore it is clear that steel frames with discontinuous columns can easily satisfy the requirements for Class 2A. This means that satisfying the building regulation for disproportionate collapse for 4-storey residential or office buildings is simple.

9.6.3 Class 2B buildings

For Class 2B buildings, BS 5950-1 requires that the horizontal ties comply with Section 2.4.5.2 *Minimum requirements* and 2.4.5.3 *Limiting effects of accidental removal of supports*. Following the Approved Document A, Section 2.4.5.3 presents three different approaches to limit the effects.

Horizontal and vertical tying

Notional removal of columns

Design of members as “key elements”

In the aftermath of the Ronan Point collapse, designers had to demonstrate that new designs were not sensitive to accidents by one of two approaches. One was to show that removal of any one vertical element did not cause extensive collapse, which is the philosophy of notional removal of columns. The other was to show that the important support members would not be blown away by the pressure of a gas explosion, which is the philosophy of

“key elements”. The tying requirements are a derivative of the methods used to justify a frame by notional removal of columns, served up as a recipe that is comparatively easy to apply to the majority of conventional building frames. Designers of conventional steel frames should try to use the requirements for horizontal and vertical tying because these were developed by the steelwork industry to make it simpler to show that a frame is sufficiently robust. The application of horizontal and vertical tying to frames with discontinuous columns is investigated in 9.7.

9.7 Connection design to avoid disproportionate collapse

9.7.1 Horizontal and vertical tying

For frames of hot-rolled steelwork, the relevant BS remains BS 5950-1 because Approved Document A of the Building Regulations refers to this for the design forces for horizontal and vertical tying. Eurocode 1 Part 7 contains a similar Annex, but the factors applied to the loads give less onerous requirements than BS 5950-1, which is not thought to have been intended. Therefore the requirements of BS 5950-1 will be applied in this study.

The clauses in BS 5950-1 are written on the assumption that steel frames follow the common practice of continuous columns, so does not consider discontinuous columns explicitly. However, initially it seems reasonable to design frames with discontinuous columns to resist the loads specified for continuity of columns at column splices. For this, BS 5950-1 Clause 2.4.5.3(c) requires that the splice should be capable of resisting a tensile force equal to the largest total factored vertical dead and imposed load applied to the column at a single floor level. In the case of discontinuous column construction this might be interpreted simply as the factored load applied to the column by the floor at that floor level.

The tying clauses in BS 5950-1 have been developed from the option of “notional removal”. The philosophy of the tying clauses is to find a structure that will limit the deformations throughout the structure when a column is removed or damaged so that it has almost no capacity. The structural behaviour assumed is as shown in Figure 9.17.

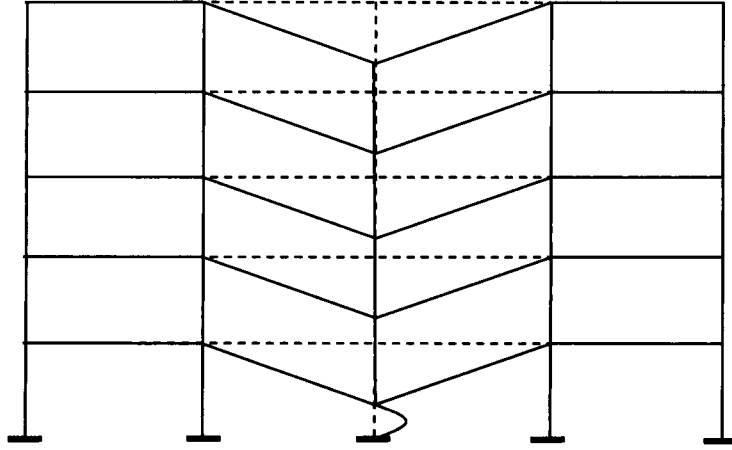


Figure 9.17 Model assumed in BS 5950-1 tying

The beams above the damaged column act as inclined ties to support the loads on the columns above the damaged columns. The vertical tying requirement is to share unequal reactions on the damaged column line amongst all the beam-ties. The unequal reactions may arise either from different design load intensities or from the different amount of load actually applied on each floor. This is important in the majority of steel-frame buildings because the design values of the tie forces are small to ensure economy in normal frames of “simple construction”.

Vertical tying should not be brittle so it is wise to use bolts of no higher grade than Grade 8.8. These have a minimum ultimate tensile strength of 800 N/mm^2 and a minimum 0.2% proof stress of 640 N/mm^2 . The tension capacity of Grade 8.8 bolts is

$$F_{t,Rd} = 0.9 \times f_u \times A_s / \gamma_{M2} \quad \text{Eq 9.28}$$

where $f_u = 800 \text{ N/mm}^2$ and $\gamma_{M2} = 1.25$

$$0.9 \times f_u / \gamma_{M2} = 0.9 \times 800 / 1.25 = 576 \text{ N/mm}^2 \quad \text{Eq 9.29}$$

The tying forces depend on the column grid and the floor loads. To demonstrate a range of details, the tying forces required for a larger grid commercial building and a smaller grid residential building are calculated. The calculations use loads derived from SCI P 342 Design of Asymmetric Slimflor Beams with Precast Concrete Slabs.

9.7.2 Vertical tying for a larger grid commercial building

Taking a 7.5m by 9.0m grid, the reactions based on grid area are:

PC units	$(1.25 \times 3.3) \times 9.0 \times 7.5$	=	278 kN
Concrete	$(1.25 \times 1.23) \times 9.0 \times 7.5$	=	104
Beam weight	$(1.25 \times 0.2) \times 9.0 \times 7.5$	=	17
Ceilings and services	$(1.25 \times 0.1) \times 9.0 \times 7.5$	=	8
Partitions	$(1.5 \times 1.0) \times 9.0 \times 7.5$	=	101
Imposed loading	$(1.5 \times 2.5) \times 9.0 \times 7.5$	=	<u>253</u>
TOTAL		=	762 kN

A typical column for a four storey building with this floor load and 2 kN/m² for the roof load would carry $2 \times 9 \times 7.5 + 3 \times 762 = 135 + 2286 = 2421$ kN. At $0.7 f_y / \gamma_{M1}$, the area required is 9741mm².

200×200×16 SHS has A = 11500mm² and 200×200×12.5 has A = 9210mm², so the column would probably not be less than a 200×200 SHS.

The tying force must be resisted by the end plate. If the column is assumed to be a 200 SHS, a reasonable width for the end-plate is 220mm or more. An example beam-column connection is shown in Figure 9.18. Assuming that the bolts are 70mm from the face of the column and that the end-plate is S275 plate 25mm thick by 260mm wide, the vertical tying resistance is 797kN. Therefore, at plastic deformation of the end-plate, the tying force per bolt is 199kN. If the end-distance of the bolts is 70mm, the prying force at full plasticity increases the total bolt tension to 276kN/bolt. The tensile resistance of an M30 Grade 8.8 bolt is 323kN. The tensile resistance of an M24 Grade 8.8 is only 203kN which is insufficient. However, this end-plate arrangement gives a load-path of the tying force from the column into the end-plate concentrated through two sides of the column only. This would necessitate 10mm leg welds along these two sides because the weld strength is governed by the yield of the S275 plate. The other two sides could use 6mm leg fillets.

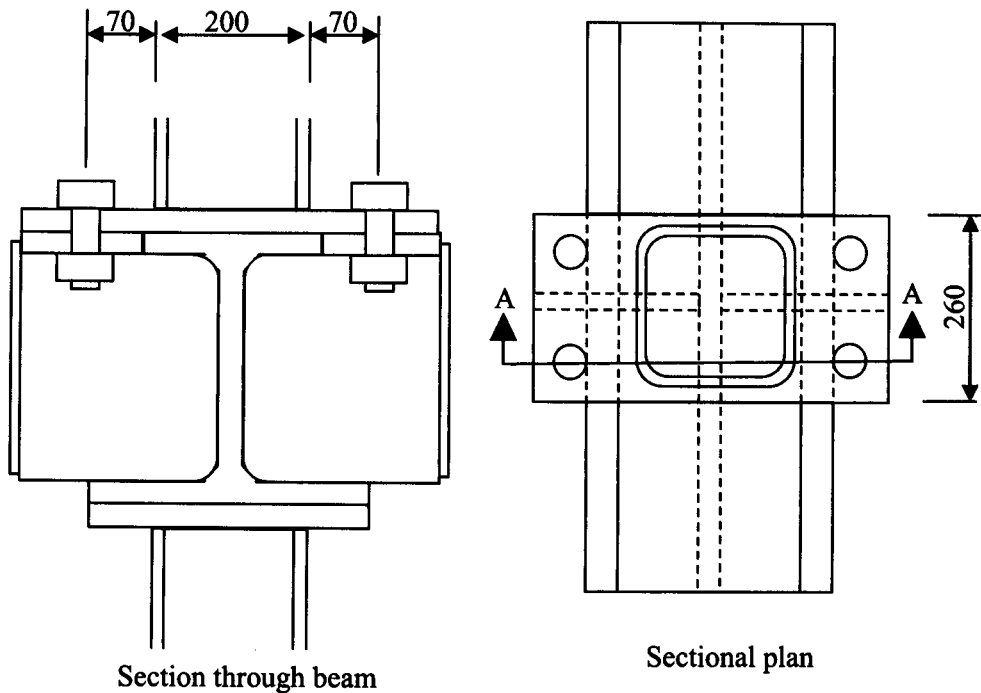


Figure 9.18 Example beam-column connection

Normally a 10mm weld will require 3 passes of weld so it is more expensive than normal. To reduce the weld leg size, either a greater length of weld must be mobilised or a higher grade of plate must be used. Raising the grade of plate to S355 gives a higher weld resistance, but does not allow the use of an 8mm leg weld that only requires 1 run of weld, so it does not help reduce the cost of the weld. Mobilising a greater length of weld would mean using a much wider plate, approximately square on plan. This would also need the bolts to be spaced out further, necessitating two vertical stiffeners either side of the web, instead of the one shown. While this is possible for the connection above the beam, it is less attractive for the connection below the beam because asymmetric beams have wide bottom flanges and the spacing of the bolts clashes with the edges of the flanges making the details even more difficult. The larger end-plates and the extra web stiffeners add to the costs making this a less attractive detail for economy.

The ductility of the end connection must also be considered. The column-beam connections are quite stiff if they are to resist vertical tying forces, so any column end-moments will cause significant end moments. These might be so large as to fracture the bolts and welds, so either the bolts and welds must be clearly stronger than the plate, or the end moments must be calculated so that the welds and bolts can be checked for strength. The welds could be increased to 12mm without increasing the number of weld passes above 3. For rotation

of the column in the plane of the column and the beam, the bolts in tension will develop individual yield-line patterns, as shown in Figure 9.19.

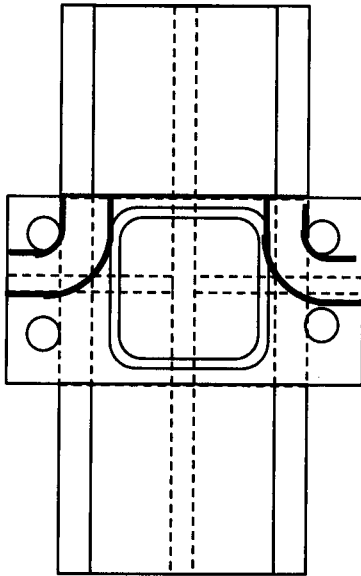


Figure 9.19 End-plate yield line patterns

The plate resistance per bolt is now so great that the bolts and the welds need to be even larger than those required to resist the vertical tying force, making the connection even larger and more expensive.

9.7.3 Vertical tying for a smaller grid residential building

Taking a 7.5m by 6.0m grid, the reactions for the 1.5 kN/m² areas based on grid area are:

PC units	$(1.25 \times 3.3) \times 6.0 \times 7.5$	=	186 kN
Concrete	$(1.25 \times 1.23) \times 6.0 \times 7.5$	=	69
Beam weight	$(1.25 \times 0.2) \times 6.0 \times 7.5$	=	11
Ceilings and services	$(1.25 \times 0.1) \times 6.0 \times 7.5$	=	6
Partitions	$(1.5 \times 1.0) \times 6.0 \times 7.5$	=	68
Imposed loading	$(1.5 \times 1.5) \times 6.0 \times 7.5$	=	101
TOTAL		=	440 kN

This load is resisted by 4 bolts through plastic end-plates detailed to give prying forces of 50%, then the force per bolt = $1.5 \times 440 / 4 = 165$ kN

Therefore minimum area of Grade 8.8 bolts = $165 \times 10^3 / 576 = 287 \text{ mm}^2$

M24 bolts to BS 4190 have a tensile area of 353 mm^2 , M20 bolts have only 245 mm^2 .

9.7.4 Design options

If conventional vertical tying is used to satisfy the Building Regulation, it can be seen from Sections 9.7.2 and 9.7.3 that many building types and floor grids will need bolts of 24 mm or 30 mm diameter when 4 bolts are used to make the connection.

The options are:

1. use very big bolts to allow the end moments to be ignored
2. calculate the end moments to check that the bolts will not fracture
3. find alternative methods of satisfying the disproportionate collapse regulation
4. do not use this type of construction for Class 2B buildings

9.8 Alternative methods to satisfy the regulation

9.8.1 Design as “key elements”

A standard method of design to avoid disproportionate collapse is to design the members to resist a lateral pressure defined by the design code. This method, called “key element” design in BS 5950-1, could be used for structures with discontinuous columns.

9.8.2 Notional removal

One option for demonstrating resistance to disproportionate collapse is the approach often called “notional removal”. The philosophy of notional removal is to find a structural system in the damaged structure that will limit the deformations throughout the structure when either a column or a beam is removed (or damaged so that it has almost no capacity) such that equilibrium is maintained. It is probable that many structures could be shown to satisfy this requirement if the horizontal tying resistance were sufficiently high.

If the horizontal tie resistances were high, there would be no need to share the floor loads because each floor could support its own loads. This is particularly appropriate for the form of construction foreseen in this study because the beams are well restrained by the floor in the depth of the beams, the beams can form plastic hinges if there are no holes in the top flanges at the columns and it is easy to provide beam splices that will develop large tying resistances. Therefore, for this type of construction it is appropriate to design for horizontal tying alone, but with larger forces than in BS 5950-1.

10 WORKED EXAMPLE

10.1 Introduction

The purpose of this worked example is to illustrate the calculations used in the design method. It does not include all possible load combinations and all possible structural arrangements. Designers must consider all load combinations even when they are not shown below.

The design method comprises two parts:

1. Design of the floor slab and main beams.
2. Design of the columns to be compatible with the slopes of the slab and beams at Ultimate Limit State.

The design process is shown with pattern loading for the slab, because this is the more complicated case. It is shown both with and without pattern loading for the beams to show how the end slopes are calculated when plastic redistribution occurs due to plasticity in the hogging region.

The use of pattern loading or uniform loading will depend on the design code specified for a particular structure and the judgement of the designer.

10.2 Structural arrangement

The structural arrangement is shown in Figure 10.1. The beam span is 6.0 metres, so, if these are continuous over two spans, the piece length is 12 metres which is reasonable for transport. The slab is assumed to be made of precast concrete units with a concrete overlay with some continuity steel across the tops of the main beams.

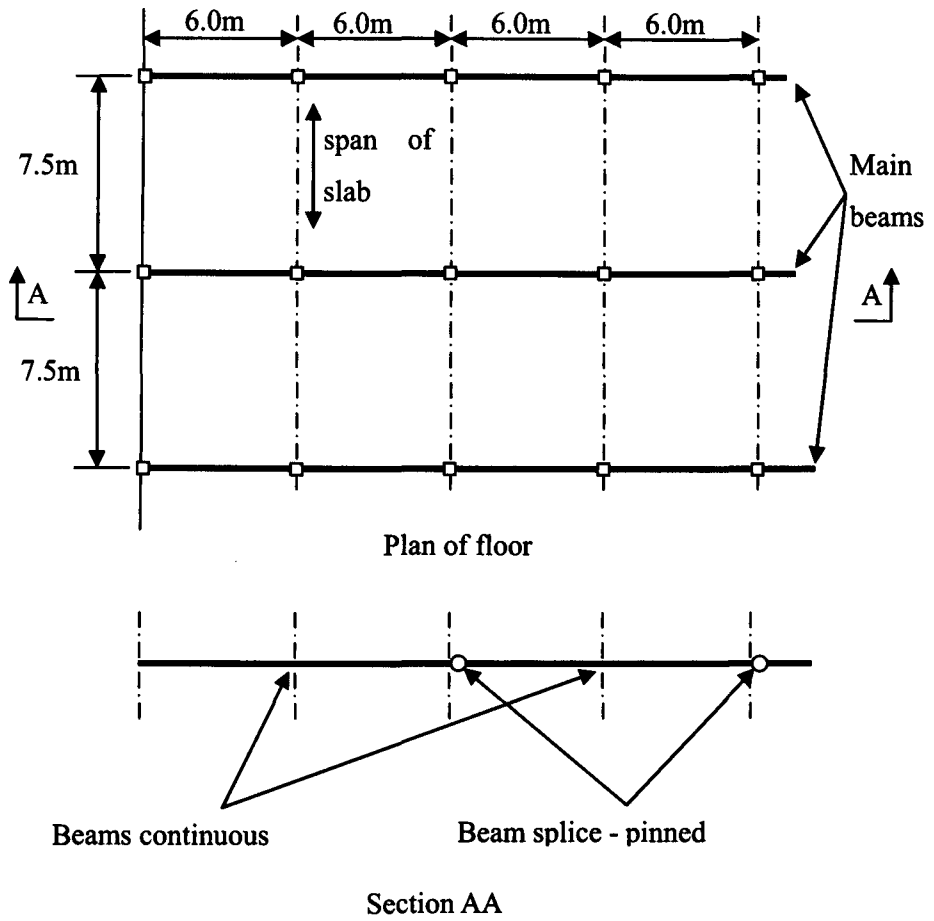


Figure 10.1 Structural arrangement

10.3 Loading

The loading used in the example is given in Table 10.1

Table 10.1 Loading

Item	Gamma	Specified load (kN/m ²)	Factored Load
PC units	1.25	3.3	
Concrete	1.25	1.23	
Beam weight	1.25	0.2	
Ceilings and services	1.25	0.1	
Total permanent load	1.25	4.83	6.04 kN/m ²
Partitions	1.5	1.0	
Imposed loading	1.5	1.5	
Total variable load	1.5	2.5	3.75 kN/m ²

10.4 Slab

In this example it is assumed that the slab is constructed so that the self-weight of the floor is carried as if the slab were simply supported along each main beam, but that the continuity steel across the main beams is sufficient for the slab to act as continuous for support of the variable loads (imposed floor load and partition load).

10.4.1 Column end-rotation due to slab deflections

The deflection of the slab can cause end-rotation of the column. For this particular structure, the self-weight is assumed to be supported as if the slab were simply supported and that there is no end-rotation induced in the column due to self-weight when the structure is complete. Therefore the only cause of end-rotation in the columns arising from the slab in the completed structure is from the variable load effects and these effects will be worst with alternate spans loaded. This condition is shown for an infinitely long structure in Figure 10.2.

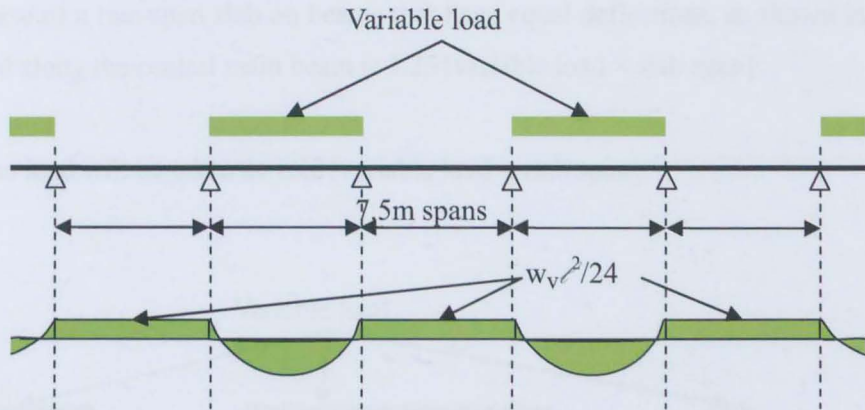


Figure 10.2 Slab variable load and bending moment diagram

The EI value of the concrete floor is taken as 18.3×10^{12} N-mm²/metre-width.

The end slope of the slab if simply supported is

$$\theta_{ss} = \frac{1}{24} \frac{w \ell^3}{EI} = \frac{1}{24} \frac{3.75 \times 7.5^3 \times 10^9}{18.3 \times 10^{12}} = 0.0036 \text{ radians} \quad \text{Eq 10.1}$$

The end slope is reduced by any hogging moments at supports

$$\theta_{end} = \theta_{ss} - \left(\frac{M_{near} \ell}{3EI} + \frac{M_{far} \ell}{6EI} \right) = \theta_{ss} - \left(\frac{M_{near}}{3} + \frac{M_{far}}{6} \right) \frac{\ell}{EI} \quad \text{Eq 10.2}$$

Taking the hogging moment at the support as

$$M = \frac{w_v \ell^2}{24} = \frac{3.75 \times 7.5^2}{24} = 8.79 \text{ kN-m/metre-width} \quad \text{Eq 10.3}$$

$$\begin{aligned} \theta_{end} &= 0.0036 - \left(\frac{8.79}{3} + \frac{8.79}{6} \right) \times 10^6 \times \frac{7500}{18.3 \times 10^{12}} \\ &= 0.0036 - 0.0018 = 0.0018 \text{ radians} \end{aligned} \quad \text{Eq 10.4}$$

In this case the column end-rotation in the plane transverse to the main beam is very small. However this cannot be assumed in all cases, especially if a beam carrying significant floor load frames into the column in this plane.

10.4.2 Slab reaction on main beams

The slab reaction along the main beams due to variable load should not be expected to be equal to {variable load \times slab span}. Where pattern loading is applied, as shown in Figure 10.3, the load along the most heavily loaded beam will be increased significantly. Even

where pattern loading is not applied, the load along the beam next to the edge beam will be increased. In the case of a two-span slab on beams that have equal deflections, as shown in Figure 10.4, the load along the central main beam is $1.25 \{\text{variable load} \times \text{slab span}\}$.

For this example, the load will be taken as $1.20 \{\text{variable load} \times \text{slab span}\}$.

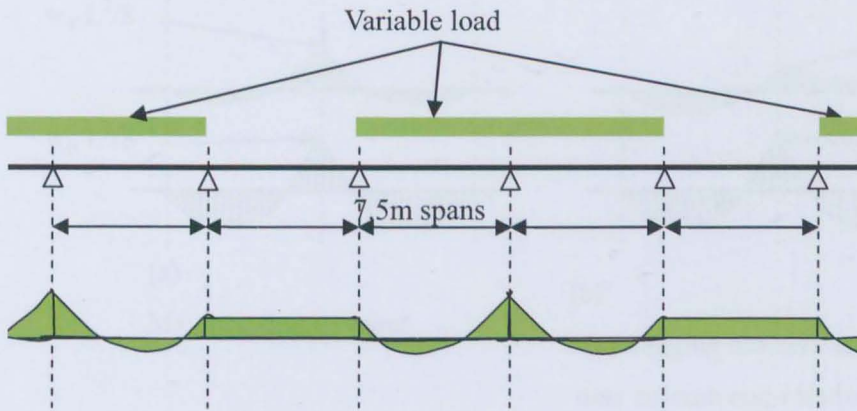


Figure 10.3 Slab variable load for max reaction on main beams

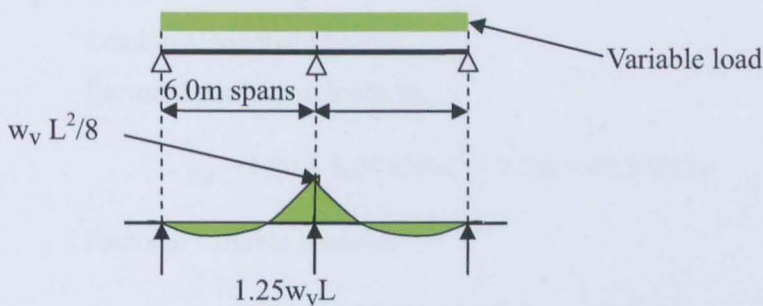


Figure 10.4 Two-span slab

10.5 Main beams

10.5.1 Initial analysis of main beam

The main beams are two-span continuous beams with pinned splices to one side of a column. This will give high moment and shear in the beam where it is continuous across the column line. However, the highest column end-rotation can be expected in the columns at the pinned splice in the beam.

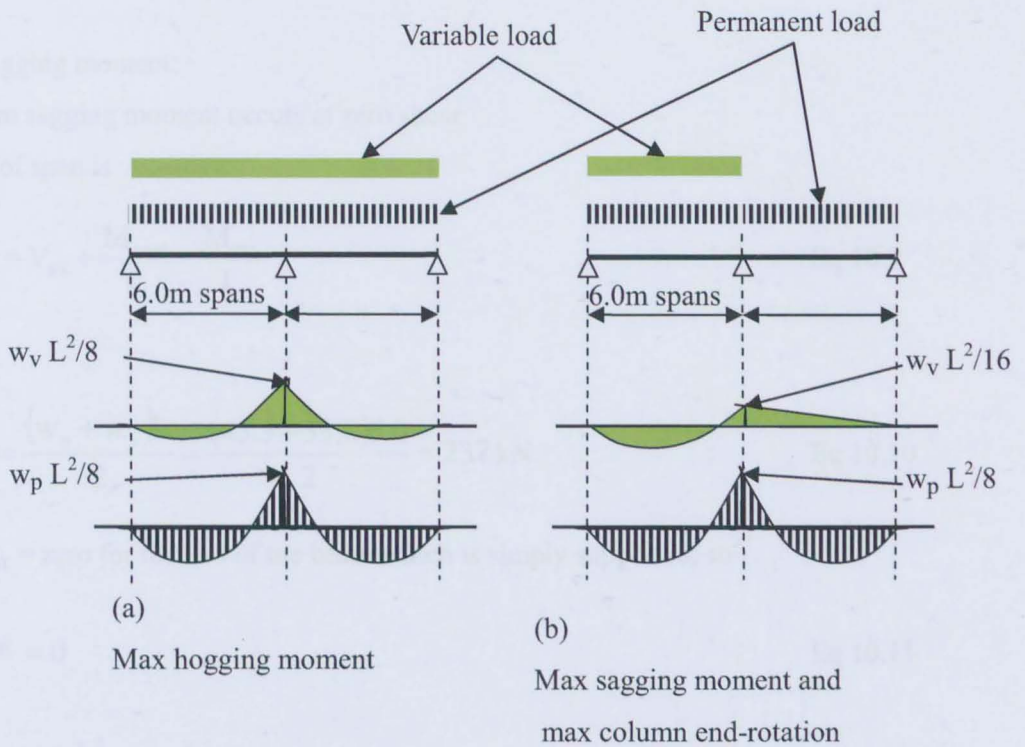


Figure 10.5 Main beam load and bending moment

Load/m along main beam:

Factored permanent loads/m,

$$w_p = 1.00 \times 6.04 \text{ kN/m}^2 \times 7.5\text{m} = 45.3 \text{ kN/m} \quad \text{Eq 10.5}$$

Factored variable loads/m,

$$w_v = 1.20 \times 3.75 \text{ kN/m}^2 \times 7.5\text{m} = 33.8 \text{ kN/m} \quad \text{Eq 10.6}$$

Assuming elastic behaviour:

The maximum hogging moment is

$$M_{Ed} = \frac{w_p L^2}{8} + \frac{w_v L^2}{8} \quad \text{Eq 10.7}$$

$$= \frac{45.3 \times 6.0^2}{8} + \frac{33.8 \times 6.0^2}{8} = 204 + 152 = 356 \text{ kN-m}$$

The coincident shear force is

$$V_{Ed} = 1.25w_p L + 1.25w_v L \quad \text{Eq 10.8}$$

$$= 1.25 \times 6.04 \times 6.0 + 1.25 \times 3.75 \times 6.0 = 169.8 + 126.6 = 296 \text{ kN}$$

Maximum sagging moment:

The maximum sagging moment occurs at zero shear

Shear at end of span is

$$V_{\text{end}} = V_{\text{SS}} + \frac{M_{\text{near}}}{L} - \frac{M_{\text{far}}}{L} \quad \text{Eq 10.9}$$

where

$$V_{\text{SS}} = \frac{(w_p + w_v)L}{2} = \frac{(45.3 + 33.8)6.0}{2} = 237 \text{ kN} \quad \text{Eq 10.10}$$

$M_{\text{near}} = \text{zero}$ for the end of the beam which is simply supported, so

$$\frac{M_{\text{near}}}{L} = 0 \quad \text{Eq 10.11}$$

$$M_{\text{far}} = \frac{w_p L^2}{8} + \frac{w_v L^2}{16} \quad \text{Eq 10.12}$$

$$= \frac{45.3 \times 6.0^2}{8} + \frac{33.8 \times 6.0^2}{16} = 203.8 + 75.9 = 280 \text{ kN-m,}$$

$$\Rightarrow \frac{M_{\text{far}}}{L} = \frac{280}{6.0} = 46.6 \text{ kN-m} \quad \text{Eq 10.13}$$

$$\Rightarrow V_{\text{end}} = 237 + 0 - 46.6 = 190.5 \text{ kN} \quad \text{Eq 10.14}$$

so the shear force is zero at a distance x from the end of the beam is

$$x = \frac{V_{\text{end}}}{(w_p + w_v)} = \frac{190.5}{(45.3 + 33.8)} = 2.410 \text{ m} \quad \text{Eq 10.15}$$

$$M_{\text{sag}} = V_{\text{end}} x - \frac{(w_p + w_v)x^2}{2} \quad \text{Eq 10.16}$$

$$= 190.5 \times 2.410 - \frac{(45.3 + 33.8) \times 2.41^2}{2} = 459 - 229.5 = 230 \text{ kN-m}$$

10.5.2 Choice of beam size

Max hogging moment = 356 kN-m with coincident shear force = 296 kN

Max sagging moment = 230 kN-m from pattern loading

Try 280 ASB 74, yield stress = 355 MPa

$$W_{el} = 776 \text{ cm}^3,$$

$$M_{c,el} = 355 \times 776 \times 1000 = 275 \text{ kN-m} \quad \text{Eq 10.17}$$

$$\frac{M_{sag}}{M_{c,el}} = \frac{230}{275} = 0.833 \Rightarrow \text{OK} \quad \text{Eq 10.18}$$

Check classification to see if plastic cross-sectional resistance can be used

Bottom flange:

$$c = \frac{B_b - t_w - 2r}{2} = \frac{285 - 10 - 2 \times 24}{2} = 113.5 \quad \text{Eq 10.19}$$

$$\text{so } \frac{c}{t_f} = \frac{113.5}{14} = 8.107 \quad \text{Eq 10.20}$$

Class2 limit is

$$\frac{c}{t_f} = 10\epsilon = 10 \sqrt{\frac{235}{f_y}} = 10 \sqrt{\frac{235}{355}} = 8.136 \quad \text{Eq 10.21}$$

Therefore 280 ASB 74 is Class 2, so the plastic moment of resistance can be used.

Check if the plastic moment of resistance is reduced by shear:

$$V_{pl,Rd} = \frac{A_v \left(\frac{f_y}{\sqrt{3}} \right)}{\gamma_{M0}} = \frac{3742 \left(\frac{355}{\sqrt{3}} \right)}{1.0} = 767 \text{ kN} \quad \text{Eq 10.22}$$

$$\therefore \frac{V_{Ed}}{V_{pl,Rd}} = \frac{296}{767} = 0.386 < 0.5 \quad \text{Eq 10.23}$$

so the moment of resistance need not be reduced for the effects of coexistent shear force.

$$W_{pl} = 979 \text{ cm}^3,$$

$$M_{c,pl} = 355 \times 979 \times 1000 = 348 \text{ kN-m} \quad \text{Eq 10.24}$$

$$\frac{M_{hog}}{M_{c,pl}} = \frac{356}{348} = 1.082 \quad \text{Eq 10.25}$$

EN 1993-1-1 Section 5.4.1(4)B allows 15% redistribution from elastic analysis for Class 2 cross-sections provided that the conditions of this Section are satisfied, which they are for this particular structure. For this beam, the required redistribution is $(356 - 348)/356 \times 100\% = 2.3\%$, so the redistribution is acceptable.

The sagging moment resulting from the redistribution must also be checked, but the pattern load case used to check sagging above is more onerous, so the sagging resistance is acceptable.

Therefore the 280 ASB 74 is satisfactory.

10.5.3 Calculation of beam slopes

$E = 210000 \text{ MPa}$,

$I \text{ of } 280 \text{ ASB } 74 = 12190 \text{ cm}^4$,

The end slope of the beam if simply supported:

$$\begin{aligned}\theta_{ss} &= \frac{1}{24} \frac{(w_p + w_v)L^3}{EI} && \text{Eq 10.26} \\ &= \frac{1}{24} \frac{(45.3 + 33.8) \times 6.0^3 \times 10^9}{210 \times 10^3 \times 121.9 \times 10^6} = 0.0278 \text{ radians}\end{aligned}$$

The end slope is reduced by any hogging moments at supports

$$\theta_{\text{end}} = \theta_{ss} - \left(\frac{M_{\text{near}}L}{3EI} + \frac{M_{\text{far}}L}{6EI} \right) \quad \text{Eq 10.27}$$

At end of two-span beam, $M_{\text{near}} = 0$,

$$\text{so } \theta_{\text{end}} = \theta_{ss} - \frac{M_{\text{far}}L}{6EI} \quad \text{Eq 10.28}$$

At centre of two-span beam, $M_{\text{far}} = 0$,

$$\theta = \theta_{ss} - \frac{M_{\text{near}}L}{3EI} \quad \text{Eq 10.29}$$

With pattern loading:

The hogging moment at mid-length of the two-span beam = 280 kN-m

At end of two-span beam,

$$\begin{aligned}\theta_{\text{end}} &= \theta_{ss} - \frac{M_{\text{far}}L}{6EI} && \text{Eq 10.30} \\ &= \theta_{ss} - \frac{280 \times 10^6 \times 6000}{6 \times 210 \times 10^3 \times 121.9 \times 10^6} = 0.0278 - 0.0109 = 0.0169 \text{ radians}\end{aligned}$$

At centre of two-span beam,

$$\theta = \theta_{ss} - \frac{M_{near} L}{3EI} \quad \text{Eq 10.31}$$

$$= \theta_{ss} - \frac{280 \times 10^6 \times 6000}{6 \times 210 \times 10^3 \times 121.9 \times 10^6} = 0.0278 - 0.0219 = 0.0059 \text{ radians}$$

Without pattern loading:

The hogging moment at mid-length of the two-span beam is limited to the cross-sectional moment of resistance of the beam, reduced by shear if appropriate. In this case is no reduction from shear because the applied shear is less than 50% of the plastic shear resistance. Therefore the hogging moment = 348 kN-m

At end of two-span beam,

$$\theta_{end} = \theta_{ss} - \frac{M_{near} L}{3EI} - \frac{M_{far} L}{6EI} \quad \text{Eq 10.32}$$

$$= \theta_{ss} - 0 - \frac{348 \times 10^6 \times 6000}{6 \times 210 \times 10^3 \times 121.9 \times 10^6} = 0.0278 - 0.0136 = 0.0142 \text{ radians}$$

At centre of two-span beam,

$$\theta_{end} = \theta_{ss} - \frac{M_{near} L}{3EI} - \frac{M_{far} L}{6EI} \quad \text{Eq 10.33}$$

$$= \theta_{ss} - \frac{348 \times 10^6 \times 6000}{3 \times 210 \times 10^3 \times 121.9 \times 10^6} - 0 = 0.0278 - 0.0272 = 0.0006 \text{ radians}$$

10.6 Column

10.6.1 Design values of end-rotations

The design values of end rotations are taken from the beam analysis without pattern loading to show the values calculated to the Eurocodes.

The greatest end-rotation in Section 10.5.3 is at the end of the two-span beam, so this case will be used to show the design method. It should be noted that the axial load in this column will be less than in the column at mid-length of the two-span beam because of the hogging moments in the beams at mid-span. Therefore, the columns at mid-length might be the most heavily loaded and must be checked.

Table 10.2 Design end-rotation (end of two-span beam)		
End of two-span beam		End-rotation (radians)
In plane of beam and column	Beam slope	0.0142
	Frame imperfection	0.005
	Horiz deflection from wind	0.005
	TOTAL	0.0242
Perpendicular to main beam	Slab, see Note 1	0.0018
Design end-rotation	End-rotation = $\theta = \sqrt{\theta_1^2 + \theta_2^2}$	0.0243
Note 1: The end-rotation was calculated with a different pattern of floor loading (alternate spans of slab loaded) from the pattern that gives the highest beam slopes, but the value is so small that it is not worth re-calculating the slope for the coexistent case.		

10.6.2 Wall thickness of column

The design limits are given in Figure 9.2. From this it can be seen that the limiting B/t is approximately 18 for the design end-rotation of 0.0243 radians = 24.3 milliradians.

Using the formula for the limiting B/t:

$$B/t = 37.5 - 14 \log_{10}(\text{end-rotation in milliradians}) \quad \text{Eq 10.34}$$

$$B/t = 37.5 - 19.4 = 18.1$$

If the section is a 140×140 SHS, then B = 140, so the minimum wall thickness of the column is 140/18.1 = 7.7 mm.

10.6.3 Design equations

Where there is no externally applied moment from lateral loads, the design equation is

$$N_{\theta, Rd} \left\{ \left(\frac{h}{2} \right) \theta + e_i \right\} \leq M_{N, Rd} \quad \text{Eq 10.35}$$

Where there is an externally applied moment from lateral loads, the design equation is

$$N_{\theta, Rd} \left\{ \left(\frac{h}{2} \right) \theta + e_i \right\} + M_{\text{ext}} \leq M_{N, Rd} \quad \text{Eq 10.36}$$

but $N_{\theta,Rd} \leq$ flexural buckling resistance of a pin-ended strut with the the same lateral loading.

The resistance equation for the column depends on the axial compression applied.

If the axial compression resistance does not exceed $0.5 N_{cRd}$, the resistance may be calculated from Appendix A.2.4:

$$\therefore N_{\theta,Rd} = -4t f_{yd} e + \sqrt{(4t f_{yd} e)^2 + 8t f_{yd} (M_{pl,Rd} - M_{ext})} \quad \text{Eq 10.37}$$

If the axial compression resistance is not less than $0.5 N_{cRd}$, the resistance may be calculated from Appendix A.3.4:

$$\therefore N_{\theta,Rd} = \frac{N_{pl,Rd} \left(\frac{b}{2} \right) - M_{ext}}{\left(e + \frac{b}{2} \right)} \quad \text{Eq 10.38}$$

where $b = B - t =$ the distance between mid-planes of the SHS walls

10.6.4 Resisting vertical loads only

Design end-rotation, $\theta = 0.0269$ radians and storey height, $h = 3.0$ metres.

Find the resistance of a $140 \times 140 \times 10$ SHS with yield stress of 355 N/mm^2 ,

Find the design imperfection e_d

The design imperfection $e_d = e_s$, the imperfection calculated from the flexural buckling resistance of the column if acting as a pin-ended strut.

Calculate the pin-ended strut resistance to EN1993-1-1:

$$\bar{\lambda} = \frac{\lambda}{\lambda_1} = \frac{\left(\frac{L_{cr}}{i} \right)}{\left(\pi \sqrt{\frac{E}{f_y}} \right)} = \frac{\left(\frac{3000}{52.7} \right)}{\left(\pi \sqrt{\frac{210000}{355}} \right)} = \frac{56.9}{76.4} = 0.745 \quad \text{Eq 10.39}$$

$$\phi = 0.5 \left[1 + \alpha(\bar{\lambda} - 0.2) + \bar{\lambda}^2 \right] = 0.5 \left[1 + 0.21(0.745 - 0.2) + 0.745^2 \right] \quad \text{Eq 10.40}$$

$$= 0.5[1 + 0.114 + 0.555] = 0.835$$

$$\chi = \frac{1}{\left[\phi + \sqrt{\phi^2 - \bar{\lambda}^2} \right]} = \frac{1}{\left[0.835 + \sqrt{(0.835^2 - 0.745^2)} \right]} = 0.826 \quad \text{Eq 10.41}$$

$$\therefore N_{b,Rd} = \frac{A\chi f_y}{\gamma_{M1}} = \frac{5090 \times 0.826 \times 355}{1.0} = 1492 \text{ kN} \quad \text{Eq 10.42}$$

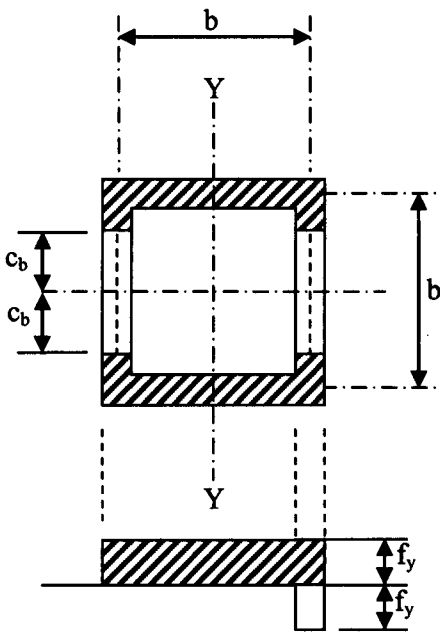
Calculate the squash load:

$$N_{pl,Rd} = \frac{Af_y}{\gamma_{M0}} = \frac{5090 \times 355}{1.0} = 1807 \text{ kN} \quad \text{Eq 10.43}$$

Calculate strut action moment M_s assuming rectangular stress blocks:

In this case, the area required to resist axial compression alone is more than the area of the two sides acting as webs. Therefore the area resisting bending is confined to the two sides acting as flanges as shown in Figure 10.6 as the two unshaded areas. The force resisted by

each unshaded area is equal to $\frac{(N_{pl,Rd} - N_{b,Rd})}{2}$.



plastic stress diagram


 = area resisting axial compression $N_{\theta,Rd}$

Figure 10.6 Plastic stress blocks in column

Therefore the strut action moment resistance available is

$$M_s = \frac{(N_{pl,Rd} - N_{b,Rd})b}{2} = \frac{(1807 - 1492)0.130}{2} = 20.47 \text{ kN-m} \quad \text{Eq 10.44}$$

Calculate imperfection e_s :

$$e_s = \frac{M_s}{N_{b,Rd}} = \frac{20.47}{1492} = 0.01372 \text{ metres} = 13.72 \text{ mm} \quad \text{Eq 10.45}$$

Calculate total eccentricity on column:

$$e = e_s + \left(\frac{h_s}{2}\right)\theta = 13.72 + \left(\frac{3000}{2}\right) \times 0.0243 \quad \text{Eq 10.46}$$

$$= 13.72 + 36.45 = 50.18 \text{ mm}$$

Calculate the axial compression that can be resisted at the end of the two-span beam from either Appendix A.2.4 for $N_{\theta,Rd}$ not more than $0.5N_{c,Rd}$ or Appendix A.3.4 for $N_{\theta,Rd}$ not less than $0.5N_{pl,Rd}$.

Initially try $N_{\theta,Rd}$ not less than $0.5N_{pl,Rd}$.

When there is no externally applied bending moment:

$$N_{\theta,Rd} = N_{pl,Rd} \frac{\left(\frac{b}{2}\right)}{e + \left(\frac{b}{2}\right)} \quad \text{Eq 10.47}$$

$$= 1807 \frac{0.065}{0.05018 + 0.065} = 1807 \times 0.564 = 1020 \text{ kN}$$

From Eq 10.43, $0.5N_{pl,Rd} = 0.5 \times 1807 = 904 \text{ kN} \Rightarrow N_{\theta,Rd} > 0.5N_{pl,Rd}$

$$\frac{N_{\theta,Rd}}{N_{b,Rd}} = \frac{1020}{1492} = 0.684 \text{ even for single curvature of the column} \quad \text{Eq 10.48}$$

For the column at mid-span of the two-span beam, the design end-rotation is 0.0106 radians,

$$\text{so } \frac{N_{\theta,Rd}}{N_{b,Rd}} = \frac{1241}{1492} = 0.832 \quad \text{Eq 10.49}$$

even for single curvature of the column

10.6.5 Resisting reduced vertical and lateral loads

Therefore the design equation derived from moment equilibrium at mid-height becomes:

$$N_{\theta,Rd} \left\{ \left(\frac{h}{2} \right) \theta + e_s \right\} + M_{ext} \leq M_{N,Rd} \quad \text{Eq 10.50}$$

but $N_{\theta,Rd} \leq$ resistance of a pin-ended strut with the the same lateral loading.

Take the factored horizontal load for this load combination $w_H = 15 \text{ kN/m}$ acting on the storey height of 3.0 metres as a uniformly distributed load,

Therefore the bending moment applied to the column is:

$$M_{ext} = \frac{w_H h^2}{8} = \frac{15 \times 3.0^2}{8} = 16.88 \text{ kN-m} \quad \text{Eq 10.51}$$

Using EN 1993-1-1 Section 6.3.3 and Annex B, the maximum axial compression coincident with this moment is 1107kN.

Using the new design model:

$$N_{\theta,Rd} \left\{ \left(\frac{h}{2} \right) \theta + e_d \right\} + M_{ext} \leq M_{N,Rd} \quad \text{Eq 10.52}$$

The resistance function for the column depends on the axial compression applied.

If the axial compression resistance is not less than $0.5 N_{cRd}$, the resistance may be calculated from Appendix A.3.4:

$$N_{\theta,Rd} = \frac{N_{pl,Rd} \left(\frac{b}{2} \right) - M_{ext}}{\left(e + \frac{b}{2} \right)} = \frac{1807 \left(\frac{0.130}{2} \right) - 16.88}{\left(0.05018 + \frac{0.130}{2} \right)} = 873 \text{ kN} \quad \text{Eq 10.53}$$

If the axial compression resistance does not exceed $0.5 N_{cRd}$, the resistance may be calculated from Appendix A.2.4:

$$\therefore N_{\theta,Rd} = -4t f_{yd} e + \sqrt{(4t f_{yd} e)^2 + 8t f_{yd} (M_{pl,Rd} - M_{ext})} = 871 \text{ kN} \quad \text{Eq 10.54}$$

$$0.5 N_{pl,Rd} = 0.5 \frac{A f_y}{\gamma_{M1}} = 903 \text{ kN} \quad \text{Eq 10.55}$$

so N does not exceed $0.5 N_{pl,Rd}$,

Therefore with externally applied moment = 16.88 kN-m, max compression = 871 kN.

This is less than the compression resistance of 1107 kN for the pin-ended strut resisting the same applied bending moment of 16.88 kN-m because the design end-rotations, caused by the beam slopes, give a lower resistance than the pin-ended condition.

11 CONCLUSIONS

11.1 Summary of what has been achieved

11.1.1 Design philosophy

A design model has been developed for discontinuous square hollow section (SHS) steel columns with flexible end-connections. It uses the non-linear behaviour of the column arising from extensive plasticity. This has necessitated a thorough investigation of the behaviour of columns with zones of plasticity that extend beyond the zones of plasticity that occur in columns designed using current structural design codes such as BS 5950-1 and EN 1993-1-1.

The model allows beams to be designed as beams independently of the columns and the columns designed for end-rotations equal to the rotation of the beam. The design model assumes that the column is not required to resist externally applied moments to maintain static equilibrium, eg moments from the beams, so the resistance to axial loads for a given end-rotation is higher than allowed by normal codified design methods.

11.1.2 Column design model

The column design model uses the classic plastic cross-sectional resistance model about a rectangular axis together with a member model that is rigid-plastic with an initial imperfection. The initial imperfection is calibrated from whatever design code is specified so that at zero end-rotation, the column model gives the same resistance to axial compression as the code gives for a pin-ended strut. The design model has been demonstrated to be conservative so it is safe for use in the design of structures.

11.1.3 Design of a complete frame

Beams may be designed as simple or continuous, either entirely elastic or elastic in the spans and plastic at the interior supports. Appropriate design methods are given for the beams, connections and to ensure overall frame stability and compatibility of the frame sway deflections with the column design. A worked example including beam and column design is included.

11.1.4 Economy of structural material

The design method requires the beams to carry all the bending moments from the loads on the beams, leaving the column to resist axial load alone. Thus the reduction of resistance of the column below the pin-ended strut resistance is not as severe as in normal codified methods. Therefore this design method offers economy of material relative to current frame and column design methods in appropriate frames.

11.1.5 Economy of design effort

The beams are designed independently from the columns, either as simply supported beams or continuous beams on knife edge supports. Therefore the analysis is very simple. The column design model has simple “closed solutions” to calculate the resistance, so this also is simple.

11.2 Suggestions for further developments

Further work would be valuable in the following areas:

11.2.1 Circular hollow sections

Verifying that the model is applicable to circular hollow sections (CHS).

11.2.2 Rectangular hollow sections

Checking the application to rectangular (not square) hollow sections (RHS) and finding how to benefit from the greater inertia about one rectangular axis.

11.2.3 I-sections

Investigating the application to I-sections. It is expected that application to end-rotation about the minor axis will be similar to the behaviour of SHS sections, but with restrictions on the slenderness of the flange outstands to be defined. Rotation about the major axis forces shortening in one flange more than in the other, so the behaviour is likely to be similar to two SHS sections side-by-side. In single curvature bending about the major axis of the column, one flange can be expected to deflect out-of-plane much more than the other flange, resulting in significant twisting along the length of the member. This is likely to be a complicated investigation.

11.2.4 Avoiding disproportionate collapse in Class 2B and Class 3 buildings

As discussed in Section 9.8.2, the verification strategy of “notional removal” appears ideally suited to demonstrating the robustness of frames with discontinuous columns. Reference to older design documents from the period after Ronan Point would show the methods used by designers to employ the notional removal philosophy.

REFERENCES

- Access-steel SN005a 2005 Determination of moments on columns in simple construction,
SN005a-EN-EU; 2005
Access-steel website: www.access-steel.com
- AISC 2005 ANSI/AISC 360-05
Specification for Structural Steel Buildings
American Institute of Steel Construction, 2005
- AISC 2005a ANSI/AISC 341-05 + ANSI/AISC 341s1-05
Seismic Provisions for Structural Steel Buildings
Including Supplement No.1
American Institute of Steel Construction, 2005
- ASCE 1971 Plastic Design in Steel; A Guide and Commentary
ASCE - Manuals and Reports on Engineering Practice - No. 41
American Society of Civil Engineers, 1971
- BCSA 2002 National Structural Steelwork Specification for Building Construction
(commonly known as the NSSS)
The British Constructional Steelwork Association
Fourth Edition, 2002
- BSI 1969 BS 449-2:1969
Specification for the use of structural steel in building,
Part 2, Metric units
British Standards Institution 1969
- BSI 2000a BS 5950-1:2000
Structural use of steelwork in building -
Part 1: Code of practice for design - Rolled and welded sections
British Standards Institution 2000

- BSI 2000b BS 5400-3:2000
Steel, concrete and composite bridges
Part 3: Code of practice for design of steel bridges
British Standards Institution 2000
- BSI 2001 BS 5950-2:2001
Structural use of steelwork in building -
Part 2: Specification for material, fabrication and erection
- Rolled and welded sections
British Standards Institution 2001
- BSI 2002a BS EN 1990:2002
Eurocode 0, Basis of structural design.
British Standards Institution 2002
- BSI 2002b BS EN 1991-1-1:2002
Eurocode 1, Actions on structures. General actions.
Densities, self-weight, imposed loads for buildings.
British Standards Institution 2002
- BSI 2005a BS EN 1993-1-1:2005
Eurocode 3: Design of steel structures - general rules and rules for
buildings
British Standards Institution 2005
- BSI 2005b BS EN 1993-1-8:2005
Eurocode 3: Design of steel structures: Part 1.8: design of joints
British Standards Institution 2005
- BSI 2006a BS EN 10210-1:2006
Hot finished structural hollow sections of non-alloy and fine grain
steels
Part 1: Technical delivery conditions

- BSI 2006b BS EN 10210-2:2006
Hot finished structural hollow sections of non-alloy and fine grain steels
Part 2: Tolerances, dimensions and sectional properties
- BSI 2008 BS EN 1090-2:2008
Execution of steel structures and aluminium structures.
Part 2: Technical requirements for the execution of steel structures.
- Calladine 1969 Calladine, C.R.,
Engineering Plasticity,
Pergamon Press 1969
- Carr 1993 Carr, J.F.,
A simplified approach to the design of semi-rigidly connected columns
in multi-storey non-sway steel framed buildings
M. Phil Thesis, University of Sheffield, 1993
- CEN 2002a EN 1990:2002
Eurocode 0, Basis of structural design.
CEN (European Committee for Standardization), 2002
- CEN 2002b EN 1991-1-1:2002
Eurocode 1, Actions on structures. General actions.
Densities, self-weight, imposed loads for buildings.
CEN (European Committee for Standardization), 2002
- CEN 2005a EN 1993-1-1:2005
Eurocode 3: design of steel structures - Part 1.1: General rules and
rules for buildings
CEN (European Committee for Standardization), 2005
- CEN 2005b BS EN 1993-1-8:2005
Eurocode 3: Design of steel structure -: Part 1.8: Design of joints
CEN (European Committee for Standardization), 2005

- CEN 2006a EN 10210-1:2006
Hot finished structural hollow sections of non-alloy and fine grain steels
Part 1: Technical delivery conditions
- CEN 2006b EN 10210-2:2006
Hot finished structural hollow sections of non-alloy and fine grain steels
Part 2: Tolerances, dimensions and sectional properties
- CEN 2008 EN 1090-2:2008
Execution of steel structures and aluminium structures.
Part 2: Technical requirements for the execution of steel structures.
- Davies 1966 Frame instability and strain hardening in plastic theory
Journal of the Structural Division,
Proceedings of the American Society of Civil Engineers, June 1966
- Dowrick 1977 Dowrick, D J,
Earthquake Resistant Design,
John Wiley & Sons, 1977
- ECCS 1976 European Convention for Constructional Steelwork
Second International Colloquium on Stability
Introductory Report
(includes the ECCS Manual on Stability of Steel Structures)
Tokyo, September 1976
Liege, April 1977
Washington, May 1977
- ECCS 2006 Boissonnade N., Greiner R., Jaspart J.P. and Lindner J.
Rules for member Stability in EN 1993-1-1, Background
documentation and design guidelines
ECCS Technical Committee 8 – Stability;
ECCS No 119, 2006

- Fewster et al 1993 Fewster M., Giradier V., Owens G.,
Economic Design and the Importance of Standardised Connections,
New Steel Construction, February 1993
- Galambos 1998 Galambos T. V.
Guide to Stability Design Criteria for Metal Structures, fifth edition,
John Wiley & Sons, 1998
- Gent 1966 Gent A.R.,
Elastic-plastic column stability and the design of no-sway frames,
Proceedings of the Institution of Civil Engineers, 34, June 1966 p129-
152
- Gent & Milner 1968 Gent, A.R. and Milner, H.R.,
The ultimate load capacity of elastically restrained H-columns under
biaxial bending,
Proceedings of the Institution of Civil Engineers, 43, December 1968
p685-704
- Gibbons 1990 Gibbons, C
The strength of biaxially loaded beam-columns in flexibly connected
steel frames,
Ph.D. Thesis, Department of Civil and Structural Engineering,
University of Sheffield, 1990
- Gibbons et al 1993 Gibbons, C., Nethercot, D.A., Kirby, P.A., and Wang, Y.C.,
An appraisal of partially restrained columns behaviour in non-sway
steel frames,
Proceedings of the Institution of Civil Engineers,
Structures and Buildings, 99, Feb 1993, p15-28
- Gibbons et al 1993a Gibbons, C., Kirby, P.A., and Nethercot, D.A.,
Experimental behaviour of partially restrained steel columns,
Proceedings of the Institution of Civil Engineers,
Structures and Buildings, 99, Feb 1993, p29-42

- Greiner et al 1998 Greiner R., Ofner R. and Salzgeber G.,
Review of rules for members in bending and axial compression,
Report 3, Flexural buckling of beam-columns,
ECCS Validation Group, Working Item 8
Institut für Stahlbau, Holzbau und Flachentragwerke,
Technische Universität Graz,
- Horne 1960 Horne, M.R.,
Instability and the plastic theory of structures
Transactions of the Engineering Institute of Canada, Vol 4, No.2, 1960
- Horne 1963 Horne, M.R.,
Elastic-plastic failure loads of plane frames
Proceedings of the Royal Society, Vol A, Part 274, pp 343-64, 1963
- King 2006 King, C.M.,
Column design for axial compression and end rotation
Report to the University of Sheffield and the SCI
SCI RT 1111, 2006
- King 2007 King, C.M.,
Design of discontinuous columns for axial load and end-rotations in
rigid jointed braced frames
SSRC, 2007 Annual Stability Conference, April 18 – 21,
New Orleans, Louisiana
- Kirby et al 1992 Kirby, P.A., Bitar, S. and Gibbons, C.,
Design of columns in non-sway, semi-rigidly connected frames,
Proceedings of First World Conference on Constructional Steelwork
Design, ed. Bowlins, P., J., et al.,
Elsevier Applied Science, London, 1992, pp 54-63.
- ODPM 2004 Approved Document A – Structure
The Building Regulations 2000, 2004 edition,
Office of the Deputy Prime Minister

- SCI 1997 Lawson, R.M., Mullett, D.L., Rackham, J.W.,
P175, Design of asymmetric Slimfor beams using deep composite
decking.
The Steel Construction Institute, 1997
- SCI 2001 P 202, Steelwork Design Guide to BS 5950-1:2000, Volume 1
Section Properties and Member Capacities
(commonly referred to as the “Blue Book”)
The Steel Construction Institute, 2001
- SCI 2004 Brown, D.G., King, C.M., Rackham, J.W., Way, A.,
P334, Design of multi-storey braced frames.
The Steel Construction Institute, 2004
- SCI 2005a AD 281: The use of discontinuous columns in simple construction
New Steel Construction, February 2005
- SCI 2005b AD 283: The use of discontinuous columns in simple construction
(Part 2)
New Steel Construction, March 2005
- SCI 2005c AD 285: Floor systems for simple construction using discontinuous
columns and continuous beams.
New Steel Construction, April 2005
- SCI 2005d AD 288: Discontinuous columns in simple construction: Beam-column
connection.
New Steel Construction, July/Aug 2005
- SCI 2005e AD 292: The use of discontinuous columns and shallow deck
composite slabs on floor beams.
New Steel Construction, Oct 2005

SCI 2009 Brown, D.G., Iles, D.C, Yandzio, E.,
Steel Building Design: Medium Rise Braced Frames
The Steel Construction Institute, 2009

Wood 1973 Wood, R.H.,
A new approach to column design
Building Research Establishment Report
Department of the Environment, HMSO, 1974

APPENDIX A SHS SECTION PROPERTIES

A.1 Introduction

A.1.1 General

There are two basic cases of resistance to axial and bending. One is where the axial compression is sufficiently small to be resisted only by the “webs”. In a square section, this occurs when the axial compression is not greater than $0.5 N_{pl}$. The other is where the area of the “webs” alone is not sufficient to resist the axial compression. In a square section, this occurs when the axial compression is greater than $0.5 N_{pl}$.

The calculations are made using an “ideal square” section. This is a perfectly square centreline model, to avoid the complexities of rounded corners with varying thickness. The finite slice model used an equivalent thickness and distance from mid-plane to mid-plane of the walls calculated to give the same area and inertia (second moment of area) as the real SHS section. In the Abaqus model, the distance from mid-plane to mid-plane of the walls is the same as in the SHS being analysed. It used the thickness of the SHS being analysed because the local stability of the walls is automatically included in the Abaqus model. Therefore the comparison of resistance of the Abaqus model with actual SHS sections, as in the analysis of the laboratory tests, requires that the Abaqus prediction is reduced according to the ratio of cross-sectional area of the SHS to the Abaqus model.

The formulae are written to be compatible with EN 1993-1-1 and are based on N_{pl} and M_{pl} to avoid the difference between an “ideal square” section and the actual SHS section with rounded corners.

A.1.2 Partial safety factors for resistance

The calculation of the resistance uses the strut buckling resistance to establish the design value of initial imperfection and uses plastic cross-sectional resistance calculations to find the resistance with applied end-rotations. The calculation of resistance could be done either by using characteristic values of resistance and then dividing the characteristic value by the appropriate partial safety factor for resistance or it could be done by using the design values of both strut resistance and cross-sectional resistance.

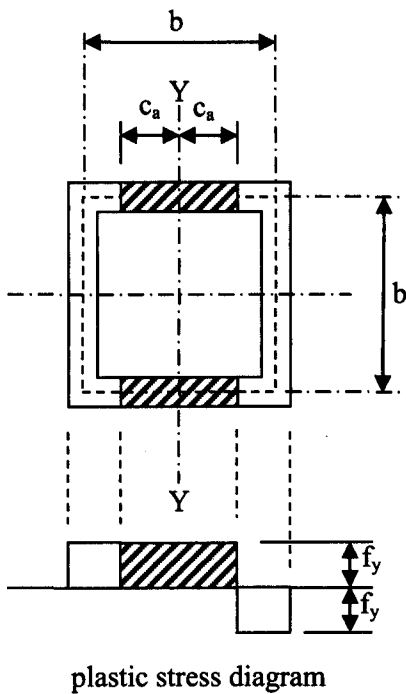
Most designers will not be accustomed to working with characteristic values, so this report recommends the use of design values. In EN 1993-1-1, different partial safety factors are

used for cross-sectional resistance (γ_{M0}) and for buckling (γ_{M1}). In many countries, including the UK, the National Annex for EN 1993-1-1 will use the same numerical value for both γ_{M0} and for γ_{M1} so there is no difference in the partial safety factor used. In countries using a higher value of γ_{M1} than for γ_{M0} , the design value of initial imperfection will be higher, so even though γ_{M0} is used in the cross-sectional resistance calculations, the resistance will be correctly calculated.

A.2 Axial not exceeding 50% squash load

A.2.1 Plastic stress blocks

An idealised SHS section is shown in Figure A1. It is subject to axial compression and bending about the YY axis. The area required to resist axial compression at yield stress is denoted by the length of wall within the shaded area which extends to the distance “ c_a ” either side of the YY axis.



= area resisting axial compression $N_{\theta,Rd}$

Figure A.1 Plastic stress distribution, low axial load

A.2.2 Derivation of depth of block resisting axial, dimension “c_a”

In an ideal square cross-section, the plastic moment of resistance with no axial compression is given by:

$$M_{pl,Rd} = \frac{2 \left[(b t f_y) \frac{b}{2} \right] + 4 \left[\left(\frac{b}{2} t f_y \right) \frac{b}{4} \right]}{\gamma_{M0}} = \frac{b^2 t f_y + \frac{b^2 t f_y}{2}}{\gamma_{M0}} = \frac{3 b^2 t f_y}{2 \gamma_{M0}} \quad \text{Eq A 1}$$

For compression resistance not exceeding 50% N_{pl}, ie N_{θ,Rd} ≤ 2htf_y/ γ_{M0}, the axial compression resisted is

$$N_{\theta,Rd} = 4t c_a f_y / \gamma_{M0} \quad \text{Eq A 2}$$

therefore the plastic moment of resistance of the section is reduced by the plastic moment of resistance of the wall lengths “c_a” either side of the YY axis

Therefore the reduced plastic moment of resistance is

$$M_{N,Rd} = \frac{3 b^2 t f_y}{2 \gamma_{M0}} - \frac{4 c_a t f_y}{\gamma_{M0}} \left(\frac{c_a}{2} \right) = \left(\frac{3}{2} b^2 - 2 c_a^2 \right) \frac{t f_y}{\gamma_{M0}} \quad \text{Eq A 3}$$

If there is no externally applied bending moment such as from wind

$$M_{N,Rd} = N_{\theta,Rd} e \quad \text{Eq A 4}$$

then

$$\left(\frac{3}{2} b^2 - 2 c_a^2 \right) \frac{t f_y}{\gamma_{M0}} = \frac{4 c t f_y}{\gamma_{M0}} e \quad \text{Eq A 5}$$

$$\therefore \frac{3}{2} b^2 - 2 c_a^2 = 4 c_a e \quad \text{Eq A 6}$$

$$\therefore 3 b^2 - 4 c_a^2 = 8 c_a e \quad \text{Eq A 7}$$

$$\therefore 4 c_a^2 + 8 e c_a - 3 b^2 = 0 \quad \text{Eq A 8}$$

$$\text{Then from } ax^2 + bx + c = 0 \Rightarrow x = \frac{-b \pm \sqrt{b^2 - 4ac}}{2a}$$

$$4 c_a^2 + 8 e c_a - 3 b^2 = 0 \quad \text{Eq A 9}$$

$$\Rightarrow c = \frac{-8e \pm \sqrt{(8e)^2 - 4(4)(-3b^2)}}{2(4)} = \frac{-8e \pm \sqrt{64e^2 + 48b^2}}{8} \quad \text{Eq A 10}$$

$$\therefore c_a = -e \pm \sqrt{e^2 + \frac{3}{4}b^2} = \pm e \sqrt{1 + \frac{3}{4} \frac{b^2}{e^2}} - e = e \left(\pm \sqrt{1 + \frac{3}{4} \left(\frac{b}{e} \right)^2} - 1 \right) \quad \text{Eq A 11}$$

A.2.3 Derivation of “e” from failure load N_θ

To calculate e so that the design model gives the correct failure load N_θ as calculated by Abaqus:

$$N_\theta e = M_N - M_{\text{ext}} \quad \text{Eq A 12}$$

where M_{ext} is an externally applied moment on column, for example from wind load,

$$\text{Therefore } e = (M_N - M_{\text{ext}}) / N_\theta \quad \text{Eq A 13}$$

$$\text{where } M_N = M_{\text{pl}} - N_\theta \left(\frac{c_a}{2} \right) \quad \text{Eq A 14}$$

$$\text{and } N_\theta = 4t c_a f_y \Rightarrow c_a = \frac{N_\theta}{4t f_y} \quad \text{Eq A 15}$$

A.2.4 Derivation of failure load $N_{\theta, \text{Rd}}$ from “e”

To calculate $N_{\theta, \text{Rd}}$ from “e”:

$$N_{\theta, \text{Rd}} e = M_{N, \text{Rd}} - M_{\text{ext}} \quad \text{Eq A 16}$$

where M_{ext} is an externally applied moment on column, for example from wind load,

$$\text{For } N \leq 0.5N_{\text{pl}}, N_{\theta, \text{Rd}} = 4t c_a f_y / \gamma_{M0} \quad \text{Eq A 17}$$

$$\text{and } M_{N, \text{Rd}} = M_{\text{pl}, \text{Rd}} - N_{\theta, \text{Rd}} \left(\frac{c_a}{2} \right) \quad \text{Eq A 18}$$

$$\therefore N_{\theta, \text{Rd}} e = M_{\text{pl}, \text{Rd}} - M_{\text{ext}} - N_{\theta, \text{Rd}} \left(\frac{c_a}{2} \right) \quad \text{Eq A 19}$$

$$\therefore N_{\theta, \text{Rd}} e + N_{\theta, \text{Rd}} \left(\frac{c_a}{2} \right) = M_{\text{pl}, \text{Rd}} - M_{\text{ext}} \quad \text{Eq A 20}$$

$$N_{\theta, \text{Rd}} = \frac{4c_a t f_y}{\gamma_{M0}} \Rightarrow c_a = \frac{N_{\theta, \text{Rd}}}{4t f_y} \quad \text{Eq A 21}$$

$$\therefore N_{\theta,Rd} e + \left(\frac{N_{\theta,Rd}}{2} \right) \left(\frac{N_{\theta,Rd}}{4t f_{yd}} \right) = M_{pl} - M_{ext} \quad \text{Eq A 22}$$

$$\therefore \frac{N_{\theta,Rd}^2}{8t f_{yd}} + N_{\theta,Rd} e = M_{pl,Rd} - M_{ext} \quad \text{Eq A 23}$$

$$\therefore N_{\theta,Rd}^2 + 8t f_{yd} N_{\theta,Rd} e - 8t f_{yd} (M_{pl,Rd} - M_{ext}) = 0 \quad \text{Eq A 24}$$

$$\therefore N_{\theta,Rd} = \frac{-8t f_{yd} e \pm \sqrt{(8t f_{yd} e)^2 + 4 \times 1 \times 8t f_{yd} (M_{pl,Rd} - M_{ext})}}{2} \quad \text{Eq A 25}$$

in which “+” gives the relevant root

$$\therefore N_{\theta,Rd} = -4t f_{yd} e + \sqrt{(4t f_{yd} e)^2 + 8t f_{yd} (M_{pl,Rd} - M_{ext})} \quad \text{Eq A 26}$$

A.3 Axial compression exceeding $0.5 N_{pl}$.

A.3.1 Plastic stress blocks

An idealised SHS section is shown in Figure A2. It is subject to axial compression and bending about the YY axis. The area required to resist axial compression at yield stress is denoted by the length of wall within the shaded area which extends beyond the “webs”. This idealisation uses a “centre-line” model, so the area of the flange is taken to extend to the distance “ c_b ” either side of the XX axis.

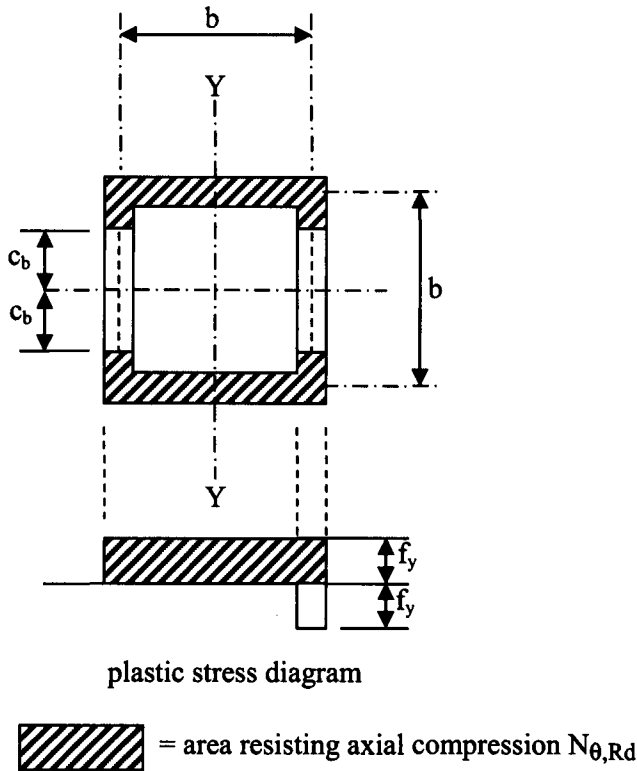


Figure A.2 Plastic stress distribution, high axial load

A.3.2 Derivation of depth of block resisting bending, dimension “ c_b ”, assuming no externally applied moments

In an ideal square cross-section, for axial compression exceeding 50% $N_{pl,Rd}$,

The axial compression resisted is

$$N_{\theta,Rd} = \frac{4btf_y - 4c_b tf_y}{\gamma_{M0}} = 4(b - c_b)tf_{yd} \quad \text{Eq A 27}$$

The reduced plastic moment of resistance is

$$M_{N,Rd} = \frac{4c_b tf_y \left(\frac{b}{2}\right)}{\gamma_{M0}} = 2c_b btf_{yd} \quad \text{Eq A 28}$$

If there is no externally applied bending moment such as from wind

$$M_{N,Rd} = N_{\theta,Rd}e, \text{ then} \quad \text{Eq A 29}$$

$$2c_b btf_{yd} = 4(b - c_b)tf_{yd}e \quad \text{Eq A 30}$$

$$\therefore 2c_b b = 4(b - c_b)e \quad \text{Eq A 31}$$

$$\therefore 2c_b b = 4be - 4c_b e \quad \text{Eq A 32}$$

$$\therefore 2c_b b + 4c_b e = 4be \quad \text{Eq A 33}$$

$$\therefore c_b = \frac{4be}{2b + 4e} = \frac{2be}{b + 2e} \quad \text{Eq A 34}$$

A.3.3 Derivation of “e” from failure load N assuming no externally applied moments

To calculate e so that the design model gives the correct failure load N_θ as calculated by Abaqus:

$$M_N = N_\theta e, \quad \text{Eq A 35}$$

where $M_{N,Rd}$ is the plastic moment of resistance of the plastic stress block NOT resisting the axial force,

$$\text{Therefore } M_N = (N_{pl} - N_\theta)(b/2) \quad \text{Eq A 36}$$

$$\text{Therefore } e = [(N_{pl} - N_\theta)/N_\theta](b/2) \quad \text{Eq A 37}$$

A.3.4 Derivation of failure load $N_{\theta,Rd}$ from “e”

To calculate $N_{\theta,Rd}$ from “e”:

For $N \geq 0.5N_{pl}$, the moment resistance is

$$M_{N,Rd} = \frac{(N_{pl,Rd} - N_{\theta,Rd})b}{2} \quad \text{Eq A 38}$$

$$\therefore N_{\theta,Rd} e + M_{ext} = \frac{(N_{pl,Rd} - N_{\theta,Rd})b}{2} \quad \text{Eq A 39}$$

$$\therefore N_{\theta,Rd} e + M_{ext} = \frac{(N_{pl,Rd} - N_{\theta,Rd})b}{2} = \frac{N_{pl,Rd} b}{2} - \frac{N_{\theta,Rd} b}{2} \quad \text{Eq A 40}$$

$$\therefore N_{\theta,Rd} e + \frac{N_{\theta,Rd} b}{2} = \frac{N_{pl,Rd} b}{2} - M_{ext} \quad \text{Eq A 41}$$

$$\therefore N_{\theta,Rd} \left(e + \frac{b}{2} \right) = N_{pl,Rd} \left(\frac{b}{2} \right) - M_{ext} \quad \text{Eq A 42}$$

$$\therefore N_{\theta, Rd} = \frac{N_{pl, Rd} \left(\frac{b}{2} \right) - M_{ext}}{\left(e + \frac{b}{2} \right)}$$

Eq A 43

APPENDIX B BS 5950 CALCULATIONS

B.1 Buckling resistance of Square Hollow Sections

This Appendix gives the calculations for the axial compression resistance according to BS 5950-1:2000 [BSI 2000] and conventional analysis.

BS 5950-1:2000 clause 4.8.3.3.3, More exact method for CHS, RHS or box sections with equal flanges gives:

For square hollow sections (so no lateral-torsional buckling) with moments about one axis only:

$$\frac{F_c}{P_{cx}} + \frac{m_x M_x}{M_{cx}} \left(1 + 0.5 \frac{F_c}{P_{cx}} \right) \leq 1 \quad \text{Eq B. 1}$$

$$\frac{F_c}{P_{cx}} + 0.5 \frac{m_{LT} M_{LT}}{M_{cx}} \leq 1 \quad \text{Eq B. 2}$$

By inspection, the first equation is seen to be critical

$$\frac{F_c}{P_{cx}} + \frac{m_x M_x}{M_{cx}} \left(1 + 0.5 \frac{F_c}{P_{cx}} \right) \leq 1 \quad \text{Eq B. 3}$$

$$\therefore \frac{F_c}{P_{cx}} + 1 \times \frac{m_x M_x}{M_{cx}} + 0.5 \frac{F_c}{P_{cx}} \times \frac{m_x M_x}{M_{cx}} \leq 1 \quad \text{Eq B. 4}$$

$$\therefore \frac{F_c}{P_{cx}} \left(1 + 0.5 \frac{m_x M_x}{M_{cx}} \right) + \frac{m_x M_x}{M_{cx}} \leq 1 \quad \text{Eq B. 5}$$

$$\therefore \frac{F_c}{P_{cx}} \left(1 + 0.5 \frac{m_x M_x}{M_{cx}} \right) \leq 1 - \frac{m_x M_x}{M_{cx}} \quad \text{Eq B. 6}$$

$$\therefore F_c \leq \frac{\left(1 - \frac{m_x M_x}{M_{cx}} \right)}{\left(1 + 0.5 \frac{m_x M_x}{M_{cx}} \right)} P_{cx} \quad \text{Eq B. 7}$$

Hot finished 140×140×10 SHS in S355

$S_x = S_y = 246 \text{ cm}^3$, so $M_p = 355 \times 246 \times 10^{-3} = 87.3 \text{ kN/m}$

B.2 Single curvature

B.2.1 3 metre column height

General

$P_{cx} = 1550$ kN from Blue Book

$$M = \frac{2EI}{L} \theta = \frac{2 \times 205000 \times 14.2 \times 10^6}{3000} \theta \times 10^{-6} = 1941\theta \text{ kN-m} \quad \text{Eq B. 8}$$

$m = 1.0$ for single curvature

40 milli-radians end slope

End slope = 0.040 radians at the top and -0.040 radians at the bottom for single curvature.

$$M = \frac{2EI}{L} \theta = 1941\theta = 1941 \times 0.040 = 77.6 \text{ kN-m} \quad \text{Eq B. 9}$$

$$\frac{m_x M_x}{M_{cx}} = \frac{1.0 \times 77.6}{87.3} = 0.889 \quad \text{Eq B. 10}$$

$$\therefore F_c \leq \frac{\left(1 - \frac{m_x M_x}{M_{cx}}\right)}{\left(1 + 0.5 \frac{m_x M_x}{M_{cx}}\right)} P_{cx} \quad \text{Eq B. 11}$$

$$= \frac{1 - 0.889}{1 + 0.5 \times 0.889} 1550 = \frac{0.111}{1.445} 1550 = 119 \text{ kN}$$

30 milli-radians end slope

End slope = 0.030 radians at the top and -0.030 radians at the bottom for single curvature.

$$M = \frac{2EI}{L} \theta = 1941\theta = 1941 \times 0.030 = 58.2 \text{ kN-m} \quad \text{Eq B. 12}$$

$$\frac{m_x M_x}{M_{cx}} = \frac{1.0 \times 58.2}{87.3} = 0.667 \quad \text{Eq B. 13}$$

$$\therefore F_c \leq \frac{\left(1 - \frac{m_x M_x}{M_{cx}}\right)}{\left(1 + 0.5 \frac{m_x M_x}{M_{cx}}\right)} P_{cx} \quad \text{Eq B. 14}$$

$$= \frac{1 - 0.667}{1 + 0.5 \times 0.667} 1550 = \frac{0.333}{1.334} 1550 = 387 \text{ kN}$$

20 milli-radians end slope

End slope = 0.020 radians at the top and -0.020 radians at the bottom for single curvature.

$$M = \frac{2EI}{L} \theta = 1941\theta = 1941 \times 0.020 = 38.8 \text{ kN-m} \quad \text{Eq B. 15}$$

$$\frac{m_x M_x}{M_{cx}} = \frac{1.0 \times 38.8}{87.3} = 0.444 \quad \text{Eq B. 16}$$

$$\therefore F_c \leq \frac{\left(1 - \frac{m_x M_x}{M_{cx}}\right)}{\left(1 + 0.5 \frac{m_x M_x}{M_{cx}}\right)} P_{cx} \quad \text{Eq B. 17}$$

$$= \frac{1 - 0.444}{1 + 0.5 \times 0.444} 1550 = \frac{0.556}{1.222} 1550 = 705 \text{ kN}$$

End slope = 0.010 radians at the top and -0.010 radians at the bottom for single curvature.

$$M = \frac{2EI}{L} \theta = 1941\theta = 1941 \times 0.010 = 19.4 \text{ kN-m} \quad \text{Eq B. 18}$$

$$\frac{m_x M_x}{M_{cx}} = \frac{1.0 \times 19.4}{87.3} = 0.222 \quad \text{Eq B. 19}$$

$$\therefore F_c \leq \frac{\left(1 - \frac{m_x M_x}{M_{cx}}\right)}{\left(1 + 0.5 \frac{m_x M_x}{M_{cx}}\right)} P_{cx} \quad \text{Eq B. 20}$$

$$= \frac{1 - 0.222}{1 + 0.5 \times 0.222} 1550 = \frac{0.778}{1.111} 1550 = 1085 \text{ kN}$$

APPENDIX C FINITE ELEMENT MODEL DETAILS

C.1 Introduction

This Appendix contains details of the finite element models numbering systems.

C.2 Full model

The key nodes are shown in Figure C.1 and Figure C.2. The wall node numbering scheme is shown in Figure C.4, Figure C.5, Figure C.6 and Figure C.7. The nodes used to predict the inclinometer output are shown in Figure C.8. The input lines for the end constraints and rigid bodies are shown Table C.1.

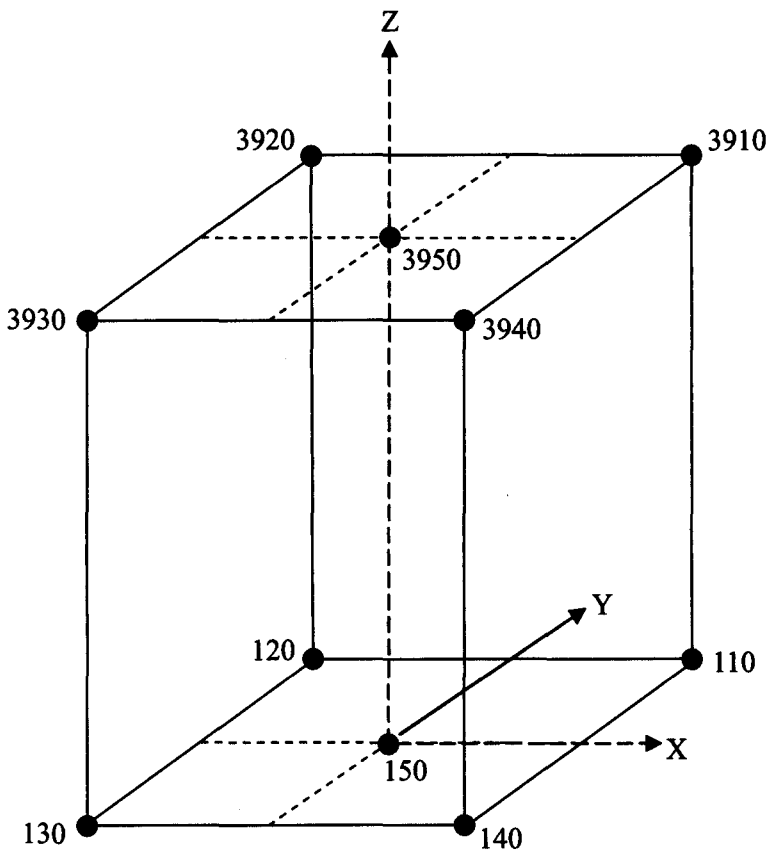
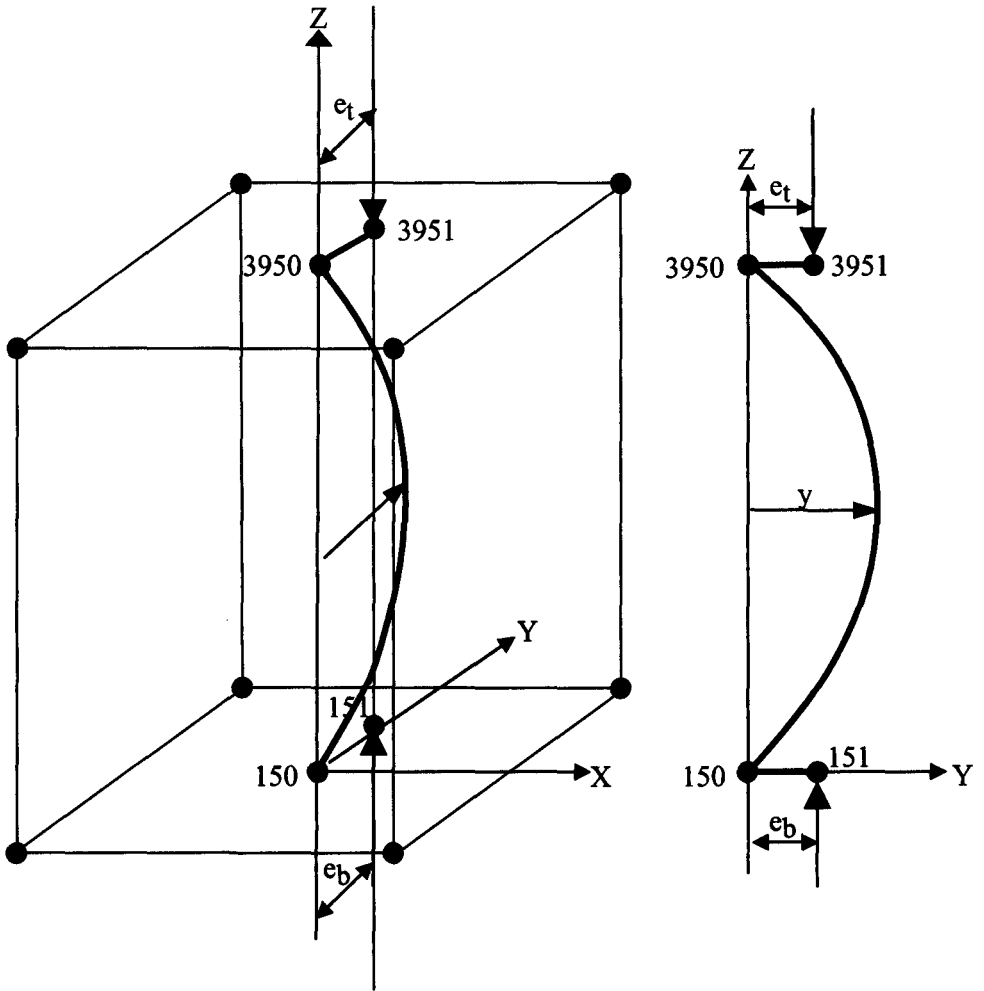


Figure C.1 Node numbering of corner nodes of SHS



Imperfections and nodes to apply eccentric load

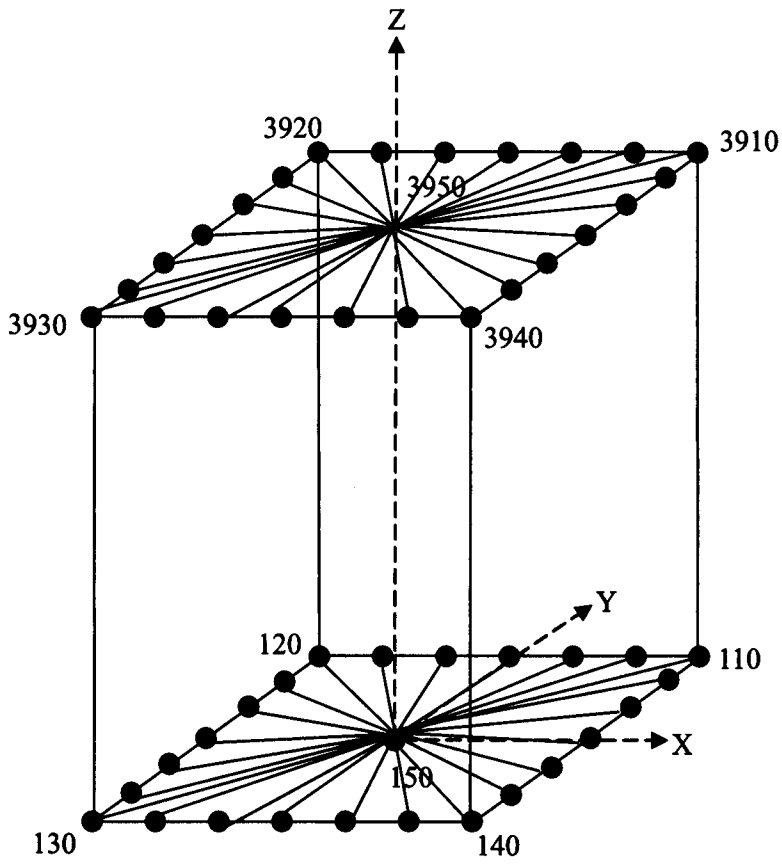


Figure C.3 Node numbering of rigid bodies at ends

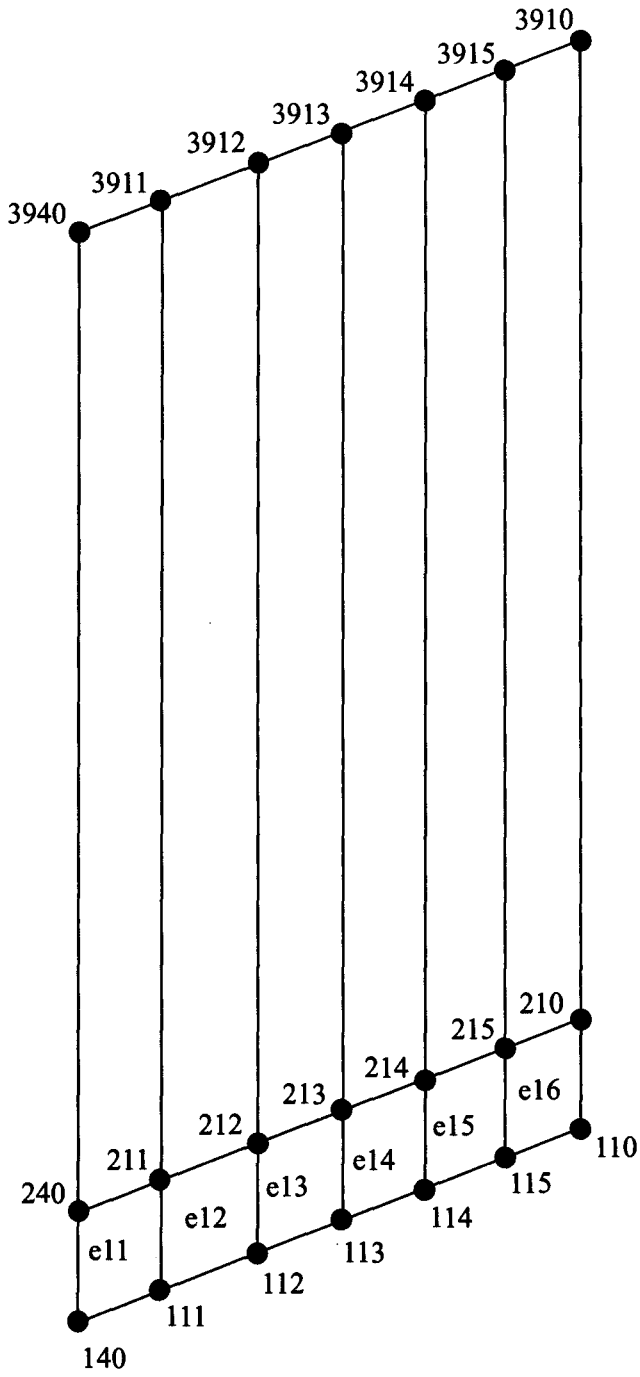


Figure C.4 Wall 1, node and element numbering

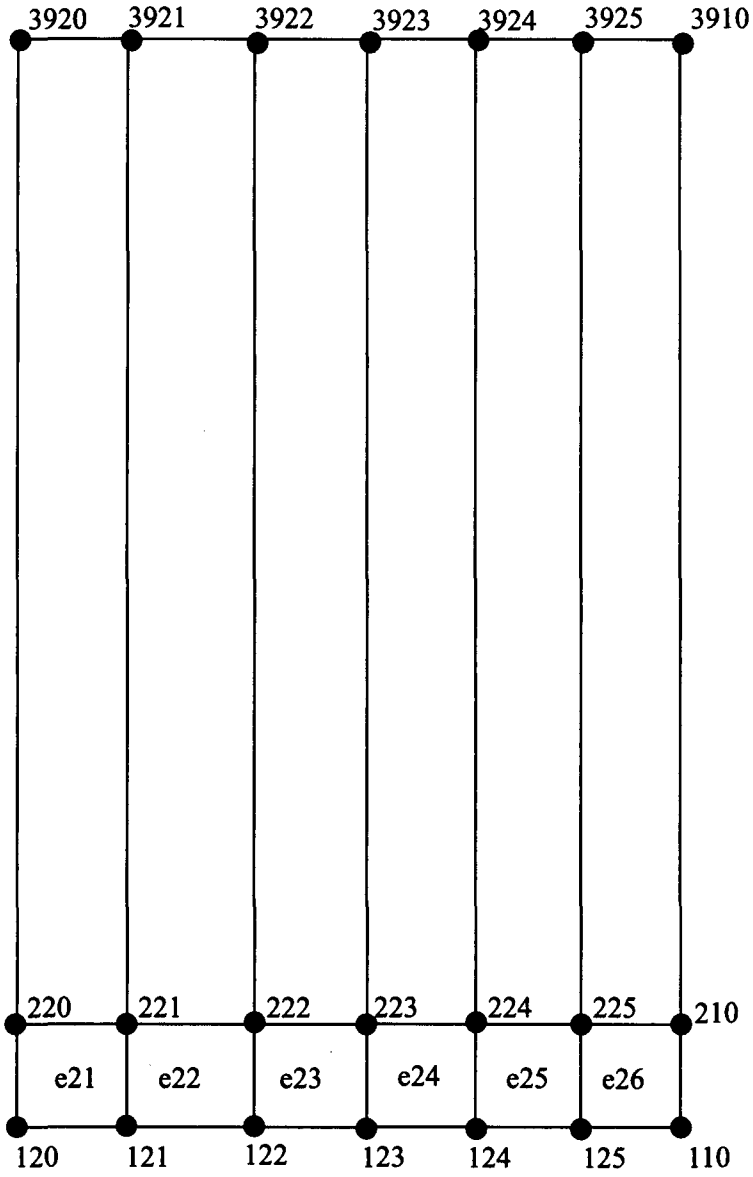


Figure C.5 Wall 2, node and element numbering

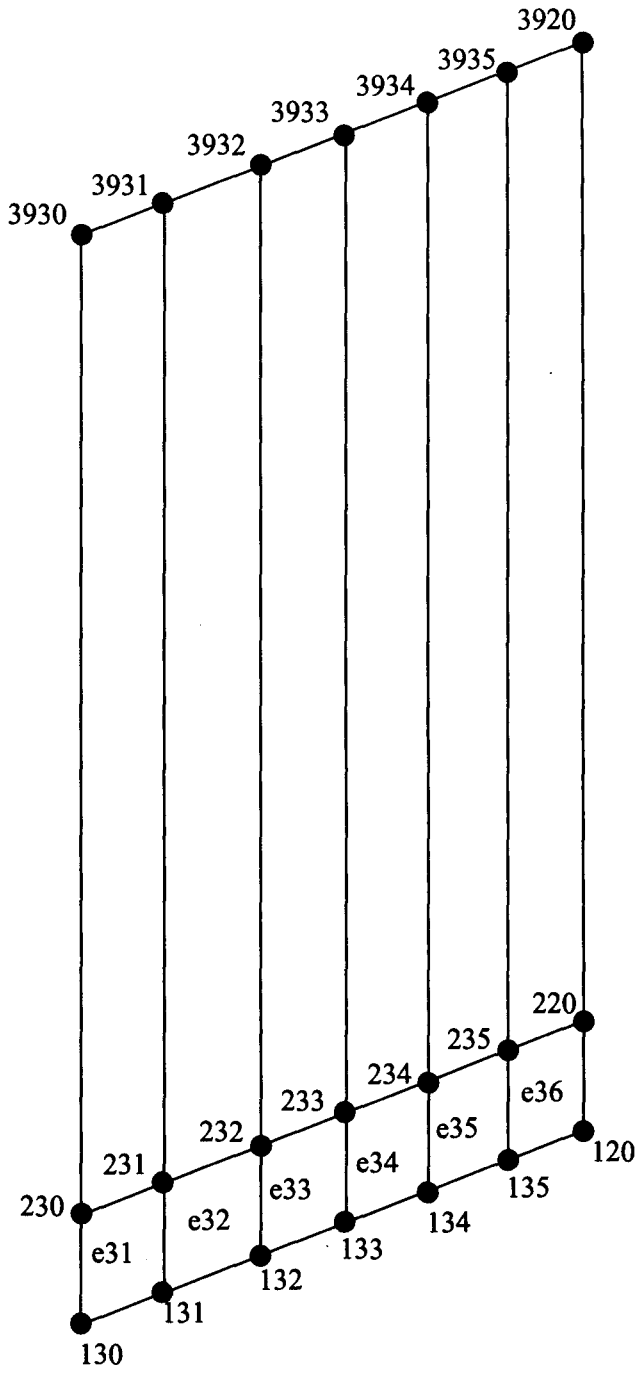


Figure C.6 Wall 3, node and element numbering

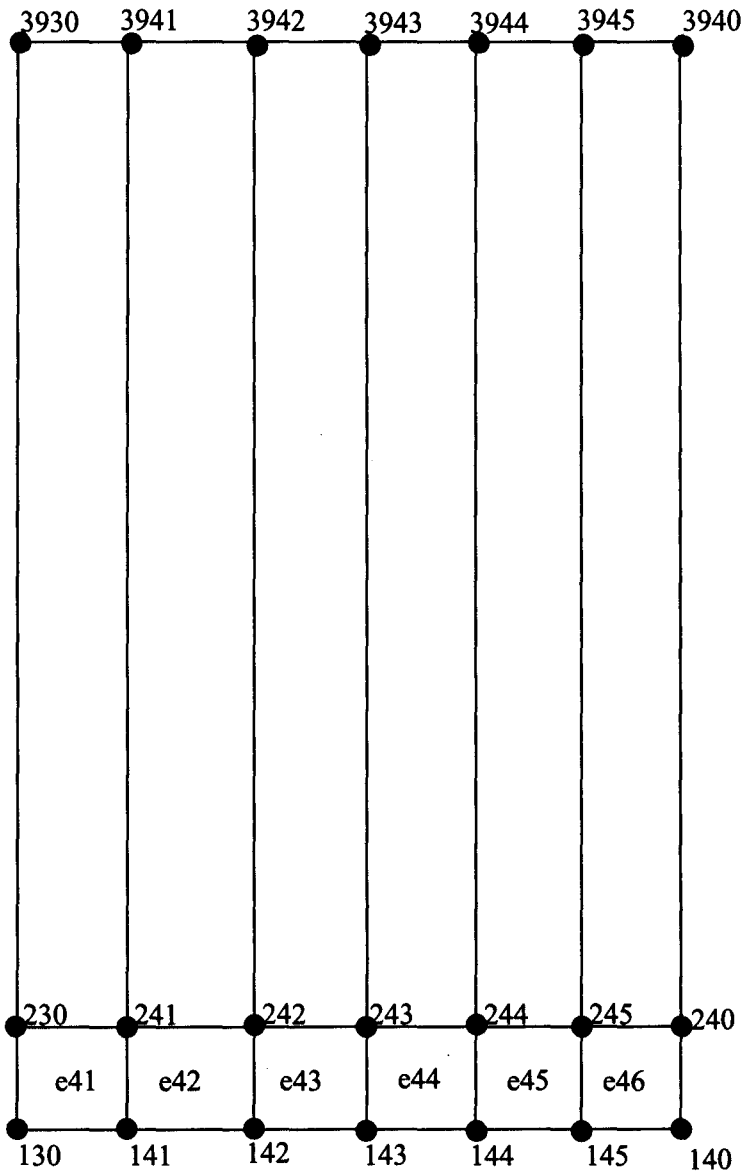


Figure C.7 Wall 4, node and element numbering

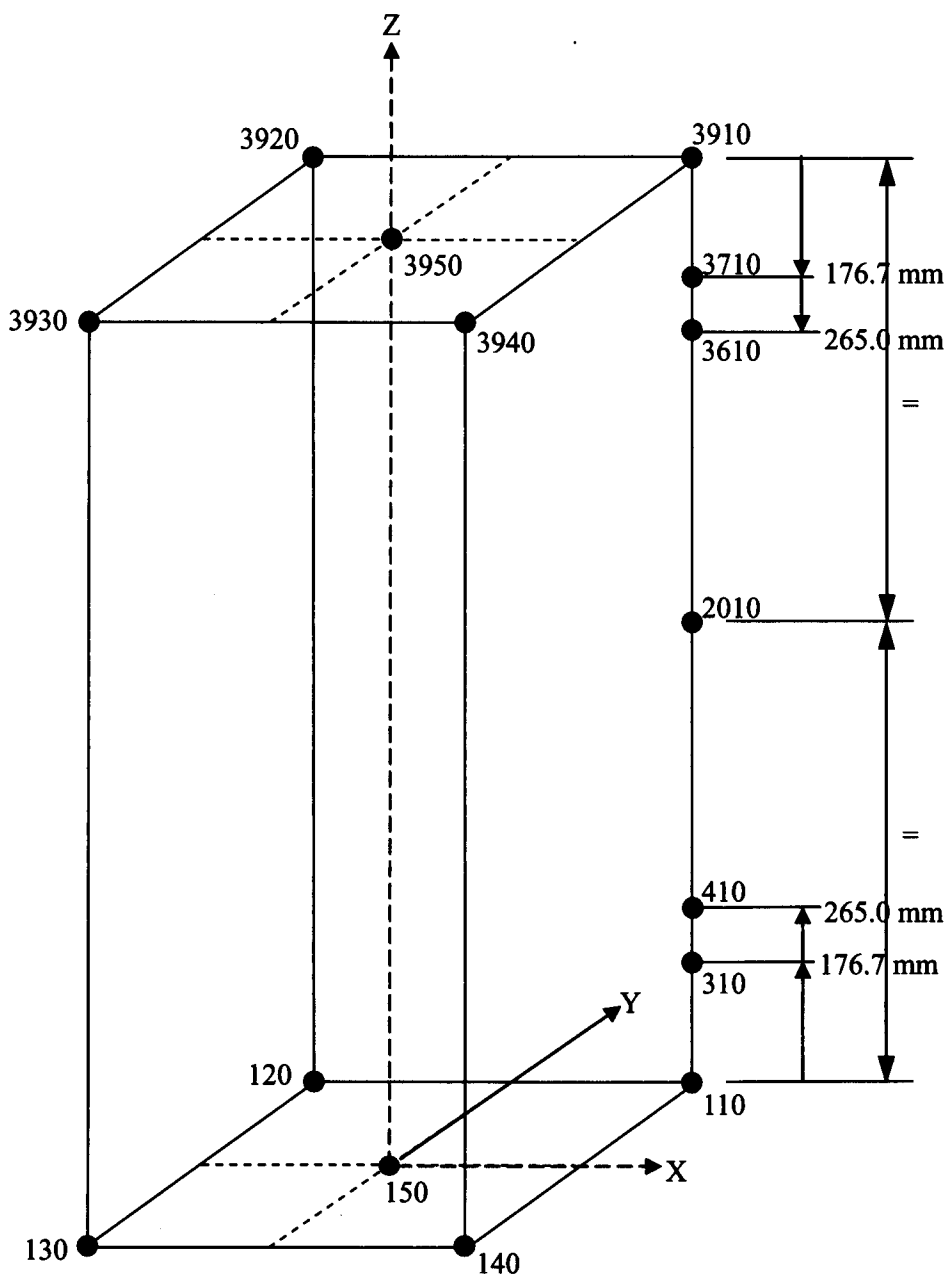


Figure C.8 Node numbering at mid-height and inclinometers


```

3950
*NSET, NSET=BOTTOMREFNODE
150
**
*NSET, NSET=TOPNODESPLUS
3910, 3911, 3912, 3913, 3914, 3915,
3920, 3921, 3922, 3923, 3924, 3925,
3930, 3931, 3932, 3933, 3934, 3935,
3940, 3941, 3942, 3943, 3944, 3945, 3950,
3951
**
*NSET, NSET=BOTTOMNODESPLUS
110, 111, 112, 113, 114, 115,
120, 121, 122, 123, 124, 125,
130, 131, 132, 133, 134, 135,
140, 141, 142, 143, 144, 145, 150,
151
**
*****
** Boundary conditions
**
*BOUNDARY, TYPE=VELOCITY
151,1
151,2
**150,3,,10
151,3,,10
151,5
151,6
3951,1
3951,2
**3950,3,,-10
3951,3,,-10
3951,5
3951,6
**

```

C.3 Half model

The key nodes of the finite element model are shown in Figure C.9 and Figure C.10. The nodes on line 123 to 7623 and 143 to 7643 are constrained against displacement in the X direction and against rotations about the Y and Z axes using the Abaqus XSYMM boundary constraint command. The nodes used to predict the inclinometer output are shown in Figure C.11.

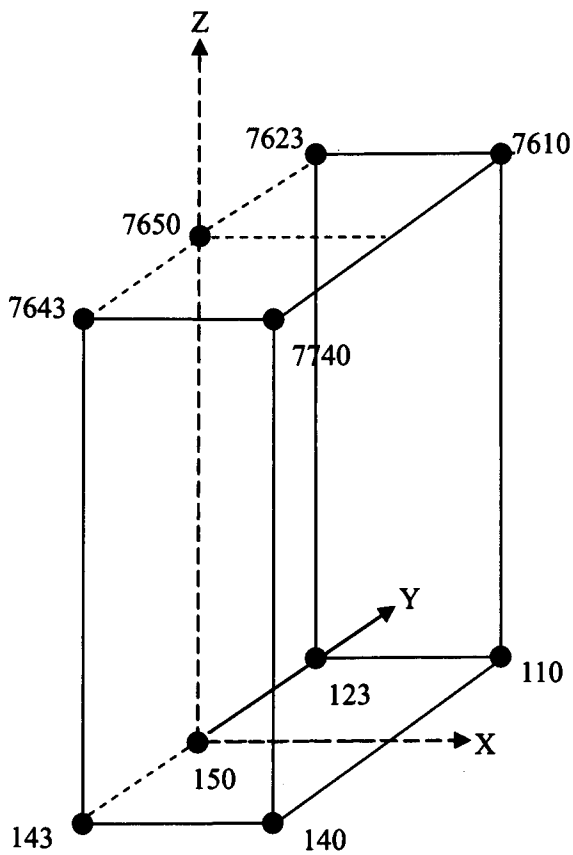


Figure C.9 Node numbering of SHS – half model

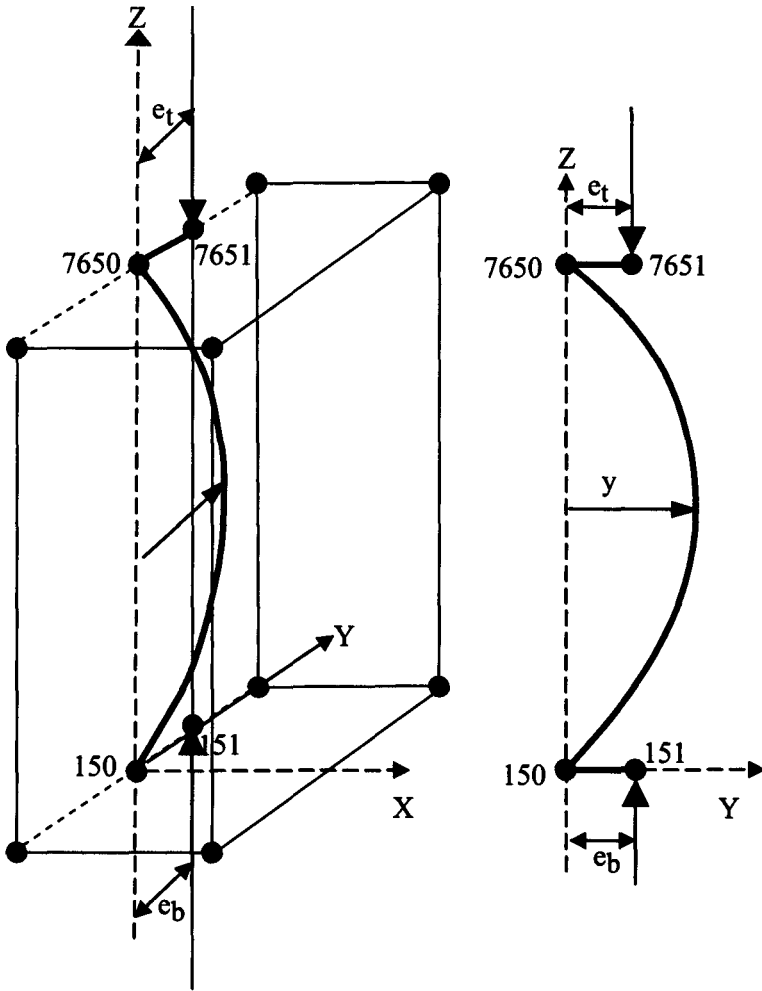


Figure C.10 Imperfections and eccentric load application – half model

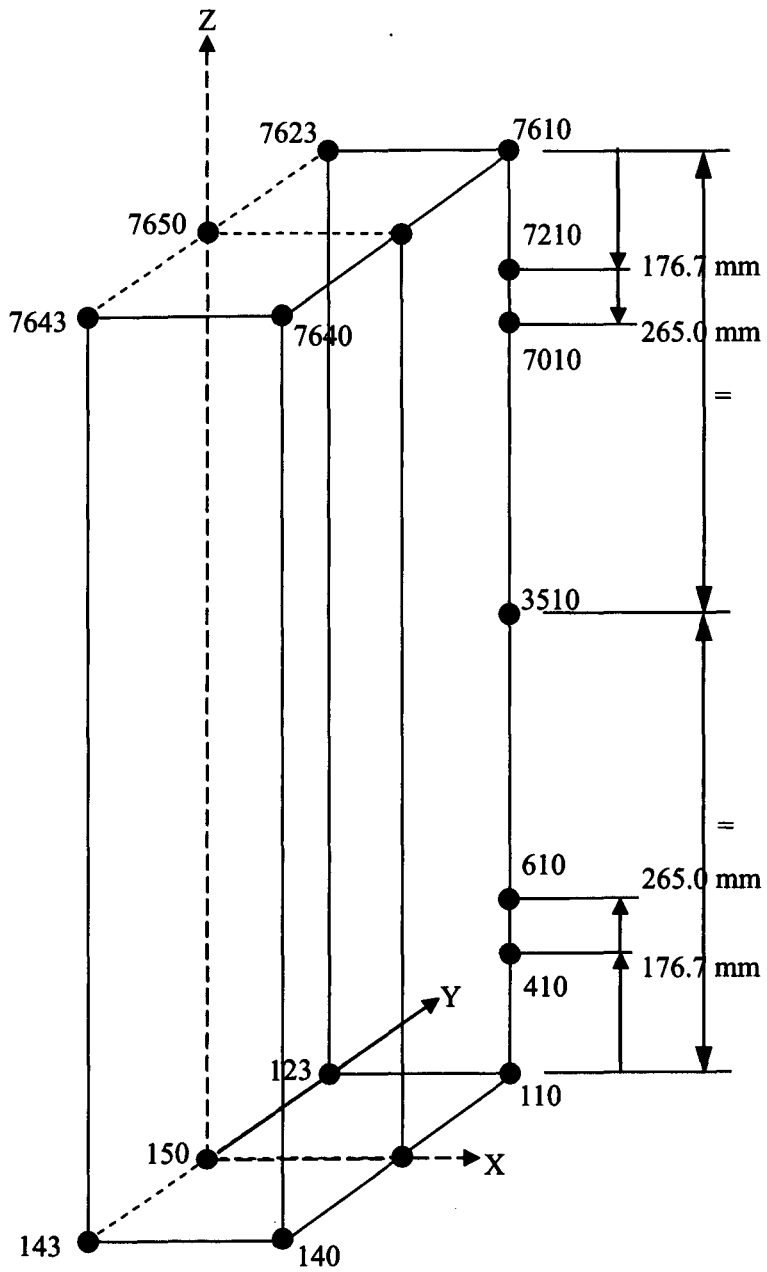


Figure C.11 Node numbering at mid-height and inclinometers – half model

APPENDIX D STRUT RESISTANCE FROM INITIAL IMPERFECTIONS

D.1 Introduction

This appendix shows how the strut imperfection is used in BS 5400-3 [BSI 2000b] Annex G in the Perry strut approach. It is included as an example of a strut buckling formula in which there is magnification of the design imperfection.

D.2 Equilibrium

Calculate the equilibrium stresses in the simple strut with an initial imperfection in the shape of a half-sine wave

Using the Perry type of formulation for strut stability:

$$\sigma_{\max} = \sigma_a + \sigma_b = \frac{N}{A} + \frac{M}{W_e} = \frac{N}{A} + \frac{Ne_N}{W_e} = \frac{N}{A} + \frac{Ne_0}{W_e} \left(\frac{1}{1 - N/N_{cr}} \right) \quad \text{Eq D. 1}$$

where

σ_{\max} is the maximum stress in the strut assuming elasticity

σ_a is the mean axial stress in the strut

σ_b is the bending stress in the strut at the extreme fibre assuming elasticity

N is the axial compressive force on the strut

M is the moment caused by strut buckling

A is the cross-sectional area of the strut

W_e is the elastic modulus resisting bending in the plane of buckling

e_N is the equivalent geometrical imperfection in the plane of buckling under load N

e_0 is the initial equivalent geometrical imperfection in the plane of buckling

N_{cr} is the relevant buckling force

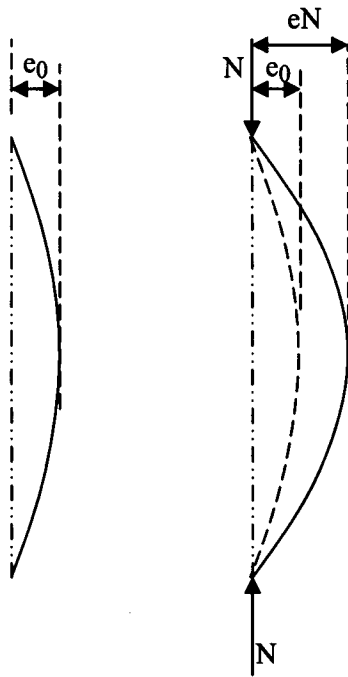


Figure D.1 Imperfections; e_0 at zero load and e_N at load N

D.3 Derivation of strut formula

$$= \sigma_a + \frac{\sigma_a A e_0}{W_e} \left(\frac{1}{1 - \frac{\sigma_a A}{\sigma_{cr} A}} \right) \quad \text{Eq D. 2}$$

$$= \sigma_a + \sigma_a \left(\frac{A e_0 y}{I} \right) \left(\frac{1}{1 - \frac{\sigma_a}{\sigma_{cr}}} \right) \quad \text{Eq D. 3}$$

$$= \sigma_a + \sigma_a \left(\frac{e_0 y}{r^2} \right) \left(\frac{\sigma_{cr}}{\sigma_{cr} - \sigma_a} \right) \quad \text{Eq D. 4}$$

$$= \sigma_a + \sigma_a \eta \left(\frac{\sigma_{cr}}{\sigma_{cr} - \sigma_a} \right) \quad \text{Eq D. 5}$$

where

$$\eta = \left(\frac{e_0 y}{r^2} \right)$$

σ_{cr} is the elastic critical buckling stress in the strut

I is the inertia in the plane of buckling

r is the radius of gyration in the plane of buckling

$$\therefore \sigma_{\max} (\sigma_{cr} - \sigma_a) = \sigma_a (\sigma_{cr} - \sigma_a) + \sigma_a \eta \sigma_{cr} \quad \text{Eq D. 6}$$

When $\sigma_{\max} = \sigma_y$, where σ_y is the yield stress,

$$\sigma_y (\sigma_{cr} - \sigma_a) = \sigma_a (\sigma_{cr} - \sigma_a) + \sigma_a \eta \sigma_{cr} \quad \text{Eq D. 7}$$

$$\therefore \sigma_y (\sigma_{cr} - \sigma_a) - \sigma_a (\sigma_{cr} - \sigma_a) = \sigma_a \eta \sigma_{cr} \quad \text{Eq D. 8}$$

$$\therefore \sigma_{cr} \sigma_y - \sigma_a \sigma_y - \sigma_a \sigma_{cr} + \sigma_a^2 = \sigma_a \eta \sigma_{cr} \quad \text{Eq D. 9}$$

$$\therefore \sigma_a^2 = \sigma_a \sigma_{cr} + \sigma_a \eta \sigma_{cr} + \sigma_a \sigma_y - \sigma_{cr} \sigma_y \quad \text{Eq D. 10}$$

Dividing through by σ_y^2

$$\therefore \frac{\sigma_a^2}{\sigma_y^2} = \frac{\sigma_a}{\sigma_y} (\sigma_{cr} + \eta \sigma_{cr} + \sigma_y) - \frac{\sigma_{cr} \sigma_y}{\sigma_y^2} \quad \text{Eq D. 11}$$

$$\therefore \left(\frac{\sigma_a}{\sigma_y} \right)^2 = \frac{\sigma_a}{\sigma_y} \left[\frac{\sigma_{cr}}{\sigma_y} + \eta \frac{\sigma_{cr}}{\sigma_y} + 1 \right] - \frac{\sigma_{cr}}{\sigma_y} \quad \text{Eq D. 12}$$

Re-writing with $\frac{\sigma_a}{\sigma_y} = k$ and $\frac{\sigma_y}{\sigma_{cr}} = \bar{\lambda}^2$

$$\therefore k^2 = k \left[\frac{1}{\bar{\lambda}^2} + \eta \frac{1}{\bar{\lambda}^2} + 1 \right] - \frac{1}{\bar{\lambda}^2} = k \left[1 + (1 + \eta) \frac{1}{\bar{\lambda}^2} \right] - \frac{1}{\bar{\lambda}^2} \quad \text{Eq D. 13}$$

$$\therefore k^2 - k \left[1 + (1 + \eta) \frac{1}{\bar{\lambda}^2} \right] + \frac{1}{\bar{\lambda}^2} = 0 \quad \text{Eq D. 14}$$

From $ax^2 + bx + c = 0 \Rightarrow x = \frac{-b \pm \sqrt{b^2 - 4ac}}{2a}$

$$k = \frac{1}{2} \left[\left(1 + (1 + \eta) \frac{1}{\bar{\lambda}^2} \right) \pm \sqrt{\left(1 + (1 + \eta) \frac{1}{\bar{\lambda}^2} \right)^2 - 4 \frac{1}{\bar{\lambda}^2}} \right] \quad \text{Eq D. 15}$$

The relevant root is

$$k = \frac{1}{2} \left[\left(1 + (1 + \eta) \frac{1}{\lambda^2} \right) - \sqrt{\left(1 + (1 + \eta) \frac{1}{\lambda^2} \right)^2 - 4 \frac{1}{\lambda^2}} \right] \quad \text{Eq D. 16}$$

$$\frac{1}{\lambda^2} = \frac{1}{\frac{\sigma_y}{\sigma_{cr}}} = \frac{\sigma_{cr}}{\sigma_y} = \frac{\left(\frac{\pi^2 EI}{L^2 A} \right)}{355} = \frac{\left(\frac{\pi^2 E r^2}{L^2} \right)}{355} = \frac{\left(\frac{\pi^2 E}{355} \right)}{\frac{L^2}{r^2}} = \frac{\left(\frac{\pi^2 205000}{355} \right)}{\lambda^2} = \frac{5700}{\lambda^2} \quad \text{Eq D. 17}$$

$$\therefore k = 0.5 \left[\left(1 + (1 + \eta) \frac{5700}{\lambda^2} \right) - \sqrt{\left(1 + (1 + \eta) \frac{5700}{\lambda^2} \right)^2 - \frac{22800}{\lambda^2}} \right] \quad \text{Eq D. 18}$$

This is the form of strut buckling equation that appears in BS 5400-3 [BSI 2000b] Annex G.

APPENDIX E TRANSVERSE BENDING OF WALLS

E.1 Introduction

This appendix contains the study of wall thickness made in the early phase of this project. The goal was to establish if the requirements of codes such as BS 5950-1 and EN 1993-1-1 are sufficient for the type of column behaviour considered in this project. The study was made on columns of 140×140×10 SHS, 3 metres long, in S355 steel bending about a rectangular axis. The study showed clearly that the limits given in these codes are not sufficient. The application of the method in this appendix was not extended to other geometries of column because the column analysis method was changed from the finite slice method of Section 4.2 to the Abaqus finite element analysis of Section 4.3 which incorporates the effects of wall thickness as seen in Section 7.

The structural mechanics of the effects of curvature are discussed in Section 7.1. In conventional design procedures, the transverse bending of the walls of members is not analysed explicitly. Instead, the wall thickness is chosen to satisfy the “classification” requirements of the design code for the particular use of the member. For example, designing to BS 5950-1, a beam required to develop a plastic hinge must satisfy the breadth to thickness limits of Class 1. These are given for flanges and webs of ‘open’ sections and for walls of hollow sections.

The limits in BS 5950-1 for Class 1, Class 2 and Class 3 for a 140×140 SHS in S355 steel are as follows:

$$\epsilon = \sqrt{(275/355)} = 0.880 \quad \text{Eq E. 1}$$

$$\text{Class 1: } b/t = 28\epsilon = 28 \times 0.880 = 24.64 \quad \text{Eq E. 2}$$

$$\text{so } B/t = 3 + 24.64 = 27.64 \quad \text{Eq E. 3}$$

$$\text{so } t \geq 140/27.64 = 5.1 \text{ mm} \quad \text{Eq E. 4}$$

$$\text{Class 2: } b/t = 32\epsilon = 32 \times 0.880 = 28.16 \quad \text{Eq E. 5}$$

$$\text{so } B/t = 3 + 28.16 = 31.16 \quad \text{Eq E. 6}$$

$$\text{so } t \geq 140/31.16 = 4.5 \text{ mm} \quad \text{Eq E. 7}$$

$$\text{Class 3: } b/t = 40\epsilon = 40 \times 0.880 = 35.2 \quad \text{Eq E. 8}$$

$$\text{so } B/t = 3 + 35.2 = 38.2 \quad \text{Eq E. 9}$$

$$\text{so } t \geq 140/38.2 = 3.7 \text{ mm} \quad \text{Eq E. 10}$$

In certain cases, such as in design for earthquake resistance of some forms of structures, greater wall thickness is required as shown in textbooks and codes such as the AISC Seismic Provisions [AISC 2005a]. The dominant phenomenon requiring extra wall thickness is transverse bending of the wall caused by the curvature of the member. The curvature of the member produces radial forces in the members across the full width. These radial forces cause transverse bending moments. If these are large, they will cause distortion of the cross-section such that the resistance might be significantly reduced. In this Appendix, the issues involved in defining a suitable breadth to thickness ratio are considered because the normal classification limits may not be adequate for the high curvatures that may occur in columns checked to the proposed design method.

Finite element analysis using 3-D elements with 3-D elasto-plastic material properties are commonly used for detailed studies of this issue. However, it is possible to develop a good understanding of this behaviour by using the simplified analyses in this Appendix.

All common columns carrying their maximum load will have plastic strains on the most compressed face, so the behaviour is not entirely elastic. However, it is helpful to develop understanding of the phenomena involved by starting with a study of behaviour that is elastic. Therefore, the following studies start with elastic behaviour in Section E.3 and then develop equations for elastic-plastic behaviour in Section E.4. Equations are developed for columns bending about a rectangular axis and about a diagonal axis. It was observed in Section 7 that members with applied end-rotations in the $X = Y$ axis tend to deflect as expected in that plane, but as they approach maximum load, they tend to deflect towards a rectangular axis if the initial imperfection was in that rectangular axis. This results in an end-rotation in the rectangular plane that approaches $1/\text{Sin}45^\circ$ times the end-rotation in the $X = Y$ axis. Therefore columns with applied end-rotations in the $X = Y$ axis need to have wall slenderness suitable for $1/\text{Sin}45^\circ$ times the end-rotation if it were to be applied in a rectangular plane.

E.2 Second order elastic behaviour

The deflections of the wall due to the radial pressure vary along the member because the curvature varies and so the radial pressure varies. The variation of deflection causes an additional curvature along the centre-line of the wall which will cause additional deflections. A simple model of this effect can be made by assuming that this curvature is a Sine curve with a certain effective half-wave length of l_{eff} and maximum displacement = δ .

The radial pressure then becomes the sum of

1. The radial pressure from the member curvature, $p_{\text{RC}} = t\sigma_c/R = t\sigma_c(d^2y/dx^2)$, as described in Section 7.1, plus
2. The pressure from the curvature of the local buckling of the wall, $p_{\text{RC}} = t\sigma_c(d^2y/dx^2)$.

It is most convenient to represent the curve of the local buckling as a Sine curve, so that

$$p_{\text{RC}} = \sigma_c t \frac{d^2 y_m}{dx^2} + \left| \sigma_c t \frac{d^2}{dx^2} \left(\delta \sin \frac{\pi x}{l_{\text{eff}}} \right) \right| \quad \text{Eq E. 11}$$

$$\therefore p_{\text{RC}} = \sigma_c t \frac{d^2 y_m}{dx^2} + \sigma_c t \delta \left(\frac{\pi}{l_{\text{eff}}} \right)^2 \sin \frac{\pi x}{l_{\text{eff}}} \quad \text{Eq E. 12}$$

At the maximum value of Sine,

$$p_{\text{RC}} = \sigma_c t \frac{d^2 y_m}{dx^2} + \sigma_c t \delta \left(\frac{\pi}{l_{\text{eff}}} \right)^2 = \sigma_c t \left[\frac{d^2 y_m}{dx^2} + \delta \left(\frac{\pi}{l_{\text{eff}}} \right)^2 \right] \quad \text{Eq E. 13}$$

Assuming the transverse stiffness depends on transverse bending stiffness alone, the deflection may be written for the general case as

$$\delta = d \frac{p_{\text{RC}} b^4}{EI_{\text{wall}}} \quad \text{Eq E. 14}$$

$$\therefore p_{\text{RC}} = \sigma_c t \left[\frac{d^2 y_m}{dx^2} + d \frac{p_{\text{RC}} b^4}{EI_{\text{wall}}} \left(\frac{\pi}{l_{\text{eff}}} \right)^2 \right] \quad \text{Eq E. 15}$$

$$\therefore p_{\text{RC}} = \sigma_c t \frac{d^2 y_m}{dx^2} + \sigma_c t d \frac{p_{\text{RC}} b^4}{EI_{\text{wall}}} \left(\frac{\pi}{l_{\text{eff}}} \right)^2 \quad \text{Eq E. 16}$$

$$\therefore p_{\text{RC}} - p_{\text{RC}} \sigma_c t d \frac{b^4}{EI_{\text{wall}}} \left(\frac{\pi}{l_{\text{eff}}} \right)^2 = \sigma_c t \frac{d^2 y_m}{dx^2} \quad \text{Eq E. 17}$$

$$\therefore p_{RC} = \left(\sigma_c t \frac{d^2 y_m}{dx^2} \right) \frac{1}{\left[1 - \sigma_c t d \frac{b^4}{EI_{wall}} \left(\frac{\pi}{\ell_{eff}} \right)^2 \right]} \quad \text{Eq E. 18}$$

The term $\frac{1}{\left[1 - \sigma_c t d \frac{b^4}{EI_{wall}} \left(\frac{\pi}{\ell_{eff}} \right)^2 \right]}$ is an elastic magnifier.

E.3 Elastic behaviour bending about X or Y axes

E.3.1 Radial pressure

As described in Section 3, curvature causes radial pressure on the wall:

$$p_{RC} = t\sigma_c/R = p_{RC} = t\sigma_c C \text{Eq} \quad \text{E. 19}$$

where C is the curvature = 1/R

For the case of a 140×140×10 SHS 3 metres long in S355 steel bending about a rectangular axis, the curvature, C, reaches 2×10^{-4} for the case of single curvature with both the initial imperfection and the imposed end rotations acting in the same plane.

Taking

the wall thickness is 10mm and

the axial stress in the wall is at yield stress of 355N/mm²

$$\therefore \text{Axial force/mm, } t\sigma_c = 10 \times 355 = 3550 \text{ N/mm} \quad \text{Eq E. 20}$$

$$\therefore \text{Radial pressure, } p_{RC} = t\sigma_c C = 3550 \times 2 \times 10^{-4} = 0.71 \text{ N/mm}^2 \quad \text{Eq E. 21}$$

E.3.2 Transverse bending moments

Assuming the stress along the tension face of the section is also at yield, there is symmetry of the bending moment diagram about the axis of curvature of the section.

The free bending moment on curved wall = $wL^2/8$ with free end slope = $wL^3/24EI$ where $w = p_{RC}$ because member under consideration is bending about a rectangular axis so the radial pressure is perpendicular to the wall of the SHS.

The symmetry of the bending moment diagram gives a uniform moment along the walls in the plane of curvature. Writing this uniform moment as M, the end slope = $ML/2EI$

For strain compatibility,

the end slope at end of wall in the plane of curvature = End slope at end of curved wall

$$\frac{Mb}{2EI} = \frac{wb^3}{24EI} - \frac{Mb}{2EI} \quad \text{Eq E. 22}$$

$$\therefore 2\left(\frac{Mb}{2EI}\right) = \frac{wb^3}{24EI} \quad \text{Eq E. 23}$$

$$\therefore M = \frac{wb^2}{24EI} \quad \text{Eq E. 24}$$

Therefore the moment along walls in the plane of curvature is constant and is:

$$M = wb^2/24 \quad \text{Eq E. 25}$$

Therefore the moment at mid-span of curved wall is:

$$M = wb^2/8 - wb^2/24 = wb^2/12 \quad \text{Eq E. 26}$$

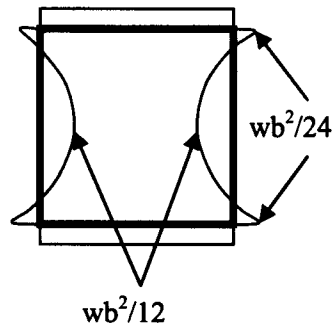


Figure E.1 BMD with equal stresses in the compression and tension flanges

E.3.3 Stresses

The span of the walls is the width of the section minus half the wall thickness at each end

Therefore maximum moment is

$$wb^2/12 = \frac{0.71 \times 130^2}{12} = 1000 \text{ N-mm} \quad \text{Eq E. 27}$$

If $t = 10 \text{ mm}$, the elastic modulus of a 1 mm wide strip is

$$Z = \frac{BD^2}{6} = \frac{1 \times 10^2}{6} = 16.7 \text{ mm}^3/\text{mm} \quad \text{Eq E. 28}$$

Therefore, bending stress is

$$\sigma = 1000/16.7 = 60 \text{ N/mm}^2 \quad \text{Eq E. 29}$$

Shear force (at inside face of wall at right-angles) is

$$V = 0.71 \times 120/2 = 42.6 \text{ N} \quad \text{Eq E. 30}$$

Average shear stress is

$$\tau_{\text{ave}} = 42.6/10 = 4.3 \text{ N/mm}^2 \quad \text{Eq E. 31}$$

At extreme fibre, shear stress = 0

At mid-plane, shear stress is

$$\tau = 1.5 \times 42.6/10 = 6.4 \text{ N/mm}^2 \quad \text{Eq E. 32}$$

E.3.4 First order deflections

The deflection of wall at mid-span of the wall is:

$$\delta = \frac{5}{384} \frac{wb^4}{EI_{\text{wall}}} - \frac{1}{8} \frac{Mb^2}{EI_{\text{wall}}} = \frac{5}{384} \frac{wb^4}{EI_{\text{wall}}} - \frac{1}{8} \frac{wb^2}{24} \frac{b^2}{EI_{\text{wall}}} \quad \text{Eq E. 33}$$

$$\therefore \delta = \frac{3}{384} \frac{wb^4}{EI_{\text{wall}}} \quad \text{Eq E. 34}$$

$$\text{where } I = \frac{BD^3}{12} = \frac{1 \times 10^3}{12} = 83.3 \text{ mm}^4 / \text{mm} \quad \text{Eq E. 35}$$

$$\therefore \delta = \frac{3}{384} \frac{0.71 \times 130^4}{210 \times 1000 \times 83.3} = 0.091 \text{ mm} \quad \text{Eq E. 36}$$

E.4 Effects of plastic flow

E.4.1 Introduction

Where material reaches yield and is strained beyond the onset of yield, there is deformation due to plastic flow of the material in addition to deformations due to the elastic strains. This means that the deflections arising from transverse bending will be different from that calculated by assuming pure elastic behaviour.

Plastic flow is explained with elegant simplicity by Calladine, *Engineering Plasticity*, (Calladine 1969) in section 2.8 *Yield Surface for Three-dimensional Stress*, especially page 36, and in section 2.13 *The Mises Yield Condition and Associated Flow Rule*, especially page 49. From this we have that the plastic flow vector, $(\delta\epsilon_1, \delta\epsilon_2, \delta\epsilon_3)$ is parallel to the deviatoric stress vector, $(\sigma'_1, \sigma'_2, \sigma'_3)$ in which

$$\sigma'_1 = \sigma_1 - \sigma_0 \quad \text{Eq E. 37}$$

$$\sigma'_2 = \sigma_2 - \sigma_0 \quad \text{Eq E. 38}$$

$$\sigma'_3 = \sigma_3 - \sigma_0 \quad \text{Eq E. 39}$$

$$\text{where } \sigma_0 = (\sigma_1 + \sigma_2 + \sigma_3)/3 \quad \text{Eq E. 40}$$

and σ_1, σ_2 and σ_3 are the principal stresses.

At the extreme fibre, the transverse direct stress, σ_2 , is at its maximum and the shear stress is zero. In this study, the maximum shear stress is small compared with the maximum transverse direct stresses, so the study will focus on the zones of maximum direct stresses, which are at the extreme fibres.

Clearly there is an interaction between the longitudinal stress at which yield will occur and the transverse bending stresses. In a wall with longitudinal compressive stresses, on the face with tensile transverse bending stresses, the stress at yield is less than the uni-axial compressive yield whereas on the face with compressive transverse bending stresses, the stress at yield is greater than the uni-axial compressive yield.

Strain hardening will affect the actual behaviour. So also will the unloading of longitudinal stress as the longitudinal “slices” deflect towards the centre of the section due to the transverse bending deflections. Both of these effects will be ignored to simplify the analysis.

The plastic strains are calculated from the plastic flow vector, $(\delta\epsilon_1, \delta\epsilon_2, \delta\epsilon_3)$. The plastic flow vector is found by calculating the deviatoric stress vector, $(\sigma'_1, \sigma'_2, \sigma'_3)$, which is found from the principal stresses, σ_1, σ_2 and σ_3 .

E.4.2 Calculating the principal stresses at the surface

The von Mises solution for stresses in 2 directions only is used, because there is no through-thickness stress along the flat regions of the walls. This is solved to find the value of longitudinal direct stress, σ_1 , that causes yield in the presence of the bending stress that was calculated from the member curvature.

$$\sigma_y^2 = \sigma_1^2 + \sigma_2^2 - \sigma_1\sigma_2 + 3\tau^2 \quad \text{Eq E. 41}$$

$$\therefore \sigma_1^2 + \sigma_2^2 - \sigma_1\sigma_2 + 3\tau^2 - \sigma_y^2 = 0 \quad \text{Eq E. 42}$$

$$\therefore \sigma_1^2 - \sigma_1\sigma_2 - (\sigma_y^2 - \sigma_2^2 - 3\tau^2) = 0 \quad \text{Eq E. 43}$$

$$\therefore \sigma_1 = \frac{\sigma_2 \pm \sqrt{\sigma_2^2 + 4(\sigma_y^2 - \sigma_2^2 - 3\tau^2)}}{2} \quad \text{Eq E. 44}$$

$$\therefore \sigma_1 = \frac{\sigma_2}{2} \pm \sqrt{\frac{\sigma_2^2}{4} + (\sigma_y^2 - \sigma_2^2 - 3\tau^2)} \quad \text{Eq E. 45}$$

$$\therefore \sigma_1 = \frac{\sigma_2}{2} \pm \sqrt{\sigma_y^2 - \frac{3\sigma_2^2}{4} - 3\tau^2} \quad \text{Eq E. 46}$$

$$\therefore \sigma_1 = \frac{\sigma_2}{2} \pm \sqrt{\sigma_y^2 - 3\left(\frac{\sigma_2}{2}\right)^2 - 3\tau^2} \quad \text{Eq E. 47}$$

At the surface, $\tau = 0$, so substituting $\tau = 0$ into Eq E. 47

$$\sigma_1 = \frac{\sigma_2}{2} \pm \sqrt{\sigma_y^2 - 3\left(\frac{\sigma_2}{2}\right)^2} \quad \text{Eq E. 48}$$

E.4.3 Calculating the deviatoric stress vector at the surface

At the surface, $\sigma_3 = 0$, and σ_1 is defined by Eq E. 48, so Eq E. 40 becomes

$$\sigma_0 = \frac{\sigma_1 + \sigma_2 + \sigma_3}{3} = \frac{\left(\frac{\sigma_2}{2} \pm \sqrt{\sigma_y^2 - 3\left(\frac{\sigma_2}{2}\right)^2}\right) + \sigma_2}{3} \quad \text{Eq E. 49}$$

$$\therefore \sigma_0 = \frac{\left(\frac{3\sigma_2}{2} \pm \sqrt{\sigma_y^2 - 3\left(\frac{\sigma_2}{2}\right)^2}\right)}{3} = \frac{\sigma_2}{2} \pm \frac{\left(\sqrt{\sigma_y^2 - 3\left(\frac{\sigma_2}{2}\right)^2}\right)}{3} \quad \text{Eq E. 50}$$

Calculating σ'_1

$$\therefore \sigma'_1 = \sigma_1 - \sigma_0 = \left[\frac{\sigma_2}{2} \pm \left(\sqrt{\sigma_y^2 - 3\left(\frac{\sigma_2}{2}\right)^2}\right)\right] - \left[\frac{\sigma_2}{2} \pm \frac{1}{3}\left(\sqrt{\sigma_y^2 - 3\left(\frac{\sigma_2}{2}\right)^2}\right)\right] \quad \text{Eq E. 51}$$

$$\therefore \sigma'_1 = \sigma_1 - \sigma_0 = \pm \frac{2}{3}\left(\sqrt{\sigma_y^2 - 3\left(\frac{\sigma_2}{2}\right)^2}\right) \quad \text{Eq E. 52}$$

Calculating σ'_2

$$\sigma'_2 = \sigma_2 - \sigma_0 = \sigma_2 - \frac{\sigma_2}{2} \mp \frac{\left(\sqrt{\sigma_y^2 - 3\left(\frac{\sigma_2}{2}\right)^2} \right)}{3} = \frac{\sigma_2}{2} \mp \frac{\left(\sqrt{\sigma_y^2 - 3\left(\frac{\sigma_2}{2}\right)^2} \right)}{3} \quad \text{Eq E. 53}$$

Calculating σ'_2

$$\sigma'_3 = \sigma_3 - \sigma_0 = 0 - \frac{\sigma_2}{2} \mp \frac{\left(\sqrt{\sigma_y^2 - 3\left(\frac{\sigma_2}{2}\right)^2} \right)}{3} = -\frac{\sigma_2}{2} \mp \frac{\left(\sqrt{\sigma_y^2 - 3\left(\frac{\sigma_2}{2}\right)^2} \right)}{3} \quad \text{Eq E. 54}$$

Therefore the deviatoric stress vector $(\sigma'_1, \sigma'_2, \sigma'_3) =$

$$\pm \frac{2}{3} \left(\sqrt{\sigma_y^2 - 3\left(\frac{\sigma_2}{2}\right)^2} \right), \frac{\sigma_2}{2} \mp \frac{\left(\sqrt{\sigma_y^2 - 3\left(\frac{\sigma_2}{2}\right)^2} \right)}{3}, -\frac{\sigma_2}{2} \mp \frac{\left(\sqrt{\sigma_y^2 - 3\left(\frac{\sigma_2}{2}\right)^2} \right)}{3} \quad \text{Eq E. 55}$$

E.4.4 Calculating the normalised plastic flow vector at the surface

The plastic flow vector is parallel to the deviatoric stress vector, so the plastic flow vector, $(\delta\epsilon_1, \delta\epsilon_2, \delta\epsilon_3)$, normalised to a longitudinal plastic strain of 1.0 =

$$\left\{ \begin{array}{l} \pm \frac{2}{3} \left(\sqrt{\sigma_y^2 - 3\left(\frac{\sigma_2}{2}\right)^2} \right), \frac{\sigma_2}{2} \mp \frac{\left(\sqrt{\sigma_y^2 - 3\left(\frac{\sigma_2}{2}\right)^2} \right)}{3}, -\frac{\sigma_2}{2} \mp \frac{\left(\sqrt{\sigma_y^2 - 3\left(\frac{\sigma_2}{2}\right)^2} \right)}{3} \\ \pm \frac{2}{3} \left(\sqrt{\sigma_y^2 - 3\left(\frac{\sigma_2}{2}\right)^2} \right), \pm \frac{2}{3} \left(\sqrt{\sigma_y^2 - 3\left(\frac{\sigma_2}{2}\right)^2} \right), \pm \frac{2}{3} \left(\sqrt{\sigma_y^2 - 3\left(\frac{\sigma_2}{2}\right)^2} \right) \end{array} \right\} \quad \text{Eq E. 56}$$

$$= \left\{ 1, \frac{\frac{\sigma_2}{2} \mp \frac{1}{3} \left(\sqrt{\sigma_y^2 - 3\left(\frac{\sigma_2}{2}\right)^2} \right)}{\pm \frac{2}{3} \left(\sqrt{\sigma_y^2 - 3\left(\frac{\sigma_2}{2}\right)^2} \right)}, \frac{-\frac{\sigma_2}{2} \mp \frac{1}{3} \left(\sqrt{\sigma_y^2 - 3\left(\frac{\sigma_2}{2}\right)^2} \right)}{\pm \frac{2}{3} \left(\sqrt{\sigma_y^2 - 3\left(\frac{\sigma_2}{2}\right)^2} \right)} \right\} \quad \text{Eq E. 57}$$

$$= \left\{ 1, \pm \frac{\frac{3\sigma_2}{4} \mp \frac{1}{2}}{\left(\sqrt{\sigma_y^2 - 3\left(\frac{\sigma_2}{2}\right)^2} \right)}, \mp \frac{\frac{3\sigma_2}{4} \mp \frac{1}{2}}{\left(\sqrt{\sigma_y^2 - 3\left(\frac{\sigma_2}{2}\right)^2} \right)} \right\} \quad \text{Eq E. 58}$$

The vector is non-linear in terms of σ_2 .

The effect of plastic flow is shown schematically (ie not to scale) in Figure E.2 in which the elastic stress-strain is compared with stress-strain when there is plastic flow form a longitudinal strain of 2 yield strain and 3 yield strain.

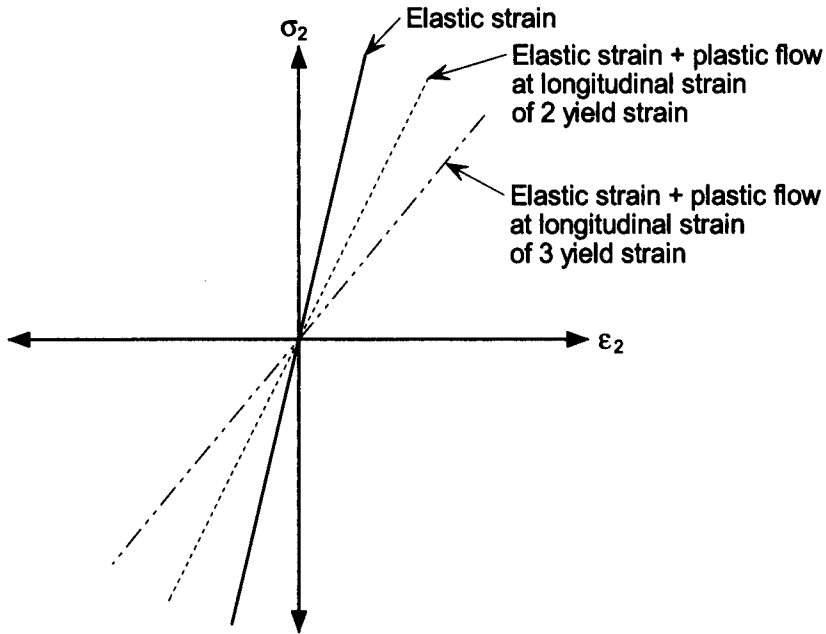


Figure E.2 Schematic comparison of (elastic strain) v (elastic strain + plastic flow)

For the purposes of this present report, the relationships will be assumed to be linear to estimate the magnitude of the effects of transverse bending and the associated deflections.

From Eq E. 58, it is seen that

$$\delta\epsilon_2 = \left\{ \pm \frac{\frac{3\sigma_2}{4}}{\left(\sqrt{\sigma_y^2 - 3\left(\frac{\sigma_2}{2}\right)^2} \right)} \mp \frac{1}{2} \right\} \delta\epsilon_1 \quad \text{Eq E. 59}$$

The term $\left\{ \mp \frac{1}{2} \right\}$ is the component of plastic strain that expands the total width of the wall, but does not affect the deflection of the wall.

The term $\left\{ \pm \frac{\frac{3\sigma_2}{4}}{\left(\sqrt{\sigma_y^2 - 3\left(\frac{\sigma_2}{2}\right)^2} \right)} \right\}$ is the component of plastic strain that increases the

curvature of the wall. It is proportional to the bending stresses and inversely proportional to the yield stress modified by the transverse bending stress. This means that the deflections from transverse bending are magnified according to both the transverse bending stresses and the longitudinal plastic strain. The term is not linear in σ_2 , but for smaller values of σ_2 it is not far from linear. To make a simple calculation possible, for small values of σ_2 , this term can be taken as:

$$\left\{ \frac{\frac{3\sigma_2}{4}}{\left(\sqrt{\sigma_y^2 - 3\left(\frac{\sigma_2}{2}\right)^2} \right)} \right\} \approx \frac{\frac{3\sigma_2}{4}}{\left(\sqrt{\sigma_y^2} \right)} = \frac{\frac{3\sigma_2}{4}}{\sigma_y} = \frac{3\sigma_2}{4\sigma_y} \quad \text{Eq E. 60}$$

Calling the plastic strain that increases the curvature of the wall ϵ_{2b} , then Eq E. 59 becomes

$$\delta\epsilon_{2b} = \delta\epsilon_1 \times \frac{3\sigma_2}{4\sigma_y} \quad \text{Eq E. 61}$$

E.4.5 Second-order effects where plasticity occurs

It is shown in Section E.2 that, for elastic behaviour, the deflections are magnified by:

$$\frac{1}{\left[1 - \sigma_c \text{td} \frac{b^4}{EI_{\text{wall}}} \left(\frac{\pi}{\ell_{\text{eff}}} \right)^2 \right]}$$

where $d \frac{b^4}{EI_{\text{wall}}}$ is the deflection of the wall calculated by first-order elastic analysis.

The bending moment diagram will be modified by plastic flow. The parts of the cross-section experiencing plastic flow deflect as if they have reduced stiffness, so the restraint from the walls in the plane of the curvature will be somewhat increased. However, a simplified study of the wall behaviour can be made by assuming that the elastic amplifier can be modified to represent behaviour in the presence of plasticity by increasing the deflections by an amplification factor, A. Therefore, the magnification factor would become:

$$\frac{1}{\left[1 - \sigma_y t A d \frac{b^4}{EI_{\text{wall}}} \left(\frac{\pi}{\ell_{\text{eff}}} \right)^2 \right]}$$

The amplification factor, A, may be calculated approximately without iterations. The amplification is due to the plastic strains that increase the curvature of the wall. These are the strains in direction '2' of the plastic flow vector ($\delta\epsilon_1, \delta\epsilon_2, \delta\epsilon_3$) assuming that the plastic strain along the column is in direction '1'. Integrating Eq E. 61, in which ϵ_{2b} is the plastic strain that increases the curvature of the wall,

$$\epsilon_{2b} = \int \frac{3\sigma_2}{4\sigma_y} \delta\epsilon_1 \quad \text{Eq E. 62}$$

Both the transverse bending stress, σ_2 , and the longitudinal strain in the column, ϵ_1 , are functions of the overall curvature of the column. In Section 7.1 it was shown that the radial pressure is a function of the curvature and in Section E.3.3 the transverse stresses were calculated from the radial pressure.

Writing the overall curvature of the column, $\frac{d^2y}{dx^2}$, as 'C' for convenience, and writing

$$\sigma_2 = D \times C \quad \text{Eq E. 63}$$

$$\text{and } \epsilon_1 = F \times C, \quad \text{Eq E. 64}$$

where D and F may be considered to be independent of C, then

$$\epsilon_{2b} = \int_{\epsilon_y}^{\epsilon_{\text{max}}} \frac{3\sigma_2}{4\sigma_y} d\epsilon_1 = \frac{3}{4\sigma_y} \int_{\epsilon_y}^{\epsilon_{\text{max}}} (DC)d(FC) = \frac{3DF}{4\sigma_y} \int_{\epsilon_y}^{\epsilon_{\text{max}}} C dC = \frac{3DF}{4\sigma_y} \left[\frac{C^2}{2} \right]_{\epsilon_y}^{\epsilon_{\text{max}}} \quad \text{Eq E. 65}$$

$$\therefore \epsilon_{2b} = \frac{3DF}{8\sigma_y} \left[C_{\text{em}}^2 - C_y^2 \right] \quad \text{Eq E. 66}$$

where C_{em} is the curvature at a cross-section

and C_y is the curvature at a cross-section when the longitudinal strain reaches 1.0 yield strain.

The total bending strain is the sum of the elastic bending strain and the plastic bending strain.

Writing the elastic bending strain as ϵ_{2be} , the total bending strain = $\epsilon_{2be} + \epsilon_{2b}$.

The amplification factor, A, is the ratio of the total bending strain, including plasticity, to the elastic bending strain, therefore

$$A = \frac{\epsilon_{2be} + \epsilon_{2b}}{\epsilon_{2be}} \quad \text{Eq E. 67}$$

where $\epsilon_{2be} = \frac{\sigma_2}{E} = \frac{DC}{E}$ Eq E. 68

$$\therefore A = \frac{\frac{DC_{\epsilon m}}{E} + \frac{3DF}{8\sigma_y} [C_{\epsilon m}^2 - C_y^2]}{\frac{DC_{\epsilon m}}{E}} = 1 + \frac{3E}{8\sigma_y} F \left[1 - \left(\frac{C_y}{C_{\epsilon m}} \right)^2 \right] C_{\epsilon m} \quad \text{Eq E. 69}$$

where $C_{\epsilon m}$ is the maximum curvature at the cross-section under consideration.

The factor F was defined in Eq E. 64 as $\epsilon_1 = F \times C$, therefore

$$F = \frac{\epsilon_1}{C} \quad \text{Eq E. 70}$$

Writing the number of yield strains at maximum strain as 'n',

$$\epsilon_1 = n \left(\frac{\sigma_y}{E} \right), \quad \text{Eq E. 71}$$

$$F = \frac{\epsilon_1}{C_{\epsilon m}} = \frac{n \left(\frac{\sigma_y}{E} \right)}{C_{\epsilon m}} \quad \text{Eq E. 72}$$

Substituting into Eq E. 69

$$\therefore A = 1 + \frac{3E}{8\sigma_y} \frac{n \left(\frac{\sigma_y}{E} \right)}{C_{\epsilon m}} \left[1 - \left(\frac{C_y}{C_{\epsilon m}} \right)^2 \right] C_{\epsilon m} \quad \text{Eq E. 73}$$

$$\therefore A = 1 + \frac{3n}{8} \left[1 - \left(\frac{C_y}{C_{\epsilon m}} \right)^2 \right] \quad \text{Eq E. 74}$$

E.4.6 Minimum thickness of wall to avoid local instability

The wall thickness needs to be sufficient to prevent gross deformation of the wall of the column, because gross deformation would reduce the resistance of the column and

precipitate failure. The minimum thickness of the wall cannot be less than the thickness at which the magnifier would become infinite. From the formula for the magnifier above, we see that the magnifier becomes infinite when:

$$\left[1 - \sigma_y t A d \frac{b^4}{EI_{\text{wall}}} \left(\frac{\pi}{\ell_{\text{eff}}} \right)^2 \right] = 0 \quad \text{Eq E. 75}$$

$$\therefore 1 = \sigma_y t A d \frac{b^4}{EI_{\text{wall}}} \left(\frac{\pi}{\ell_{\text{eff}}} \right)^2 = \sigma_y t A d \frac{b^4}{E(t^3/12)} \left(\frac{\pi}{\ell_{\text{eff}}} \right)^2 \quad \text{Eq E. 76}$$

$$\therefore 1 = 12 \sigma_y A d \frac{b^4}{E t^2} \left(\frac{\pi}{\ell_{\text{eff}}} \right)^2 \quad \text{Eq E. 77}$$

$$\therefore t = \sqrt{12 \sigma_y A d \frac{b^4}{E} \left(\frac{\pi}{\ell_{\text{eff}}} \right)^2} = \sqrt{\frac{12 A d \sigma_y}{E} \left(\frac{\pi}{\ell_{\text{eff}}} \right)} b^2 \quad \text{Eq E. 78}$$

E.5 Elastic-plastic behaviour bending about X or Y axes

E.5.1 Example of strains

For the case of a 140×140×10 SHS 3 metres long in S355 steel, for the case of single curvature with end rotations equal and opposite of 0.040 radians and with both the initial imperfection and the imposed end rotations acting in the same plane, the curvature reaches 2×10^{-4} .

On the face with **compressive** stresses of $\sigma_2 = 60 \text{ N/mm}^2$ from transverse bending, as calculated in Eq E. 29, and the shear stress of zero at an extreme fibre,

$$\begin{aligned} \sigma_1 &= \frac{\sigma_2}{2} \pm \sqrt{\sigma_y^2 - 3 \left(\frac{\sigma_2}{2} \right)^2 - 3\tau^2} \\ &= 30 \pm \sqrt{355^2 - 3(30)^2 - 3 \times 0^2} = 30 + 351.2 = 381.2 \text{ N/mm}^2 \end{aligned} \quad \text{Eq E. 79}$$

Therefore the “hydrostatic” stress is

$$\sigma_0 = (\sigma_1 + \sigma_2 + \sigma_3)/3 = (381.3 + 60 + 0)/3 = 147.1 \text{ N/mm}^2 \quad \text{Eq E. 80}$$

Therefore

$$\sigma'_1 = \sigma_1 - \sigma_0 = 381.2 - 147.1 = 234.1 \text{ N/mm}^2 \quad \text{Eq E. 81}$$

$$\sigma'_2 = \sigma_2 - \sigma_0 = 60.0 - 147.1 = -87.1 \text{ N/mm}^2 \quad \text{Eq E. 82}$$

$$\sigma'_3 = \sigma_3 - \sigma_0 = 0.0 - 147.1 = -147.1 \text{ N/mm}^2 \quad \text{Eq E. 83}$$

Therefore the deviatoric stress vector is

$$(\sigma'_1, \sigma'_2, \sigma'_3) = (234.1, -87.1, -147.1) \quad \text{Eq E. 84}$$

The plastic flow vector, $(\delta\epsilon_1, \delta\epsilon_2, \delta\epsilon_3)$ is parallel. Dividing through by σ'_1 , so that $\delta\epsilon_1 = 1.0$,

$$\text{the plastic flow vector} = (1.0, -0.372, -0.628) \quad \text{Eq E. 85}$$

On the face with **tensile** stresses of $\sigma_2 = 60 \text{ N/mm}^2$ from transverse bending, as calculated in Eq E. 29, and the shear stress of zero at an extreme fibre,

$$\begin{aligned} \sigma_1 &= \frac{\sigma_2}{2} \pm \sqrt{\sigma_y^2 - 3\left(\frac{\sigma_2}{2}\right)^2 - 3\tau^2} \\ &= -30 \pm \sqrt{355^2 - 330^2 - 3 \times 0^2} = -30 + 351.2 = 321.2 \text{ N/mm}^2 \end{aligned} \quad \text{Eq E. 86}$$

Therefore the “hydrostatic” stress is

$$\sigma_0 = (\sigma_1 + \sigma_2 + \sigma_3)/3 = (321.2 - 60 + 0)/3 = 87.1 \text{ N/mm}^2 \quad \text{Eq E. 87}$$

Therefore

$$\sigma'_1 = \sigma_1 - \sigma_0 = 321.2 - 87.1 = 234.1 \text{ N/mm}^2 \quad \text{Eq E. 88}$$

$$\sigma'_2 = \sigma_2 - \sigma_0 = -60.0 - 87.1 = -147.1 \text{ N/mm}^2 \quad \text{Eq E. 89}$$

$$\sigma'_3 = \sigma_3 - \sigma_0 = 0.0 - 87.1 = -87.1 \text{ N/mm}^2 \quad \text{Eq E. 90}$$

Therefore, the deviatoric stress vector is

$$(\sigma'_1, \sigma'_2, \sigma'_3) = (234.1, -147.1, -87.1) \quad \text{Eq E. 91}$$

The plastic flow vector, $(\delta\epsilon_1, \delta\epsilon_2, \delta\epsilon_3)$ is parallel. Dividing through by σ'_1 , so that $\delta\epsilon_1 = 1.0$,

$$\text{the plastic flow vector} = (1.0, -0.628, -0.372) \quad \text{Eq E. 92}$$

Therefore, under longitudinal plastic straining, the compression face plastic flow (or plastic strain) is -0.372 and the tension face plastic flow (or plastic strain) is -0.628. The mean value is -0.500, so the difference from mean to maximum is +/-0.128. This means that for an increment of longitudinal strain of 1.0, there is a plastic flow equivalent to a transverse bending strain of 0.128. For each increment of longitudinal strain of one yield strain,

$\epsilon_y = \sigma_y/E$, the increase in the bending strain at the surface of the wall will be equivalent to an elastic bending stress of $0.128 \times \text{yield stress} = 0.128 \times 355 = 45 \text{ N/mm}^2$ due to plastic strain.

For the same member in single curvature with an end rotation of 0.020 radians, the most severe curvature is 5.3×10^{-5} and the maximum strain is less than 5 yield strains. Therefore the radial pressure and the transverse bending stress are reduced by a factor of about 4, giving commensurately reduced plastic flows.

E.5.2 Example of minimum thickness for high end-rotation

The elasto-plastic second-order finite slice model of Section 4.2 of a $140 \times 140 \times 10$ SHS 3 metres long in S355 steel bending about a rectangular axis gave the following results for the case of single curvature with both the initial imperfection and the imposed end rotations of 40 milliradians acting in the same plane. Assuming no strain hardening:

1. at mid-height (the point of maximum curvature), the curvature reaches 2×10^{-4} and the strain reaches 14 yield strain,
2. at 100 mm from mid-height of the member, the curvature is 1×10^{-4} and the strain is 7 yield strain.

At mid-height of the member, the maximum strain is $14\epsilon_y$, so taking

$$C_y/C_{\epsilon m} = 1\epsilon_y/14 \epsilon_y = 0.07 \quad \text{Eq E. 93}$$

$$\therefore A = 1 + \frac{3n}{8} \left[1 - \left(\frac{C_y}{C_{\epsilon m}} \right)^2 \right] = 1 + \frac{3 \times 14}{8} \left[1 - (0.07)^2 \right] = 6.2 \quad \text{Eq E. 94}$$

At 100 mm from mid-height of the member, the maximum strain is $7\epsilon_y$ and $C_{\max} = 1 \times 10^{-4}$, so taking

$$C_y/C_{\epsilon m} = 1\epsilon_y/7 \epsilon_y = 0.14 \quad \text{Eq E. 95}$$

$$\therefore A = 1 + \frac{3n}{8} \left[1 - \left(\frac{C_y}{C_{\epsilon m}} \right)^2 \right] = 1 + \frac{3 \times 7}{8} \left[1 - (0.14)^2 \right] = 3.6 \quad \text{Eq E. 96}$$

To find the magnification factor, the effective length l_{eff} needs to be found. Assuming that the effective length remains the same, this can be calculated from the ratio of the deflections at mid-length of the column and at the points 100mm either side.

The deformation arising from the second order effects described in Section E.2 is a half Sine curve of length l_{eff} . The deformation can equally be defined as a half Cosine curve with the maximum displacement at mid-length of the column and the curve form:

$$\delta = \delta_{max} \text{Cos} \frac{\pi x}{l_{eff}} \quad \text{Eq E. 97}$$

Therefore, the deflection at 100mm from mid-length is

$$\delta_{100} = \delta_{max} \text{Cos} \frac{\pi \times 100}{l_{eff}} \quad \text{Eq E. 98}$$

$$\therefore \text{Cos} \frac{\pi \times 100}{l_{eff}} = \frac{\delta_{100}}{\delta_{max}} \quad \text{Eq E. 99}$$

from which l_{eff} can be calculated.

The elastic deflection of the wall was calculated in E.3.4 as $\delta = \frac{3}{384} \frac{p_{RC} b^4}{EI_{wall}}$

Therefore the total deflection, δ_t , including the effects of plasticity is

$$\delta_t = \frac{3A}{384} \frac{p_{RC} b^4}{EI_{wall}} \quad \text{Eq E. 100}$$

Using Eq E. 100 to calculate $\frac{\delta_{100}}{\delta_{max}}$

$$\frac{\delta_{t,100}}{\delta_{t,max}} = \frac{\left(\frac{3A_{100} p_{RC,100} b^4}{384 EI_{wall}} \right)}{\left(\frac{3A_{max} p_{RC,max} b^4}{384 EI_{wall}} \right)} = \frac{A_{100} p_{RC,100}}{A_{max} p_{RC,max}} = \frac{A_{100} (\sigma_y t C_{100})}{A_{max} (\sigma_y t C_{max})} = \frac{A_{100} C_{100}}{A_{max} C_{max}} \quad \text{Eq E. 101}$$

$A_{100} = 3.6$ from Eq E. 96

$A_{max} = 6.2$ from Eq E. 94

$C_{100} = 1 \times 10^{-4}$ from finite slice model

$C_{max} = 2 \times 10^{-4}$ from finite slice model

$$\therefore \frac{\delta_{t,100}}{\delta_{t,max}} = \frac{A_{100} C_{100}}{A_{max} C_{max}} = \frac{3.6 \times 1 \times 10^{-4}}{6.2 \times 2 \times 10^{-4}} = 0.290 \quad \text{Eq E. 102}$$

$$\text{Cos} \frac{\pi \times 100}{l_{eff}} = \frac{\delta_{100}}{\delta_{max}} = 0.290 = \text{Cos}(1.277 \text{rads}) \quad \text{Eq E. 103}$$

$$\therefore \frac{\pi \times 100}{l_{\text{eff}}} = 1.277 \quad \text{Eq E. 104}$$

$$\therefore l_{\text{eff}} = \frac{\pi \times 100}{1.277} = 246 \text{ mm} \quad \text{Eq E. 105}$$

Substituting into Eq E. 78, $t = \sqrt{\left(\frac{12A\sigma_y}{E} d\right) \left(\frac{\pi}{l_{\text{eff}}}\right) b^2}$

$$= \sqrt{\left(\frac{12 \times 6.2 \times 355}{205000} \frac{3}{384}\right) \left(\frac{\pi}{246}\right) 130^2} = 6.8 \text{ mm} \quad \text{Eq E. 106}$$

Therefore the estimate of the thickness for wall stability is clearly greater than the thickness required for Class 1 to BS 5950-1 which is $140/27.6 = 5.1$ mm for a 140×140 SHS. The thickness for wall stability is $6.8/5.1 = 1.3 \times$ Class 1 thickness to BS 5950-1.

E.5.3 Example of lower end-rotation and lower curvature

To show the influence of the end-rotation, the calculation is repeated for the case of equal end rotations (point of contraflexure at mid-height of column) with the end-slope equal to 0.020 radians bending about a rectangular axis.

Assuming no strain hardening:

1. at mid-height (the point of maximum curvature), the curvature reaches 0.58×10^{-4} and the strain reaches 4.7 yield strain,
2. at 100 mm from mid-height of the member, the curvature is 0.41×10^{-4} and the strain is 3.5 yield strain.

At mid-height of the member, the maximum strain is $4.7\epsilon_y$, so taking

$$C_y/C_{\text{max}} = 1\epsilon_y/4.7\epsilon_y = 0.21 \quad \text{Eq E. 107}$$

$$\therefore A = 1 + \frac{3n}{8} \left[1 - \left(\frac{C_y}{C_{\text{max}}} \right)^2 \right] = 1 + \frac{3 \times 4.7}{8} [1 - (0.21)^2] = 2.7 \quad \text{Eq E. 108}$$

At 100 mm from the point of maximum strain, the greatest strain is $3.5\epsilon_y$.

$$C_y/C_{\text{max}} = 1\epsilon_y/3.5\epsilon_y = 0.29 \quad \text{Eq E. 109}$$

$$\therefore A = 1 + \frac{3n}{8} \left[1 - \left(\frac{C_y}{C_{\max}} \right)^2 \right] = 1 + \frac{3 \times 3.5}{8} [1 - (0.29)^2] = 2.20 \quad \text{Eq E. 110}$$

$$A_{100} = 2.2 \text{ from Eq E. 110}$$

$$A_{\max} = 2.7 \text{ from Eq E. 108}$$

$$C_{100} = 0.41 \times 10^{-4}$$

$$C_{\max} = 0.58 \times 10^{-4}$$

$$\therefore \frac{\delta_{t,100}}{\delta_{t,\max}} = \frac{A_{100} C_{100}}{A_{\max} C_{\max}} = \frac{2.2 \times 0.41 \times 10^{-4}}{2.7 \times 0.58 \times 10^{-4}} = 0.576 \quad \text{Eq E. 111}$$

$$\text{Cos} \frac{\pi \times 100}{\ell_{\text{eff}}} = \frac{\delta_{100}}{\delta_{\max}} = 0.576 = \text{Cos}(0.957 \text{rads}) \quad \text{Eq E. 112}$$

$$\therefore \frac{\pi \times 100}{\ell_{\text{eff}}} = 0.957 \quad \text{Eq E. 113}$$

$$\therefore \ell_{\text{eff}} = \frac{\pi \times 100}{0.957} = 328 \text{ mm} \quad \text{Eq E. 114}$$

Substituting into the Eq E. 78, $t = \sqrt{\frac{12Ad\sigma_y}{E} \left(\frac{\pi}{\ell_{\text{eff}}} \right) b^2}$

$$t = \sqrt{\left(\frac{12A\sigma_y}{E} d \right) \left(\frac{\pi}{\ell_{\text{eff}}} \right) b^2}$$

$$= \sqrt{\left(\frac{12 \times 2.7 \times 355}{205000} \frac{3}{384} \right) \left(\frac{\pi}{328} \right) 130^2} = 3.4 \text{ mm} \quad \text{Eq E. 115}$$

This is less than 6.7mm required for single curvature with end-slopes of 0.040 radians. It is also much less than the BS 5950-1 Class 1 limit of 5.1mm. Therefore, the simplified analysis above suggests that it is sufficient for the columns to be Class 3 for equal end slopes and 0.020 radians end slope.

E.6 Summary

From the analysis shown above it is clear that some columns can be Class 3 or Class 2 if the end-rotations are low, but guidance is needed to say under what conditions they need to be or Class 1 of even thicker walled than Class 1. Wall slenderness is investigated in Sections 5, 6 and 7 and design limits are given in Section 7.4 and repeated in Section 9.2.2. Generally this will not be an issue because designers will almost always choose the thicker walled sections

available to allow them to use the smallest overall section size to be hidden in the walls of the building with the greatest ease. There is also an incentive to use the thickest walls so that the columns designed for least load, ie for the higher floors, are easily distinguished on site by having smaller breadth and width than the sections with higher design loads.

APPENDIX F FINITE SLICE SPREADSHEET

F.1 Outline of spreadsheet calculations

F.1.1 Introduction

This Appendix describes the CMK elasto-plastic analysis spreadsheet used to calculate the axial compression resistance of columns for particular end rotations and end moments.

The spreadsheet allows the calculation of the resistance for any end rotations both in the region between zero load and maximum resistance and in the region beyond maximum load, often referred to as the “falling branch”.

At October 2005, the calculation considers only flexural buckling. It does not consider torsional or lateral-torsional effects. It is intended to add the calculation steps to consider lateral-torsional effects in the future.

F.1.2 Overall method

The solution is iterative.

The core of the method is to find the axial compression that can be resisted at any cross-section along the column by the moment induced by the curvature of the column, as shown in Figure F.1. The axial load resisted, N_r (kN), at any section is equal to the moment, M_x or M_y (kN/m), divided by the eccentricity from the line of thrust at that section, D_{a_mod} (mm), so that:

$$N_r = \frac{M_x}{\left(\frac{D_{a_mod,x}}{1000}\right)} \text{ or } = \frac{M_y}{\left(\frac{D_{a_mod,y}}{1000}\right)}$$

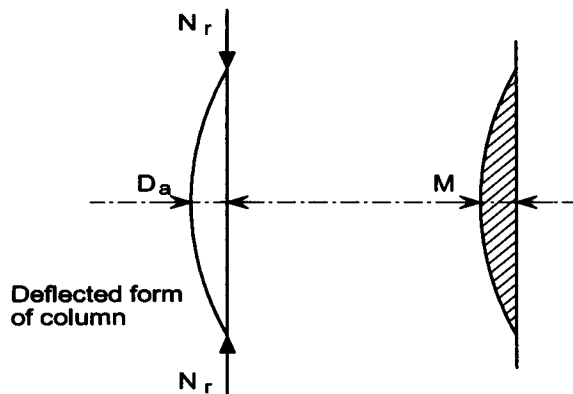


Figure F.1 Bending moment in column

The curvature of the column is the principal variable in the analysis. It is the variable that is modified to start each new cycle of iteration. At the end of each cycle of the iteration, a modified curvature is calculated from the difference between the moment induced by curvature and the moment from axial load at the eccentricity between the line of thrust and the centre line of the column at each section.

Cycles of iteration are repeated until the equilibrium at each section along the length of the column is within acceptable limits of convergence. In early September 2005, a new method was developed for improving the curvature and the convergence achievable is now closer than 0.1%.

Variables at October 2005 are:

1. curvature
2. initial geometrical imperfection
3. residual stress (to date considered to be parabolic)
4. length
5. yield stress
6. elastic modulus
7. section properties

Strain hardening is not yet included. Strain hardening is an extremely complicated issue because local buckling phenomena often reduce or cancel the benefits that would be expected.

F.2 Calculation of the 'line of thrust'

The line of thrust is defined as the straight line off-set by the distance D_N (mm) from the undeformed column centre-line and passing through points at the ends of the member defined by the end-moment M_{end} (kN/m) divided by the applied axial load N (kN), so that the ends:

$$D_N = \frac{M_{end} \times 1000}{N}$$

The eccentricity for the deformed column from the line of thrust, D_{a_mod} (mm) is:

$$D_{a_mod} = D_a - D_N$$

For pin-ended columns with zero end moments, the line of thrust passes through the ends of the column, because the end moments are zero.

The end moment is defined on the Sheet “Data” - at October 2005 it is the [joint+beam stiffness]*[the end rotation of the column in excess of the end rotation of the beam if the beam were simply supported].

The axial load is defined on “Sheet 1”

The eccentricity of the line of thrust from the column at the ends is calculated

The line of thrust at intermediate points is calculated by interpolation

The eccentricity of the column centre line from the line of thrust is found from the deformed shape of the column.

F.3 Generation of the curvature and the deflected shape

F.3.1 Outline

The initial geometrical imperfection D_0 , the initial curvature (ie the curvature from the initial geometrical imperfection) K_0 , the curvature due to bending K_{flexF} and the deflections due to bending D_{flexF} are calculated on Sheets “Mode Shape Y” and “Mode Shape X” and exported to Sheet 1. On Sheet 1, the total deflection of the member D_a is calculated from $D_a = D_0 + D_{flexF}$.

F.3.2 Generation of initial imperfection and imperfection curvature

The initial geometrical imperfection and the imperfection curvature are generated on sheet “Mode Shape Y” in columns E to K (I, J and K are not used at October 2005). At October 2005, it is assumed that the initial imperfection is a sine curve. The maximum displacement is defined on the sheet as a_i in row 5.

F.3.3 Generation of curvature due to bending

Starting curvature

The starting curvature is most conveniently generated by using the imperfection curvature plus a number of multiples of the imperfection curvature by setting U9 to the multiple required. End moments are most conveniently included in the starting curvature by copying them into column S. At October 2005, when end moments are being taken as equal and opposite, the values are copied by Copy/Paste Special - Values from $S8 = M_{end}/(dM/dK) = M_{end} * 1000000/N10$ where $N10 = dM/dK$ copied from Sheet 1. For defined end slopes, the value of U9 must be adjusted until the defined values of end slope, θ_d , is generated. This can be found by finding the end slope with curvatures from end moments alone, θ_{Mends} then finding the end slope from imperfection curvature alone, θ_i , and then finding the necessary value of U9 from S45

$$U9 = \left(\frac{\theta_d - \theta_{Mend}}{\theta_i} \right) - 1$$

Calculation of improved curvature

The subsequent values of curvature are generated with $U9 = 0$.

On Sheet 1, after calculating the axial load that can be resisted, a curvature correction is calculated for each section. This is done by finding the difference between the moment at the section and the moment required at the section to resist the applied axial load.

The curvature correction is calculated from [curvature correction] = [difference in moment]/[dM/dK], in which [dM/dK] can either be the secant value or a value nearer to the tangent stiffness as the user chooses. The ratio dM/dK is calculated on Sheet 1 in column DO as (My - old My)/(KflexF - old K) in which 'old My' and 'old K' are in column DM and column DN. They are imported manually from column DV and column DW into which they were imported from column DK and column DL. For the secant value of dM/dK, DM and DN are set to zero. For a value nearer the tangent dM/dK, DM and DN are generated from a cycle in which the curvature KflexF is reduced on sheet Mode Shape Y by using a value in Z9 less than 1.0 so that the K values in column Z (used to generate the output from Mode Shape Y) are reduced.

The curvature corrections are exported to sheet "Mode Shape Y" into columns P and Q. When ready to iterate on Mode Shape Y, these values in P and Q are copied into R and S. T9 must be set to 1.0 if 1.0 times the correction is to be used in the iteration. T41 shows the sum of the curvature corrections from Sheet1. If this is not zero, the end slopes will change unless a further correction equal and opposite to T41 is also added. This further correction is applied in column W, which adds column V times -T41 at each section. The sum of column V should be 1.0 and the sum of column W should be equal to -T41. The values of V are entered manually, generally at the central section alone or shared by the central three sections.

F.3.4 Generation of the deflected shape due to bending

Outline

The deflected shape due to bending is calculated on sheet Mode Shape Y, columns AA to BL.

The method is, on each section in turn, to

1. calculate the change of angle of the member, N_i , at each section from the curvature times segment length,
2. impose the change of angle on the member at that section, as Figure F.2.
3. calculate the displacements at all the sections from the change of angle at this section

4. sum the displacements from all the changes of angle
5. correct at each section for the difference between change of angle at a point and curvature, as Figure F.3.

Internal sections, sections 2 to 30 inclusive:

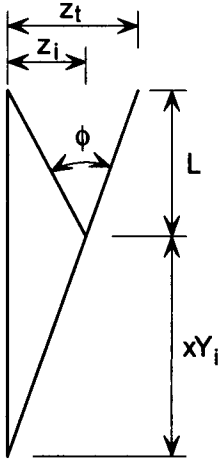


Figure F.2 Displacements of nodes from curvature at node "i"

$\phi_i = K_i \times s_i$, where 's_i' is the segment length at section 'i'

$$z_{ii} = (L - xY_i)\phi_i$$

$$z_i = z_{ii} \left(\frac{xY_i}{L} \right) = [(L - xY_i)\phi_i] \left(\frac{xY_i}{L} \right) = (L - xY_i) \left(\frac{xY_i}{L} \right) \phi_i = (L - xY_i) \left(\frac{xY_i}{L} \right) K_i s_i$$

In this model, the segments are all of equal length $s = \frac{L}{n}$, where 'n' is the number of segments

$$\therefore z_i = (L - xY_i) \left(\frac{xY_i}{L} \right) K_i \left(\frac{L}{n} \right) = \frac{(L - xY_i)(xY_i)}{n} K_i$$

The deflection at other sections, 'j', due to the curvature K_i at section 'i' is given by

$$j < i \rightarrow z_j = z_i \left(\frac{j}{i} \right)$$

$$j = i \rightarrow z_j = z_i$$

$$j > i \rightarrow z_j = z_i \left(\frac{n-j}{n-i} \right)$$

where

n = the number of segments of the member = 30,

in the spreadsheet, n = nsegments,

i = the number of segments from the bottom of the column at which the change of angle occurs

in the spreadsheet =

nofsr - 1 = number of section (for rows), from 1 to 31, -1.

j = the number of segments from the bottom of the column at which the deflection is calculated

in the spreadsheet =

nofsc - 1 = number of section (for columns), from 1 to 31, -1.

The formula in each cell for all the internal sections (sections 2 to 30) and the end sections (sections 1 and 31) is:

=KYr*(IF((nofsc-1)<(nofsr-1),zir*(nofsc-1)/(nofsr-1),IF((nofsc-1)=(nofsr-1),zir,zir*((nsegments+1-nofsc)/(nsegments+1-nofsr))))))

The deflections calculated as above for the change of angle at each section are summed to find the total deflection at each section. This sum is an over-estimate of the deflection because it assumes that the change of angle occurs as an abrupt change at a point, whereas it occurs as a curve over the length of a segment, as shown in Figure F.3:

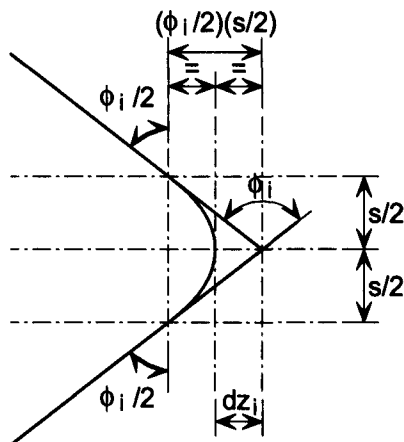


Figure F.3 Correction of displacements

$$dz_i = -\frac{1}{2} \left(\frac{\phi_i}{2} \right) \left(\frac{s}{2} \right) = -\frac{1}{2} \left(\frac{K_i \times s}{2} \right) \left(\frac{s}{2} \right) = -\frac{K_i \times s^2}{8} = -\frac{K_i}{8} \left(\frac{L}{n} \right)^2$$

$$= -KYc \cdot (L/nsegments)^2 / 8$$

Ends of member, sections 1 and 31

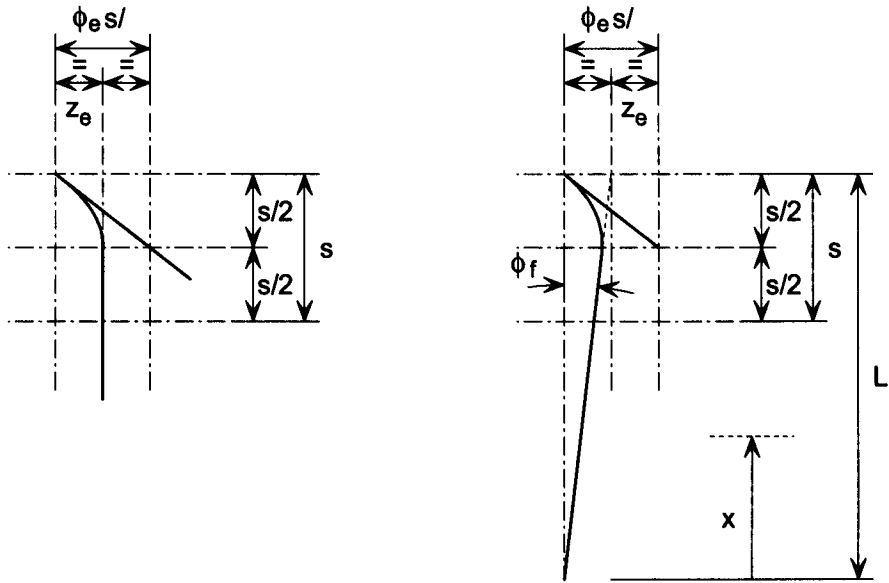


Figure F.4 Member shape at ends

At the ends of the member, the change of angle is shown in Figure F.4.

$$\phi_e = K_e \left(\frac{s}{2} \right)$$

therefore the offset of the straight line projected to the end of the member would be z_e :

$$z_e = \frac{1}{2} [\phi_e] \left(\frac{s}{2} \right) = \frac{1}{2} \left[K_e \left(\frac{s}{2} \right) \right] \left(\frac{s}{2} \right) = \frac{K_e \times s^2}{8} = \frac{K_e}{8} \left(\frac{L}{n} \right)^2$$

$$= -KYc * (L/nsegments)^2 / 8$$

It should be noted that the spreadsheet only considers no-sway columns, so 'z' at the end of the column = 0,

The deflection at other sections, 'j', due to the curvature K_e at the end is given by

$$x_j < x_i \rightarrow z_j = z_i \left(\frac{x_j}{x_i} \right), \text{ which gives the deflections due to curvature at the top}$$

$$x_j > x_i \rightarrow z_j = z_i \left(\frac{L - x_j}{L - x_i} \right), \text{ which gives the deflections due to curvature at the bottom}$$

where

n = the number of segments of the member = 30,

in the spreadsheet, n = nsegments,

i = the number of segments from the bottom of the column at which the change of angle occurs

in the spreadsheet =

nofsr -1 = number of section (for rows), from 1 to 31, -1.

j = the number of segments from the bottom of the column at which the deflection is calculated

in the spreadsheet =

nofsc - 1 = number of section (for columns), from 1 to 31, -1.

The formula in each cell for all the internal sections (sections 2 to 30) and the end sections (sections 1 and 31) is:

$$=KYr*(IF((nofsc-1)<(nofsr-1),zir*(nofsc-1)/(nofsr-1),IF((nofsc-1)=(nofsr-1),zir,zir*((nsegments+1-nofsc)/(nsegments+1-nofsr))))))$$

The values of deflection due to the curvature concentrated at each section are summed in column BI:

$$Sumzi = \sum_1^{31} z$$

The value of the deflection at section 'i' due to flexure allowing for the curvature dz_i is given in column BL:

$$DiF = Sumzi + dz_i$$

The values of DiF are copied into the column BS via BQ and exported automatically from BS into Sheet 1 in which they are the values of DflexF, the deflection due to flexure.

F.3.5 Calculation of end-slope

The end slope is calculated from the sum of:

the slope due to the deflection of the internal sections

the slope from the curvature at the end sections.

The slope due to the deflection of the internal sections is given by the slope of a straight line from the end of the member to the penultimate section

= z_{pt}/s , where $z_{pt} = SumziY$ at the penultimate section at the top of the member

= z_{pb}/s , where $z_{pb} = SumziY$ at the penultimate section at the bottom of the member

see Figure F.5.

The slope from the curvature at the end sections = ϕ_{er} shown in Figure F.5.

$$\phi_{er} = \phi_e - \phi_{ep} \text{ where } \phi_e = K_e \left(\frac{s}{2} \right) \text{ and } \phi_{ep} = \frac{z_e}{s}$$

$$\text{where } z_e = \frac{1}{2} [\phi_e] \left(\frac{s}{2} \right) = \frac{1}{2} \left[K_e \left(\frac{s}{2} \right) \right] \left(\frac{s}{2} \right) = \frac{K_e \times s^2}{8}$$

$$\phi_{er} = \phi_e - \phi_{ep} = K_e \left(\frac{s}{2} \right) - \frac{z_e}{s} = K_e \left(\frac{s}{2} \right) - \frac{1}{s} \frac{K_e \times s^2}{8} = K_e \left(\frac{s}{2} - \frac{s}{8} \right) = \frac{3}{8} K_e s$$

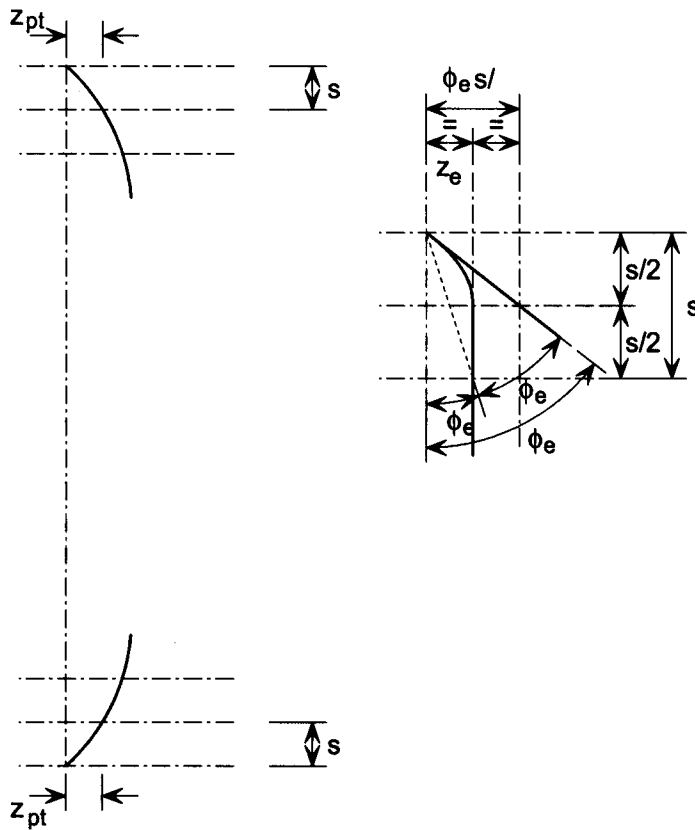


Figure F.5 End-shape from curvature in end sections

F.3.6 Calculation of next shape

On Sheet "Mode Shape Y", the next shape is generated as follows:

1. the total change of slope at all 31 nodes is found by summing dK
2. for solutions with a defined (equal and opposite) end slope, an equal and opposite total curvature is assigned to the nodes so that there is no change to the end-slopes. This assignment is done manually according to the deformed shape. Generally the most efficient method is to assign all this to the central nodes, often assigning all to the central node.
3. the new curvature from flexure is generated by adding
 - the previous values of curvatures from flexure, K_{flexY} from Sheet 1,
 - the change in curvature, dKY from Sheet 1,
 - the manually assigned equal and opposite curvatures
4. the new deflections from flexure arising from the new curvature from flexure are generated
5. the new curvature from flexure and the new deflections from curvature are exported to Sheet 1

F.4 Calculation of the moment induced by curvature

The calculated moment allows for the effects of plasticity and for the effects of residual stresses and of the axial load.

The calculations, performed for each of 30 sections along the length of the section, are as follows:

1. Calculate the total stresses from curvature + axial load + residual stresses, assuming the section remains elastic
2. Calculate the elastic-plastic stress diagram
3. Calculate the moment about the centre-line of the column limiting the compressive stresses to yield
4. Check that the calculated tensile stresses do not exceed yield.

Step 4 is required because at October 2005, the spreadsheet does not handle tensile strains in excess of yield strain.

F.4.1 Calculate the total “elastic” stresses

Calculate the residual stresses

The residual stresses are defined on Sheet 1 and a stress distribution is calculated on Sheet “res stress”

Input data are:

1. f_r/f_y , the ratio of maximum compressive residual stress to the yield stress
2. A_w , the web area, which appears because the spread sheet is derived from a spreadsheet for I-sections; for SHS, $A_w = 0$ **but it needs reconsidering for RHS**

$$f_{rmin} = -f_r / (2 + 3A_w / 4t_f Y)$$

$$a = (f_r - b) / Y^2$$

It is assumed that the stress distribution is parabolic, with compression at the corners of the section, as shown in Figure F.6.

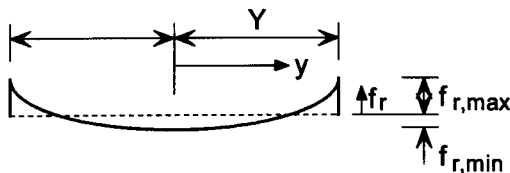


Figure F.6 Residual stress distribution

Assuming that the residual stress distribution is parabolic

$$f_r = ay^2 + f_{rmin}$$

At the edge of the section, $f_{r \max} = aY^2 + f_{r \min}$

$$\therefore aY^2 = f_{r \max} - f_{r \min}$$

$$\therefore a = \frac{(f_{r \max} - f_{r \min})}{Y^2}$$

The total force on the flange is:

$$\begin{aligned} N &= \int_{-Y}^Y f_r dA = \int_{-Y}^Y (ay^2 + f_{r \min}) (T dy) = T \left[\frac{ay^3}{3} + (f_{r \min})y \right]_{-Y}^Y \\ &= T \left[\left(\frac{aY^3}{3} \right) - \left(-\frac{aY^3}{3} \right) + (f_{r \min}Y) - (-f_{r \min}Y) \right] = 2T \left[\left(\frac{aY^3}{3} \right) + (f_{r \min}Y) \right] \end{aligned}$$

But the total force from residual stresses = 0, so:

$$\begin{aligned} 0 &= 2T \left[\left(\frac{aY^3}{3} \right) + (f_{r \min}Y) \right] \\ &= 2T \left[\left(\frac{f_{r \max} - f_{r \min}}{Y^2} \right) \frac{Y^3}{3} + (f_{r \min}Y) \right] = 2T \left[(f_{r \max} - f_{r \min}) \frac{Y}{3} + (f_{r \min}Y) \right] \\ &= 2T \left[\frac{f_{r \max}}{3} - \frac{f_{r \min}}{3} + f_{r \min} \right] Y = 2T \left[\frac{f_{r \max}}{3} + \frac{2f_{r \min}}{3} \right] Y = \frac{2TY}{3} [f_{r \max} + 2f_{r \min}] \\ \therefore f_{r \min} &= \frac{f_{r \max}}{2} \text{ for a Square Hollow Section} \end{aligned}$$

Calculate the "elastic" stress from axial compression

The "elastic" stress from axial compression $f_a = f_{ave} = \frac{N}{A_g}$, as shown in Figure F.7.

where N is the applied axial compression

and A_g is the gross area of the section

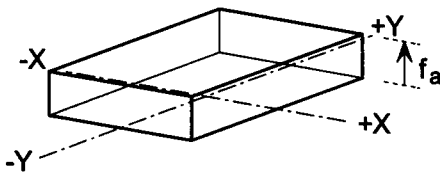


Figure F.7 Average compression stress

Calculate the “elastic” stress from curvature

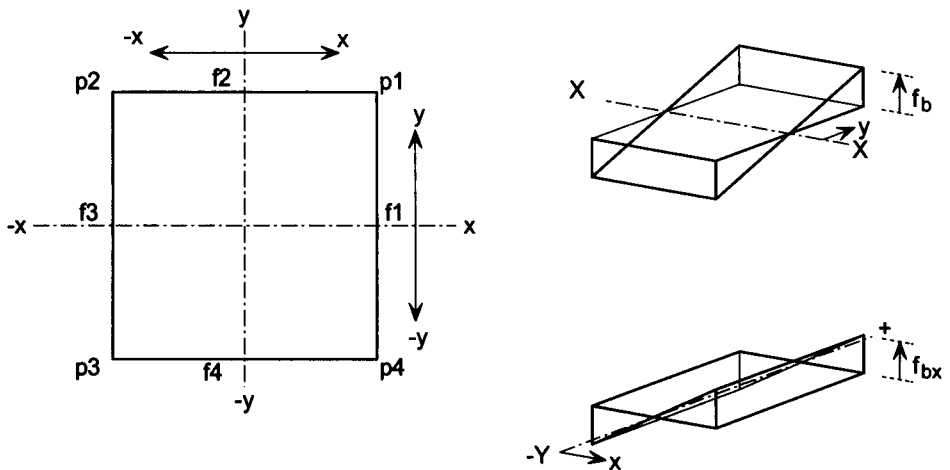


Figure F.8 “Elastic” bending stresses

The “elastic” stress from curvature, as shown in Figure F.8, is given by:

$$f_{bx} = E \times y \times K_{\text{flex } F_x} \text{ for curvature about the x-x axis}$$

$$f_{by} = E \times x \times K_{\text{flex } F_y} \text{ for curvature about the y-y axis}$$

where E is Young’s modulus

y is the distance from the elastic neutral axis parallel to the x-x axis

x is the distance from the elastic neutral axis parallel to the y-y axis

$K_{\text{flex } F_x}$ is the curvature due to flexure about the x-x axis

and $K_{\text{flex } F_y}$ is the curvature due to flexure about the y-y axis

F.4.2 Calculate the elastic-plastic stress diagram

The elasto-plastic stress diagram is shown in Figure F.9 for one side of a member of total width = $2X$. The procedure followed by the spreadsheet is:

1. Find where the “elastic” stresses exceed the yield stress.
2. Limiting the stresses to yield stress in compression, calculate the axial load resisted
3. Find the axial load error between the design axial load and the axial load resisted
4. Find the increase required of the axial stresses to correct the axial load error
5. Iterate to correct axial compression

For an SHS

Find where the “elastic” stresses exceed the yield stress

The “elastic” stress is the stress the would occur if there were no plasticity. This is the strain multiplied by the Young’s modulus = ϵE .

The “elastic” stress along any side is the sum of:

the residual stress which along faces 2 and 4 is $f_r = ay^2 + f_{r \min}$

the mean axial stress $f_a = f_{ave} = \frac{N}{A_g}$

the bending stress which is $f_b = E \times K_{flexFy} \times x + E \times K_{flexFx} \times y$

along faces 2 and 4, the “elastic” bending stress from curvature about the x-x axis is:

$$f_{bx} = \pm f_{bxY} = E \times K_{flexFx} (\pm Y)$$

$$\therefore f_b = E \times K_{flexFy} \times x + E \times K_{flexFx} \times (\pm Y) = E \times K_{flexFy} \times x \pm f_{bxY}$$

The general case of the “elastic” stresses is:

along faces 1 and 3, $f_e = (f_{r \min} + ay^2) + f_a \pm f_{byX} + E \times K_{flexFx} \times y$

along faces 2 and 4, $f_e = (f_{r \min} + ax^2) + f_a \pm f_{bxY} + E \times K_{flexFy} \times x$

The “elastic” stresses at each of the corners p1, p2, p3, p4 are f_{ep1} , f_{ep2} , f_{ep3} , f_{ep4} , where

$$f_{ep} = f_a \pm f_{bxY} \pm f_{byX} + f_{r \max}$$

eg, $f_{ep1} = f_a + f_{bxY} + f_{byX} + f_{r \max}$

the “elastic” stresses at mid-length of each of the sides f1, f2, f3, f4 are f_{ef1Y0} , f_{ef2X0} , f_{ef3Y0} , f_{ef4X0} , where:

eg $f_{ef2X0} = f_a + f_{bxY} + f_{r \min}$

The coordinates of the point of minimum “elastic” stress in the plane of each side, which may occur outside the section, are $y_{f \min f1}$, $x_{f \min f2}$, $y_{f \min f3}$, $x_{f \min f4}$.

For the minimum stress along face 2, $\frac{d(f_e)}{dx} = 0$,

$$\therefore 0 = \frac{d(f_e)}{dx} = \frac{d}{dx} \left\{ (f_{r \min} + ax^2) + f_a \pm f_{bxY} + E \times K_{flexFy} \times x \right\}$$

$$\therefore 0 = \left\{ (0 + 2ax) + 0 \pm 0 + E \times K_{flexFy} \right\}$$

$$\therefore 2ax + E \times K_{flexFy} = 0$$

$$\therefore x_{\min f2} = -\frac{E \times K_{flexFy}}{2a}$$

The minimum “elastic” stress in the plane of each face is $f_{\min f1}$, $f_{\min f2}$, $f_{\min f3}$, $f_{\min f4}$, where:

along face 2, $f_{\min f2} = (f_{r \min} + ax_{\min f2}^2) + f_a + f_{bxY} + E \times K_{flexFy} \times x_{\min f2}$

the coordinates of the points at which the “elastic” stress reaches yield in the plane of each face, which may occur outside the section, are y_{pfyf1} , y_{nfyf1} , x_{pfyf2} , x_{nfyf2} , y_{pfyf3} , y_{nfyf3} , x_{pfyf4} , x_{nfyf4} .

If f_{minf} is greater than the yield, f_y , then the value of are y_{pfyf1} , y_{nfyf1} , x_{pfyf2} , x_{nfyf2} , y_{pfyf3} , y_{nfyf3} , x_{pfyf4} , x_{nfyf4} is taken as 0 because this value is used to define the extent of the plastic zone.

Along face 2, where $f_{minf2} \leq f_y$ the point at which the “elastic” stress reaches yield is

calculated from $f_e = f_y = (f_{rmin} + ax_{fyf2}^2) + f_a + f_{bxY} + E \times K_{flexFy} \times x_{fyf2}$

$$\therefore (f_{rmin} + ax_{fyf2}^2) + f_a + f_{bxY} + E \times K_{flexFy} \times x_{fyf2} - f_y = 0$$

Re-arranging in the classic solution of a quadratic equation:

$$ax^2 + bx + c = 0 \Rightarrow x = \frac{-b \pm \sqrt{b^2 - 4ac}}{2a}$$

$$\therefore ax_{fyf2}^2 + E \times K_{flexFy} \times x_{fyf2} + (-f_y + f_{rmin} + f_a + f_{bxY}) = 0$$

$$\therefore x_{fyf2} = \frac{-(E \times K_{flexFy}) \pm \sqrt{(E \times K_{flexFy})^2 - 4a(-f_y + f_{rmin} + f_a + f_{bxY})}}{2a}$$

$$\therefore x_{pfyf2} = \frac{-(E \times K_{flexFy}) + \sqrt{(E \times K_{flexFy})^2 - 4a(-f_y + f_{rmin} + f_a + f_{bxY})}}{2a}$$

$$\therefore x_{nfyf2} = \frac{-(E \times K_{flexFy}) - \sqrt{(E \times K_{flexFy})^2 - 4a(-f_y + f_{rmin} + f_a + f_{bxY})}}{2a}$$

$$x_{pfyf2} = \text{IF}(f_{minf2} > f_y, 0, (-(E \times K_{flexFy}) + \text{SQRT}((E \times K_{flexFy})^2 - 4 \times a \times (-f_y + f_{rmin} + f_a + f_{bxY})))) / (2 \times a)$$

$$x_{nfyf2} = \text{IF}(f_{minf2} > f_y, 0, (-(E \times K_{flexFy}) - \text{SQRT}((E \times K_{flexFy})^2 - 4 \times a \times (-f_y + f_{rmin} + f_a + f_{bxY})))) / (2 \times a)$$

The limit of the elastic zone (p = positive, n = negative) along each face is defined as y_{pecf1} , y_{necf1} , x_{pecf2} , x_{necf2} , y_{pecf3} , y_{necf3} , x_{pecf4} , x_{necf4}

If the “elastic” stress does not reach yield within the section, then the values of y_{pecf1} , y_{necf1} , x_{pecf2} , x_{necf2} , y_{pecf3} , y_{necf3} , x_{pecf4} , x_{necf4} are taken as the distance to the edge of the section from the neutral axis as follows:

$$y_{pecf1} = Y, y_{necf1} = -Y, y_{pecf3} = Y, y_{necf3} = -Y$$

$$x_{pecf2} = X, x_{necf2} = -X, x_{pecf4} = X, x_{necf4} = -X$$

If the “elastic” stress does reach yield within the section, then the values of ypecf1, ynecf1, xpecf2, xnecf2, ypecf3, ynecf3, xpecf4, xnecf4 are as follows:

$$ypecf1 = ypfyf1, ynecf1 = ynfyf1, ypecf3 = ypfyf3, ynecf3 = ynfyf3,$$

$$xpecf2 = xpfyf2, xnecf2 = xnfyf2, xpecf4 = xpfyf4, xnecf4 = xnfyf4,$$

Where the “elastic” stress exceeds yield throughout the length of the side, the IF statements will use the values for reaching yield, eg xpfyf2 and xnfyf2 which will be =0 if the “elastic” stress exceeds yield throughout the length of the side.

$$=IF(xpfyf2 > X, X, (IF(xpfyf2 < -X, -X, xpfyf2)))$$

$$=IF(xnfyf2 < -X, -X, (IF(xnfyf2 > X, X, xnfyf2)))$$

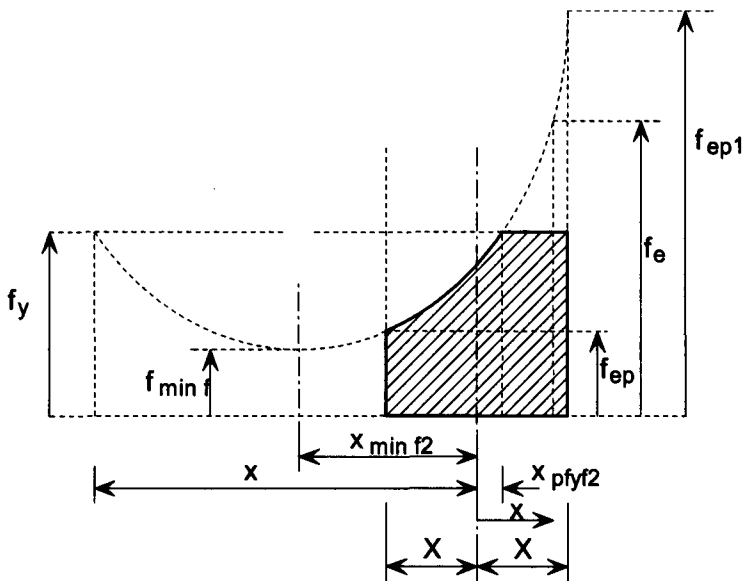


Figure F.9 Stress diagram for one wall of width 2X

Calculate the axial load resisted

The axial compression resisted by the plastic zones, if any, are defined as Nef1, Nef2, Nef3, Nef4.

The force is the integral of the stress over the elastic area (which is the area where the stress is less than yield).

$$N_{ef} = \int_{Ae} f_e \times dA \text{ where } f_e = (f_{r \min} + ax^2) + f_a \pm f_{bxY} + E \times K_{flexFy} \times x$$

The extent of the elastic zone depends on the “elastic” stresses along each face.

As shown in Figure F.10(a), the stresses in the section might all be less than yield, so the extent is from -X to +X or to -Y to +Y. Alternatively, the “elastic” stress may reach yield within the width of the section, giving a reduced extent of the elastic zone, as shown in Figure F.10(b) and (c). The variables ypecf1, ynecf1, xpecf2, xnecf2, ypecf3, ynecf3, xpecf4, xnecf4 are so defined as to give the limit as either the edge of the section or the point

at which the “elastic” stresses reach yield. Writing the positive extent as “xp”, eg instead of xpecf2, and the negative extent as “xn”, eg instead of xnecf2, the integral can be written:

$$\begin{aligned}
 N_{ef} &= \int_{x_n}^{x_p} \{f_e\} \times (t \times dx) = t \int_{x_n}^{x_p} \left\{ ax^2 + (E \times K_{flexFy})x + (f_{r\ min} + f_a + f_{bxY}) \right\} dx \\
 &= t \left[a \frac{x^3}{3} + (E \times K_{flexFy}) \frac{x^2}{2} + (f_{r\ min} + f_a + f_{bxY})x \right]_{x_n}^{x_p} \\
 &= t \left[a \frac{x_p^3 - x_n^3}{3} + (E \times K_{flexFy}) \frac{x_p^2 - x_n^2}{2} + (f_{r\ min} + f_a + f_{bxY})(x_p - x_n) \right]
 \end{aligned}$$

eg for face 2, $N_{ef2} = t * (a * ((x_{pecf2})^3 - (x_{necf2})^3) / 3 + E * K_{flexFy} * ((x_{pecf2})^2 - (x_{necf2})^2) / 2 + (f_{rmin} + f_a + f_{bxY}) * (x_{pecf2} - x_{necf2})) / 1000$

The axial compression resisted by the plastic zones, if any, are defined as Npp1f1, Npp1f2, Npp2f2, Npp2f3, Npp3f3, Npp3f4, Npp4f4, Npp4f1. Where there is a plastic zone, the force is the integral from the end of the elastic zone to the edge of the section.

$$N_p = \int_{A_p} f_y \times dA = \int_{A_p} f_y (t \times dx)$$

This is calculated using the variables ypecf1, ynecf1, xpecf2, xnecf2, ypecf3, ynecf3, xpecf4, xnecf4 and the distances to the extreme fibres of the section along the side considered, +X, -X, +Y, -Y. For example, on face 2 and at point 1,

$$N_{pp1f2} = \int_{x_{pecf2}}^X f_y (t \times dx) = f_y \times t \int_{x_{pecf2}}^X dx = f_y \times t [x]_{x_{pecf2}}^X = f_y \times t (X - x_{pecf2})$$

The axial force on all the plastic and elastic zones that is actually resisted by the stress diagram derived above is defined as Na:

$$N_a = \sum_{ij} N_{ppifj} + \sum_j N_{efj}$$

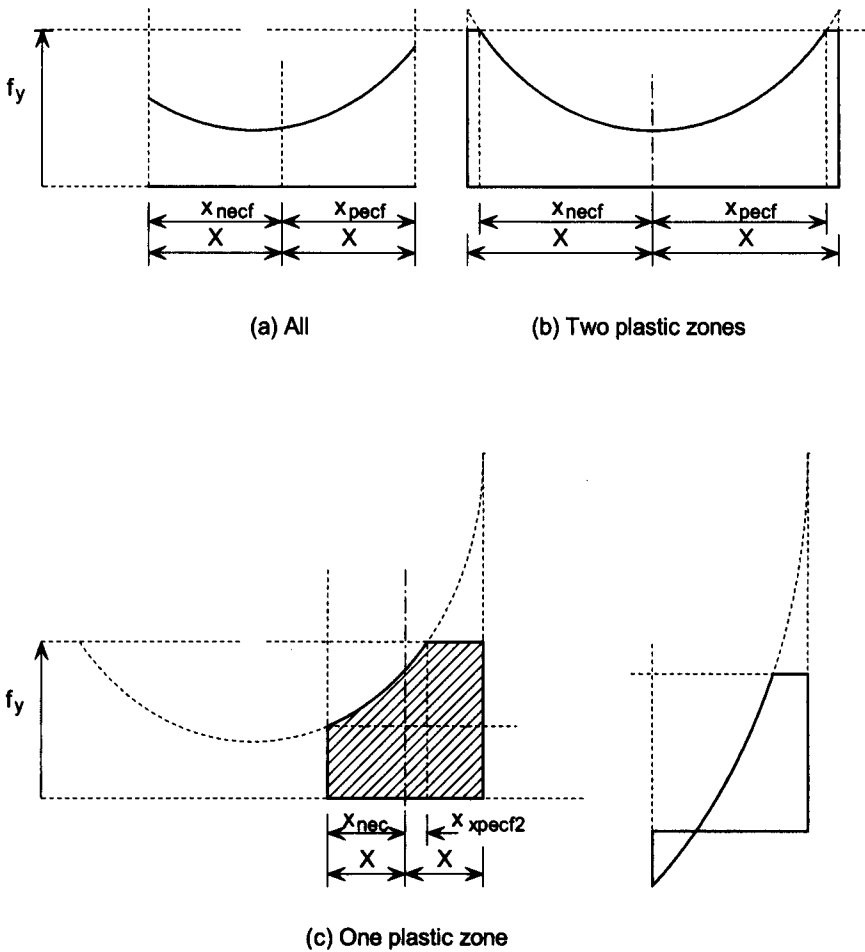


Figure F.10 Possible stress distributions

Find the error in the axial compression actually on the section

dN_a = the difference between the design load, N , and the force actually resisted by the stress diagram above load, N_a .

$$dN_a = N - N_a$$

Calculate the correction required for the axial compression

To increase the axial force resisted by the stress diagram, the axial strain must be increased. This is shown below in terms of a corrective compressive “elastic” stress, f_c , which equals the corrective compressive strain, ϵ_c , multiplied the Young’s modulus, E . The spreadsheet uses f_c and does not explicitly use $\epsilon_c \times E$.

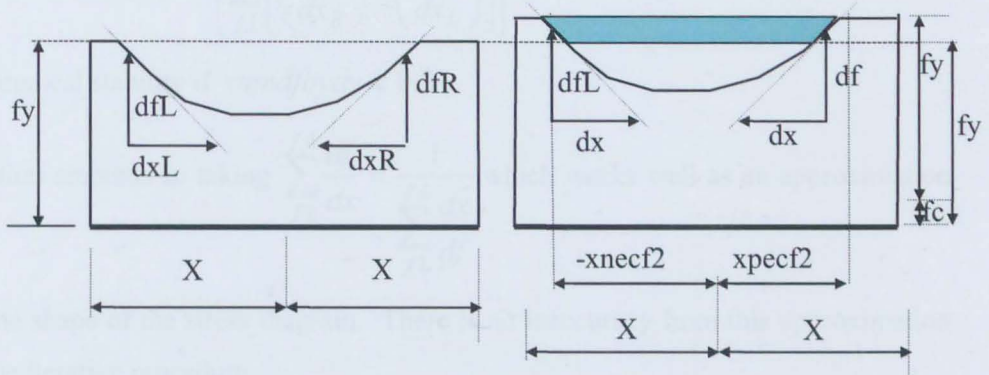


Figure F.11 Correction of axial force resisted

The increase in the axial force resulting from the “elastic” stress f_c is shown by the shaded area in Figure F.11. The areas either side are at yield stress, so there is no increase in axial force resisted from the increased strain. Assuming the sides of the shaded area are straight lines at the slope of the stress diagram at the top of the shaded area, with slopes of $-df_L/dx_L$ and $+df_R/dx_R$, then

$$dN = f_c (x_{pecf2} - x_{necf2})t - \frac{1}{2}f_c \left(\frac{dx_R}{df_R} f_c \right)t + \frac{1}{2}f_c \left(\frac{dx_L}{df_L} f_c \right)t$$

$$= \left\{ -\frac{1}{2} \left[\left(\frac{dx_R}{df_R} \right) + \left(\frac{dx_L}{df_L} \right) \right] t \right\} f_c^2 + \left\{ (x_{pecf2} - x_{necf2})t \right\} f_c$$

For convenience write in terms of “y” instead of “x” for faces 2 and 4 and “y” for faces 1 and 3

$$\sum_{f1}^{f4} dN = \left\{ -\frac{1}{2} \sum_{f1}^{f4} \left[\left(\frac{dx_R}{df_R} \right) + \left(\frac{dx_L}{df_L} \right) \right] t \right\} f_c^2 + \left\{ \sum_{f1}^{f4} (x_{pecf2} - x_{necf2})t \right\} f_c$$

Writing $A_e = \left\{ \sum_{f1}^{f4} (x_{pecf2} - x_{necf2})t \right\}$,

To limit the number of columns in the spreadsheet, which is an important issue for a manageable spreadsheet, a substitution of an approximation is used as follows:

$$sumdybydf = \left\{ \sum_{f1}^{f4} \left[\left(\frac{dx_R}{df_R} \right) + \left(\frac{dx_L}{df_L} \right) \right] \right\}, \text{ where } sumdybydf = \frac{1}{mod\ dfbydy} \text{ where}$$

$$\text{mod } dfbydy = \text{sum}dfbydy = \left\{ \sum_{f1}^{f4} \left[\left(\frac{df_R}{dx_R} \right) + \left(\frac{df_L}{dx_L} \right) \right] \right\} \text{ but taking mod } dfbydy = 0.01 \text{ to}$$

retain mathematical stability if $\text{sum}dfbydy < 0.01$

The substitution amounts to taking $\sum_{f1}^{f4} \frac{df}{dx} = \frac{1}{\sum_{f1}^{f4} \frac{dx}{df}}$ which works well as an approximation

because of the shape of the stress diagram. There is no inaccuracy from this approximation because of the iterative procedure.

$$\text{Also writing } \sum_{f1}^{f4} dN = dN_a$$

Then

$$-\frac{1}{2} \{ \text{sum}dybydf \} f_c^2 + A_e f_c - dN_a = 0$$

$$\therefore \frac{1}{2} \{ \text{sum}dybydf \} f_c^2 - A_e f_c + dN_a = 0$$

Re-arranging in the classic solution of a quadratic equation

$$ax^2 + bx + c = 0 \Rightarrow x = \frac{-b \pm \sqrt{b^2 - 4ac}}{2a}$$

$$f_c = \frac{A_e \pm \sqrt{A_e^2 - 4 \left[\frac{1}{2} (\text{sum}dybydf) \right] (dN_a)}}{2 \left[\frac{1}{2} (\text{sum}dybydf) \right]}$$

If there is no plasticity, then there is no effect of the slope of the stress diagram and the change of stress is equal to f_{capp} , where

$$f_{capp} = \frac{dN_a}{A_e}$$

The formula for f_c in the spreadsheet is written

$$=IF(\text{sum}dybydf=0, f_{capp}, (A_e - \text{SQRT}(A_e^2 - 4 * (\text{tf} * \text{sum}dybydf / 2) * (dNa * 1000))) / (2 * (\text{tf} * \text{sum}dybydf / 2)))$$

The values of dy/df and dx/df are found by inverting the values of df/dy and df/dx where the latter are found for example by

$$\frac{d(f_e)}{dx} = \frac{d}{dx} \left\{ (f_{r \min} + ax^2) + f_a \pm f_{bxY} + E \times K_{flexFy} \times x \right\} = \left\{ (0 + 2ax) + 0 \pm 0 + E \times K_{flexFy} \right\} T$$

herefore $\frac{d(f_e)}{dx} = 2ax + E \times K_{flexFy}$ and $\frac{d(f_e)}{dy} = 2ay + E \times K_{flexFx}$ calculated at the points

where the stress diagram reaches yield, ie at y_{pecf1} , y_{necf1} , x_{pecf2} , x_{necf2} , y_{pecf3} , y_{necf3} , x_{pecf4} , x_{necf4} .

Iterate to correct axial compression

The final step in the iterative procedure is to calculate $f_{aplustc}$ = the previous “elastic” axial stress, f_a , plus the correction, f_c . For subsequent iterations, the calculations in 4.2.1 to 4.2.4 above are repeated after feeding $f_{aplustc}$ into f_a for the next iteration of finding the stress diagram. The criterion to show conversion is that the axial force resisted, N_a , is equal to the design axial force, N , at all sections. At October 2005, this has always been achieved to less than 1kN in 3 iterations after the first set of calculations.

Check that the tensile stresses do not exceed yield.

Check that the calculated tensile stresses do not exceed yield because, at October 2005, the spreadsheet does not handle tensile strains in excess of yield strain.

Check is done on the minimum of f_{ep1} , f_{ep2} , f_{ep3} , f_{ep4} and f_{ef1Y0} , f_{ef2X0} , f_{ef3Y0} , f_{ef4X0}

F.4.3 Calculate the moment resisted by the column

The moment is calculated about the centre-line of the column using the “elastic-plastic” stress diagram calculated in 4.2 above, in which the compressive stresses do not exceed yield.

The moments from plastic zones are calculated from the lever-arm multiplied by the force, as shown in Figure F.12. For the unshaded areas, the contribution to the bending moment is calculated from the axial force resisted \times the lever-arm from the geometrical centres of the area. For the shaded areas, it is calculated by integration about the axis of bending.

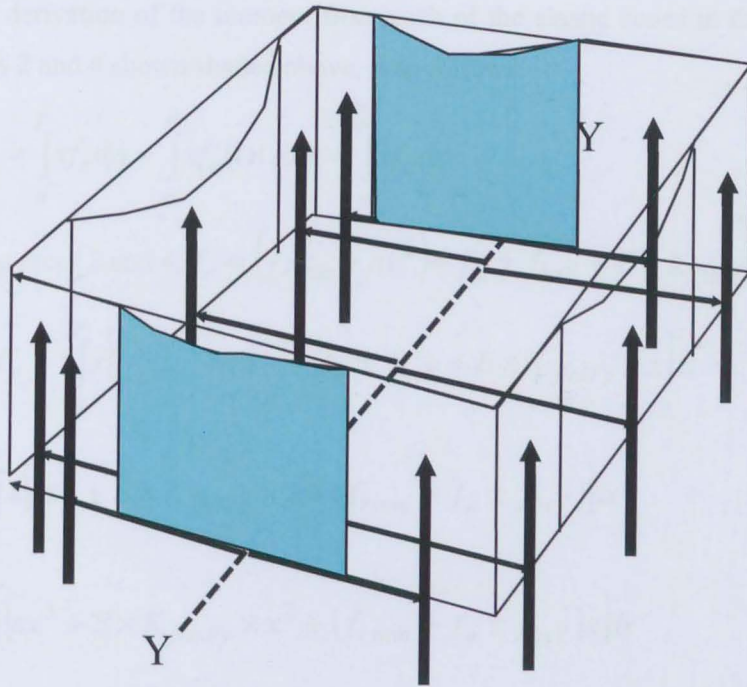


Figure F.12 Calculation of bending moment resisted

The lever arms from the centre of force of the plastic zones about the neutral axis of the column are defined as $layNpp1f1$, $layNpp1f2$, $layNpp2f2$, $layNpp2f3$, $layNpp3f3$, $layNpp3f4$, $layNpp4f4$, $layNpp4f1$, where lay is about the y-y axis.

My = the total moment about the y-y axis

$$My = Myf1 + Myf2 + Myf3 + Myf4$$

$Myf1$, $Myf2$, $Myf3$, $Myf4$ = the moments about the y-y axis from faces 1, 2, 3, 4

$$Myf1 = (Npp1f1 + Nef1 + Npp4f1) * X / 1000$$

$$Myf2 = Meyf2 + layNpp1f2 * Npp1f2 / 1000 + layNpp2f2 * Npp2f2 / 1000$$

$$Myf3 = (Npp2f3 + Nef3 + Npp3f3) * (-X) / 1000$$

$$Myf4 = Meyf4 + layNpp4f4 * Npp4f4 / 1000 + layNpp3f4 * Npp3f4 / 1000$$

$Meyf2$, $Meyf4$ = the moments about the y-y axis from the elastic zone on each face

$$Meyf2 = tf * (a * ((xpecf2)^4 - (xnecf2)^4) / 4 + E * KflexFy * ((xpecf2)^3 - (xnecf2)^3) / 3$$

$$+ (frmin + fa + fbxY) * ((xpecf2)^2 - (xnecf2)^2) / 2) / 1000000$$

$$Meyf4 = tf * (a * ((xpecf4)^4 - (xnecf4)^4) / 4 + E * KflexFy * ((xpecf4)^3 - (xnecf4)^3) / 3$$

$$+ (frmin + fa - fbxY) * ((xpecf4)^2 - (xnecf4)^2) / 2) / 1000000$$

Similar expressions are used for the moment about the x-x axis

M_x = the total moment about the x-x axis

$M_{xf1}, M_{xf2}, M_{xf3}, M_{xf4}$ = the moment about the x-x axis from faces 1, 2, 3, 4

M_{exf1}, M_{exf3} = the moments about the x-x axis from the elastic zone on each face

The derivation of the moment from each of the elastic zones in the plane of the curvature, faces 2 and 4 shown shaded above, is as follows:

$$M_e = \int_n^p x f_e dA = \int_n^p x f_e (t \times dx) = t \int_n^p x f_e dx$$

along faces 2 and 4, $f_e = (f_{r\min} + ax^2) + f_a \pm f_{bxY} + E \times K_{flexFy} \times x$

$$\therefore M_e = t \int_n^p x [(f_{r\min} + ax^2) + f_a \pm f_{bxY} + E \times K_{flexFy} \times x] dx$$

$$= t \int_n^p x [ax^2 + E \times K_{flexFy} \times x + (f_{r\min} + f_a \pm f_{bxY})] dx$$

$$= t \int_n^p [ax^3 + E \times K_{flexFy} \times x^2 + (f_{r\min} + f_a \pm f_{bxY})x] dx$$

$$= t \left[a \frac{x^4}{4} + E \times K_{flexFy} \times \frac{x^3}{3} + (f_{r\min} + f_a \pm f_{bxY}) \frac{x^2}{2} \right]_n^p$$

$$= t \left[a \frac{(x_p^4 - x_n^4)}{4} + E \times K_{flexFy} \times \frac{(x_p^3 - x_n^3)}{3} + (f_{r\min} + f_a \pm f_{bxY}) \frac{(x_p^2 - x_n^2)}{2} \right]$$

APPENDIX G TABLES OF RESULTS OF PARAMETRIC STUDY

G.1 Introduction

This Appendix gives the results of the results from the parametric study of the compression resistance of the columns. All the results are for 140×140×10 SHS sections in S355 steel.

G.2 Mid-height displacements

Figure G.1 shows the mid-height displacements for members with an initial imperfect in the +Y direction and imposed end rotations in different planes. The figure includes a list of the Abaqus analysis runs used to generate the mid-height displacements.

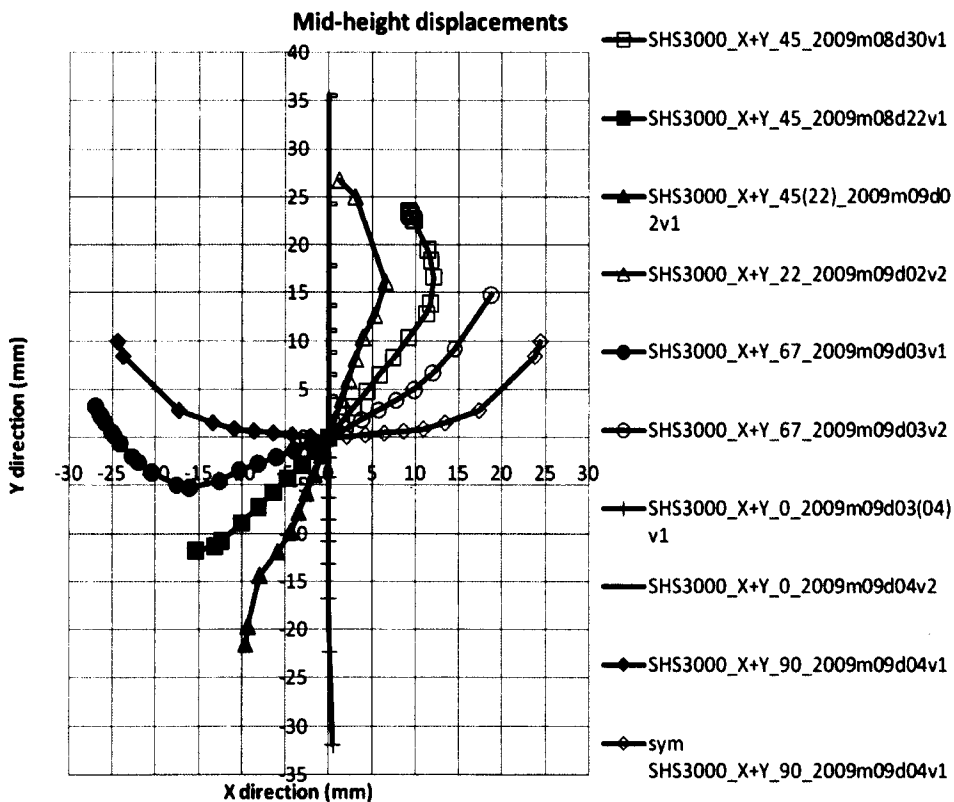


Figure G.1 Mid-height displacements – rotations at 22.5° intervals

G.3 1.5m columns

The results of the Abaqus analysis for columns of 1.5m length are presented in Table G.1 for the initial imperfection and end-rotations in the $X = 0$ plane.

Table G.2 for the initial imperfection in the $X = 0$ plane and end-rotations in the $Y = 0$ plane. Table G.3 for the initial imperfection in the $X = 0$ plane and end-rotations in the $X = Y$ plane by imposing rotation about $X = Y$ axis, rotation forcing displacement in the same direction as the initial imperfection.

Table G.4 for the initial imperfection in the $X = 0$ plane and end-rotations in the $X = Y$ plane by imposing equal rotations about X and Y axes, rotation forcing displacement in the opposite direction as the initial imperfection. This case is not a worst case so is not especially interesting.

Table G.5 lists early analyses performed for the 2007 SSRC paper [King 2007] for the initial imperfection in the $X = 0$ plane and end-rotations in the $X = Y$ plane by imposing equal rotations about X and Y axes. The results of these analyses were somewhat uncertain because the maximum load was that at the point where the end moment passes through zero from destabilising to stabilising, but this occurred at different loads for the two axes of enforced rotation, the X and Y axes. Therefore these results are inferior to those of Table G.3.

Table G.1 1.5m column, rotation in X=0 plane

Initial imperfection in the X = 0 plane in Y +ve direction

End rotations in the plane of the initial imperfection and in the same direction as the initial imperfection

Max from SHS2006m10d22_130by10_by1500v1 All results other from SHS2006m10d22_130by10_by1500v2	UR1 = end rot (radians)	RF3 = compn (kN)	end of analysis	End moment (kN-m)
Max pin-ended	0.00220	1769.8	buckled	0 (pinned)
	0.00291	1767.1	continued	0 (pinned)
	0.00446	1747.3	continued	0 (pinned)
	0.00596	1726.7	continued	0 (pinned)
	0.00741	1707.0	continued	0 (pinned)
	0.00952	1679.1	continued	0 (pinned)
	0.01254	1640.7	continued	0 (pinned)
	0.01680	1589.6	continued	0 (pinned)
	0.02272	1524.0	continued	0 (pinned)
	0.03081	1443.4	continued	0 (pinned)
	0.04168	1348.4	continued	0 (pinned)
	0.05696	1233.6	continued	0 (pinned)

Table G.2 1.5m column, rotn in Y=0 plane				
Initial imperfection in the X = 0 plane in Y +ve direction				
End rotations <u>perpendicular</u> to the plane of initial imperfection				
	UR1 = end rot (radians)	RF3 = compn (kN)	end of analysis	End mmt kN-m
SHS2006m10d24_130by10by1500 _2planes_v1	0.00481	1730.7	buckles	2.18 destabilising
SHS2006m10d24_130by10by1500 _2planes_v2	0.00942	1696.1	buckles	0.45 destabilising
SHS2006m10d24_130by10by1500 _2planes_v3	0.01386	1663.6	continues	0
SHS2006m10d24_130by10by1500 _2planes_v4	0.01797	1617.6	ditto	0
SHS2006m10d24_130by10by1500 _2planes_v5b	0.03252	1465.2	ditto	0
End moment zero by interpolation				

Table G.3 1.5m column, rotation in the X=Y plane (1)				
Initial imperfection in the X = 0 plane in Y +ve direction				
End rotations at 45° to the plane of initial imperfection with the component in the plane of the initial imperfection in the <u>same</u> direction as the initial imperfection				
	max end rot in X=Y plane (radians)	RF3 = compn (kN)	end of analysis	End moment (kN-m)
SHS1500_X+Y_45_2009m09d27v1	0.00905	1659	end moment changing to stabilising	0 by interpola tion
SHS1500_X+Y_45_2009m08d30v2	0.01695	1559	ditto	ditto
SHS1500_X+Y_45_2009m08d30v4	0.02165	1508	ditto	ditto
SHS1500_X+Y_45_2009m09d28v2	0.02418	1483	ditto	ditto
SHS1500_X+Y_45_2009m09d29v3	0.03096	1424	ditto	ditto

Table G.4 1.5m rotation in the X=Y plane (2)				
Initial imperfection in the X = 0 plane in Y +ve direction				
End rotations at 45° to the plane of initial imperfection with the component in the plane of the initial imperfection in the opposite direction as the initial imperfection				
	max end rot (radians)	RF3 = compn (kN)	end of analysis	End moment (kN-m)
SHS1500_X+Y_45_2009m08d30v1	0.01520	1566	end moment changing to stabilising	0 by interpolation

Table G.5 1.5m column, imperfection in X=0 plane, rotn in X = Y plane (3)				
Column end-rotations at 45° to the plane of initial imperfection				
Cor_130by10by1500 _rotn_in_2planes _2009m08d16.xls/plots	max end rot (radians)	RF3 = compn (kN)	end of analysis	End moment (kN-m)
SHS_X+Y_2009m08d13v1b	0.00997	1620	end moment changing to stabilising	0 by interpolation
SHS_X+Y_2009m08d13v2	0.02014	1474	ditto	ditto
SHS_X+Y_2009m08d16v1	0.03034	1326	ditto	ditto
SHS_X+Y_2009m08d16v2	0.04032	1188	ditto	ditto

G.4 3.0m columns

The results of the Abaqus analysis for columns of 3.0m length are presented in:

All the tables, except Table G.10 and Table G.11, have the initial imperfection in the $X = 0$ plane with the imperfection in the +Y direction. Table G.10 and Table G.11 have the initial imperfection in the $X + Y$ plane and the imperfection in the $X \& Y$ +ve direction.

Table G.15 lists early analyses performed for the 2007 SSRC paper [King 2007] for the initial imperfection in the $X = 0$ plane and end-rotations in the $X = Y$ plane by imposing equal rotations about X and Y axes. The results of these analyses were somewhat uncertain because the maximum load was that at the point where the end moment passes through zero from destabilising to stabilising, but this occurred at different loads for the two axes of enforced rotation, the X and Y axes.

Table G.6 3.0m column, rotation in $X=0$ plane				
Initial imperfection in the $X = 0$ plane in Y +ve direction				
End rotations <u>in the plane of</u> the initial imperfection and in the <u>same</u> direction as the initial imperfection				
Max from SHS2006m10d09_130by10_ v1 All other results from SHS2006m10d10_130by10_ v2	UR1 = end rot (radians)	RF3 = compn (kN)	end of analysis	End moment (kN-m)
	0.00086	728.6	continued	0 (pinned)
	0.00237	1456.4	continued	0 (pinned)
Max pin-ended	0.00459	1582.8	buckled	0 (pinned)
	0.01362	1430.6	continued	0 (pinned)
	0.02417	1254.1	continued	0 (pinned)
	0.03105	1158.0	continued	0 (pinned)
	0.03663	1089.5	continued	0 (pinned)
	0.04374	1013.1	continued	0 (pinned)
	0.05283	927.6	continued	0 (pinned)
	0.06466	833.4	continued	0 (pinned)

Table G.7 3.0m column, rotn in Y=0 plane				
Initial imperfection in the X = 0 plane in Y +ve direction				
End rotations <u>perpendicular</u> to the plane of initial imperfection				
	UR2 = end rot (radians)	RF3 = compn (kN)	end of analysis	End moment (kN-m)
SHS2006m10d13_130by10_v4	0.00451	1556	buckled	destabilising
SHS2006m10d13_130by10_v6	0.00662	1522	buckled	destabilising
SHS2006m10d13_130by10_v5	0.00861	1483	buckled	destabilising
SHS2006m10d13_130by10_v3	0.01313	1404	buckled	destabilising
SHS2006m10d13_130by10_v2	0.02422	1257	buckled	destabilising
SHS3000_X+Y_90_ 2009m09d12v4	0.03197	1169	end moment changing to stabilising	0 by interpolation
SHS2006m10d13_130by10_v7	0.04012	1078	ditto	ditto

Table G.8 3.0m column, rotation in the X=Y plane (1)				
Initial imperfection in the X = 0 plane in Y +ve direction				
End rotations at 45° to the plane of initial imperfection with the component in the plane of the initial imperfection in the <u>same</u> direction as the initial imperfection				
	max end rot in X=Y plane (radians)	RF3 = compn (kN)	end of analysis	End moment (kN-m)
SHS3000_X+Y_45_2010m03d14v2	0.00516	1548		
SHS3000_X+Y_45_2010m03d14v1	0.01552	1345		
SHS3000_X+Y_45_2009m09d12v1	0.03063	1119	buckled	5.89 kN-m destabilising
SHS3000_X+Y_45_2010m03d14v3	0.04041	1010		
SHS3000_X+Y_45_2010m03d14v4	0.06342	846		

Table G.9 3.0m column, rotation in the X=Y plane (2)				
Initial imperfection in the X = 0 plane in Y +ve direction				
End rotations at 45° to the plane of initial imperfection with the component in the plane of the initial imperfection in the <u>opposite</u> direction as the initial imperfection				
	max end rot in X=Y plane (radians)	RF3 = compn (kN)	end of analysis	End moment (kN-m)
SHS3000_X+Y_45_2009m08d22v1	0.02206	1254.8		
SHS3000_X+Y_45_2009m08d25v1	0.03092	1129.5		
SHS3000_X+Y_45_2009m08d27v1	0.04930	946.0		
SHS3000_X+Y_45_2009m08d29v2	0.07243	800.1		

Table G.10 3.0m column, rotn in the Y=X plane (3)				
Initial imperfection in the X = Y plane in X & Y +ve direction				
End rotations in the plane of initial imperfection (Y=X plane) and in the <u>same</u> direction as the initial imperfection				
Axial force/shortening only, no applied end rotations				
initial imperfection in both Y=0 plane and X=0 plane = 0.75L/1000	max end rot about either axis (radians)	RF3 = compn (kN)	end of analysis	End moment (kN-m)
max axial load SHS3000_X+Y_45_2009m08d30v5		1584.2	buckled	

Table G.11 3.0m column, rotationn in the Y=X plane (4)				
Initial imperfection in the X = Y plane in X & Y +ve direction				
End rotations in the plane of initial imperfection (Y=X plane) and in the <u>same</u> direction as the initial imperfection				
initial imperfection in both Y=0 plane and X=0 plane = 0.75L/1000	max end rot about either axis (radians)	RF3 = compn (kN)	end of analysis	End moment (kN-m)
SHS3000_X+Y_45_2009m09d01v6	28.50	1239.2	end moment changing to stabilising	0 by interpolation
SHS3000_X+Y_45_2009m09d01v5	46.61	1033.5	ditto	ditto

Table G.12 3.0m column, rotation in $X = Y \tan 22.5^\circ$ (1)

Initial imperfection in the $X = 0$ plane in Y +ve direction

End rotations at 22.5° to the plane of initial imperfection ($X=Y \tan 22.5^\circ$), with the component in the plane of the initial imperfection in the **same** direction as the initial imperfection

	max end rot about either axis (radians)	RF3 = compn (kN)	end of analysis	End moment (kN-m)
SHS3000_X+Y_22_2009m09d02v2	0.02232	1269.6		
SHS3000_X+Y_22_2009m09d12v1	0.03125	1141.5	end moment changing to stabilising	0 by interpolat ion

Table G.13 3.0m column, rotation in $X = Y \tan 22.5^\circ$ (2)

Initial imperfection in the $X = 0$ plane in Y +ve direction

End rotations at 22.5° to the plane of initial imperfection ($X=Y \tan 22.5^\circ$) with the component in the plane of the initial imperfection in the **opposite** direction as the initial imperfection

	max end rot about either axis (radians)	RF3 = compn (kN)	end of analysis	End moment (kN-m)
SHS3000_X+Y_22_2009m09d02v1	0.02348	1356.6		

Table G.14 3.0m column, rotation in $X = Y \tan 67.5^\circ$ plane				
Initial imperfection in the $X = 0$ plane in Y +ve direction				
End rotations at 67.5° to the plane of initial imperfection ($X=Y \tan 67.5^\circ$) towards				
	max end rot about either axis (radians)	RF3 = compn (kN)	end of analysis	End moment (kN-m)
SHS3000_X+Y_67_2009m09d03v1	21.99	1251.0	buckled	destabilising
SHS3000_X+Y_67_2009m09d12v2	32.51	1187.7	end moment changing to stabilising	0 by interpolat tion

Table G.15 3.0m column, rotation in the $X=Y$ plane (5)				
Initial imperfection in the $X = 0$ plane in Y +ve direction				
End rotations at 45° to the plane of initial imperfection with the component in the plane of the initial imperfection in the <u>same</u> direction as the initial imperfection				
	max end rot about both X and Y axes (radians)	RF3 = compn (kN)	end of analysis	End moment (kN-m)
SHS2006m11d14_130by10 _X+Y_v4	0.006452	1549.4	end moment changing to stabilising	0 by interpolatio n
SHS2006m11d14_130by10 _X+Y_v5b	0.01549	1316.2	ditto	ditto
SHS2006m11d14_130by10 _X+Y_v1	0.02285	1185.4	ditto	ditto
SHS2006m11d14_130by10 _X+Y_v6b	0.03581	976.7	ditto	ditto

G.5 6.0m columns

The results of the Abaqus analysis for columns of 6.0m length are presented in

Table G.16, for end-rotations in the plane of the initial imperfection

Table G.17, for end-rotations out of the plane of the initial imperfection

Both the tables have the initial imperfection in the $X = 0$ plane with the imperfection in the +Y direction.

Table G.16 6.0m column, rotation in the X=0 plane				
Initial imperfection in the X = 0 plane in Y +ve direction				
End rotations in the plane of initial imperfection and in the <u>same</u> direction as the initial imperfection				
Max from SHS2006m10d14_130by10_by6000v1 All results other from SHS2006m10d14_130by10_by6000v2	UR1 = end rot (radians)	RF3 = compn (kN)	end of analysis	End moment (kN-m)
	0.0184	671.1	continued	0 (pin)
Max pin-ended	0.0270	755.7	buckled	0 (pin)
	0.0394	690.8	continued	0 (pin)
	0.0460	645.1	continued	0 (pin)
	0.0538	596.1	continued	0 (pin)
	0.0633	543.5	continued	0 (pin)
	0.0751	477	continued	0 (pin)
	0.0852	423	continued	0 (pin)

Table G.17 6.0m column, rotation in the Y=0 plane

Initial imperfection in the X = 0 plane in Y +ve direction

	UR1 = end rot (radians)	RF3 = compn (kN)		End mmt (kN-m)
Max pin-ended	0.0270	755.7		
SHS2006m10d19_130by10by6000 _2planes_v10	0.00469	750.5		0.29 destab
SHS2006m10d19_130by10by6000 _2planes_v9	0.00924	738.9		0.83 destab
SHS2006m10d19_130by10by6000 _2planes_v8	0.01320	726.2		1.45 destab
SHS2006m10d19_130by10by6000 _2planes_v7	0.01780	711.9		2.23 destab
SHS2006m10d19_130by10by6000 _2planes_v6	0.02176	696.4		3.04 destab
SHS2006m10d19_130by10by6000 _2planes_v5	0.02404	686.8		3.40 destab
SHS2006m10d19_130by10by6000 _2planes_v2	0.02552	680.5		3.68 destab
SHS2006m10d19_130by10by6000 _2planes_v4	0.02696	674.1		3.95 destab
SHS2006m10d19_130by10by6000 _2planes_v3	0.02908	664.6		0.43 destab
SHS2006m10d19_130by10by6000 _2planes_v1	0.03606	631.1		
SHS6000_X+Y_90_2010m05d06v1	0.07156	447		buckled

Table G.18 6.0m column, rotation in the X=Y plane

Initial imperfection in the X = 0 plane in Y +ve direction

	UR1 = end rot (radians)	RF3 = compn (kN)		End mmt (kN-m)
SHS6000_X+Y_45_2010m05d03v2	0.0804	453		

APPENDIX H IMPROVED ECONOMY WITH VARIABLE IMPERFECTION

For end-rotations applied in the rectangular planes of the SHS section, the parametric study showed that use of a constant for e_0 ($e_0 = e_s$) is unnecessarily conservative and the resistance could be modelled more accurately by using a value of e_0 that reduces with increased end-rotation. This is of practical interest because there might be many structures in which the slab is very stiff relative to the steel beams, so the end-rotations orthogonal to the end-rotations caused by the steel beam might be very small.

The values of e_0 needed for the design model to give the correct failure load for that end-rotation for rotations in a rectangular plane are shown in Figure H.1 together with the dotted line e_0/e_s that shows a possible tri-linear design line for e_0/e_s that could be used for rotations in a rectangular plane. The equation of the dotted line shown is:

$$\begin{aligned} \text{if } & \theta(h/2) < a_e e_s, \\ & e_0 = e_s (1 - \theta(h/2)/(n_e e_s)), \end{aligned} \quad \text{Eq H 1}$$

$$\begin{aligned} \text{if } & a_e e_s < \theta(h/2) < m_e e_s, \\ & e_0 = e_s (1 - a_e/n_e - b_e) (1 - (\theta(h/2) - a_e \times e_s)/(m_e e_s - a_e e_s)) + b_e e_s, \end{aligned} \quad \text{Eq H 2}$$

$$\begin{aligned} \text{if } & \theta(h/2) > m_e e_s, \\ & e_0 = b_e e_s, \end{aligned} \quad \text{Eq H 3}$$

where θ is the end-rotation applied to the column

h is the column height

and the constants have values:

$$a_e = 1.50, b_e = 0.15, m_e = 5.0 \text{ and } n_e = 3.5.$$

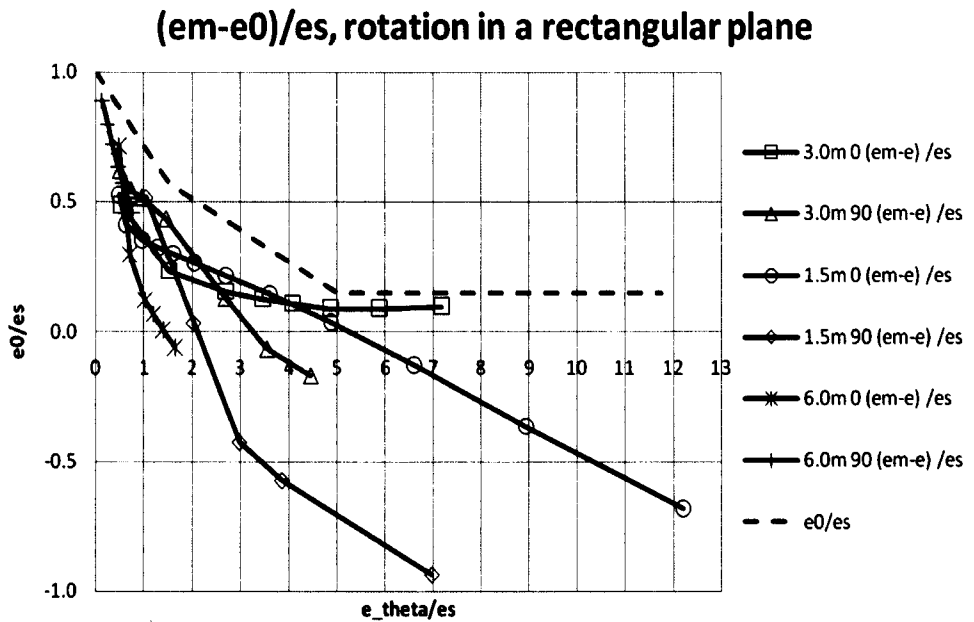


Figure H.1 e_0 for failure load for rotations in a rectangular plane.

For rotations that are not entirely in a rectangular plane, the dotted design line in Figure H.1 should not be used unless there is a method to account for the effect of being out of plane. One method to account for the effect of the end-rotation being out of a rectangular plane uses the projection of the applied rotation, θ , onto a rectangular axis. The resistance is calculated by taking the end-rotation, θ_r , about the rectangular axis “r” (where the axis “r” is either of the rectangular axes of the SHS section) as $\theta_r = \theta/\text{Cos}\phi$, where θ is the end-rotation applied to the column and this end rotation is in the plane at an angle ϕ to the nearest rectangular axis (ie $\phi \leq 45^\circ$).

Another method to account for the effect of the end-rotation being out of a rectangular plane uses the sum of the end-rotations θ_x and θ_y . The resistance is calculated by taking the end-rotation, θ_r , about the rectangular axis “r” (where the axis “r” is either of the rectangular axes of the SHS section) as $\theta_r = \theta\text{Sin}\phi + \theta\text{Cos}\phi$, where θ is the end-rotation applied to the column and this end rotation is in the plane at an angle ϕ to the nearest rectangular axis (ie $\phi \leq 45^\circ$). For both of these methods to account for the effect of the end-rotation being out of a rectangular plane, the imperfection e_0 needs to be calibrated to ensure it is reliable. The data available is shown in Figure H.2 compared with the design line shown in Figure H.1. Data labelled e_{0p} is derived using the projection onto a rectangular plane and data labelled e_{0sum} is derived using the sum of θ_x and θ_y .

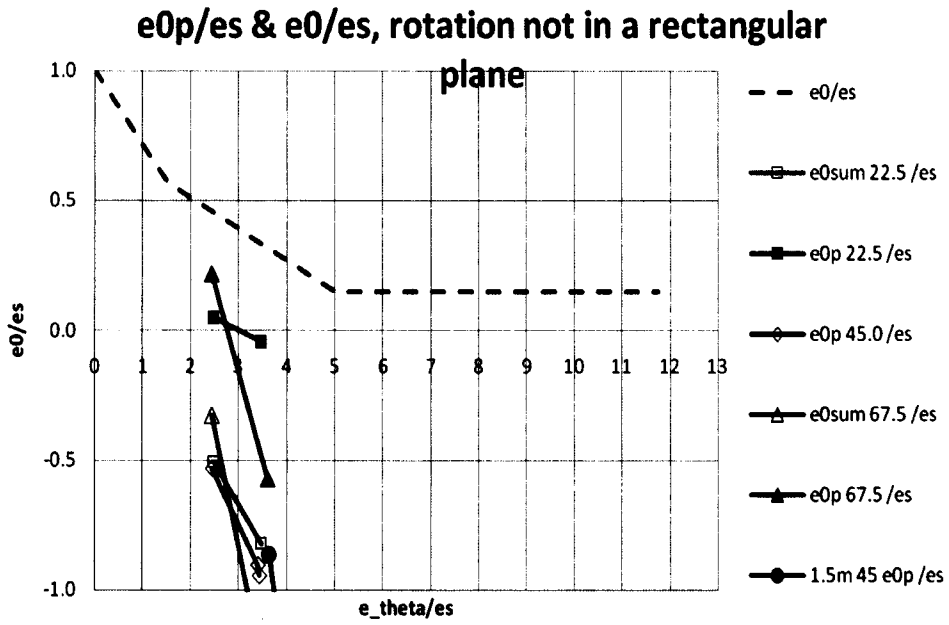


Figure H.2 e_0 for failure load for rotations not in a rectangular plane

APPENDIX I DEFORMED SHAPE OF TEST SPECIMEN

The correlation factors varies between tests as shown in Figure 6.26 Correlation factors for rotation. The possibility that these differences arose from a differences in deformed shape of the members (due to differences in the extent of plasticity) was investigated by studying the relationship of mid-length displacement to end-rotation for different forms of curve. The ratio of (mid-height displacement/height) to (end-rotation) in a circular curve is approximately $\frac{1}{4}$ and for a half-sine curve is $\frac{1}{\pi}$. The plots in Figure I.1 show ratios from 0.28 to 0.33 at the unloading cycles, the points at which the correlation factors c_f are calculated, but there is no apparent correlation between these ratios and the correlation factor, c_f .

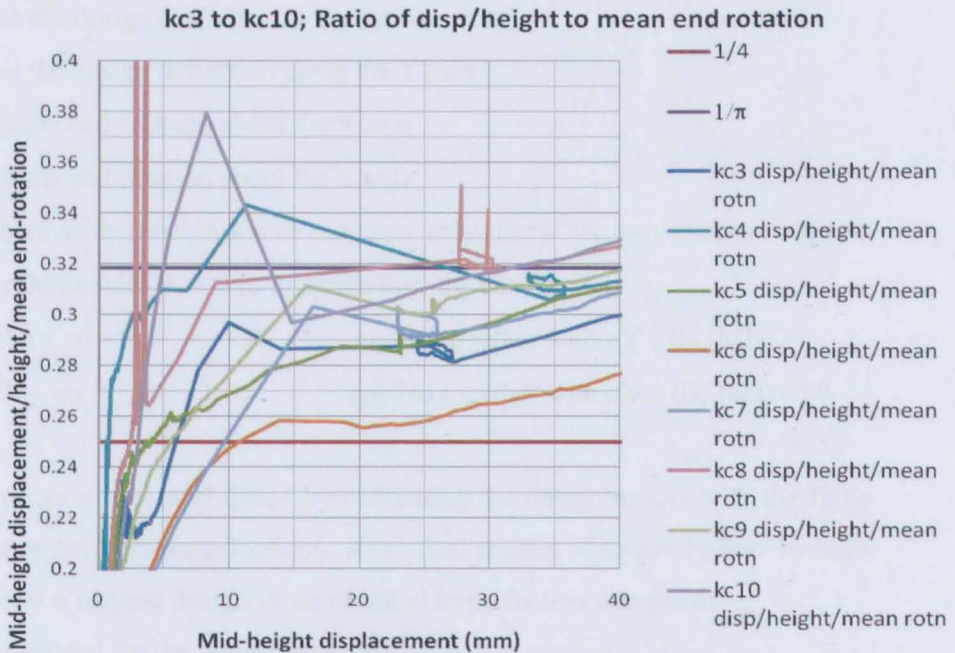


Figure I.1 Deflected shape of test columns

APPENDIX J CMK 2007 SSRC MODEL

At the 2007 SSRC conference [King 2007], a model was proposed using the data and understanding at that date. The model proposed is described below. As a result of the full scale tests reported in Section 5, the analysis reported in Section 6 and further parametric studies reported in Sections 7 and 8, this model is now superseded by the 2009 basic design model. The 2007 model is described here for reference purposes only.

The 2007 model was as follows:

In cases where there are end rotations in both planes, the design deflections in both planes must be included. The appropriate value of imperfection, e_0 , (see below) is added in only one plane. Therefore the total design deflections, e_X and e_Y are:

either $e_X = \theta_Y (h/2) + e_0$ and $e_Y = \theta_X (h/2)$

or $e_Y = \theta_X (h/2) + e_0$ and $e_X = \theta_Y (h/2)$

where e_X is the design deflection along the X axis

e_Y is the design deflection along the Y axis

θ_X is the end-rotation about the X axis

θ_Y is the end-rotation about the Y axis

Note that for members with rotation about one axis only, there are two checks required.

Using the case of a column with $\theta_Y = 0$ to illustrate this, the checks are:

(1) $e_X = (\theta_Y (h/2) + e_0) = e_0$ applied together with $e_Y = \theta_X (h/2)$

(2) $e_Y = \theta_X (h/2) + e_0$ applied together with $e_X = (\theta_Y (h/2)) = 0$

The proposed imperfection was established by calibrating the design model with the finite element analyses using different imperfections. Analytical studies of square hollow sections at that date showed that a varying design value of initial imperfection was possible.

The following was proposed for the imperfection, e_0 :

if $e\theta \leq 2es$, $e_0 = es [1 - (e\theta / 2es)]$

but if $e\theta > 2es$, $e_0 = 0$

where $e\theta = \theta \times (h/2)$

Following full scale testing and further analytical studies, the imperfection was simplified to the use of e_s in the basic design model proposed in Section 8.5.1. This is required because the formulae above were derived

1. before the full scale laboratory testing and calibration reported in Chapters 5 and 6 and
2. before knowing about the difference in the directions of the displacement at midheight of the column caused by end-rotations not in a rectangular plane, as described in Section 3.4.5

Both of these show that the resistance may be lower than predicted by the 2007 model [King 2007], so that model should not be used in design.